UNIVERSITY OF NAPLES FEDERICO II

Ph.D PROGRAM

IN STRUCTURAL, GEOTECHNICAL ENGINEERING AND SEISMIC RISK

COORDINATOR PROF. IUNIO IERVOLINO

XXXIV Cycle

ANDREA NATALE

Ph.D THESIS

EFFECTIVENESS AND ECONOMIC FEASIBILITY OF BASE ISOLATED SEISMIC RETROFIT SOLUTIONS FOR BUILDINGS AND INFRASTRUCTURES

TUTOR

PROF. MARCO DI LUDOVICO

DOTT. ING. CIRO DEL VECCHIO

2022

Because limits like fears are often just an illusion

(Michael Jordan)

If you can dream it, you can do it

(Walt Disney)

Acknowledgements/Ringraziamenti

Since I was a child, I had the aim to become an engineer because I has been always attracted from the structures, moreover the recent seismic events and the consequent losses moved on me the purpose to avoid the sufferance in the people after an earthquake and the need to ensure them the safety in their home; because in own home ‘we have to feel safe’ in every aspect of our life. The Ph.D program gave me the opportunity to follow this purpose and despite my contribution was very little, I am very grateful to a lot of people that gave me this possibility.

First, I would like to thank Prof. Marco Di Ludovico, that gave me the opportunity to participate at this Ph.D program. His guide in these years allowed to improve my skills as an engineer and my scientific knowledge. His kindness and honesty are rare.

A big thank to Eng. Ciro Del Vecchio, for the constant help and presence in my research path. He taught me the approach to the work and the unsatiable desire to discover each aspect of a research topic. He spurred me to improve and overcome my limits.

I am very grateful to Prof. Alp Caner for its kindness and availability to welcome me at M..E.T.U (Middle East Technical University) during my exchange period in Turkey. With his suggestions and advice, he allowed me to discover more deeply the topic of base isolation, and the world of the experimental tests. To this aim a thank to the General Directorate of Highways, Ankara, Turkey, for test setup for the experimental tests and the Ozdekan Rubber for providing the test specimens.

I am very grateful to Tobia Zordan and Bolina Ingegneria for the kindness and the hospitality showed during my period there. This experience gave me the opportunity to improve my skills and my knowledge.

I am very grateful to RINA that gave me the opportunity to participate a project on base isolation, allowing to investigate further aspect of this topic.

I would like to thank the reviewers that improve the work with their advice.

A special thanks to my colleagues and in particular to Davide and Marzia that shared every day the issue and the joys of this path and supporting me.

A big thank to my parents that supported and encouraged me in this journey. Their advice and education have been the basis to all the objective achieved.

A special thanks to my friends in particular Gianluca and Francesco, that made this journey lighter.

A particular thanks to my brother, Davide, that in every day of this journey encouraged me and believed in me more than I do. With its happiness and presence, he gave me the force to follow this objective.

At last, an enormous thank to the only person that has the capacity to make every day a beautiful day despite the difficulties. She supported me in each day of this journey and gave me the force to face up every obstacle. I have no words to describe the importance of her in my life. Thank you to Giulia.

Information

Part of the content of this thesis has been already published on research journals or conference proceedings, as reported in the list below

- Natale A, Del Vecchio C, Di Ludovico M, (2019) The role of the infills in the seismic retrofit of existing buildings using base isolation, ANIDIS 2019
- Natale A, Del Vecchio C, Di Ludovico M, (2019) Seismic retrofit of R.C buildings by using base isolation: Superstructure modelling issues, FIB SYMPOSYUM YOUNG 2019
- Natale A, Del Vecchio C, Di Ludovico M, (2021) Seismic retroift solutions using base isoaltion for existing RC buildings: economic feasibility and pay-back time. Bulletin of Earthquake Engineering 19:843-512. https:/doi.org/10.007/s10518-020-00988-9
- Del Vecchio C, Natale A, Caner A, Di Ludovico M, (2022) Experimental and analytical investigation on the lateral response of ball rubber bearing isolators. Soil Dynamics and Earthquake Engineering,
- Natale A, Del Vecchio C, Di Ludovico M, Caner A, Karimzadeh N.A, Jacak M, (2022) Creep effects on elastomeric and ball rubber bearings under sustained lateral loads, Structure and Infrastructure Engineering

Table of Contents

CHAPTER 1 – INTRODCUTION…………………………………………………………1

1.1 Scope and Objective………………………………………………………….......4

1.2 Thesis Outline……………………………………………………………………. 8

CHAPTER 2 - BASE ISOLATION: PRINCIPLES AND APPLICATION……………….11

2.1 Overview and design principles for base isolated structures…………………………..15

2.2 Overview and design principles for the retrofitting of existing buildings using of base isolation…………………………………………………………………………………19

2.3 Isolation devices…………………………………………………………………34

2.3.1 Rubber Bearing……………………………………………………………….36

2.3.2 Sliding Bearing……………………………………………………………….39

CHAPTER 3 – SEISMIC PERFORMANCE ASSESSMENT OF BASE ISOLATED REINFORCED CONCRETE STRUCTURE……………………………………………..45

3.1 Performance-Based Earthquake Engineering…………………………………....46

3.2 The role of the infills in the seismic performance assessment………………………..50

3.3 Selection of a case study…………………………………………………………....54

3.4 Case Study…………………………………………………………………………56

3.4.1 Numerical Model…………………………………………………………..57

3.4.2 Analyses Matrix…………………………………………………………....60

3.4.3 Assessment of the structure……………………………………………….61

3.5 Results……………………………………………………………………………64

3.6 Base isolation of a bare structure……………………………………………………...66

3.7 Base isolation of an infill structure…………………………………………………68

CHAPTER 4 –A FRAMEWORK FOR THE QUANTIFICATION OF THE ECONOMIC FEASIBILITY AND PAYBACK TIME……………………………………………………..71

4.1 Methodology………………………………………………………………………..72

4.2 Application to a case study ……………………………………………………...77

4.2.1 Hazard analysis……………………………………………………………78

4.2.2 Seismic performance assessment and design of the retrofit alternatives…..79
4.2.3 Quantification of EDPs…………………………………………………….82
4.2.4 Loss assessment ……………………………………………………...85
4.2.4.1 Building component model ……………………………………...85
4.2.4.2 Assessment of EALs……………………………………………...89
4.2.4.3 Cost of the strengthening interventions……………………………..94
4.2.4.4 Pay-Back Time ………………………………………………..96
4.3 PBT as design a parameter……………………………………………………99

CHAPTER 5 – A TOOL FOR THE RAPID ASSESSMENT OF THE PBT KNOWING BUILDING CHARACTERISTICS……………………………………………...105

5.1 Simplified methodology…………………………………………………..106
5.2 Implementation in a Matlab code……………………………………………111
5.2.1 Input…………………………………………………………………111
5.2.2 Dynamic properties…………………………………………………114
5.2.3 Numerical integration and first output……………………………………117
5.2.4 Verification and collapse definition……………………………………118
5.2.5 Damage and loss analysis……………………………………………...122
5.3 Application to case study buildings…………………………………………128
5.3.1 Validation code………………………………………………………...137
5.4 Results………………………………………………………………………148
5.5 Discussion of Results………………………………………………………..171

CHAPTER 6 - BASE ISOLATED INFRASTRUCTURES…………………………….175

6.1 Novel isolation devices: the Ball Rubber Bearings………………………………176
6.1.1 Experimental characterization……………………………………....177
6.1.1.1 Experimental program to assess the influence of displacement and axial load………………………………………………………...177
6.1.1.2 Experimental program to assess the influence of creep …………..184
6.1.2 Analytical model of the main BRB's characteristics…………………….198
6.1.2.1 Prediction of BRBs characteristic ad maximum strength…………205
6.1.2.2 Prediction of damping for BRBs…………………………………..210

6.1.2.3 Influence of design variables…………………………………….....211
6.1.3 Long terms effect on BRB……………………………………………..214
6.2 Certification and acceptance of isolation device (curved surface sliders) for bridge..217
6.2.1 UNI EN 15129………………………………………………………218
6.2.2 Application to a case study……………………………………………221
6.2.2.1 Acceptance protocol test…………………………………………...222
6.2.2.1.1 Benchmark test...……………………………………..225

CONCLUSIONS……………………………………………………………………...229

References……………………………………………………………………………237

List of Figures

Figure 1. Base isolation system on buildings a) and bridge b)……………………………12

Figure 2. Effect of base isolation based on the elongation of the period…………………12

Figure 3. Effects of damping on displacement……………………………………………13

Figure 4. The use of base isolation on new building in the world…………………………16

Figure 5. The seismically isolated Del Mare Hospital in Naples (2004–2017) and view of some of its 327 HDRBs after their installation (Clemente and Martelli 2018)……………17

Figure 6. Procedure of design of base isolation system on a new building (Dolce et al,2004)..18

Figure 7. Failure of beam-column joint a), and column b)………………………………..20

Figure 8. Interaction between infills and structure: a), b) out plane mechanism, c) column failure…………………………………………………………………………...20

Figure 9. Repair and Strengthening Interventions: RC structures a); masonry structures b) (Di Ludovico 2017)………………………………………………………………..21

Figure 10. Installation technique: a) Cutting columns, b) SOLES' system……………....23

Figure 11. The cut of one column of the Poly-functional Centre Rione Traiano in Naples (courtesy of ALGA) (Clemente and Martelli 2018)………………………………………24

Figure 12. The school of Riposto, Catania (courtesy of FIP Industriale)(Clemente and Martelli 2018)……………………………………………………………..............24

Figure 13. Aerial view of Palazzo Ciuffini-Cricchi-Volpi in L′Aquila and an HDRB (courtesy of FIP Industriale and R. Vetturini) (Clemente and Martelli 2018)…………....25

Figure 14. View of the historical masonry building called "La Silvestrella", L′Aquila, and a HDRB (courtesy of FIP Industriale and R. Vetturini) (Clemente and Martelli 2018)….26

Figure 15. Emiciclo building at l′Aquila (courtesy of Somma and R. Vetturini) (Clemente and Martelli 2018)……………………………………………………………...27

Figure 16. The use of base isolation for existing RC buildings in the L'Aquila reconstruction process ……………………………………………………………………………………27

Figure 17. Procedure of retrofit design of base isolation system on an existing building (Dolce et al)…………………………………………………………………………..32

Figure 18. Identification of the minimum period for the base isolated configuration……33

Figure 19. Rubber bearing: a) Low rubber bearing or high damping rubber bearing, b) lead rubber bearing ………………………………………………………………………….37

Figure 20. Sliding bearing: a) Friction Pendulum, b) Double Concave Friction Pendulum, c) Triple Concave Friction Pendulum……………………………………………………..42

Figure 21. PBEE Methodology(Porter 2003)…………………………………………......47

Figure 22. Repair costs as a function of the building damage state (DS) at the component category level (Del Vecchio et al. 2020)………………………………………………….49

Figure 23. The effect of the infills on the seismic response of a structure in terms of a) accelerations, b) displacement……………………………………………………….51

Figure 24. Infill's cracks for cyclic loads…………………………………………………...51

Figure 25. Interaction columns and infills with opening…………………………………52

Figure 26. Soft-storey mechanism…………………………………………………………..52

Figure 27. Failure of the infills at medium floors………………………………………...53

Figure 28. Cyclic behavior for infills (Panagiotakos and Fardis 1996)…………………..54

Figure 29. Case study building: a) building front view and b) plan view and moment resisting frames…………………………………………………………………………56

Figure 30. Numerical model of the case study building …………………………………58

Figure 31. Matrix Analysis………………………………………………………………….61

Figure 32. Push-Over curves of the case study building in the as-built bare configuration ………………………………………………………………………………………..63

Figure 33. Procedure to define the safety index in x direction a) and y direction b)……..64

Figure 34. Distribution of floor acceleration on the case study building in the as-built and isolated configurations: in the x direction a); y direction………………………………….65

Figure 35. Drift comparison between fixed base, isolated bare and isolated infilled configurations: in the x direction a); y direction b)……………………………………..66

Figure 36. Non-linear behaviour of the superstructure on bare configuration……………67

Figure 37. Results of bare a) and infilled b) configuration in linear and non-linear modelling……………………………………………………………………………..68

Figure 38. Linear behaviour of superstructure in infilled configuration and interaction with infills…………………………………………………………………………………69

Figure 39. Results of linear a) and non-linear b) configuration in bare and infilled modelling……………………………………………………………………………..70

Figure 40. Methodology proposed to assess the PBT of retrofit solution………………...73

Figure 41. Compatibility in terms of acceleration a) and displacement b) with code spectra at LSLS (T_R= 475 y)………………………………………………………………….79

Figure 42. Assessment of the structure and preliminary design of the retrofit alternatives…………………………………………………………………………...82

Figure 43. Results in the NLTHs in terms of EDPs for T_R= 475 years (IM7): a) Maximum Drift in the X direction; b) Maximum Drift in the Y direction; c) Peak Floor Acceleration in the X direction; d) Peak Floor Acceleration in the Y direction………………………...84

Figure 44. Component-based model for loss-assessment with focus on the adopted fragility and consequence functions………………………………………………………88

Figure 45. a) Loss distribution for as-built configuration for T_R 475 years, Loss curves related to direct repair costs for the case study building in the as-built and retrofitted configurations: b) lognormal fitting, c) binned value……..…………………………......90

Figure 46. Disaggregation of direct repair costs at increasing IMs for each building configuration……………………………………………………………………………92

Figure 47. Pay-Back Time for the different retrofit solutions…………………………….96

Figure 48. Fitting for the evaluation of discount rate……………………………………..98

Figure 49. PBT accounting for the influence of the discount rate………………………..99

Figure 50. Correlation between the PBT and main characteristic of the building: a) Surface, b) Stories, c) Years of construction, d) Safety index in the as-built configuration…………………………………………………………………………..101

Figure 51. Pay-Back Time for the database of 59 base isolated buildings in L'Aquila: (a) return of the investment curves; (b) interpolation of the PBT as function of the safety index $(PGA_C/PGA_D)_{LSLS}$…………………………………………………………………...102

Figure 52. Flow chart of the tool's functionality……………………………………...108

Figure 53. MDOF model and stiffness definition………………………………………114

Figure 54. Mass Matrix…………………………………………………………………115

Figure 55. Stiffness Matrix……………………………………………………………....115

Figure 56. Distribution of the shear on the columns…………………………………....116

Figure 57. Shear behavior for cyclic loads………………………………………………120

Figure 58. Collapse fragility function for hypothetical building………………………...123

Figure 59. Hypothetical fragility function……………………………………………....124

Figure 60. Hypothetical consequence curve……………………………………………..125

Figure 61. Hypothetical loss distribution………………………………………………..126

Figure 62. Hypothetical seismic hazard curve…………………………………………..127

Figure 63. Case study building 2: a) building front view and b) plan view and moment resisting frames…………………………………………………………………….....129

Figure 64. Case study building 3: a) building front view and b) plan view and moment resisting frames……………………………………………………………………..130

Figure 65. Case study building 4: a) building front view and b) plan view and moment resisting frames……………………………………………………………………..130

Figure 66. Case study building 5: a) building front view and b) plan view and moment resisting frames……………………………………………………………………..131

Figure 67. Case study building 6: a) building front view and b) plan view and moment resisting frames……………………………………………………………………..132

Figure 68. Spectrum compatibility for building 2: a) acceleration and b) displacement..134

Figure 69. Spectrum compatibility for building 3: a) acceleration and b) displacement..135

Figure 70. Spectrum compatibility for building 4-5: a) acceleration and b) displacement………………………………………………………………………...136

Figure 71. Spectrum compatibility for building 6: a) acceleration and b) displacement..137

Figure 72. Comparison between the acceleration estimate with MATLAB code and SAP2000 for base isolated configuration at LSLS: a) record 1, b) record 2, c) record 3, d) record 4, e) record 5, f) record 6, g) record 7, h) mean and all records, i) mean………...139

Figure 73. Comparison between the drift estimate with MATLAB code and SAP2000 for base isolated configuration at LSLS: a) record 1, b) record 2, c) record 3, d) record 4, e) record 5, f) record 6, g) record 7, h) mean……………………..141

Figure 74. Comparison between the acceleration estimate with MATLAB code and SAP2000 for fixed based configuration at LSLS: a) record 1, b) record 2, c) record 3, d) record 4, e) record 5, f) record 6, g) record 7, h) mean…………………………………...142

Figure 75. Comparison between the drift estimate with MATLAB code and SAP2000 for fixed based configuration at LSLS: a) record 1, b) record 2, c) record 3, d) record 4, e) record 5, f) record 6, g) record 7, h) mean………………………………………………………144

Figure 76. Comparison between the acceleration estimate with MATLAB code and SAP2000 for fixed based configuration at DS: a) record 1, b) record 2, c) record 3, d) record 4, e) record 5, f) record 6, g) record 7, h) mean……………………………………………146

Figure 77. Comparison between the drift estimate with MATLAB code and SAP2000 for fixed based configuration at DS: a) record 1, b) record 2, c) record 3, d) record 4, e) record 5, f) record 6, g) record 7, h) mean and all records, i) mean……………………………..147

Figure 78. Acceleration in x direction for a) as-built , b) base-isolated configuration and in y direction for c) as-built , d) base-isolated, drift in x direction for e) as-built , f) base-isolated configuration and in y direction for g) as-built , h) base-isolated for building 1…………149

Figure 79. Variation of EALs with the f_{cm} and A_{sw}/s for the building 1 for the different configuration: a) As-Built, b) FRP, c) Rebuilt, d) Base Isolation………………………..150

Figure 80. Variation of PBT with the f_{cm} and A_{sw}/s for the building 1 for the different configuration: a) FRP, b) Rebuilt, c) Base Isolation……………………………………..151

Figure 81. Acceleration in x direction for a) as-built , b) base-isolated configuration and in y direction for c) as-built , d) base-isolated, drift in x direction for e) as-built , f) base-isolated configuration and in y direction for g) as-built , h) base-isolated for building 2…………154

Figure 82. Variation of EALs with the f_{cm} and A_{sw}/s for the building 2 for the different configuration: a) As-Built, b) FRP, c) Rebuilt, d) Base Isolation………………………..155

Figure 83. Variation of PBT with the f_{cm} and A_{sw}/s for the building 2 for the different configuration: a) FRP, b) Rebuilt, c) Base Isolation……………………………………..156

Figure 84. Acceleration in x direction for a) as-built , b) base-isolated configuration and in y direction for c) as-built , d) base-isolated, drift in x direction for e) as-built , f) base-isolated configuration and in y direction for g) as-built , h) base-isolated for building 3…………158

Figure 85. Variation of EALs with the f_{cm} and A_{sw}/s for the building 3 for the different configuration: a) As-Built, b) FRP, c) Rebuilt, d) Base Isolation………………………..159

Figure 86. Variation of PBT with the f_{cm} and A_{sw}/s for the building 3 for the different configuration: a) FRP, b) Rebuilt, c) Base Isolation……………………………………..160

Figure 87. Acceleration in x direction for a) as-built , b) base-isolated configuration and in y direction for c) as-built , d) base-isolated, drift in x direction for e) as-built , f) base-isolated configuration and in y direction for g) as-built , h) base-isolated for building 4…………162

Figure 88. Variation of EALs with the f_{cm} and A_{sw}/s for the building 4 for the different configuration: a) As-Built, b) FRP, c) Rebuilt, d) Base Isolation………………………..163

Figure 89. Variation of PBT with the f_{cm} and A_{sw}/s for the building 4 for the different configuration: a) FRP, b) Rebuilt, c) Base Isolation……………………………………..164

Figure 90. Acceleration in x direction for a) as-built , b) base-isolated configuration and in y direction for c) as-built , d) base-isolated, drift in x direction for e) as-built , f) base-isolated configuration and in y direction for g) as-built , h) base-isolated for building 5…………165

Figure 91. Variation of EALs with the f_{cm} and A_{sw}/s for the building 5 for the different configuration: a) As-Built, b) FRP, c) Rebuilt, d) Base Isolation………………………..166

Figure 92. Variation of PBT with the f_{cm} and A_{sw}/s for the building 5 for the different configuration: a) FRP, b) Rebuilt, c) Base Isolation……………………………………..167

Figure 93. Acceleration in x direction for a) as-built , b) base-isolated configuration and in y direction for c) as-built , d) base-isolated, drift in x direction for e) as-built , f) base-isolated configuration and in y direction for g) as-built , h) base-isolated for building 6…………169

Figure 94. Variation of EALs with the f_{cm} and A_{sw}/s for the building 6 for the different configuration: a) As-Built, b) FRP, c) Rebuilt, d) Base Isolation………………………..170

Figure 95. Variation of PBT with the f_{cm} and A_{sw}/s for the building 6 for the different configuration: a) FRP, b) Rebuilt, c) Base Isolation……………………………………..171

Figure 96. Geometry (a) and front view (b) of the tested BRBs (dimensions in mm)………………………………………………………………………………....178

Figure 97. Test setup…………………………………………………………………….178

Figure 98. Cyclic response of tested BRBs at 3 MPa axial pressure: a) d_{max}=15mm; b) d_{max}=30mm; c) d_{max}=45mm; d) d_{max}=60mm; e) d_{max}=75mm; f) comparison of the cyclic response at different maximum displacement……………………………………………180

Figure 99. Cyclic response of tested BRBs at 6 Mpa axial pressure: a) d_{max}=15mm; b) d_{max}=30mm; c) d_{max}=45mm; d) d_{max}=60mm; e) d_{max}=75mm; f) comparison of the cyclic response at different maximum displacement……………………………………………181

Figure 100. Cyclic response of tested BRBs at 9 Mpa axial pressure: a) d_{max}=15mm; b) d_{max}=30mm; c) d_{max}=45mm; d) d_{max}=60mm; e) d_{max}=75mm; f) comparison of the cyclic response at different maximum displacement……………………………………………183

Figure 101. Geometric dimensions (in mm) and overview of the tested specimens: a) Elastomeric Bearing (EB), b) Tube Ball Rubber Bearing (TBRB)……………………....186

Figure 102. Test setup……………………………………………………………...186

Figure 103. Results of Test 1: a) Elastomeric Bearings (EBs), b) Tube Ball Rubber Bearings (TBRBs), c) comparison of EBs and TBRBs……………………………………………189

Figure 104. Creep tests for the Elastomeric Bearing (EBs), a-b-c) EBs_Test 2, d-e-f-) EBs_Test 3, g-h-i) EBs_Test 4………………………………………………………...192

Figure 105. Creep tests for the Tube Ball Rubber Bearing (TBRBs), a-b-c) TBRBs_Test 2, d-e-f) TBRBs_Test 3, g-h-i) TBRBs_Test 4……………………………………………..193

Figure 106. Comparison creep's tests between EBs and TBRBs: a-b-c) EBs-TBRBs_Test 2, d-e-f) EBs-TBRBs_Test 3, g-h-i) EBs-TBRBs_Test 4………………………………..194

Figure 107. a) EBs_Test 5, b) EBs_Test 6, c) Comparison between EBs_Test 1 and EBs_Test 5, d) Comparison between EBs_Test 5 and EBs_Test 6……………………...197

Figure 108. a) TBRBs_Test 5, b) TBRBs_Test 6, c) Comparison between TBRBs_Test 1 and TBRBs_Test 5, d) Comparison between TBRBs_Test 5 and TBRBs_Test 6………198

Figure 109. Variability of the hysteretic response with the axial pressure at different maximum imposed displacement: a) d_{max}=15mm, b) d_{max}=30mm%, c) d_{max}=45mm, d) d_{max}=60mm%, e) d_{max}=75mm……………………………………………………….199

Figure 110. Percentage increase of F_{max}, $Q_{d,BRB}$ and $Q_{d,BRB}/F_{max}$ as function of P_{ver} and d_{max}: ΔF_{max} vs. P_{ver} a); $\Delta Q_{d,BRB}$ vs. P_{ver} b); $\Delta Q_{d,BRB}/F_{max}$ vs. P_{ver} c); $\Delta \beta_{eq}$ vs. P_{ver} d); ΔF_{max} vs. d_{max} e); $\Delta Q_{d,BRB}$ vs. d_{max} f); $\Delta Q_{d,BRB}/F_{max}$ vs. d_{max} g); $\Delta \beta_{eq}$ vs. d_{max} h)………………………..200

Figure 111. Bilinear behaviour of BRB…………………………………………………202

Figure 112. Correlation of the maximum force with different parameters of BRBs: a) dimension of the central hole, *d*; b) maximum displacement, d_{max}; c) Axial Load, P_{ver}; d) height, *h*; e), maximum displacement to height ratio, d_{max}/h; f) height to diameter ratio,*h/D*………………………………………………………………………………203

Figure 113. Correlation of the characteristic strength due to the core with different parameters of BRBs: a) dimension of the central hole, *d*; b) maximum displacement, d_{max}; c) Axial Load, P_{ver}; d) height, *h*; e), maximum displacement to height ratio, d_{max}/h; f) height to diameter ratio,*h/D*……………………………………………………………………...204

Figure 114. Investigating the friction coefficient of the steel balls: characteristic strength vs. core axial pressure a); mean friction coefficient vs. maximum displacement b)…………………………………………………………………………………207

Figure 115. Comparison of experimental results and analytical predictions in terms of: a) Characteristic strength, b) Post-Elastic stiffness, c) Maximum force……………………210

Figure 116. Comparison of experimental results and analytical predictions in terms of damping a) $Q_{d,BRB}/F_{max}$ calculated through regression, b) $Q_{d,BRB}$ and F_{max} calculate as single parameter……………………………………………………………………....211

Figure 117. Comparison experimental vs prediction trend, variability of damping: a) with maximum displacement for h =85mm, b) with maximum displacement for h =60mm, c) with dimension of central hole, d) with axial pressure…………………………………………212

Figure 118. Parametric study on the damping a) Dependence from d and d_{max}, b) Dependence from d and P_{ver}……………………………………………………………...213

Figure 119. Long span bridge subjected to thermal distortion a), Displacement of bearing subjected to service condition on long span bridge b), Creep effect in terms of losses related to the Q_d: c) EBs, d) TBRBs…………………………………………………………...215

Figure 120. Ratio between the losses and the characteristic strength of the EB and TBRB…………………………………………………………………………………….216

Figure 121. The acceptance for the curved surface sliders summarized in a flow-chart (Cademartori et al 2021)…………………………………………………………………220

Figure 122. View of the bridge (Cademartori et al 2021)……………………………….221

Figure 123. Plan view of the bridge with the piers' identification (Miano eta al) ……...222

Figure 124. Displacement-force plot for the 3 cycles of the benchmark test…………...227

Figure 125. Displacements-time and forces-time plots for the 3 cycles..…………………..227

Figure 126. Stability check of the 3 cycles for the curved surface sliders………………228

List of Tables

Table 1. Details of 59 buildings retrofitted by means of base isolation in L'Aquila…..…29

Table 2. List of the selected building having design's details……………………….….……..54

Table 3. List of the selected building satisfy ¾ requirements……………….…….….…..55

Table 4. List of the selected building satisfy all requirements……………….…….….……..55

Table 5. Reinforcement details of beam and columns……………………….….….……57

Table 6. Properties of the selected records…………………………………….…...……..79

Table 7. Cost of the proposed retrofit solutions………………………………...……..95

Table 8. Masses implemented in the tool for each building……………….…..……..133

Table 9. Record selected for the building 2…………………………………..….…..…...134

Table 10. Record selected for the building 3………………………………...………..134

Table 11. Record selected for the building 4-5……………………………………….135

Table 12. Record selected for the building 6………...…………………………...…...136

Table 13. Main characteristics and results for the 6 buildings in exam…………...…....171

Table 14. Experimental program…………………………………………………...…179

Table 15. Experimental data and results……………………………………………...…184

Table 16. Test matrix for each bearing (EBs, TBRBs)…………………………….....187

Table 17. Results of the creep test on EBs and TBRBs………………………………....191

Table 18. Results of cyclic tests……………………………………………………196

Table 19. Comparison of experimental results for tests at same maximum displacement…………………………………………………………………………..201

Table 20. Experimental data using for the prediction model……………………………202

Table 21. Experimental damping for the prediction of $Q_{d,EB}$……………………………206

Table 22. Summary of devices under investigation and relevant tests (see Figure for labels)…………………………………………………………………………………….223

Table 23. Load application method for the benchmark test (UNI EN 15129 8.3.4.1.5)..225

Table 24. Summary of the dynamic frictional coefficient in the three cycles………….228

CHAPTER 1 – INTRODUCTION

Most of the existing reinforced concrete (RC) buildings in the Mediterranean area are designed with obsolete code prescriptions far from the modern ones. This made these constructions often inadequate to meet essential structural requirements, especially when subjected to seismic shaking. According to current Italian building code, seismic safety at the LSLS (Life Safe Limit State) can be quantified as the capacity of a structure to resist the design earthquake. For ordinary residential building, the latter is calculated considering the reference earthquake with a return period of 475 years. The capacity of existing buildings often results significantly lower than the code requirements at LSLS, making them vulnerable to seismic actions. In recent years, several seismic events demonstrated the high vulnerability of the existing building stock with number of fatalities and significant direct and indirect losses. This remarked the importance of research studies aiming at the development of novel technologies and design strategies to mitigate the seismic risk of existing buildings. In the past decades many advances were made in the development seismic retrofit interventions that might improve the structural safety. Nowadays, various retrofit techniques are available on the market, and they have been extensively used in the repair and retrofitting of existing building in the recent reconstruction processes showing to the researcher and practitioners the advantages and disadvantages of each technique. Generally speaking, retrofit techniques can be grouped into three macro categories: those mainly increasing the ductility, those increasing the strength and stiffness and those acting in reducing the seismic demand on the superstructure. The first category includes traditional techniques widely used in design practice, such as FRP (Fiber Reinforce Polymer), steel or concrete +jacketing; the second group includes the introduction of novel RC walls, infilling of bays, cross-section enlargement, steel bracing; the third group includes innovative techniques developed in recent years, such as base isolation, dampers, TMD (Tuned Mass Dampers). The selection of retrofit technique is often related to the confidence of the designer with design principles of a technique respect to another one. Thus, in most of the cases, this selection is based on subjective considerations without any cost-benefit analysis of possible alternatives. This approach is exacerbated by the fact that, in the last decade, the seismic retrofitting mainly aimed at increase structural safety at the LSLS without any consideration on the improvement of the performance of the building under frequent and low-intensity earthquake (i.e. at the damage limit state, DLS). Thus, efficient but expensive techniques, such as the base isolation, might be difficult to promote to stakeholders unless a simple strategy to communicate benefits related to reduction of damage is used.

Recent reconstruction processed followed to catastrophic seismic events, showed that most of the repair cost is related to repairing of damage to non-structural components. Thus, a design of a retrofit intervention aimed at pursuing modern concepts of resilience and sustainability should aim at both increasing the structural safety and minimizing the damage to non-structural components. Recent scientific progresses in the field of seismic performance assessment pushed the use of modern performance-based earthquake engineering (PBEE) concepts in the design practice. To this end user-friendly software or design-oriented methodology were developed to help practitioners to assess seismic losses. Other studies demonstrated that most of the economic losses in a building during a seismic event are due to the damage of non-structural components, such as hollow clay brick infills. Such components are sensitive to both drift demand (responsible of in-plane damage) and acceleration demand (responsible of out-of-plane failures). In this context, traditional retrofit techniques such as FRP, steel or RC jacketing mainly devoted at the seismic safety enhancement, do not help in reducing drift and acceleration demand and, in turn they are not very effective in reducing the expected damage and related losses.

This revamped the interest in the use of low damage retrofit techniques such as base isolation. It mainly acts in reducing the acceleration demand transmitted to the superstructure resulting in a reduction of the inertial forces and drift demand on structural and non-structural components. Thus, resulting in a significant increase of the seismic safety and reduction of the expected losses. Despite of its high effectiveness and recent best-practice applications in the reconstruction processes, it is not very popular in the design practice. This is because of the high initial cost and difficulties in its design and installation. However, the direct cost should not be considered as meaningful decision variable since it does not account for the performance of the retrofitted building during its design life. The work aims at proving useful data to assess the economic convenience of base isolation as seismic retrofit solution. Comprehensive methodology available in literature based on the refined FEMA P-58 loss-assessment framework properly adapted to the characteristics of RC buildings in the Mediterranean area are used. This framework can be used to assess the breakeven time of different retrofit solutions and to have useful insights for the selection of the most convenient one. In this work, this loss-assessment framework is adapted to accurately assess the return period of the economic investment in a seismic retrofit solution. The PBT (Pay-Back Time) of the economic investment is defined and a procedure for its calculation and for the selection of the proper modelling assumptions is proposed. The PBT could be a meaningful parameter to guide the designer in comparing different retrofit techniques and selecting the most cost-effective solution.

Although the seismic performance of buildings is of paramount importance in the development of modern resilient communities, recent earthquakes also demonstrated that the seismic performance of road infrastructures are critical to guarantee a rapid recover and to reduce direct and indirect economic losses. In this context the role of bridges is crucial in the development of a resilient road network. Bridges are subjected to a different type of loads that are not predominant in buildings, such as service loads, which have both short-term and long-term effects. Lateral movements must be allowed in order to avoid significant stress on the piers under thermal deformations. For this purpose, bridges are commonly characterized by supporting devices with a high horizontal deformability, which may also serve as base isolation when properly designed. In this case, the support devices have a dual function and should work well both under operational load and lateral loads such as seismic actions or wind loads. Due to these performance requirements the development of high-performance isolation devices for bridges is still a discusses research topic. In particular, such devices should be flexible to accommodate thermal distortion and at the same time have high energy dissipation under cyclic actions. Furthermore, the cost of the devices and maintenance cost are relevant for their widespread in the design practice. To address this further scope, this thesis also deals with the development of innovative base isolation devices and the related qualification and acceptance process governed by standard codes and national regulations.

1.1 Scope and Objective

This thesis deals with the effectives of base isolation for the seismic retrofitting of existing RC buildings and infrastructures. The objectives of the research work can be divided into two main groups.

The first refers to RC building and the main objectives are: i) determine the effectiveness of base isolation compared to other techniques; ii) provide a comprehensive PBEE-based methodology to assess the PBT of different retrofit solutions; iii) develop a simplified tool to calculate the PBT based on the building main characteristics.

The second group refers to infrastructures with emphasis on base isolated of RC bridges. The main objectives are: iv) develop and validate through experimental test a new type of rubber bearing; v) assess the influence of creep and relaxation on the lateral response this novel device; vi) provide reliable design equations to predict the main bearing characteristics to be used in the design process; vii) clarifying the acceptance and qualification process of new bearings to be used on bridges.

To achieve the first objective, an existing building representative of the entire database of the buildings retrofitted with base isolation during the L'Aquila reconstruction process is selected. It is analyzed considering different configurations and models of the structure. Normally, the design of a new isolated building takes into account the elastic behavior of the superstructure. However, this assumption is not realistic for an existing building because the structural element does not have the capacity to remain elastic. The presence of infill changes the behavior of the superstructure modifying its response in terms of drift and acceleration demand. The infills reduce the displacement of the structure often changing the failure mechanism of failure. The so-called infill-to-structure interaction may lead to premature shear failure at the top of the columns. The comparison of the results of the bare and the infilled model in the linear and the nonlinear configuration gives insights to select the most reliable model to capture the building seismic response.

The address of the second objective a novel methodology to assess the performance and the economic convenience of the base isolation as seismic retrofitting of existing RC buildings is proposed. It relies on the PBEE framework to assess the direct and indirect economic losses related to the expected reference earthquakes. It allows to calculate the PBT, that can give an idea of the return period of the economic investment, and, in turn, it can be used as a unique parameter useful to the stakeholders in the decision-making process. This parameter allows to compare different retrofit techniques having different cost of installation and different performances in terms of seismic safety at the LSLS as well as different EALs.

The third objective consists in the development of a simplified software tool to calculate the PBT based on the main building characteristics.

It is developed in MATLAB using simplified assumption to reproduce the building response. It consists of sequential scripts that allow to perform a complete structural, damage and loss analysis. Only a few input data are required, such as geometric and mechanical information of the building and the properties of the isolation system. The structural analysis is performed using the OS -Splitting method to solve the equation of motion considering a set of input records provided by a spectrum compatibility analysis. The output data for the structural analysis are the EDPs, drift and accelerations. The successive damage analysis performed according to the automatic approach implemented in the PACT tool (ATC - Applied Technology Council 2012a) and the loss analysis allow defining the EALs. Knowing the EALs and the initial cost of the retrofitting, the PBT of different retrofit solutions, namely FRP, Rebuilt and Base Isolation, can be calculated. The tool provides preliminary data to help the stakeholders to identify the best retrofit solution for an existing building and the convenience of base isolation. For this purpose, a parametric analysis was performed varying f_{cm} based on a normal distribution and each realization is combined with different ratio A_{sw}/s to obtain a total of 120 combinations for each building.

The fourth objective is to develop and validate a novel isolation device. The performance of Ball Rubber Bearing (BRB) and a further development to improve its durability are investigated by means of experimental tests and analytical studies. The lateral response of BRBs is affected by various geometrical and mechanical parameters. The experimental program focuses on the influence of displacement demand and axial load. Five values of displacement and three of axial load are investigated.

The fifth objective is to evaluate the creep on the lateral response of the BRB. Usually, creep in the vertical direction is studied and no evidence of creep in the horizontal direction is found in the literature. For this purpose, an experimental program is carried out on BRBs to investigate this phenomenon. The first test is used to evaluate the cyclic response of the device, the following three to study the lateral creep, imposing a fixed displacement for a certain period of time and observing the variation of the lateral force. The fifth test examines the influence of creep, the last one the influence of axial load, increasing the pressure from 3 MPa to 6 MPa.

The sixth objective is to provide a reliable design equation for predicting the key design parameters of bearings. All the data from the tests available in the literature on BRBs in terms of stiffness, characteristic strength, maximum force and damping are collected. The best correlation between the collected main design parameters and the main characteristics of BRBs such as diameter of the central hole, axial pressure and displacement is investigated. Finally, prediction equations for the damping, the characteristic strength and maximum strength are proposed.

The last objective is to clarify the qualification and acceptance process for the new bearing on the bridges. The large use of base isolation drives the research for novel and high-performance devices. Manufacturing a new device requires a qualification process, while using a device on a structure requires an acceptance process. The acceptance and qualification process depends on the context in which it takes place. In Italy, for example, the rules for these processes are the European ones in combination with the national rules. This combination sometimes brings difficulties in the interpretation of the tests and the development. A case study of a bridge is used to propose a clarification of the tests required for the acceptance and qualification of the equipment.

1.2 Thesis Outline

Following the objectives discussed in the previous section, this dissertation is organized as follows.

Chapter 2 describes the design principles of base isolation for new and existing buildings. An overview of the application of base isolation in Italy and worldwide to structures and infrastructures (bridges) is shown, with emphasis on the data collected during the L'Aquila reconstruction process.

Chapter 3 reports the studies conducted to assess the effectiveness of base isolation. In particular, the modelling assumptions are reported and discussed with reference to a case study RC building damaged by the L'Aquila earthquake and retrofitted by means of base isolation. The results are compared in terms of EDPs considering different modelling assumption: linear or non-linear model of the building in the bare or infilled configuration.

Chapter 4 reports the proposed methodology based on PBEE framework to estimate the Pay-Back Time (PBT) of the economic investment in the seismic retrofitting. This framework is applied to the case study RC building to validate the outcomes. Then it is extended to a database of 59 existing RC buildings retrofitted by means of base isolation during the L'Aquila reconstruction process for which data on the cost of installation and effectiveness of the retrofit intervention are available. The analyses are used to calibrate simplified equations to calculate the PBT knowing the safety index at the LSLS.

In Chapter 5, the methodology proposed in the previous chapter is implemented in MATLAB code to allow its extension to a large number of case studies. This code allows the estimation of PBT through structural, damage and loss analyses, comparing different retrofit alternatives and considering the variability in the input, concrete compressive strength and structural details. A parametric study is performed on 6 different real buildings located in different seismic zones all around Italy for which the actual retrofit costs are made available by the industrial partner Bolina Engineering. These data are later used to develop simplified correlations to assess the PBT of a base isolation retrofit intervention by using the main building characteristics.

Chapter 6 reports on two experimental campaigns on BRBs. In the first, the influence of axial load and displacement on cyclic behavior is investigated. The second one deals with the influence of horizontal creep. In the first campaign, 15 tests are performed with five values of displacement and three values of axial load. In the second campaign, 6 tests are performed on TBRBs (in this case the hole is protected with a tube) and EBs, respectively. Three tests are performed on lateral creep under different imposed displacement and speed rate. Design equation to predict the equivalent damping and the main design parameters of the BRBs are proposed. The effect of lateral creep on the TBRBs and EBs is assessed with reference to a case study RC bridge subjected to operational load. Finally, the acceptance and qualification procedure for bearings installed on a bridge are analyzed and discussed.

CHAPTER 2 – BASE ISOLATION: PRINCIPLES AND APPLICATION

Base isolation provides decoupling between the horizontal motion of the structure and that of the soil introducing a disconnection along the height of the structure. In RC building it is commonly realized by including a soft link (i.e. isolation devices) at the top, middle or bottom of the ground floor columns (Figure 1). Thus, the structure can be divided in two parts: the substructure, which is firmly connected to the ground, and the superstructure (see Figure 1a). Normally, in existing RC buildings these columns do not have adequate strength and stiffness and they may need for a structural strengthening or the introduction of an additional supporting structure. In the case of a bridge, the disconnection is located between the pier and the deck.

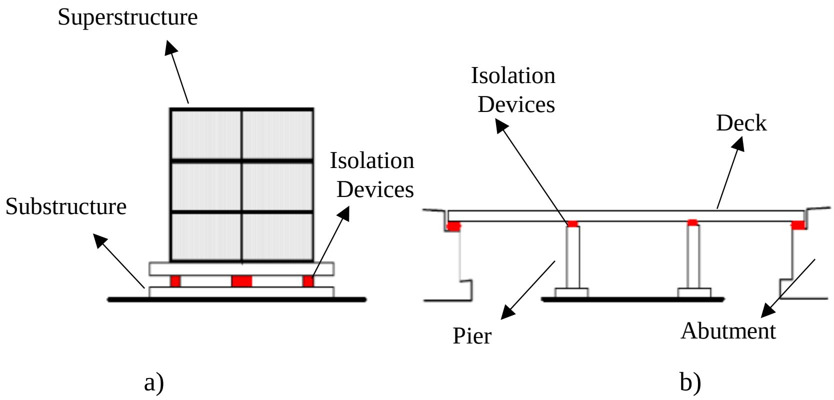

Figure 1. Base isolation system on buildings a) and bridge b)

The isolation devices should have high vertical stiffness (to transfer the vertical load to the ground) and low horizontal stiffness (to allow the relative movement between the superstructure and the substructure).

Typically, the substructure is very stiff, and it is subjected to the same acceleration as the soil, while the superstructure benefits from low stiffness of the isolation devices resulting in a significant elongation of the fundamental period of vibration and, in turn, a cut of the acceleration transmitted to the upper floors. The benefits of the period elongation can be clearly observed in the acceleration response spectra (Figure 2a). The shifting of the fundamental period related to a well-designed base isolation system allows to move in a part of the spectrum characterized by very low acceleration. However, period elongation is accompanied by an increase in displacement that can be clearly observed in the displacement response spectra (Figure 2b).

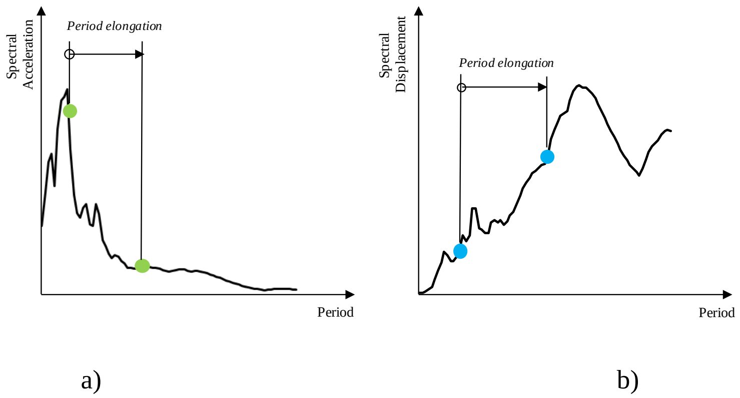

Figure 2. Effect of base isolation based on: acceleration a) and displacement demand b)

Thus, the isolation devices and all the services coming to the structure from the surrounding ground should be properly designed to accommodate large displacement demand. To overcome this issue, high damping devices can be employed. The effect of damping in terms of reduction of the displacement demand is schematically reported in (Figure 3).

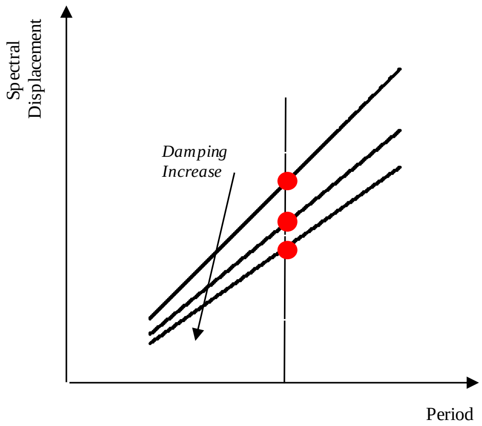

Figure 3. Effect of damping on spectral displacement demand

According to (Dolce et al. 2004), seismic protection with the base isolation can be realized with various approaches, which are essentially summarized in these two:

- Increase of the fundamental period of vibration, without or with dissipation.
- Limitation of the force, without or with dissipation

In the strategy based on increasing the fundamental period of vibration, devices with quasi-elastic behavior are usually used to reduce the accelerations acting on the structure. From the energetic point of view, the reduction of the impact on the structure is mainly due to the absorption of the seismic input energy by the device in the form of deformation energy, which is then dissipated by the hysteresis. The energy dissipation of the isolation system reduces both the displacement, and, within certain limits, the forces transmitted to the superstructure.

Instead, devices with rigid - or elastic - perfectly plastic behavior, but strongly nonlinear, with a mostly horizontal branch for high displacement (hardening almost equal to zero) are used with the strategy based on limiting the force. Reducing the impact on the structure is done by limiting the force transmitted to the superstructure by the devices (since they are implicit in the form of their hysteresis cycle). Dissipation of the base isolation system is used to contain the displacement at the base. Consequently, a reduction of the transmitted force in case of hardening is not negligible.

The strategy based on increasing the fundamental period tends to be applied in isolated buildings for various reasons, mainly technological. A positive aspect of the strategy based on limiting the force is that the effectiveness of the isolation is largely independent of the characteristics of the seismic event (intensity and frequency containment), due to the possibility of high displacement of the isolation system (Constantinou et al. 1988).

The advantages of the isolation system are many. The significant reduction of the acceleration on the structure involves:

- Reduction of inertial force, that is, the load applied to the structure by the earthquakes, in order to avoid the damage of structural elements despite the violence of the earthquake
- Significant reduction of interstorey drift to reduce or eliminate the damage to non-structural components and ensure the full functionality of the building after a strong earthquake
- High protection of the structural enclosure
- Low perception of seismic events by occupants

All these aspects imply a drastic reduction or total resetting of repair costs after a seismic event. Compared to a normal earthquake resistant structure, the initial cost may be higher, depending on several parameters:

- Dimensions, especially the number of floors
- Configuration of the building, related to the difficulty of placing the isolation plane

- Structural shape, depending on the number of devices to be used
- Frequency limitation of the design action, related to the reduction of the acceleration
- Presence of adjacent buildings, related to the realization of separation joint and the architectural aspects
- Type of isolation devices

In particular, where the number of floors it is too small the cost of the device and the interventions related to the isolation are spread over a limited number of floors, thus resulting in an inconvenience in the installation of this technique. On the other hand, for tall buildings, the fundamental period of the structure, considered fixed, could lead to severely limit the benefits of isolation in terms of seismic force reduction.

2.1 Overview and design principles for the base isolated structures

In recent years, considerable progress has been made in the development of new devices that can be used in new and existing buildings and in the development of design principles, guidelines and code prescriptions specific for base isolation. In many countries where specific rules for the design of buildings with base isolation are available, the designers are encouraged in the use of this technique and great consideration is given to the base isolation. However, these rules and the acceptance vary widely from country to country. As a result, in some parts of the world where base isolation is preferred, the number of isolated structures is increasing, while in other countries the number of applications is limited.

The country with the highest number of isolated structures is Japan, followed by China, Russia and Italy, but with large differences (Figure 4).

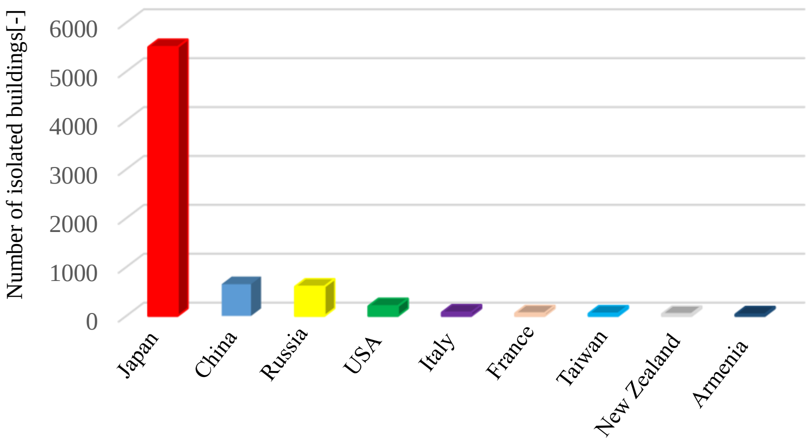

Figure 4. The use of base isolation in new buildings in the world

At the end of 2003, only 25 base isolated structures can be found in Italy. The enforcing of "Ordinanza 3274" and the seismic reclassification of the national territory provided a significant increase in the design of isolated structures. The application has been successful for both strategic and residential buildings. A new frontier, with many designs in progress, is the protection of historic monuments through base isolation. Focusing on the Italian building stock, in the 2009 there were about 70 base isolated structures in Italy. With the progressing of the "Progetto C.A.S.E." during the reconstruction process followed to the 2009 L'Aquila earthquake this number increases to 250 (Complessi Antisismici Sostenibili e Ecocompatibili) (Calvi and Spaziante 2009; Dolce and Serino 2009; Dolce and Calvi 2010). Within this project, 185 isolated platforms were built between June 2009 and February 2010, with a total of 4450 dwellings for the homeless. This operation, with its 7368 isolators, is now the largest application of base isolation in Italy and probably in the world. The basis of the project is the construction of prefabricated structures of different types (wood, steel), erected on reinforced concrete platforms with a base of 21 x 57 m and a thickness of 50 cm, supported by isolators at the top of the columns. Originally, two solutions were proposed: one with a hybrid system of 12 elastomeric bearings and 28 flat sliders, another with 40 sliders with concave surface. The second solution was chosen because it was economically

and technically compatible with the shorter intervention times. Moreover, this solution was independent of the isolated mass, which was not known because it depended on the type of building (wood, reinforced concrete, steel).
One of the most recent applications of base isolation for strategic buildings is “L’Ospedale del Mare” in Naples (Cosenza et al. 2009) (Figure 5).

Figure 5. The seismically isolated Del Mare Hospital in Naples (2004–2017) and view of some of its 327 isolators after their installation (Clemente and Martelli 2018)

The building, which has a roughly square plan with a side length of 150 m, is seismically isolated with 327 elastomeric bearings with high damping (HDRB). The size, without joint, and the number of devices make the building one of the most demanding in the world. The use of the isolation system brings several and significant advantages over traditional design. In particular, a reduction of reinforcement in beams and columns of about 40% has been identified.
In the last years, the application to bridges and viaduct, both new and existing, are significant increase in Europe and in the rest of the world, especially in the USA (where the rule isn’t penalizing as that for the buildings), Chile, Japan, China, Taiwan, and Korea.
In Japan, for example, more than 2000 isolated bridges were realized between the last decade of the 1990s and the first years of the new century (Kawashima 2001). Since 1995, after the Kobe earthquake, the use of devices has changed considerably. The devices used usually had elastoplastic behavior with energy dissipation, and most applications use elastomeric high damping (HDRB) bearings.

In Italy, there are more than 250 applications of foundation isolation systems and energy dissipation on bridges and viaducts (Martelli and Forni 2009).

The design process of a base isolated structure can be summarized as shown in Figure 6:

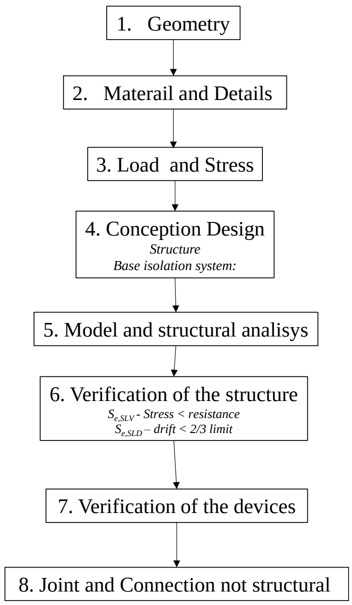

Figure 6. Procedure of design of base isolation system on a new building (Dolce et al. 2004)

The first three steps include the actions needed to define the structural system, i.e. defining the geometry, the material, the construction details and also the design loads.

The fourth step includes an initial hypothesis about the dimension of the structural elements and the definition of the properties of the structural system. The geometry of the structural system is defined based on the axial load considering the seismic checks. The isolation system is defined using the general properties of stiffness and damping as global quantities and distributed among the different devices. The verification is carried out in steps 7. The design is carried out by identifying the pair (T_{is},ξ_{esi}) that allows to obtain a reasonable reduction of the seismic actions with respect to the fixed base configuration, a limited displacement, with respect to the intensity and characteristics of the seismic actions, and a good agreement with the commercial production. In the case of a system that has a nonlinear behavior with hardening, it is possible to approximate the behavior with an equivalent period and damping and use the described procedure if the rule allows it.

Step 5 involves characterizing the structural model and performing the analyses (static or dynamic) required to evaluate the stresses and deformations of the structural elements, for the controls at DLS and ULS.

The last three steps include the verification of all components:

- Structural elements, referenced to design stress
- Isolation devices, with respect to design stress and deformation
- Structural joints and connections, related to design displacements

2.2 Overview and design principles for the retrofitting of existing buildings using of base isolation

Existing reinforced concrete (RC) buildings designed with old code provisions commonly exhibited severe damage to structural and non-structural components under medium-to- high intensity earthquakes. Recent devastating earthquakes worldwide demonstrated the high seismic vulnerability of these buildings and the need for effective retrofit interventions to increase the safety and protect the non-structural components. In the Mediterranean area the lack of proper seismic details commonly results to very low seismic performances often limited by premature shear failures at the level of joints or columns (Ricci et al. 2011a) (Figure 7a,b).

a) b)

Figure 7. Failure of beam-column joint a), and column b)

The interaction between the RC frame and hollow clay brick stiff infills can be triggering for the column shear failure (Figure 8c) (Verderame et al. 2010). Furthermore, the high sensitivity of hollow clay brick infills and partitions to lateral drift may lead to significant damage and high repair cost (Figure 8a,b) (Cardone et al. 2017; Del Vecchio et al. 2020)

a) b) c)

Figure 8. Interaction between infills and structure: a), b) out plane mechanism, c) column failure

In this context, the use of seismic retrofit strategies for existing RC buildings aiming at enhancing the seismic performance at the life-safety limit state and protecting drift and acceleration sensitive non-structural components can be a sound and efficient solution (Skinner and McVerry 1975; Naeim and Kelly 1999) The retrofit techniques available on the market are nowadays different and they are designed to increase the seismic capacity of the buildings, based on techniques to increase the strength and/or deformation capacity of the structure or to reduce the seismic demand (Di Ludovico et al. 2008). To increase the strength and/or deformation capacity, the most commonly used techniques are RC jacketing, composite systems (i.e. FRP), CAM, steel bracing, steel jacketing, beton plaque´, strengthening of foundations by jacketing or micropiles, RC shear walls. The reduction of seismic demand was mainly pursued with base isolation systems or dissipative bracing to significantly increase either the period of the structure or its damping, or both, and thereby reduce damage. The application of the retrofit intervention is related to a different number of parameters, the diffusion, or better the use, of the above cited techniques is different for several reason and an interesting overview can be provided by the reconstruction process of L'Aquila after the earthquake in 2009. The reconstruction process of damaged residential buildings was based on the usability ratings (Di Ludovico et al. 2017) assigned according to the AeDES form (ranging from A to F) (Baggio et al. 2007), with an increase damage from A to F. 654 RC and 490 masonry buildings were classified E or E_{dem} and a global strengthening intervention was designed. The distribution of the adopted retrofit solution is showed in Figure 9:

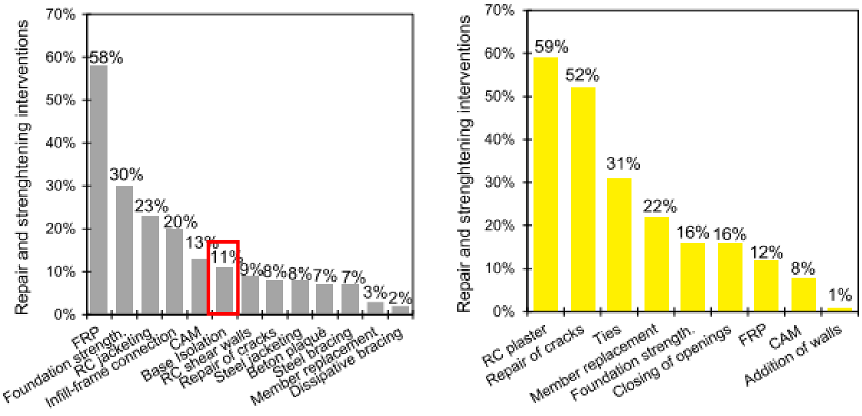

a) b)

Figure 9. Distribution of repair and strengthening intervention fors: RC buildings a); masonry buildings b) (Di Ludovico et al. 2017)

In many cases the retrofit solution consisted in an assembly of different techniques. For this reason, the sum of percentages reported in Figure 9a, b exceeds 100 %.

Figure 9a shows that the most adopted strengthening solutions for RC buildings were based on FRP systems, followed by the strengthening of foundations, and RC jacketing. It is worth noting that the category of strengthening of foundations refers only to buildings with original capacity deficiencies in the foundation members and excludes the cases of interventions caused by the use of other strengthening techniques (i.e. addition of shear walls, steel bracing or base isolation systems). Base isolations retrofit solutions were used in 11 % of the projects, corresponding to 72 existing buildings, where 59 are then effectively retrofitted and 13 were demolished due to inconvenience in the retrofitting. Figure 9b shows that for masonry buildings the most adopted interventions to increase the seismic safety index and recover usability were in-plane strengthening of masonry walls by means of RC plaster with internal steel grids and ties or, in some cases, FRP grids and spikes (Balsamo et al. 2011), out-of-plane strengthening by means of steel, RC, or tie rods, ties, strengthening of foundations.

As reported in (Clemente and Martelli 2018), base isolation has been widely applied to existing buildings in recent years due to its effectiveness in protecting structural and non-structural components, as described above. The number of buildings retrofitted with base isolation in Italy is rapidly increasing. However, there are some problems in the application of this technique, such as the cost, which is the main obstacle to the investment, and the installation.

With reference to reinforced concrete buildings, there are mainly two types of interventions for installing a seismic isolation system:

- to cut and eliminate a portion of the columns (and the walls, if any), and successively to insert the isolators. As is the case for new buildings, the best solution, when possible, is to insert the devices at the top of the columns of the lowest floor (the underground floor, if any). In this way, the floor above the isolators guarantees the horizontal stiffness level required and the portions of the columns under the isolation devices can be enlarged to obtain the stiffness needed or just to support the isolators (Figure 10a).

- to insert the devices between the existing foundations and new sub-foundations, which must be custom built. Sometimes, the existing foundation is not structurally reliable, and two new foundations should be built (Figure 10b).

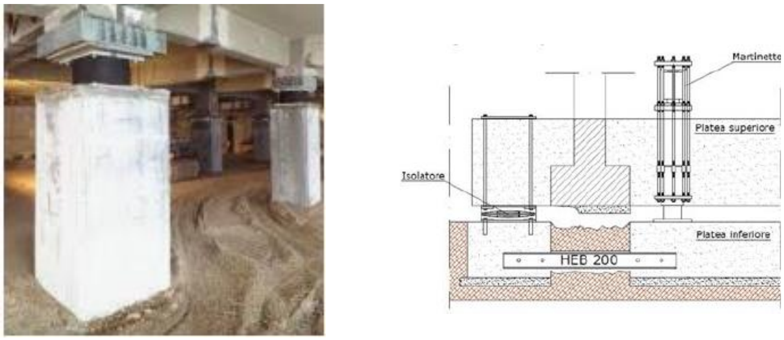

a) b)

Figure 10. Installation technique: a) Cutting of ground floor columns, b) SOLES system

The base isolation has been applied on different types of existing building for destination use and location. The application has been provided on structure designed with old code provisions, often in area previously not defined seismic or on structure suffered damage after a seismic event.

For example, the residential building in Fabriano (structural design by G. Mancinelli, acceptance certificate by A. Martelli) which suffered non-structural damaged during the earthquake of Marche Umbria in 1997-1998. The building after the retrofit intervention has been interested by the seismic action of Central Italy in 2016-2017, showing high performance with no damage compared to the other building retrofitted after the Umbria Marche earthquake. Among the other applications, we mention the Multifunctional Centre at Rione Traiano in Naples (Figure 11), which has an asymmetric shape. It had been built before the 1980 Campano-Lucano earthquake, when the area was not classified as seismic, but remained incomplete.

Figure 11. The cut of one column of the Poly-functional Centre Rione Traiano in Naples (courtesy of ALGA) (Clemente and Martelli 2018)

The building was retrofitted in accordance with the new Italian seismic classification and technical code and completed in 2005, by inserting 630 HDRBs in the columns and in the outer walls, above the foundation level. Also, the retrofit of two, four-story reinforced concrete residential buildings in Solarino, Sicily (structural design by G. Oliveto and M. Granata) (Oliveto Scalia). Seismic action was not considered in the original design (Oliveto Granata). Among the other relevant applications worth mentioning are the Quasimodo School at Riposto (Figure 12), Catania, which was seismically isolated in 2009 by means of 33 HDRBs and 16 SDs.

Figure 12. The school of Riposto, Catania (courtesy of FIP Industriale)(Clemente and Martelli 2018)

It was the first Italian application of seismic isolation in existing schools (structural design by F. Neri, Fig. 22). The IACP building at Calatabiano, Catania, built at the beginning of 1980s with a rectangular shape in plan (size 35.5 m × 11.25 m), three floors above the ground plus an underground floor. The carrying structure was composed of reinforced concrete frames and brick-concrete floors, and the foundation was a plate stiffened by a grid of beams. The structural elements were in very bad conditions, due to the carbonation of concrete and the steel corrosion. The retrofit was done by means of seismic isolators at the top of the columns at the underground floor (structural design by F. Neri). The columns of the underground floor were first enlarged, both to improve their strength and to allow the insertion of the devices, and additional beams were built just above the isolators.

The most interesting applications concern historic masonry buildings are the Palazzo Ciuffini-Cricchi-Volpi (Figure 13), a masonry building located in the historical centre of L′Aquila, which was badly damaged by the 2009 earthquake, and then retrofitted with seismic isolation (structural design by R. Vetturini); specifically, 28 HDRBs (diameter = 550 mm, total rubber thickness = 105 mm) and 25 SDs were used.

Figure 13. Aerial view of Palazzo Ciuffini-Cricchi-Volpi in L′Aquila and an HDRB (courtesy of FIP Industriale and R. Vetturini) (Clemente and Martelli 2018)

The choice of the isolation period was governed by the displacement, which had to be limited because of the presence of an ad- jacent building. The isolated period was 2.02 s and the maximum displacement 146 mm. The isolators were placed between two new sub-foundations made of reinforced concrete beams.

The historical masonry building called “La Silvestrella” (Figure 14) in L′Aquila, which was also seriously damaged by the 2009 L′Aquila earthquake. The structure had been built in the early years of the twentieth century and was kept in its original configuration, without changes or superfetation.

Figure 14. View of the historical masonry building called “La Silvestrella”, L′Aquila, and a HDRB (courtesy of FIP Industriale and R. Vetturini) (Clemente and Martelli 2018)

Therefore, it represents an uncommon example of eclectic, fantastic, grotesque architecture. A traditional strengthening intervention, which respected its historical value and guaranteed a suitable safety level, was not possible in practice, so it was decided to use seismic isolation (structural design by R. Vetturini). The executive phases were the following. The superstructure was first consolidated and protected. Then, two sub-foundations were built, one above the other and the devices were places in between (Fig. 24). The upper one consisted in continuous concrete beams, while the lower one was composed by plinths, which were successively connected by means of a reinforced concrete plate. The isolators were first connected to the upper sub-foundation, where suitable steel elements had been previously positioned. Then jacks were positioned under them, which allowed loading the isolators, by means of injection of epoxy resin. A steel floor above the isolation interface guaranteed the rigid connection, but also formed a new floor. Finally, 25 HDRBs (diameter = 450 mm, total rubber thickness = 126 mm, damping ratio = 13%) and 23 SDs were used, yielding a fundamental period of 2.35 s and a maximum displacement of 300 mm. The so-called “Emiciclo building” in L′Aquila (Figure 15), which is the main branch of the Abruzzo Region Council (Fig. 25, structural design by R. Vetturini, G. Di Marco, L. Zazzara, W. Cecchini and A. Bottone, consultancy by A. Borri); the building was seismically isolated by means of 61 HDRBs and 47 SDs, which allow a maximum displacement if 300 mm.

Figure 15. Emiciclo building at l′Aquila (courtesy of Somma and R. Vetturini) (Clemente and Martelli 2018)

A large use of the base isolation system on RC building, as described above, has been realized in the reconstruction process of L'Aquila where 59 building are retrofitted using this solution.

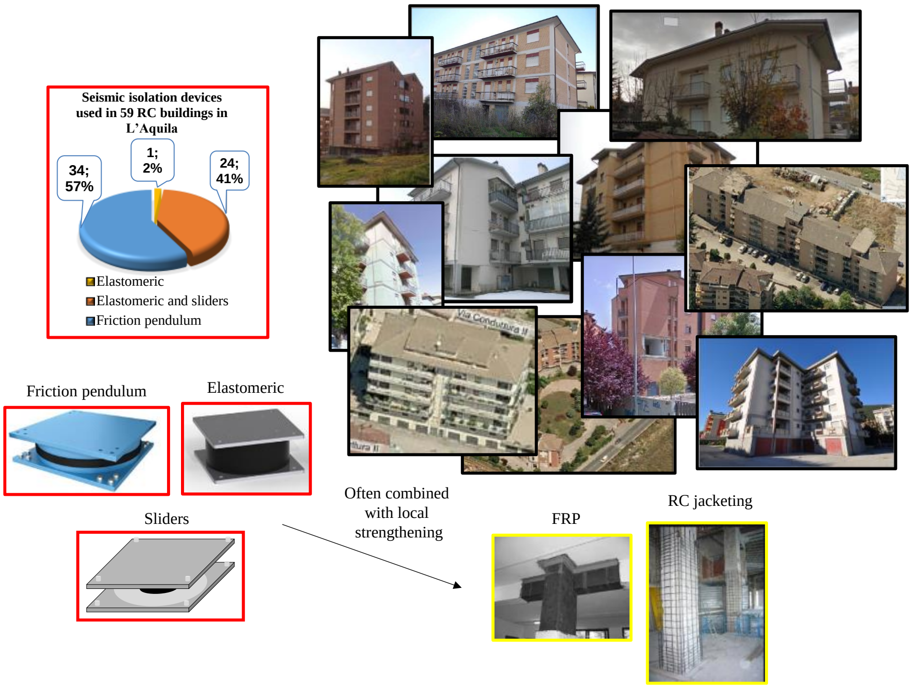

Figure 16. The use of base isolation for existing RC buildings in the L'Aquila reconstruction process

Different types of isolation devices and types of installation has been performed. In particular, the FPS were used in 57% of the structures, the elastomeric bearings combined with sliders in 41% and the elastomeric bearing alone in 2% of the buildings. While in 39% of the structure the cut of column the base has been used, in 37% the cut of the column at the top, in 14% the SOLES technique and in 10% the cut of the column at midspan (Figure 16).

Details on the 59 base isolated RC buildings are reported in Table 1 in terms of the seismic performance (PGA_C/PGA_D) of the as-built and retrofitted building. PGA_D is the design peak ground acceleration, PGA, at the building site according to the hazard map and affected by the site amplification factor (Infrastrutture and Trasporti 2018), while PGA_C is the capacity PGA defined as that required to cause the building to attain the life safety limit state, LSLS. The PGA_C can be conventionally evaluated according to the standard design methodology that accounts for the attainment of the life safety limit state (LSLS, TR = 475 years, where TR indicates the return period) considering both brittle and ductile failure modes. The adopted seismic strengthening solution and the total cost of the intervention are also reported in Table 1. The latter is expressed as a percentage of the total reconstruction cost, %RC (i.e. dividing by 1200 €/m^2 according to Di Ludovico et al. 2017). It was estimated by the practitioners engaged by the owner based on the Abruzzo region price list (STR. LL.PP. 2017) and then checked and approved by a government technical committee. This cost normalization allows to establish the convenience of the retrofitting instead of demolition and reconstruction. These data show that the base isolation systems are often combined with other strengthening techniques (i.e. 75% of buildings). The latter are usually used for the local strengthening of deficient RC members in order to avoid premature shear failures (Di Ludovico et al. 2017)

The use of base isolation as retrofit technique combined with other local strengthening solution considerably improves the seismic performance of existing buildings resulting in an increase of the safety index PGA_C/PGA_D of about the 56% on average, moving from 0.24 to 0.80.

However, this strengthening solution has a high initial cost of the installation, of about 42% of the total reconstruction cost. Furthermore, the retrofit total cost resulted significantly higher than the mean cost (about 24%, Di Ludovico

Table 1. Details of 59 buildings retrofitted by means of base isolation in L'Aquila

Building	PGA_C/PGA_D As-Built	Strengthening Intervention	PGA_C/PGA_D Strengthened	Cost of intervention (%RC)*
1	0.10	Base Isolation	1.00	43.3
2	0.10	Base Isolation	0.70	22.8
3	0.10	Base Isolation	0.70	34.1
4	0.14	Base Isolation	1.00	35.8
5	0.15	Base Isolation	0.60	40.2
6	0.17	Base Isolation	0.76	36.5
7	0.18	Base Isolation	1.00	21.6
8	0.19	Base Isolation	0.70	37.6
9	0.20	Base Isolation	1.15	45.1
10	0.21	Base Isolation	0.77	41.8
11	0.27	Base Isolation	0.62	46.8
12	0.30	Base Isolation	0.76	37.1
13	0.31	Base Isolation	0.63	51.3
14	0.31	Base Isolation	0.77	51.7
15	0.40	Base Isolation	1.00	44.5
16	0.08	Base Isolation+FRP	0.72	33.6
17	0.08	Base Isolation+FRP	0.60	48.1
18	0.10	Base Isolation+FRP	0.70	40.7
19	0.10	Base Isolation+FRP	0.76	44.8
20	0.15	Base Isolation+FRP	0.63	37.1
21	0.20	Base Isolation+FRP	0.74	49.6
22	0.21	Base Isolation+FRP	0.80	21.7
23	0.21	Base Isolation+FRP	0.80	33.3
24	0.23	Base Isolation+FRP	1.00	57.0
25	0.27	Base Isolation+FRP	1.00	34.5
26	0.27	Base Isolation+FRP	1.00	47.9
27	0.28	Base Isolation+FRP	0.80	42.7
28	0.30	Base Isolation+FRP	0.60	32.6
29	0.30	Base Isolation+FRP	0.80	24.4
30	0.30	Base Isolation+FRP	0.80	42.8
31	0.30	Base Isolation+FRP	0.80	40.2
32	0.30	Base Isolation+FRP	0.72	45.8
33	0.30	Base Isolation+FRP	0.77	36.8
34	0.30	Base Isolation+FRP	1.00	32.6
35	0.30	Base Isolation+FRP	0.80	37.2
36	0.30	Base Isolation+FRP	0.70	40.9
37	0.33	Base Isolation+FRP	0.80	38.3
38	0.16	Base Isolation+R.C Jacketing	0.60	48.5
39	0.30	Base Isolation+R.C Jacketing	1.00	49.6
40	0.30	Base Isolation+R.C Jacketing	1.00	41.4
41	0.12	Base Isolation+Steel Jacketing	0.62	35.7
42	0.15	Base Isolation+Steel Jacketing	0.80	45.7
43	0.30	Base Isolation+Steel Jacketing	0.80	49.2
44	0.34	Base Isolation+Steel Jacketing	0.80	43.3
45	0.15	Base Isolation+Stiffening Infills	0.60	34.6
46	0.30	Base Isolation+Stiffening Infills	0.60	42.6
47	0.30	Base Isolation+Stiffening Infills	0.80	47.2
48	0.30	Base Isolation+Stiffening Infills	1.00	41.9
49	0.30	Base Isolation+Steel Braces	1.00	45.1
50	0.11	Base Isolation+FRP+Steel Braces	0.61	44.3
51	0.22	Base Isolation+FRP+Steel Braces	1.00	57.9
52	0.33	Base Isolation+FRP+Steel Braces	0.80	42.9
53	0.33	Base Isolation+FRP+Steel Braces	0.80	44.6
54	0.10	Base Isolation+FRP+Steel Jacketing	0.60	44.0
55	0.10	Base Isolation+FRP+Steel Jacketing	0.60	65.7
56	0.27	Base Isolation+FRP+Steel Jacketing	0.60	57.7
57	0.30	Base Isolation+FRP+Steel Jacketing	0.80	49.5
58	0.42	Base Isolation+FRP+Steel Jacketing	0.75	40.8
59	0.38	Base Isolation+FRP+Stiffening Infills	0.80	38.1

*calculated dividing the cost of intervention by 1200 €/m^2

et al. 2017) observed in other buildings where different strengthening interventions were used.

As reported in (Del Vecchio et al. 2021) the FRP for a global strategy solution has a cost equal to 281 €/m^2, lower than those associated to the base isolation (equal to 504.0 €/m^2). The strengthening strategies which employ FRPs in some forms are those adopted the most to conduct effective and fast repairs and improve seismic performance. Usually, the improvement of seismic performance doesn't achieve the value of 1.00, where the existing buildings would have the performance on a newly designed, in fact as reported in (Del Vecchio et al. 2021) the buildings retrofitted with FRP improve their safety index between 0.6 and 0.9. Most of them achieved the lower bound of 0.6.

The high initial cost of the base isolation system strongly discourages investment in this technique as a retrofit solution when compared to a faster and less expensive alternative such as FRP. A methodology based on more detailed cost-benefit analyses using refined loss assessment frameworks has been proposed to define an objective parameter that can guide the designer in choosing the best retrofit solution for the structure under study.

The choice of retrofitting measures on an existing building raises several issues that can lead to completely different solutions, for example:

- The geometry
- Properties of the materials resistance
- Safety of the structure in relation to the axial load
- Distribution of non-structural components and their geometric configuration
- Seismic details

The evaluation of all these aspects could identify the base isolation as a retrofit solution better than the more traditional ones, if some conditions regarding the resistance and the geometry of the structure are met. It is important to emphasize that, for a fixed structure, the earthquake protection provided by the isolation system depends on the ability of the system to reduce the acceleration and therefore the inertial force on the structure. A structure with adequate resistance to horizontal action, significantly less than that required for a fixed structure, might be able to withstand a strong earthquake with elastic behavior. The critical aspect of the existing structures is the inadequacy of the seismic details and the control of the damage mechanisms, that is, the inability to sustain high inelastic deformations. The presence of structural and non-structural irregularities in plan or elevation, which usually involve concentration of inelastic loading on a few structural elements that are incapable of withstanding it, poses a minor hazard to an isolated structure due to its significant elastic behavior. The design procedure of the isolation system for an existing building could proceed as shown in Figure 17.

The first three steps involve the process necessary to define the lateral stiffness of the structure and the retrofit measure, that is, the state of knowledge. They include the knowledge of the structure: its geometry (structure, foundation, dimensions of the structural elements) and the material and details (mechanical properties of the material, structural details of the reinforcement) and the definition of the load (use destination, axial load, hazard, soil category).

The fourth step includes the seismic assessment of the structure in terms of resistance and deformability, related to the condition of LSLS and DLS of an isolated structure. This step aims to define the characteristics of the isolation system for the following fifth step. It is possible to use an approximate procedure in this stage.

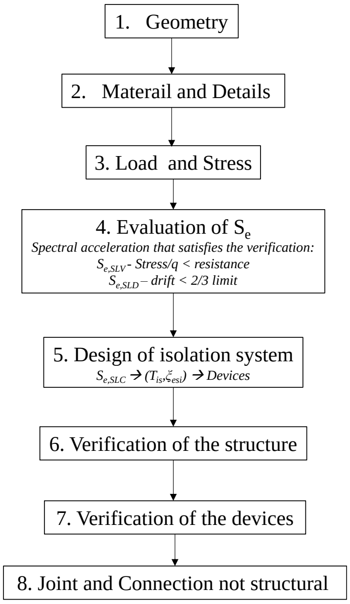

Figure 17. Procedure for the design of base isolation system for the seismic retrofittingof existing buildings (Dolce et al. 2004)

The performance of the structure is expressed in terms of spectral acceleration S_e, i.e. the acceleration suffered by the isolated structural mass (i.e. the superstructure mass).

The calculation is performed with respect to the fixed-base configuration, for example, using nonlinear static analysis, or alternatively using linear static analysis, which includes checking for different stress levels, until the compatible S_e is determined.

Design at LSLS is done by defining the capacity curve (e.g., using method N2, Fajafar) to evaluate the value of S_e that satisfies all structural elements.

The check at DLS is done by comparing the interstorey drift obtained with the analysis of acceleration S_e (DLS) and the 2/3 of the limit values of the rule.

If this check is not satisfactory S_e must be reduced in proportion to the ratio between the limit value of the rule and the maximum value of the interstorey drift that does not satisfy the check.

If the value that allows the condition to be met at LSLS and DLS is too low and it is impossible to achieve the spectral acceleration with the design of the isolation system in relation to the hazard and the characteristics of the foundation, reinforcement or modification of the structure would have to be made to increase the value of the S_e. If a few elements do not meet the verification, local reinforcement must be provided, or these elements must be considered as "secondary" structural elements.

The fifth step refers to the design of the isolation system (Figure 18). The design is characterized by the identification of the pair period-damping (T_{is},ξ_{esi}) that allows to obtain, on the elastic spectrum at LSLS and respecting the typical interval ($2 \leq T_{is} \leq 4$ sec and $10\% \leq \xi_{es} \leq 20\%$), the spectral acceleration S_e defined before. The designer's sensitivity pushes him to choose the best one between the different pairs (T_{is},ξ_{esi}).

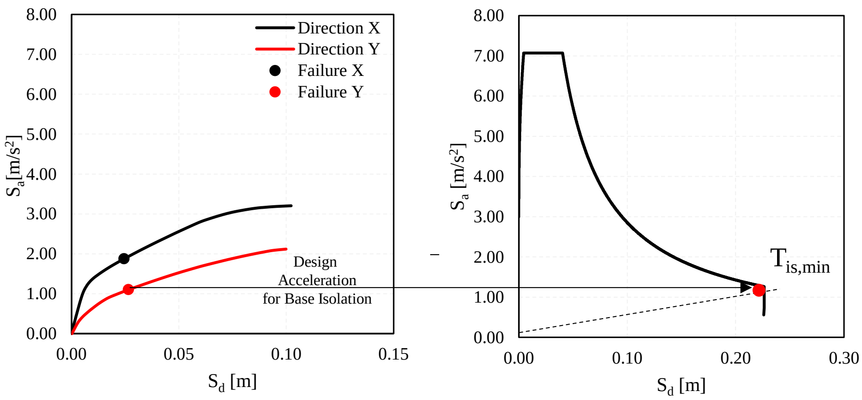

Figure 18. Identification of the minimum period for the base isolated configuration

The sixth and seventh steps are required because the design of the system is based on a nonlinear static analysis. It is possible to perform the test with a linear static analysis if the structure and the base isolation system meet the code requirements, reported in NTC 2018 (7.10.5.3.1):

- The isolation system can be modelled as linear
- The equivalent period T_{is} of the isolated structure is between $3T_{bf}$ and 3,0s, where T_{bf} is the period of the superstructure assumed fixed based
- The vertical stiffness of the base isolation system K_v is almost 800 times higher than the equivalent horizontal stiffness of the base isolation system K_{esi}

- The period in vertical direction, estimated as $T_V = 2\pi\sqrt{M/K_V}$ is lower than 0.1s
- No devices show tensile due to the combination of seismic and vertical action

If these requirements are not met, a dynamic linear or nonlinear analysis must be performed in accordance with the characteristics of the base isolation system.

The eighth step refers to the verification of the design displacements of the joints and non-structural connections between the superstructure and the adjacent fixed parts (substructure, soil, adjacent structure).

2.3 Isolation Devices

Different devices are nowadays available on the market to be used in the base isolation of buildings and bridges. An isolation system must be characterized by:

- Capacity to sustain axial load on static and seismic conditions
- High deformability (or low resistance) in the horizontal direction under seismic action
- Suitable dissipative energy
- Suitable resistance to horizontal non-seismic loads (wind, traffic)

An additional requirement could be the recentering capacity in order to avoid residual displacement after a seismic event. Other characteristics such as: durability, ease of installation, moderate cost, limited size may influence the choice of the device.

An isolation system consists of a number of devices that together provide the desired response. The devices may all be of the same type or different (usually no more than two types) and they are arranged to connect the substructure to the superstructure at the isolation level. Various devices and isolation systems have been developed over the last 20 years (Buckle and Mayes 1990; Housner et al. 1997).

The components of an isolation system can be divided into isolators and auxiliary devices. The isolators are the devices that carry the axial load. They are load-bearing devices, generally bidirectional, with high stiffness in the vertical direction and high deformability (or low resistance) in the horizontal direction. This function may or may not be related to energy dissipation, lateral restraint under horizontal non-seismic loading (wind, etc.), recentering of the structure after an earthquake. Nowadays, the isolation devices used can be divided into two categories: a) elastomeric devices with steel shims, based on the high deformability of rubber, b) sliding devices, based on the low frictional resistance between flat or curved surfaces made of different treated materials. Auxiliary devices have the function of energy dissipation and/or recentering of the system and/or lateral restraint in case of horizontal non-seismic loading (wind, etc.). They can be:

- Devices with non-linear behavior, independent of the deformation rate, based on the hysteresis of some metals, such as steel and lead, on the friction between treated surfaces, or on the superelastic property of a particular metal alloy, such as the shape memory alloy (Duerig et al. 1990), used to obtain an optimal restoring capacity.
- Device with viscous behavior depending on the deformation rate, based on the extrusion of a highly viscous fluid into the interior of a cylinder with piston provided with a hole of suitable size
- Device with linear or quasi-linear behavior, similar to a viscoelastic one, based on the shear deformation of certain polymers

An isolation system may be composed only of elastomeric devices, possibly with elastomers having high dissipation or containing an insert of dissipative materials (i.e. lead, viscous fluid), or only of sliding devices (or rollers) containing dissipative and/or re-centering functions for implicit properties or for the presence of an element capable of performing these functions, or of a suitable combination of isolators and auxiliary devices, the latter with dissipative, re-centering and/or forcing functions.

2.3.1 Rubber Bearing

The isolators made of reinforced rubber are the main components of the elastomeric isolation system. They are characterized by an alternance of rubber layers, usually with a thickness of 5-20 mm, and steel shims, with a thickness of 2-3 mm. The latter exert a limiting effect on the elastomer by limiting the vertical deformability (to limit the sinking of the device under operating load to 1-3 mm), increasing the axial capacity under axial load and not significantly affecting the shear deformation of the device in the horizontal direction.

Due to the fatigue strength and elasticity of the rubber, the elastomeric devices are capable of meeting most of the isolation system requirements. By using a special additive compound or insert that allows the dissipation capacity to be increased and the stiffness to be changed favorably, different variations can be achieved to realize an isolation system consisting only of elastomers without auxiliary devices.

Some problems are common to all elastomeric devices: i) the stability of the device under shear and compression, ii) the increase in deformation under constant load on the rubber, iii) the effectiveness of the rubber-steel bond in the presence of large displacements, iv) the variation of the mechanical behavior of the elastomer as a function of temperature, frequency and ageing.

One of the common features of all rubber isolators is the reduction in vertical capacity with increasing horizontal displacement, both in shear deformation and reduction in effective shape area (Kelly 2001).

Nowadays, there are mainly three different elastomeric devices available in the market (Figure 19a,b), grouped according to the dissipative property and the presence of an insert: i) with reinforced rubber at low damping, ii) with reinforced rubber at high damping, iii) with reinforced rubber with lead core or dissipation material. The elastomeric device with reinforced rubber at low damping (Kelly and Quiroz 1992; Taylor et al. 1992) shows essentially elastic behavior (stiffness almost constant) with increasing deformation and a very low degree of damping, about 2-4%. It is simple to implement, easy to model, and the behavior is essentially independent of frequency and insensitive to temperature. In contrast, an isolation system with these types of isolators, usually requires appropriate auxiliary devices to increase the dissipation capacity and to avoid high displacement of the structure due to horizontal effects (wind, etc.).

Elastomeric devices with reinforced rubber with high damping (Derham et al. 1985; Kelly 1991) are obtained by adding suitable additives (resin, oil, etc.) to the rubber compound, which make it possible to obtain damping values between 10% and 20% with a shear deformation of 100%. Energy dissipation is partially viscous, i.e. quadratic with displacement, and partially hysteretic, i.e. linear with displacement (Naeim and Kelly 1999). This means that the mechanical behavior depends on the frequency and there is also a non-negligible influence of temperature

Both the shear modulus and the damping depend on the applied shear deformation, γ. For a small deformation (γ <10%) the shear modulus is quite high, 5-10 times higher than for deformation under seismic condition (γ =100-150%). If you increase these values of deformation, the shear modulus increases again and defines a significant hardening of the hysteretic response of the isolators.

a) b)

Figure 19. Rubber bearing: a) Low rubber bearing or high damping rubber bearing, b) lead rubber bearing

The elastomeric device with high damping capacity can realize a complete isolation system without auxiliary devices. The high damping capacity guarantees an adequate control of the displacement caused by the seismic event. The high initial stiffness limits the displacements under service horizontal load. The quasi-elastic behavior guarantees an optimal recentering capacity. In addition, the hardening of the rubber to a deformation higher than that of the design earthquake can be useful to limit the displacements during particular seismic events in terms of intensity or frequency.

The mechanical properties of the device at high damping vary significantly during the first few cycles due to *"scragging"* (Morgan and Whittaker 2001), which corresponds to a change in the molecular structure of the rubber. After the first 2-3 cycles, the mechanical behavior is stable and repeats at deformations lower than that of *"scragging"*. During unloading, a partial recovery of the initial properties can be observed. The reinforced rubber and lead core elastomeric device (Robinson 1982; Kelly 1992) uses one or more cylindrical inserts of lead located in certain vertical internal spaces in the reinforced rubber isolators. They provide the necessary stiffness to the horizontal non-seismic load (wind, braking force in the bridge, etc.) and at the same time a high dissipation capacity during seismic events. The mechanical behavior of these devices is a combination of the elastic behavior of the elastomeric support at low damping and the elastic-plastic deformation of the lead core, which is subject to shear deformation. The shear deformation of the lead core is provided by the confining action of the steel plates of the rubber device. The viscous equivalent damping is usually between 15% and 30%, depending on the size of the lead insert and the imposed displacement (Naeim and Kelly 1999).

The secant stiffness and the equivalent viscous damping are related to the number of cycles applied. Both energy dissipation and stiffness decrease with increasing number of cycles. After 10-15 cycles, stabilization is observed, which is comparable to the phenomenon of *"scragging"* in rubber, but with more pronounced effects. The cause of this phenomenon is the overheating of the lead core due to repeated cycles with high frequency (Kelly 2001). Reducing stiffness and damping to increase cycling is related to the size of the rubber device and lead core.

A high dissipative capacity, with a higher viscous contribution and a more stable behavior, can be obtained by using a core made of polymeric material with high viscosity, such as the devices proposed by (Dolce et al. 2003a).
A more recent development is the BRBs: Ball Rubber Bearings (Ozkaya et al. 2011). They have the same geometry as LRBs but have steel balls in the inner core instead of lead. The equivalent viscous damping is usually between 15% and 35 as for the LRB due to the size of the central hole and the imposed displacement (Ozkaya et al. 2011). In the development of the BRB, the aim was to develop a high-performance device at a moderate cost. The steel balls used inside the core are made of low carbon steel rather than stainless steel. Their durability is ensured by the steel plates glued to the rubber layer, which protect them from environmental influences.

2.3.2 Slider Bearing

Sliding devices may be unidirectional or bidirectional, allowing displacement in one direction or in all directions of the horizontal plane, respectively. The first ones are used in isolation systems for bridges that have different behavior in the two directions, and usually require an isolation system that is effective in one direction (often longitudinal). In buildings where isotropic behavior (on the horizontal plane) of the isolation system is desired, multidirectional devices are preferred. The latter are characterized by internal sliding surfaces with different diameters that slide on each other and are made of a special material that develops low frictional resistance. The most commonly used sliding surfaces, widely used in bridge technology, are made of stainless steel and PTFE (Teflon) or other polymeric materials that have been developed recently. The dynamic friction coefficient for PTFE ranges from 6% to 18% and decreases to 1-3% when the surfaces are lubricated (Tyler 1977; Constantinou et al. 1988; Dolce et al. 2003b), depending on i) contact pressure, ii) sliding speed, iii) temperature (Constantinou et al. 1987; Bondonet and Filiatrault 1997). The number of cycles, or more precisely the total distance covered by the surfaces during

relative sliding, affects the dynamic coefficient of friction in a non-negligible way due to the deterioration of the sliding surface (Hwang et al. 1990).
The coefficient of friction has the following properties:

- Increases rapidly to increase velocity, remaining constant during the velocity interval usually reached during the seismic event.
- Decreases linearly as the contact pressure increases
- Decreases with increasing temperature
- Affected by the lubrication of the contact surface

Sliders on steel PTFE are never used as unique components of the isolation system unless they have elements that increase initial stiffness and dissipation capability and/or provide recentering capacity. As a rule, the energy dissipation due to friction of the slider in steel PTFE is not used because the coefficient of friction varies excessively over time and under different environmental conditions (temperature, humidity) and during cleaning. For this reason, lubricated isolators are used, whose function is only to carry the axial load, leaving the horizontal displacement free. In this case, steel PTFE sliders, lubricated on the plane surface, must be combined with auxiliary devices that have a recentering and/or dissipative capacity. Elastomeric devices (Naeim and Kelly 1999) are often used as both auxiliary devices and isolators, creating a hybrid system combining the elastomeric devices and the sliding devices. This configuration offers both technically and economically interesting advantages. It makes it possible to obtain a low stiffness (high period) system that significantly reduces the seismic impact, even if the structural mass of each isolator is limited, as well as a suitable recentering capacity. The main problem lies in the different vertical deformability both at the moment and over time (creep), which can lead to different vertical displacements for the different types of devices, both under static and seismic conditions. In this case, it is very important to limit the difference as much as possible and to evaluate the consequences of the different displacements for the structure.

Among the auxiliary devices to complete an isolation system based on sliding devices, there are the devices with a nonlinear behavior, which is strongly dissipative and based on the yielding of the steel, using elements of suitable shape deformed by bending and/or torsion, and the devices based on lead elements stressed in shear, or those in which the lead is extruded through a piston into a cylinder (*"Lead Extrusion Damper"*) (Hanson 1993; Soong and Dargush 1997; Constantinou et al. 1998).

The only sliding devices which have the power of recentration and dissipation without the combination of other elements are those with curved surfaces. The first and best known is the *"Friction Pendulum System" (FPS)* (Zayas et al. 1987; Al-Hussaini et al. 1994; Calvi and Calvi 2018), in which the recentering capacity is due to the use of spherical, non-lubricated sliding surfaces, which thus have the ability to dissipate energy. The radius of curvature of this spherical surface is related to the equivalent stiffness of the device and thus to the base period of the structure. The sliding devices with curved surface allow the realization of an isolation system with a period independent of the mass. Since the stiffness is proportional to the weight, the center of stiffness of the isolation system coincides with the projection of the center of mass, reducing the possibility of rotation of the system about a vertical axis. If we disregard friction, the behavior of these devices is similar to that of a pendulum, where the period depends only on the cable length, is equal to the radius of curvature of the spherical sliding cap and is independent of the mass.

Nowadays, two types of sliding devices are available on the market: one with one sliding surface (Figure 20a) and another with two sliding surfaces (Figure 20b). In the latter case, the sliding surfaces are opposite and contain an internal space. This makes it possible to limit the size of the device to the maximum movement, since the movement is divided between the two caps.

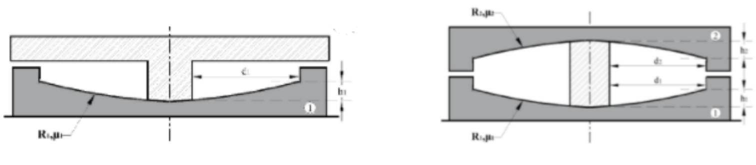

a) b)

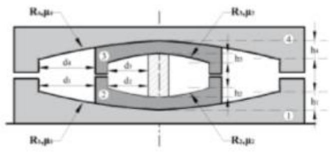

c)

Figure 20. Sliding bearing: a) Friction Pendulum, b) Double Concave Friction Pendulum, c) Triple Concave Friction Pendulum

There are some variants of the sliding pendulum available on the market that have different characteristics from those described, but they are very complex (Calvi and Ruggiero 2016; Timsina and Calvi 2021). One of them is the Triple Friction Pendulum (Figure 20c) (Fenz and Constantinou 2008; Fadi and Constantinou 2009), in which the curvature and the friction of the two sliding surfaces can be varied in such a way that the response of the device is optimally tuned to the expected seismic action In addition, the new devices use a sliding material developed ad hoc to improve the temporal constancy of the frictional properties compared to PTFE.

The main problems of the sliding pendulum are i) the large plane dimensions (while the total thickness is contained respect the elastomeric devices), which can be reduced by using a double sliding surface (Furinghetti et al. 2021), ii) the vertical movement associated with the horizontal displacements that can have parasitic effects on the structure, iii) the reliability in time of friction between the contact surfaces that must be protected. An important issue is the need to endow the isolation system with the ability to recentering. Without this capability, the isolation system will show a deviation in a certain direction and a high residual displacement at the end of the seismic event. This phenomenon may be exacerbated during a high intensity earthquake near the seismic source (*"Near Fault"*). The problem is mainly related to the possibility of using the structure after the event (high residual displacements could be incompatible with the conditions of use) and ensuring safety during the subsequent earthquakes (*"Aftershocks"*). For this reason, many codes accept the use of isolation system without recentering capacity, but allowing for a displacement higher than the design maximum displacement of the isolation system to check joints, plants, etc. The problem of displacement of the structure to its original position does not show any particular difficulty in solving it, if in the design it is possible to take into account contrasting elements to push the structure through a bushing placed horizontally, possibly disconnecting auxiliary devices to limit the force required for the displacement to the only frictional reaction in the sliding devices.

CHAPTER 3 - SEISMIC PERFORMANCE ASSESSMENT OF BASE ISOLATED REINFORCED CONCRETE STRUCTURE

Although the base isolation is becoming popular in the seismic retrofit of existing buildings, especially when high performances would be achieved, the design of a base isolation system is still challenging. Indeed, an efficient design of the base isolation system for existing buildings should aim at reducing the acceleration and, in turn, the seismic forces transmitted to the superstructure as much as possible. In the common design practice of new buildings, it is frequent the use of nonlinear dynamic analysis where the superstructure is modelled elastic while all the non-linearities are concentrated in the base isolation system. This assumption is largely demonstrated for the newly designed base-isolated buildings designed according to modern standards. By contrast, for existing buildings designed to sustain gravity loads or low-to-moderate seismic action the assumption of a linear superstructure could be not realistic also when an efficient base-isolation system is used as seismic retrofit solution. The reduced cross-section dimensions of the RC members and the lack of proper seismic details doesn’t allow to the superstructure to remain elastic, and more sophisticated nonlinear analyses capable to reproduce the nonlinear response of the superstructure and the interaction with infills are required. Indeed, the presence of stiff infills, as commonly found in RC buildings in the Mediterranea area, may significantly change the seismic response. They commonly increase the lateral stiffness of the superstructure resulting in a reduction of the lateral displacement. On the other hand, the infills attract additional force on the structure commonly leading to the shear failure at the top end of the columns. Furthermore, hollow clay brick infills commonly have a very brittle response, often showing significant damage after a seismic event. Thus, the study of the response of base isolated existing RC building considering a refined estimation of the EAL may not neglect the presence of the infills, their damage and the related losses.

To this end, a reliable assessment the response of base isolated building in terms of damage reduction to structural and non-structural components as well as of the EAL should be performed by using a proper framework capable of combining the structural analysis, hazard analysis, damage analysis and loss analysis and the related uncertainties.

3.1 Performance Based Earthquake Engineering (PBEE)

The aim of the seismic engineering is to design and build better and more economical. Nowadays it is widely acknowledged that seismic design considers explicit multiple performance objectives. There is a minimum level of protection requested by the society to safeguard adequately against various types of collapse or falling hazards that endanger the human lives. The collapse prevention is one of main objectives expressed by the seismic code that in such way are performance based. The modern approach to the seismic design pushes the use of a more refined performance-based approach as the PBEE (Performance Based Earthquake Engineering). The PBEE is based on the premise that the performance can be predicted and evaluated with quantifiable confidence and implies design, evaluation, construction and monitoring the functions and maintenance of engineered facilities whose performance under common and extreme loads responds to the diverse needs and objectives of owners-users and society.

When approaching a structure with the PBEE, one can evaluate its seismic behavior in terms of safety, but also in terms of damage and resulting losses. The evaluation is done in terms of global response and not localized to the strength capacity, which refers only to a structural performance.

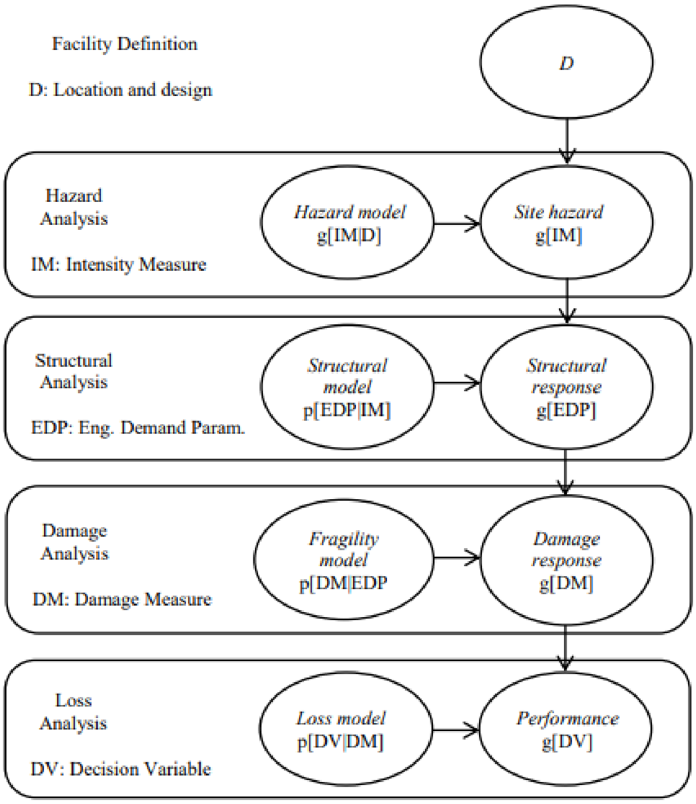

Figure 21. PBEE Methodology(Porter 2003)

The most commonly used PBEE approach for the loss-assessment analysis is the "PEER methodology" developed by the Pacific Earthquake Engineering Research (Keith Alan Porter, 2003). The main advantage of this approach is that it also incorporates the uncertainty resulting from the estimation of damage to a construction and the associated repair costs. This methodology is wholly probabilistic and consists of the numerical integration of all the conditional probabilities propagating the uncertainties from one level of analysis to the next (Goulet et al. 2007).

Figure 21 schematically shows the PEER methodology, which can be summarized in four stages: hazard analysis, structural analysis, damage analysis, and loss analysis. Their outputs are, respectively, the intensity measure (IM), the engineering demand parameters (EDPs), the damage measure (DM), and the decision variable (DV). The expression p[X|Y] refers to the probability density of X conditioned on knowledge of Y, and g[X|Y] refers to the occurrence frequency of X given Y (Porter 2003).

Consequently, the PEER framework equation is:

$$g[DV|D] = \iiint p[DV|DM,D]p[DM|EDP|D]p[EDP|IM,D]\, g[IM|D]dIMdEDPdDM \quad (1)$$

where g[DV|D] is the mean annual probability that the DV exceeds a specific value given a facility, p[DV|DM] is the conditional probability that the DV exceeds a specific value of the DM, p[DM|EDP,D] is the derivative (with respect to the DM) of the conditional probability that the DM exceeds a limit value given a value of the EDP, p[EDP|IM,D] is the derivative of the conditional probability that the EDP exceeds a limit value given a value of the earthquake IM, and g[IM|D] is the derivative of the seismic hazard curve given a site location. The hazard analysis defines the intensity measure (IM) through the selection of a ground motion set depending on the location and others parameter of the structure (i.e destination). The result is the hazard curve that describes the annual frequency with which seismic excitation is estimated to exceed various levels. Excitation is parameterized via an intensity measure (IM) such as the spectral acceleration at the fundamental period of the structure, $Sa(T_1)$. The structural analysis involves the construction of a model in order to estimate, usually through non-linear time histories analysis, the engineering demand parameters (EDPs) conditioned to the seismic excitation (EDPs|IM). EDPs can include internal member forces or local or global deformations, including ground failure. The damage analysis defined the damage suffered by each component of the structure through the use of fragility function that provide the probability to damage conditioned to the EDPs (DM|EDPs). The last analysis is the definition of the performance condition on damage and design (DV|DM, D) through the estimation of a decision variable (i.e dollars, deaths, downtime, or other metrics).

In the modern approach with the PBEE, one of the most commonly used DV (decision variables) is the expected annual losses, EALs, expressed with a monetary unit (e.g. $ or €). In Italy, the transition of the engineering design philosophy to this novel approach is pushed by the new guidelines for seismic risk classification of constructions (Cosenza et al. 2018) based on the evaluation of the seismic capacity through the definition of their EALs. This approach highlights the direction taken in the design/retrofit of civil constructions. The parameters that influence the decisions are not only safety, which always comes first, but also economic benefits in related to the reduction of expected losses.

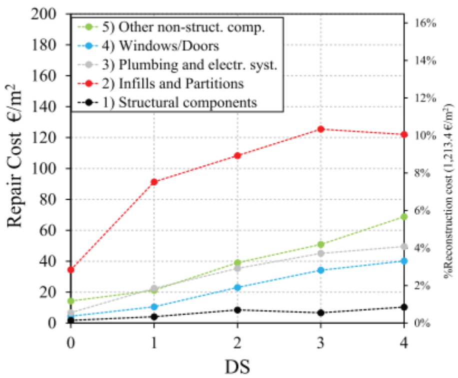

Figure 22. Repair costs as a function of the building damage state (DS) at the component category level (Del Vecchio et al. 2020)

The losses, as expressed in the above procedure, are considered by using fragility and consequence functions. These curves are developed for each component of the structure, such as infill, beam-column joints, partitions, raised access floor, lightning, water pipes, etc. They are mainly divided into acceleration and drift sensitive component, and each of them contributes with a certain value to the losses.

As reported in (Del Vecchio et al. 2020) and shown in the Figure 22, most of the repair costs concerns the infills and partitions walls. Infills play a critical role in the seismic behavior of the structure, as demonstrated by recent seismic events, but their contribution is commonly neglected in the numerical models used in the design practice.

3.2 The role of the infills in the seismic performance assessment

The infills are non-structural elements usually made of hollow clay-bricks (with a variety of thickness depending on the climatic zone) and mortar. The infill panels may have single or double leaf. Usually, the infills with single leaf have a thickness of 30 /35 cm, while those with double facing have a thickness of 8 cm for one facing and 12 cm for the other facing, with a gap in between.

The infill walls are characterized by various uncertainties in terms of resistance and stiffness, due to the different construction methods. In general, they were designed without effective connection with the surrounding RC frame, which led to their neglect in the seismic model and only the mass and weight were considered.

The bare model, which neglects the contribution of infill to stiffness and resistance, was considered conservative. However, recent seismic events have shown that unreinforced masonry (URM) infill walls, which are usually considered as non-structural elements, have a major impact on the seismic performance of the structure (Aiello et al. 2017). In recent years, there has been an increasing interest in this topic, because the infill walls indeed contribute to the lateral resistance and stiffness of the structure (Ruggieri et al. 2020) (Figure 23) and modify the dynamic properties, leading to a lower period of vibration (Ricci et al. 2011b), and thus, to a lower displacement during a seismic event.

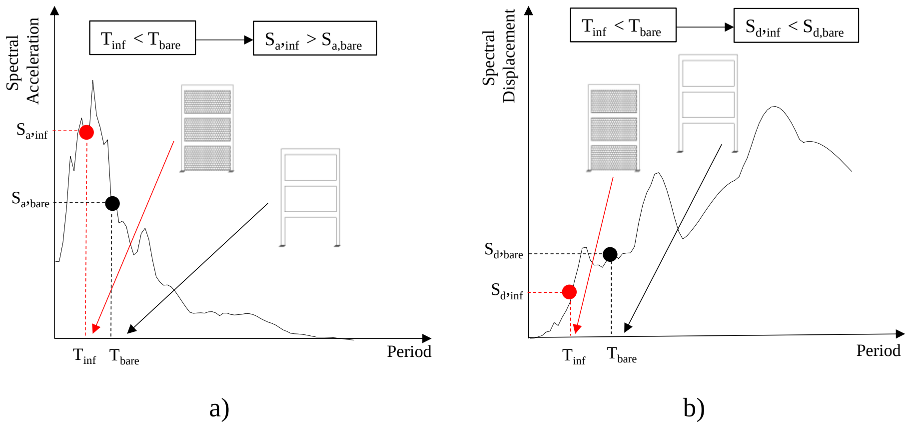

Figure 23. The effect of the infills on the seismic response of a structure in terms of a) accelerations, b) displacement

Moreover, the presence of infill reduces the deformability of the structural elements and provides an opportunity to neglect the second-order (P-Δ) effects. Although considering the bare model could be considered conservative, seismic events have shown that most buildings designed for gravity loads have seismic capacity due to the infill panels dissipating energy through the damage with X-cracks due to a cyclic loading (Figure 24) (Ricci et al. 2011a).

Figure 24. Infill's cracks for cyclic loads

On the other hand, infills may have adverse effects on the structure due to their interaction with structural elements (so-called "frame-infill interaction"). The additional mass of the infills, combined with the reduction of the vibration period, may exert additional inertial forces on the structure. The infills are characterized by a brittle behavior with a high softening that affects the response in the non-elastic field. Once the infills fail, the collapse is brittle and occurs almost instantaneously, so the seismic action previously absorbed by the infills will act on the columns; additional shear stress on the column could result in brittle failure. An example of brittle column failure is the openings in the infills that define "squat" columns (Figure 25).

Figure 25. Interaction columns and infills with opening

The irregular distribution of the infills in plan or in elevation, due to their high stiffness, may cause irregularities in the structure, worsening the behavior of the structure with respect to seismic actions. In the inelastic field, the absence of infill in some floors leads to a concentration of displacement demand in the weakest elements, resulting in local collapse. An example of this is the building on "Pilotis", where the recent seismic events have shown the soft-storey mechanism (Figure 26) in the floor where the infill walls are missing, while the rest of the building remains intact.

Figure 26. Soft-storey mechanism

The absence of infill in some parts of the floor plan results in the center of mass and the center of stiffness not coinciding, which results in a significant torsional

effect and pushes out the columns in the weak areas.
In addition, irregularities may occur during seismic event due to the separation between the infill columns and the RC frame.

Regarding seismic behavior, during a seismic event, infills are subjected to two types of actions: in-plane actions and out-of-plane actions. The in-plane action is parallel to the infill and the damage is proportional to the displacement, while the out-of-plane action is perpendicular to the infill and proportional to the acceleration. Thus, in the in-plane action, the infill walls at the ground level could be the most damaged because the displacements are usually higher, while in the out-of-plane action, the infill walls at the upper level could be the most damaged because the accelerations are usually higher. Due to the combination of actions, the infills in the middle floors are usually the most damaged (Figure 27).

Figure 27. Failure of the infills at medium floors

There are many studies in the literature on the behavior of infill. One of the most attributable works on the in-plane capacity of infills is that of (Panagiotakos and Fardis 1996), which is characterized by a trilinear model as shown in the Figure 28 and used in the next section of the work.

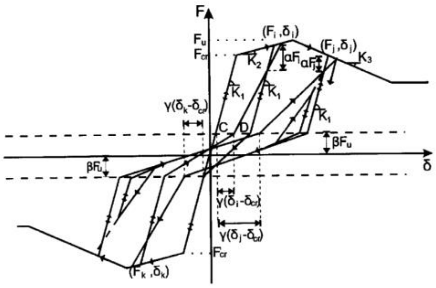

Figure 28. Cyclic behavior for infills (Panagiotakos and Fardis 1996)

In summary, neglecting the presence of infill and its contribution to the seismic response of structures can be both conservative and unconservative.

3.3 Selection of the case study

A preliminary study was conducted on the role of infill walls based on isolated existing buildings to clarify their influence on the mechanical model used to analyze the seismic performance of the structure. For this purpose, one of the 59 buildings (reported in Table 1) in L'Aquila was selected, which were retrofitted using base isolation, as described in the above section.
Several criteria were considered in the selection process in order to choose a building representative of the whole database.

Table 2. List of the selected building having design's details

Buildings	Yer of Construction	Floor Surface	ξ_{POST}	Installation Technique	C_1	C_2	C_3	C_4
1	82-'91	2347	0.76	Column at bottom	115.8	141.3	0.0	111.7
2	82-'91	293	0.8	Column at top	132.1	215.2	7.1	21.3
3	92-'01	673	0.63	Column at top	81.8	160.3	15.7	142.2
4	62-'71	434	1.14	SOLES	120.5	170.7	0.0	54.7
5	72-'81	369	1	Column at middle	109.1	71.7	52.5	236.5
6	82-'91	170	0.75	Column at bottom	177.6	104.0	27.1	84.4
7	62-'71	279	1	Column at bottom	85.1	124.9	105.8	84.2
8	82-'91	380	1	Column at middle	148.2	247.2	0.0	108.8
9	82-'91	308	0.6	SOLES	281.0	155.0	76.2	212.2
10	62-'71	455	0.79	Column at bottom	88.1	113.9	16.9	2.3
11	72-'81	450	0.79	Column at top	75.9	188.8	0.9	41.1

The main requirement was the ability to model the structure using a finite element program (e.g. SAP200, which was used in this work), as the first test was the availability of designs and details of the structure. Only 25 out of 59 buildings met this condition. In order to get a first insight into the influence of infill and to avoid further aspects, the selection focused on regular buildings in plan and elevation, which brought the number of suitable buildings to 11 (Table 2).

Table 3. List of the selected building satisfy ¾ requiremetns

Buildings	Yer of Construction	Floor Surface	ξ_{POST}	Installation Technique	C_1	C_2	C_3	C_4
2	82-'91	293	0.8	Column at top	132.1	215.2	7.1	21.3
4	62-'71	434	1.14	SOLES	120.5	170.7	0.0	54.7
5	72-'81	369	1	Column at middle	109.1	71.7	52.5	236.5
6	82-'91	170	0.75	Column at bottom	177.6	104.0	27.1	84.4
7	62-'71	279	1	Column at bottom	85.1	124.9	105.8	84.2
8	82-'91	380	1	Column at middle	148.2	247.2	0.0	108.8
10	62-'71	455	0.79	Column at bottom	88.1	113.9	16.9	2.3
11	72-'81	450	0.79	Column at top	75.9	188.8	0.9	41.1

After completing this preliminary selection, four parameters were selected to choose the case study building: the year of construction, the surface's floor, the safety index after retrofitting and the average cost. The buildings for which all of these criteria matched the mean of the entire database were selected and analyzed.

The mean value of the whole database for the year of construction until the nineties, for the floor area between 200 and 500 m^2 and for the safety index was 0.7-1. It follows that the buildings numbered 3, 1 and 9, as shown in Table 2, did not meet the requirements and were therefore excluded. This brought the number of suitable buildings to 8 (Table 3).

Table 4. List of the selected building satisfy all requirements

Buildings	Yer of Construction	Floor Surface	ξ_{POST}	Installation Technique	C_1	C_2	C_3	C_4
2	82-'91	293	0.8	Column at top	132.1	215.2	7.1	21.3
4	62-'71	434	1.14	SOLES	120.5	170.7	0.0	54.7

The cost of retrofitting the building was expressed in €/m^2 and divided into four contributions: C1, cost of base isolation, C2, cost of installation, C3, cost of further retrofit intervention, C4 cost of strengthening related to the retrofit process. A review showed that the only building with an appropriate value in terms of average cost was numbers 2 and 4 (Table 4). Finally, building number 4 was selected as case study.

3.4 Case study building

The selected case study building is depicted in Figure 29. It is located in L'Aquila, and it has a rectangular plan with dimensions 10.6 m x 27.5 m and a total height of 14.6 m. It is four floor buildings with an interstorey height of about 2.7 m, at the ground floor and 3.2 m at the upper levels. The last floor is a loft about 2.3 m height. The building is regular in plan and in the elevation. The structural system consists of RC moment resisting frames. The materials properties were identified by means of in-situ destructive and non-destructive testing. The resulting concrete compressive strength f_{cm}, is about 16.83 MPa while the yielding stress of steel, f_{ym} is about 308.9 MPa. The soil type was classified B according to NTC (2018).

a) b)

Figure 29. Case study building: a) building front view and b) plan view and moment resisting frames

The geometry of beams and columns change floor-to-floor. The cross-sections of the columns are 400x500 mm at the ground and first floor, 350x500 mm at the second floor and 350x450 mm at the third floor and loft space. The cross-sections of the beams are 350x600 mm for the external beams and 500x200 mm for the internal beams at first floor, 350x550 mm for the external beams and 500x200 mm for the internal beams at second floor, 350x550 mm for the external beams and 450x200 mm to the internal beams at third floor, 350x550 mm for the external beams and 450x200 mm to the internal beams at loft. At the staircase the sections of columns are 350x350 mm and 350x400 mm, while the sections of the beams are 300x500 mm, 200x500 mm, 300x200 mm and 400x 200 mm. The columns are reinforced with 8ϕ16 deformed steel longitudinal bars at the ground, first and second floor, while they have 8ϕ14 at the third floor. The stirrups are ϕ6/200 on columns and ϕ6/150 at beam ends.

Table 5. Reinforcement details of beam and columns

Floor	Columns		Beams (A1-A4, M1-M4, A1-M1, A4-M4)			Beams (B1-L4)		
	Long	Trans		Long	Trans		Long	Trans
I	6ϕ16	ϕ6/200	Top	5/7ϕ16	ϕ6/200	Top	5/7ϕ16	ϕ6/200
			Bottom	2/4ϕ16		Bottom	2/4ϕ16	
II	6 ϕ 16	ϕ6/170	Top	5/7ϕ16	ϕ6/200	Top	5/7ϕ16	ϕ6/200
			Bottom	2/4ϕ16		Bottom	2/4ϕ16	
III	6 ϕ 16	ϕ6/170	Top	5/7ϕ16	ϕ6/200	Top	5/7ϕ16	ϕ6/200
			Bottom	2/4ϕ16		Bottom	2/4ϕ16	
IV	6 ϕ 14	ϕ6/170	Top	5/7ϕ16	ϕ6/200	Top	5/7ϕ16	ϕ6/200
			Bottom	2/4ϕ16		Bottom	2/4ϕ16	

3.4.1 Numerical Modelling

A simple elastic linear model (Figure 30) is developed to define dynamic properties of the structure in the as-built (bare), bare isolated and isolated infilled configuration. The mass is calculated taking into account all the structure and non-structural components (i.e., beams, columns, slabs and infill walls) as well all the live loads. A quasi-permanent (QP) combination is used to combine the different weights. The total mass in the x, y and in the rotational plan is later assigned to a master joint located in the centroid of the mass distribution. For each plan a diaphragm constraint is adopted to simulate the stiffness of the slab in the horizontal direction.

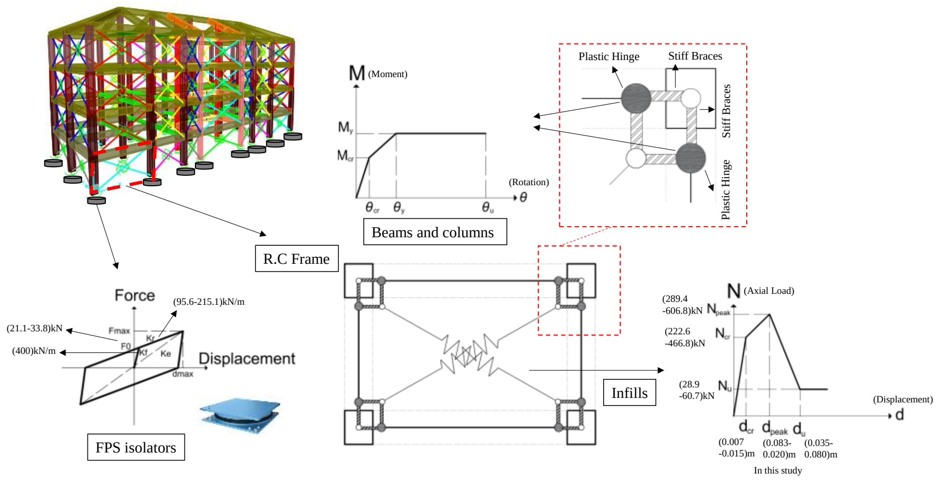

Figure 30. Numerical model of the case study building

The infills walls of the case study building are made with hollow-clay brick 200 mm thick. The mechanical properties used to characterize the infill strut are chosen according to available literature studies. In particular, the shear cracking strength τ_{cr} is set equal to 0.35 MPa (Colangelo 1999). The Young's modulus, E_{wh}, is calculated according to Colangelo (1999) and it is equal to 3188 MPa and, G_w, the shear modulus equal to 1574 MPa (Colangelo 1999). The infills were modelled through the behavior presented by Panagiatakos and Fardis (1996). This behavior is characterized by a three different stiffness (Figure 30), degrading with the increasing displacement demand. The initial stiffness K_1 (Panagiotakos and Fardis 1996) can be define as:

$$K_1 = \frac{G_w \cdot l_w \cdot t_w}{h_w} \tag{2}$$

where G_w is the shear modulus, lw is the length of the frame where the infill is located, t_w is the thickness of the infill, h_w is the height of the frame where the infill is located. The post-cracking stiffness K_2, can be set as:

$$K_2 = p \cdot K_1 \tag{3}$$

where p is assumed equal to 0.03 (Panagiotakos and Fardis 1996). The degrading stiffness K_3 can be calculated as:

$$K_3 = -p_1 \cdot K_1 \tag{4}$$

where p_1 is set equal to 0.01 (Panagiotakos and Fardis 1996). The different values of the strength are calculated from the equations below. The peak strength is:

$$F_{peak} = 1.3 \cdot \tau_{cr} \cdot l_w \cdot t_w \tag{5}$$

The cracking strength is:

$$F_{crack} = \frac{F_{peak}}{1.3} \tag{6}$$

The residual strength is:

$$F_{residual} = 0.1 \cdot F_{peak} \tag{7}$$

The infills walls are included in SAP2000 model by using the link element "Multilinear Plastic" with a kinematic cyclic behavior. The elastic stiffness to use in the linear model is taken as K_1.

The modelling of the FPS isolators was built by using the "Friction Isolator" element available in SAP2000 library. It allows to model the Friction System Bearing through a bi-linear behavior. The bilinear behavior is characterized by an initial stiffness k_i, for non-linear model, assumed equal to 400 kN/m (Ponzo et al. 2018). The horizontal force, F, is defined as function of the friction force F_0, the restoring stiffness k_b and the imposed displacement, d, see Eq (8):

$$\mathrm{F} = \mathrm{F_0} + \mathrm{k_r} \cdot \mathrm{d} \tag{8}$$

where:

$$\mathrm{F_0} = \mathrm{N_{sD}} \cdot \mu \tag{9}$$

$$\mathrm{k_b} = \frac{\mathrm{N_{sD}}}{\mathrm{R}} \tag{10}$$

N_{sd} is the axial force in the QP combination, μ is the friction coefficient of the isolators and R is the curvature radius. The parameters needed to characterize the nonlinear model in SAP2000 are the initial stiffness, k_a=400 kN/m, and the slow and the fast medium friction coefficient, 5%, so there is not dependence from the velocity, because SAP2000 used the model of Constantinou et al (1990) (Eq. 11). The curvature radius is set equal to 3100 mm.

$$\mu = \mu_{fast} - \left(\mu_{fast} - \mu_{alow}\right) \cdot e^{-\alpha|v|} \tag{11}$$

3.4.2 Analyses Matrix

In order to assess the existing structure and then clarify the role of infill on the isolated base structure, analyses were performed on various configurations of the case study, as shown in Figure 31.

First, the structure was evaluated in the as-built (bare) condition. Two configurations were considered for the assessment: linear and non-linear. (The infilled as-built configuration was considered for the successive assessment, in the next section).

NUMERICAL MODEL	***LINEAR***	***NON-LINEAR***
BARE (As Built)	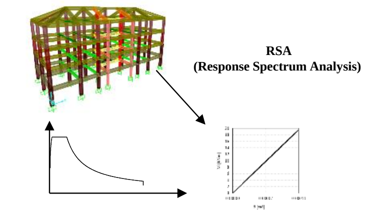	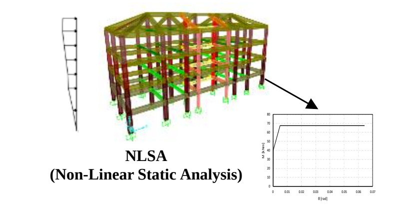
Infilled (As Built)	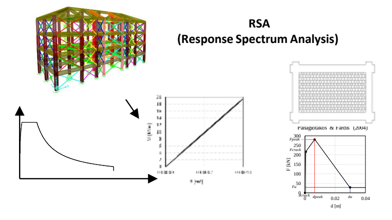	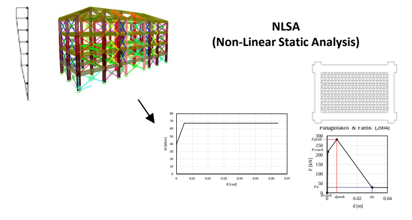

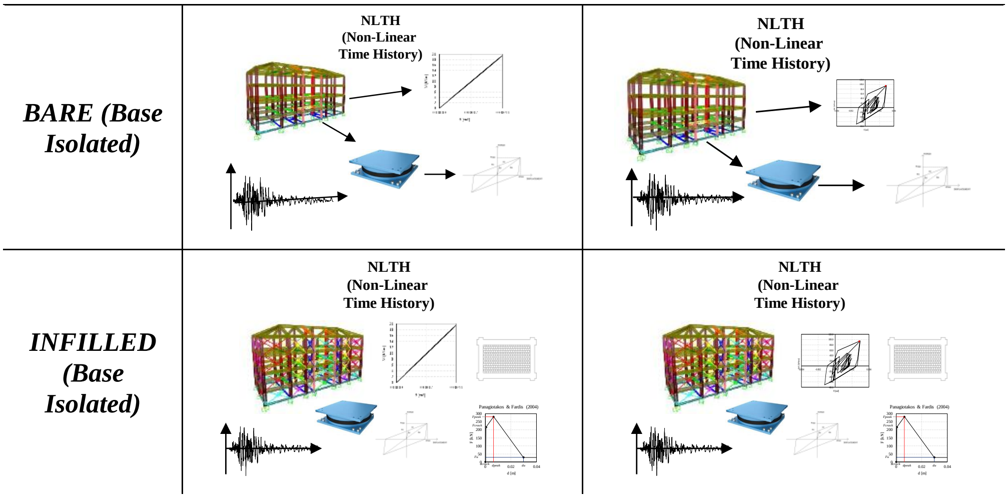

Figure 31. Matrix Analysis

To gain initial insight, a response spectrum analysis (RSA) was performed using the compliant LSLS spectrum (475 years). Subsequently, a refined evaluation was performed with a nonlinear static analysis using the N2 method to define the first failure and the safety index. The assessment of the structure allowed to design the best retrofit interventions with an isolation system. Four configurations of superstructure were considered: bare and infilled, linear and nonlinear. To clarify the role of infill in the base isolated configuration for each of the configurations studied, an NLTH was performed after performing spectral compatibility compliant with the LSLS spectrum. More information can be found in the following sections.

In order to clarify the role of the infills in the base-isolated configuration, the shear failure was checked, the results in terms of drift and acceleration were reported, and the mechanical behavior of the components was shown by comparing between the different configurations.

3.4.3 Assessment of the structure

A linear elastic model was developed in the SAP2000 (Computer and Structures 2007) environment to evaluate the dynamics properties of the as-built (bare) structure. The modal analysis outlines that the first mode of vibration is translational along the y direction with a period about 0.86 s. The second mode of vibration, torsional, with a period equal to 0.58 s and the third mode of vibration, translational along the x direction with a period equal to 0.51 s. Initially, to assess the building seismic response in the as-built configuration a response spectrum analysis, using the spectrum of L'Aquila with behavior factor equal to 1.5 to investigate only the brittle failures was carried out, resulting in a very high number of failures, due to the lack of proper seismic details and transverse reinforcement in the columns and beam-column joints. These failures may significantly limit the seismic performance of the building in the as-built configuration. To better assess the building seismic response, a non-linear static analysis was carried out according to the suggestions of the NTC (2018), Circolare (2019). A lumped plasticity model considering the nonlinear response of the RC members according to the capacity models suggested by current Italian seismic code (CS.LL.PP. 2019) is used to obtain the pushover curve of the building in the two main directions. To assess the vulnerability of the structure a set of nonlinear static analysis is carried out in displacement control. Two different loads patterns are considered according to the current code (CS.LL.PP. 2019): a displacement profile proportional to the distribution of the seismic masses along the height (MASS) and a second distribution with a displacement profile proportional to the shape of the fundamental mode of vibration in each direction (MODE). The displacement is applied at the center of the mass.

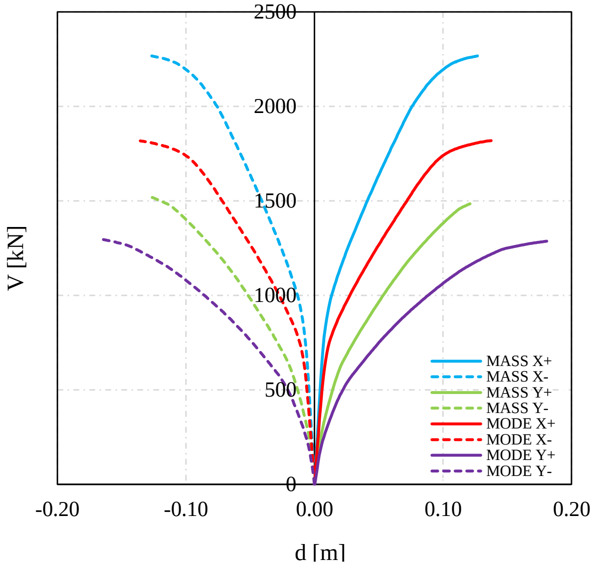

Figure 32. Push-Over curves of the case study building in the as-built bare configuration

The accidental eccentricity is not considered in this study since the curves are only used to have a first insight on the building capacity. The control point is set in the center of the mass at the top roof. The results of the non-linear static analysis are reported in Figure 32, the push-over curves. The N2 method (Fajfar 2000) is adopted to assess the seismic vulnerability of the structure at the LSLS. The safety index, ζ_e, is defined as the ratio between the peak ground acceleration, PGA, scaled to the minimum capacity of the structural system and, and the demand PGA, identify by the code compliant LSLS spectrum (TR = 475 years, soil type B, T1 category). A graphical representation of this seismic performance assessment in the ADRS format is reported in Figure 33 The assessment of the building in the as-built configuration outlines that the shear failures of the perimetral joints limit the seismic capacity to ζ_e =22%. To improve the seismic capacity of the building a retrofit intervention using base isolation is used. Once that the acceleration of the first brittle failure is defined, this value of acceleration is shifted on the ADRS design elastic spectrum at the LSLS calculated with a damping coefficient of 10% to consider the additional dissipation provided by the isolation devices.

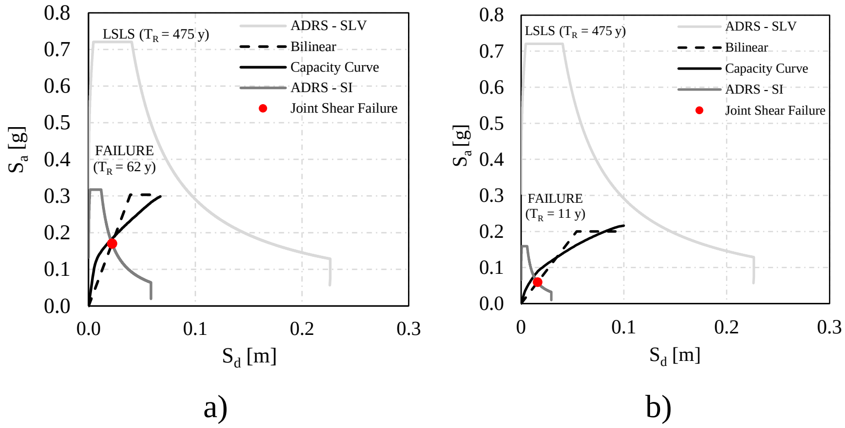

Figure 33. Procedure to define the safety index in x direction a) and y direction b)

This allows to identify the design period of the base isolation system which allows to avoid brittle failures on the superstructure. With reference to the case study building, this period is about 3.80s. For the case study building, DCFPs are selected for the isolation system. The maximum displacement, at ULS experimented by the structure is minus of 200 mm, thus a device with a maximum displacement of 200 mm is chosen, that has an associated curvature's radius of 3100 mm; the friction coefficient largely used for this device is 0.05. Both the surfaces have the same curvature's radius and friction coefficient of about 3100 mm and 0.05, respectively. These devices are selected to be representative of the dataset of buildings retrofitted during the L'Aquila reconstruction process by using base isolation systems. Indeed, DCFPs were used in 34 buildings out of 59 (Di Ludovico et al. 2017). This allows to achieve a design period of about 3.00s that is lower than the optimum design period of 3.80s. Thus, further strengthening interventions on the superstructure may be required.

3.5 Results

The distributions of the floor acceleration and drift for building in the fixed base, isolated bare and isolated infilled configurations are reported in the following Figure 34 and Figure 35.

Figure 34a,b shows that the introduction of the base isolation significantly reduces the acceleration transmitted to the superstructure. The acceleration transmitted to the first floor are about 1/3 of the imposed PGA. While the acceleration of the last floor in the base isolated configuration is about 1/6 of the one on the building in the as-built configuration. The trend of the peak floor accelerations for isolated bare and isolated infilled building are similar.

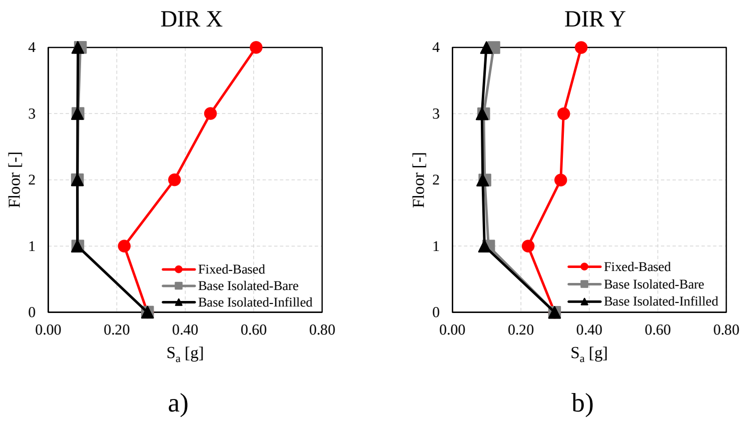

Figure 34. Distribution of floor acceleration for T_R 475 years on the case study building in the as-built and isolated configurations: in the x direction a); y direction

The drift distribution for the building in the fixed base configuration shows an increase at the second-floor respect to the first floor. This is due to the stiffness of the first-floor columns which is higher than the one of the other floors due to a shorter height. The drift demand along x direction is lower than 0,5% (i.e., the limit at DSL according to NTC 2018) while along the y direction the drift demand is considerably exceed this limit. In turn, a significant damage to infills and partitions is expected. The drift's distribution for the isolated building decreases along the height.

The drift demand on the infilled structure is considerably lower than the one on the bare structure (Figure 35a,b). The drift demand on the isolated building both in the bare and infilled configurations is the highest at the first floor. In particular, the drift demand on the infilled configuration is 1/9 in the x direction and 1/6 in the y direction with respect to that of the bare configuration. The minimum is at the last floor, and the drift on the infilled configuration is 1/7 in the x direction and 1/5 in the y direction with respect to the bare configuration.

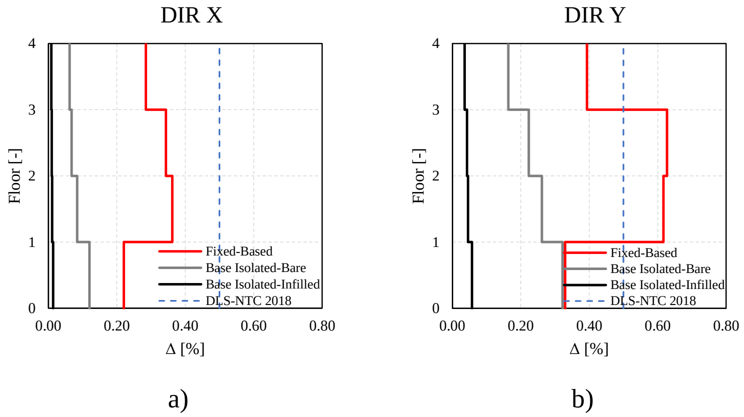

Figure 35. Drift comparison for T_R equal to 475 years between fixed base, isolated bare and isolated infilled configurations: in the x direction a); y direction b)

The presence of the infills resulted in a lower drift because the structure is stiffer than the one in the bare configuration since the infill walls remained uncracked during the simulated earthquake shaking. In conclusion, the seismic retrofit of this case study building by means of base isolation resulted in a significant improvement of seismic performance. Indeed, a significant reduction of acceleration and, in turn the drift on the superstructure can be observed. This may have a significant influence on the expected economic losses

3.6 Base isolation on bare model

In the common practice, in the seismic performance assessment and in the design of a retrofit interventions the infill action is commonly neglected. Furthermore, since the Italian building code allows the use of linear dynamic analysis, this option is often used in the design practice. However, relevant scientific studies on the seismic response of existing RC buildings retrofitted by base isolation demonstrated that these buildings can be subjected to significant nonlinear demand (Cardone et al. 2013). Thus, a comparison between the base isolated buildings in the bare configuration with linear superstructure and nonlinear superstructure is proposed. The results of the

NLTHs shows that the structural members are subjected to a significant ductility demand (see Figure 36).

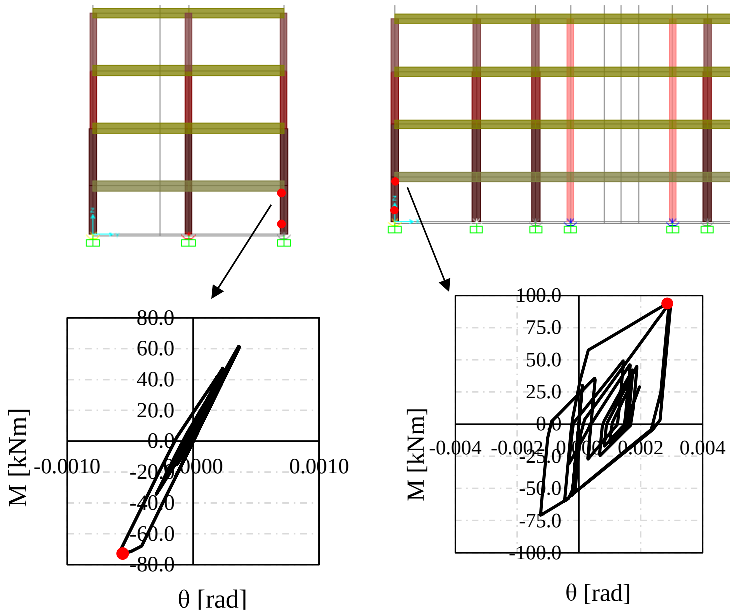

Figure 36. Non-linear behaviour of the superstructure on bare configuration

However, as also confirmed by the nonlinear static analyses discussed in the previous section, the building is capable of sustain this displacement capacity if only flexural failures are considered. By contrast, the safety checks on the shear capacity of columns and beam-columns joints outlines that many shear failures can be observed. The results are reported in Figure 37a and a comparison between the failures observed on the linear and nonlinear model is performed.

Figure 37a outlined that the shear capacity of the beam-column joints and the columns is triggering for the overall seismic performance. Furthermore, significant difference can be observed between the linear and nonlinear model. When a nonlinear model is used, a lower number of failures both for the columns and for the beam-column joints can be observed. This happens for the low seismic demands of shear forces due to the flexural yielding of some structural members.

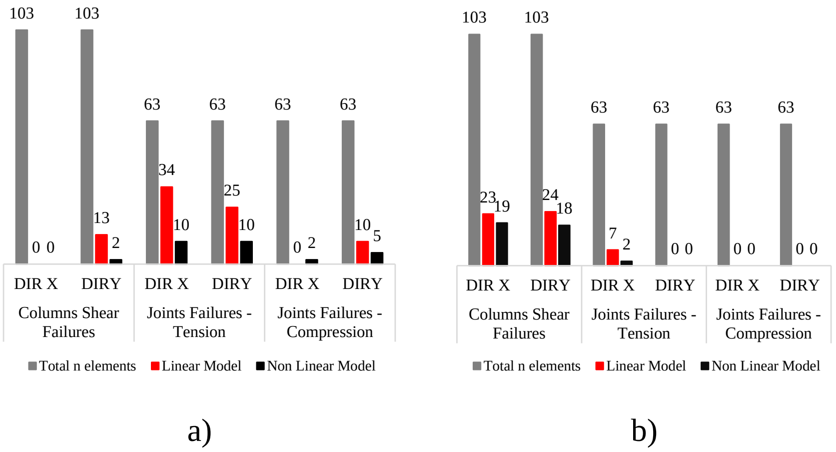

Figure 37. Results of bare a) and infilled b) configuration in linear and non-linear modelling

Thus, considering the linear superstructure, on a bare configuration of the isolated buildings, may lead to significantly overestimate the number of structural members that need for further strengthening interventions.

3.7 Base isolation on infilled model

The interaction between the infills and the structure is already known. Their presence increases the stiffness, with an increase in the accelerations and a reduction in the displacement demand on the structure. Thus, an infilled configuration is modelled, considering superstructure with linear and nonlinear behavior. The infills are modelled using the behavior of Panagiotakos and Fardis (Panagiotakos and Fardis 1996), showed in the previous section. The results of the NTLHs shows a linear elastic behavior of the structural members in both cases (see Fig 12b). The response observed is due to the reduction in the displacement demand that doesn't request a dissipative performance to the elements. Thus, the infilled configuration allows to model the superstructure with a linear behavior. A clear interaction is, therefore, showed between structure and infills in the isolated configuration.

The consequence of the interaction interests the possible failures that the structure could present. In fact, it produces an additional shear on the column, that could not satisfy the demand due to this contribution (see Fig 38). Figure 37b showed that the failures are concentrated in the columns, while the beam-column joint are quite safe. A comparison between the linear and nonlinear model doesn't show a significantly difference, due to the similar response of the superstructure.

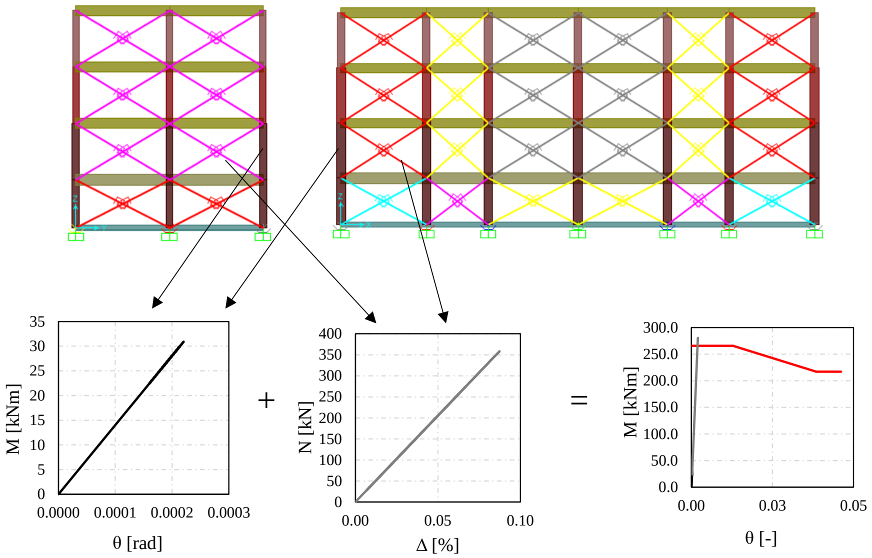

Figure 38. Linear behaviour of superstructure in infilled configuration and interaction with infills

Thus, on infilled configuration of the isolated building, a linear or nonlinear model for the superstructure is available to carry out a nonlinear time history analysis. Furthermore, accounting the infills is necessary to calibrate a suitable strengthening intervention on the buildings.

The main difference between the infilled and bare model is the different structural components that suffered damage, both for the linear and non-linear configuration as showed in Figure 39a,b. In fact, in bare configuration the beam-column joints are concentrated the shear failure while in the columns for the infilled configuration.

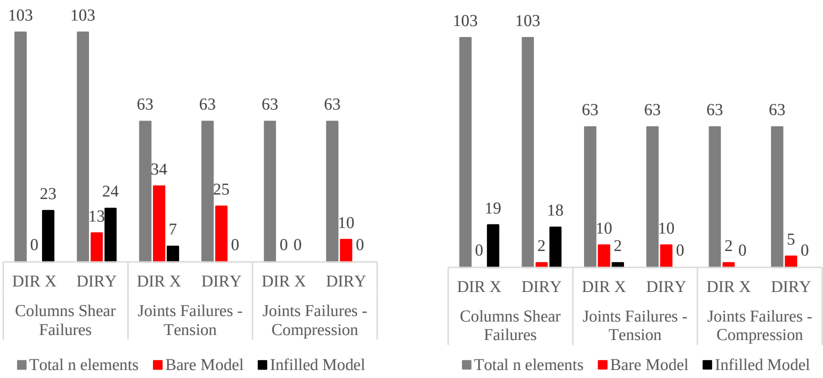

a) b)

Figure 39. Results of linear a) and non-linear b) configuration in bare and infilled modelling

The study carried out shows the different advantages and disadvantages of the bare and infilled model with linear and nonlinear behavior for an existing building isolated from the base. The results suggest that infill should be considered in the budding model and consequently a linear behavior should be assumed for the superstructure. To this end, in the next section of the paper, the building under consideration is modeled with infills and linear behavior of the superstructure.

CHAPTER 4 – A FRAMEWORK FOR THE QUANTIFICATION OF THE ECONOMIC FEASIBILITY AND PAYBACK TIME

A framework, relying on the PEER PBEE framework (Porter 2003) and the loss-assessment analyses carried out using the FEMA-58 (ATC - Applied Technology Council 2012a) approach, is proposed. The framework, discussed in detail below, can be used to estimate the Pay-Back Time, PBT. The PBT identifies the return period of the economic investment expressed in years. It can be calculated by assessing the difference between the cost of the retrofit intervention and the annual savings due to the reduction of the expected annual losses (EALs) as result of the retrofit solution. The PBT could be a useful parameter to estimate the effectiveness of the retrofit techniques combining the initial cost of the intervention, the increasing safety and the reduction of the EALs.

4.1 Methodology

The methodology proposed involves eight steps (see Figure 40): building definition, hazard analysis, structural analysis and seismic performance assessment, estimation of the Engineering Demand Parameters (EDP), evaluation of damage and losses, identification of potential weakness, design of the retrofit alternatives, estimation of the cost of the intervention, calculation of the annual savings and PBT. They are discussed in the followings with reference to the main assumptions made to adapt its application to existing RC building typical of the Mediterranean area.

- **Building Definition**: the location of the building, the soil type, details of the structural system, reinforcement details and material properties are needed to characterize the seismic response and the EDPs. The inventory of all the structural and non-structural components (drift or acceleration-sensitive) susceptible of earthquake damage is needed to conduct loss-assessment analysis. Existing RC buildings in the Mediterranean area have hollow clay-brick infills and partitions. They are susceptible of significant damage during the seismic event and they represent the major cost of building repair cost in the post-earthquake reconstruction process (Del Vecchio et al. 2020).Thus, drift and accelerations sensitive non-structural components such infills, partitions, plumbing and electrical system, floor finishes, tiles and chimneys have to be modeled in order to properly assess the expected losses and quantify the benefits due to the retrofit solution
- **Hazard Analysis**: in order to calculate a building-specific loss curve accounting for earthquakes with different intensity and the uncertainties in input selection a site-

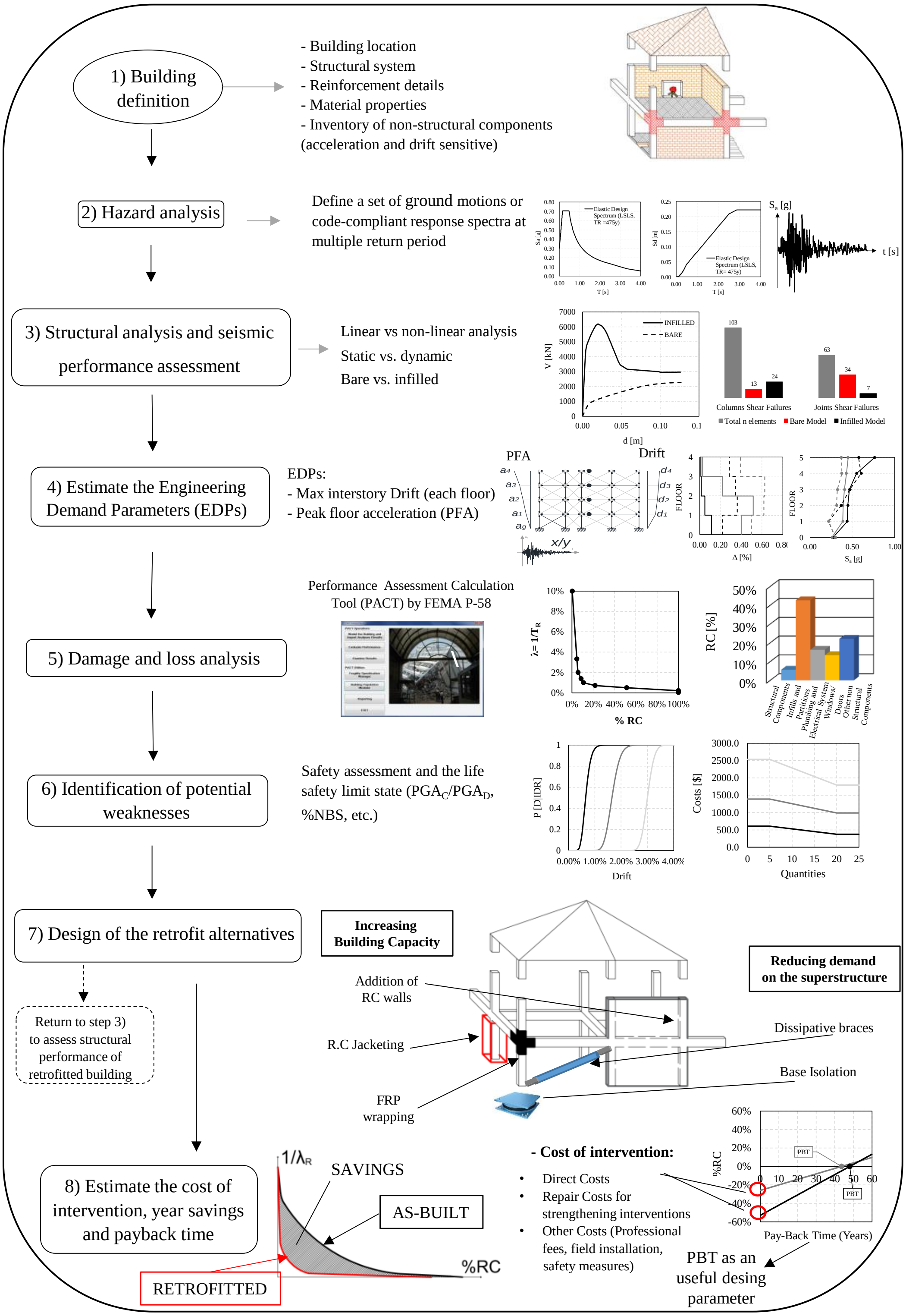

Figure 40. Methodology proposed to assess the PBT of retrofit solution

dependent hazard analysis should be carried out. The hazard curve is defined in terms of Mean Annual Frequency of Exceedance (MAFEi) vs. spectral acceleration $S_{a,i}$ (T^*) at the fundamental period of the structure. Different intensity earthquake corresponding to a return period, T_R, ranging from 30 to 2475 years have to be selected. In this work nine intensities are considered (i.e. T_R equal to 30, 50, 72, 101, 140, 201, 475, 975, 2475 years) to accurately predict the EALs.

For each of the return period, a spectrum compatibility, in acceleration and displacement is suggested for base isolated buildings. This allows to select a set of orthogonal pairs of natural records suitable to conduct non-linear time history analyses (NLTHs) to reliably assess EDPs.

- **Structural analysis and seismic performance assessment**: the vulnerability of the structure and the EDPs should be assessed using NLTHs relying on refined non-linear models. In order to properly assess the drift and acceleration demand of RC buildings with stiff infill, their contribution to the lateral response should be properly modelled. Indeed, as reported in Figure 40, the contribution of the infills may significantly change the lateral strength and stiffness of the building. The model should be capable of considering the contribution of the infills to the lateral deformation, as well-as the interaction with surrounding structural components, which may lead to premature shear failure at the top of the columns. Figure 40 reports a comparison between the type and number of failures for a RC case study building obtained by using a bare and infilled model. The presence of stiff infills significantly changes the type of failure in the structural system as-well-as the estimation of the EDPs. In case of base isolated buildings, the displacement demand on the isolation devices should be checked to account for possible collapse due to the achievement of the maximum displacement.
- **Estimation of Engineering Demand Parameters (EDP**) nonlinear time history analyses by using the previously defined sets of ground

motions are suggested. For each ground motion and return period, the maximum absolute values of interstorey drifts and peak floor accelerations have to be recorded to be used in the loss-assessment analyses. The interstorey drift and the peak floor acceleration are chosen as EDPs since most of the fragility curves available in literature use these intensity measures.

- **Evaluation damage and losses**: the damage analysis and loss assessment can be carried out by using the FEMA P-58 component-based methodology implemented in the PACT software (ATC - Applied Technology Council 2012a). A detailed component-based model of the building is needed and it should reflect the construction standard of the area (Del Vecchio et al. 2018). For this reason the fragility curves for infills and partitions (Cardone and Perrone 2015) and beam-column joints (Cardone 2016) typical of the Mediterranean area as-well-as reliable consequence functions (Del Vecchio et al. 2020) are implemented in the software. The intensity analysis option can be chosen with number demand vectors equal to the number of records selected for each intensity. The response to the earthquake in the two main building directions have to be considered according to the selected ground motions. Global collapse has to be considered because when it occurs the loss of the total value of the building is expected. The user may decide to include or not residual drift as an alternative estimation of the total loss due to the need for demolition and reconstruction. The spectral acceleration corresponding to the global collapse can be estimated by means of the numerical analysis or building-specific fragility curves (Cardone et al. 2018). In this paper, the direct economic losses, $EAL_{s,direct}$, related to damaged building components are considered. The indirect economic losses, $EAL_{s,indirect}$, related the occupants' relocation as function of the downtime are also calculated and summed to the $EAL_{s,direct}$. Injuries or fatalities are volunteering not taken into account in accordance to the Italian guidelines for seismic risk assessment of buildings (Cosenza et al. 2018).

- **Identification of potential weakness**: the assessment of the building in the as-built configuration allows to evaluate the vulnerability, the potential structural weakness as-well-as the main sources of economic losses. The explicit modelling of infills allows to identify the premature shear failure at the top of the columns as commonly found in the post-earthquake damage surveys in the aftermath of recent seismic events in the Mediterranean area. The disaggregation of the repair costs (see Figure 40) is needed to identify the most expensive component to repair and define proper seismic interventions aimed at reducing their damage.
- **Design of the retrofit alternatives**: the results of the previous step indicate the direction to select the most effective retrofit options. Two main aspects should be considered in the design of the retrofit solution: the increase of the building seismic safety (e.g. expressed as the ratio capacity over the demand at the life safety limit state) and the reduction of the EALs. Two main retrofit strategies are available (see Figure 40): increase the capacity of the structure (e.g. by using FRP wrapping, RC jacketing, addition of RC walls among many others) or reduce the demand to the super-structure (by using dissipative systems or base isolation). Once that the retrofit solutions are selected, the seismic performance and the expected losses should be assessed (return to step 3).
- **Estimation of the cost of intervention, annual savings and PBT**: the direct cost of the retrofit intervention can be estimated considering all the actions needed to install the selected techniques. Based on the experience of recent post-earthquake reconstruction processes (Del Vecchio et al. 2020), the costs of materials and the works needed for the installation as well as the costs for demolition and repair actions needed to install the selected retrofit solution should be considered

along with other costs such as professional fees, safety measures, field installation, etc. Since the indirect costs related to building downtime and occupants could be a significant portion of the total loss (Cardone et al. 2019a; Di Ludovico et al. 2019) they should be included in the loss-assessment in order to have more refined estimation of the PBT. In this study, the indirect costs related to the occupants relocation are considered. They are estimated as the product of the number of people living in the building (obtained from the AeDES form) times the average assistance cost (taken as 238.88€ assisted person/month, according to the actual costs monitored during the L'Aquila reconstruction process, (Fico et al. 2019) times the expected downtime calculated by using the PACT software. The replacement time is taken as the time to complete the great part of the heavy reconstruction in L'Aquila , about 8 years (Mannella et al. 2017). Once that the EALs related to indirect costs are calculated they are summed to the EALs related to direct costs._The annual savings can be calculated as the difference between the EALs (see Figure 40) of the building in the as built and retrofitted configurations. Finally, the PBT can be estimated as the years needed to recover the initial economic investment, which is the ratio of initial cost over the annual savings. Thus, as showed in Figure 40, the curve representing the recovery of the initial investment can be plotted. At the time of the initial investment (year zero), there is a debit equal to the cost of intervention. Every year the annual savings due to the reduction of EALs have to be deduct to the initial cost. From a graphic standpoint, the intersection between this curve and the horizontal axis identifies the PBT.

4.2 Application to the case study

The procedure described above to assess and compare different retrofit solutions in terms of the PBT time is applied to the case study building extracted from the database of the 59 existing RC buildings retrofitted by means of base isolation systems in L'Aquila. The proposed methodology is illustrated step-by-step, then it is extended to the full set of 59 buildings.

The first step, involving the building definition and the numerical model, is describe in the above section, while the assessment is newly conducted because of it considers the infilled as-built configuration, instead the bare as in the previous analysis

4.2.1 Hazard Analysis

To properly define the hazard curve in terms of Mean Annual Frequency of Exceedance, $MAFE_i$, vs spectral acceleration, $S_{a,i}$ (T^*), is considered and nine different intensities with return period ranging from 30 to 2475 years are selected. For each intensity a set of seven orthogonal pairs of records is considered, thus 14 records in total. Natural records are used for this study.

The record selection and the spectrum compatibility with the code compliant design spectrum on a soil type B, in L'Aquila, at different return periods was performed by using the software REXEL (Iervolino et al. 2010).

The range of magnitude, M_w, and distance used for the record selection is 6-6.3 and 0-30 km, respectively. This complies with the hazard disaggregation at the LSLS (T_R = 475 years) for the site of L'Aquila. The elected records are reported in Table 6 along with the main characteristics such as the M_w, the JB distance, PGA and peak ground velocity (PGV), the Arias Intensity, I_A, and the damage index, I_D (Cosenza and Manfredi 2000). Only records with I_D < 15 are considered in order to have records with a similar energy demand.

Table 6. Properties of the selected records

Record	Location	Year	Station	M_W	Soil type	Distance JB	Direction	PGA	PGV	I_A	I_D
[-]	[-]	[-]	[-]	[-]	[-]	[-]	[-]	[g]	[m/s]	[m/s]	[-]
1	L'Aquila	2009	STANT	6.1	A	23	EW	0.020	0.019	0.009	14.2
							NS	0.026	0.022	0.018	19.1
2	Golbasi	1986	ST161	6.0	A	29	EW	0.039	0.029	0.011	6.4
							NS	0.055	0.075	0.036	5.6
3	Friuli	1976	ST33	6.0	C	11	EW	0.083	0.079	0.084	8.2
							NS	0.090	0.063	0.096	10.8
							EW	0.220	0.278	0.896	9.3

4	Adana	1998	ST549	6.3	C	30	NS	0.270	0.203	1.006	11.7
5	Alkion	1981	ST121	6.3	C	25	EW	0.117	0.109	0.182	9.1
							NS	0.190	0.149	0.224	8.0
6	Umbria	1997	ST60	6.0	B	11	EW	0.524	0.319	3.304	12.6
							NS	0.463	0.290	2.821	13.4
7	Izmir	1992	ST43	6.0	B	30	EW	0.029	0.036	0.024	14.8
							NS	0.039	0.068	0.035	8.5

The records selection is made to have the average spectrum of the records matching the acceleration and displacement spectra by using the REXEL software (Iervolino et al. 2010). The mean scaling factor, i.e the mean of the all the factors used to scale each record, of the set of records should not exceed 5 for all the considered T_R. As showed in Figure 41, the spectrum compatibility is checked against the average spectrum of the 14 records. A tolerance on the lower limit of 10% (CEN 2004a) and on the upper limit of 30% in the range of period between 0.15 s (grey line in Figure 41) and 1.2 times the fundamental period of the base isolated structure T_{is} (the period of the isolated structure) is used according to the prescription of the Italian building code (MIT 2018).

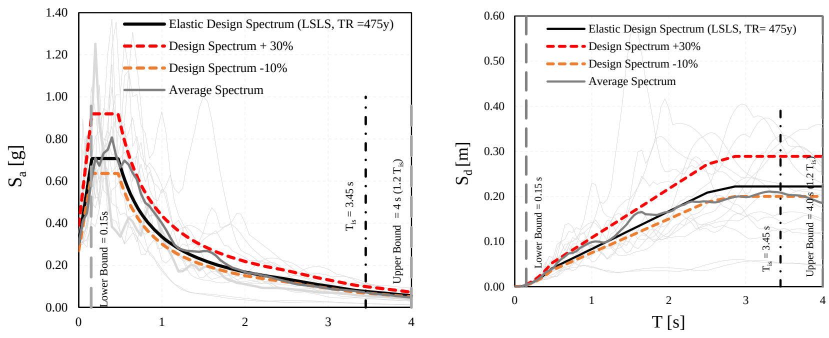

a) b)

Figure 41: Compatibility in terms of acceleration (A) and displacement (B) with code spectra at LSLS (T_R= 475 y).

4.2.2 Seismic Performance Assessment and Design of the Retrofit Alternatives

To assess the vulnerability of the structure a set of nonlinear static analysis is carried out in displacement control. Two different loads pattern are considered according to the Eurocode (CEN 2004a): a displacement profile proportional to the distribution of the seismic masses along the height and a second distribution with a displacement profile proportional to the shape of the fundamental mode of vibration in each direction. The displacement is applied at the center of the mass. The accidental eccentricity is not considered in this study since the curves are only used to have a first insight on the building seismic response. The control point is set in the center of the mass at the top roof. The N2 method (Fajfar 2000) is adopted to assess the seismic vulnerability of the structure at the LSLS. The safety index PGA_C/PGA_D at LSLS (T_R = 475 years, soil type B, T_1 category) is used to quantify the building performance. The most critical capacity curve and its linearization (dashed line) are depicted in Figure 42 along with the N2 procedure (Fajfar 2000) for the seismic performance assessment.

The seismic performance assessment outlined that premature brittle failures due to the interaction between infills and columns significantly limited the building capacity to PGA_C/PGA_D = 0.08, as shown in Figure 42, as ratio between the PGA of the scaled spectrum (red line), PGA_C = 0.024g, and the PGA of the elastic spectrum at LSLS (black line), PGA_D=0.300g.

To improve the seismic capacity of the building four different retrofit solutions are designed: *i)* FRP wrapping is considered because it was the most popular retrofit solution used during the L'Aquila reconstruction process (Di Ludovico et al. 2017); *ii)* base isolation is considered due to the high effectiveness in increasing the seismic safety and reducing the EALs including those related to non-structural components; *iii)* base isolation + FRP local retrofit, in this case the two techniques are combined to achieve high seismic performances; *iv)* demolition and reconstruction (namely Rebuilt).

FRP strengthening aims at increasing the capacity of the structural system by avoiding the premature local failure of weak members (in this case the column and joints because of the shear failures related to lack of transverse reinforcements as commonly found most of the existing RC buildings in the Mediterranean area). This technique is effective in considerably increasing the seismic safety (Frascadore et al. 2015). However, due to the debonding phenomena it commonly does not allow to strengthen the structure to sustain the 100% of the seismic demand, i.e. the demand at LSLS (T_R = 475 years). By contrast it is very simple to install and significantly cheaper than base isolation.

The seismic retrofit with FRPs was designed in accordance with the fib bulletin 90 (Fib bulletin 90 2019) and the Italian guidelines (DPC-ReLUIS 2011). The design of the strengthening system aims at achieving the highest seismic performance. In this case 103 beam-column joints were retrofitted in shear to sustain the shear demand in the joint panel (by using quadriaxial CFRP, see Figure 42) and the shear force transmitted at the top of the column due to the interaction with the infills (by using uniaxial steel FRP, see Figure 42). Due to debonding phenomena, the maximum capacity that can be achieve with this technique is $PGA_C/PGA_D = 80\%$, see the scaled spectrum at performance point (green line in Figure 42).

The preliminary design, of the base isolation is depicted in Figure 42. The acceleration at the fundamental period of the as-built structure resulting in the brittle first failure of primary structural members should be identified (red dot in Figure 42). As graphically reported in Figure 42, this acceleration is shifted on the damped ADRS (acceleration displacement response spectrum) elastic design spectrum at the LSLS (in this case a tentative damping of the 10% is considered to represent the dissipation provided by the isolation devices). This allows to identify the period of the base isolation system which allows to avoid brittle failure on the superstructure. With reference to the case study building, this period is about 4.00 s. For the case study building, friction pendulum systems FPSs (Zayas et al. 1987) are selected since they are commonly available in market worldwide. The main properties are showed in Figure 42. Although different types of commercial FPS devices are tested, the highest design period that can be achieved is about 3.38s that is lower than the optimum design period of 4.00 s but with a higher damping (about 21%). In turn, the base isolation alone is not capable of eliminating all the premature shear failures and additional FRP local strengthening of some structural members of the superstructure is required to fully satisfy the seismic code demand (i.e. $PGA_C/PGA_D = 100\%$). This solution is preferred to more complex base isolation strategies since it is widespread in the design practice (see Table 1). By contrast the base isolation alone allows to achieve a $PGA_C/PGA_D = 90\%$.

Finally, demolition and reconstruction (Rebuilt) is considered. A new building with the same dimension of the as-built one is designed but changing the reinforcement, in order to fully satisfy the requirement of current Italian building code (i.e. PGA_C/PGA_D = 100%). The structural system and the RC members have the same dimensions of the as-built structure because they have enough lateral stiffness to contain the maximum drift below the limit of 0.5% suggested by the Italian building code to contain damage to non-structural components (as demonstrated in the following sections). This is to have a lateral deformability as close as possible to the as-built one, but higher strength due to the use of code conforming internal reinforcements

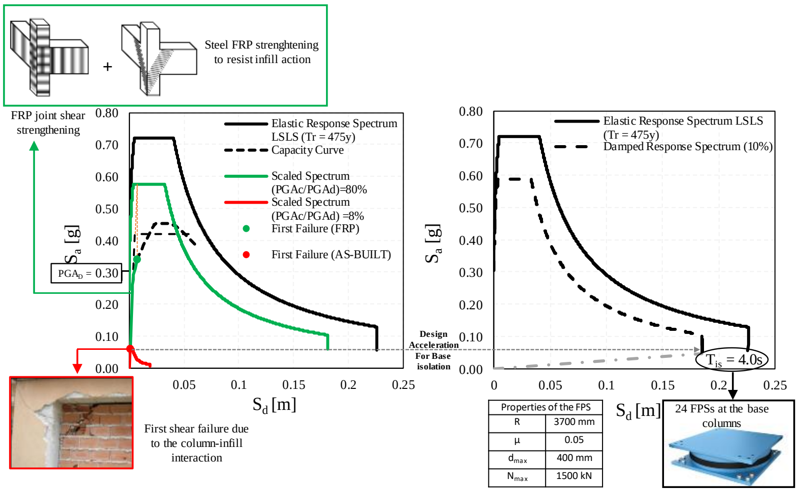

Figure 42. Assessment of the structure and preliminary design of the retrofit alternatives

The design of these different retrofit options allowed analyzing different solution corresponding to increasing effectiveness and increasing installation cost; this makes attractive the use of the PBT to quantify the most convenient solution.

4.2.3 Quantification of EDPs

The seismic performances of the case study building, for each configuration (i.e. as-built, FRP strengthened, base isolated, base isolated +FRP, rebuilt were investigated by means of the NLTH analyses using the set of seven orthogonal pairs records for each return period considered. The story-by-story estimations of the two EDPs (i.e. interstorey drift and peak floor acceleration) are reported in Figure 43 with reference to the as-built (which also corresponds to FRP and rebuilt configuration) and base isolated solutions. The data refer to set of records scaled at the return period of 475 years (LSLS). It is worth noting that the response in terms of drift and acceleration of the building in the FRP strengthened and Rebuilt configurations is the same of the as-built one. This is because in the design process it is assumed that the geometry of the structural members, the masses and the lateral stiffness does not change. Indeed, as widely demonstrated by experimental tests and analytical studies FRP systems commonly do not significantly affect the

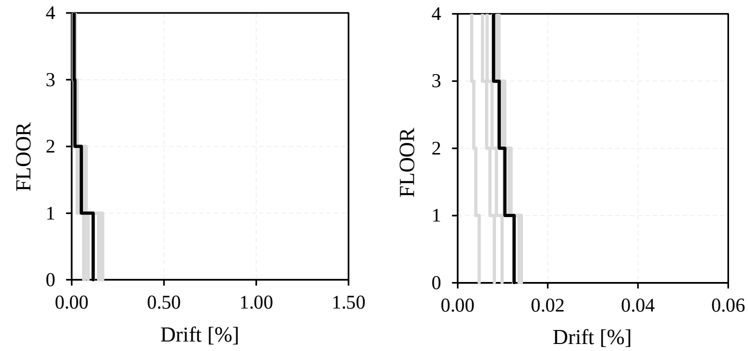

As-Built/FRP/Rebuilt   Base Isolated/ +FRP

a)

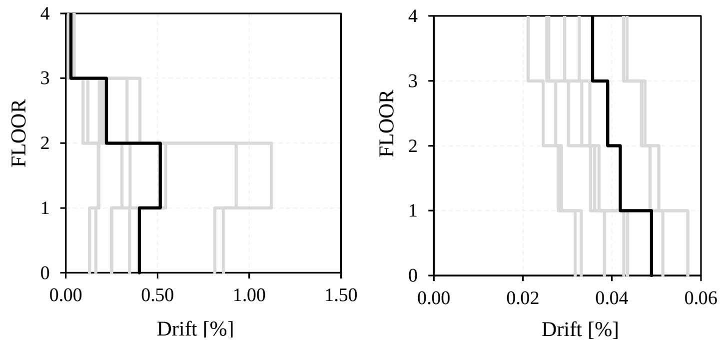

As-Built/FRP/Rebuilt   Base Isolated/ +FRP

b)

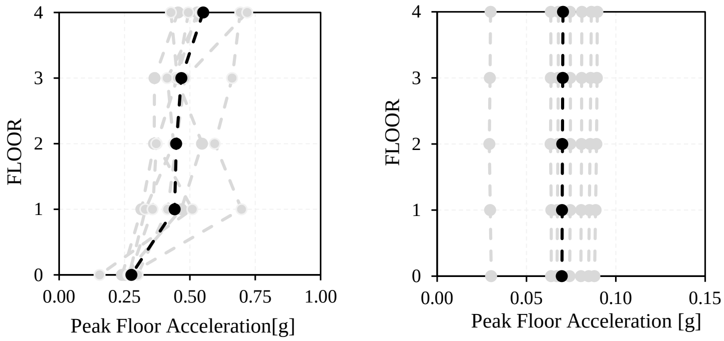

As-Built/FRP/Rebuilt Base Isolated/ +FRP

c)

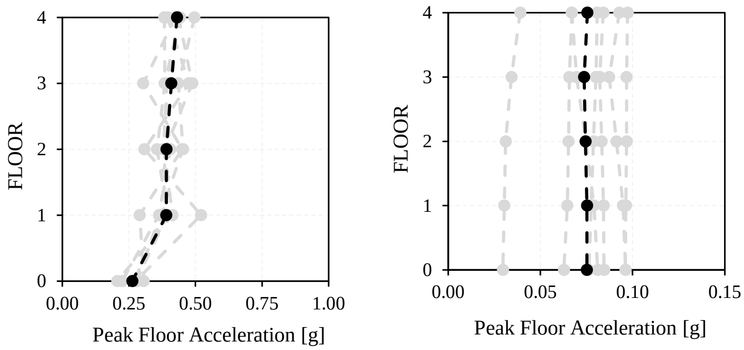

As-Built/FRP/Rebuilt Base Isolated/ +FRP

d)

Figure 43. Results in the NLTHs in terms of EDPs for T_R= 475 years (IM7): a) Maximum Drift in the X direction; b) Maximum Drift in the Y direction; c) Peak Floor Acceleration in the X direction; d) Peak Floor Acceleration in the Y direction.

stiffness of the RC structural members (Bakis et al. 2002). The role of FRP wrapping or the use of code-compliant internal reinforcement only acts at reducing the probability of collapse by avoiding the local failures of RC members.

The response of building in the as-built/FRP strengthened/Rebuilt configuration shows that the maximum interstorey drift of about 0.5% is achieved at the second floor in the Y direction. This is due to the higher stiffness of the first-floor due to a shorter height of the base columns to allocate the garage. The maximum mean drift (black line in Figure 43b) complies with the prescriptions of the Italian building code for the design of new buildings to prevent the damage to drift-sensitive non-structural components. While, the drift demand gradually reduces over the height, the acceleration demand increases resulting in a maximum amplification of the PGA of about 2.0 in the X direction (in Figure 43c)

The results reported in Figure 43 remarks the role of the designed base isolation system in significantly reducing the acceleration and drift demand to the superstructure. The drift demand at the ground floor is reduced of about 1/10 respect to the as-built configuration. Considering that the mean PGA is about 0.30 g the base isolation cuts the acceleration transmitted to the ground floor of about 1/5 in both the X and Y directions. The acceleration transmitted to the superstructure is almost constant over the building height. Furthermore, it allows to significantly contain the drift demand on the superstructure from 0.5% to 0.05% on average. This confirms the effectiveness of the designed base isolation system in reducing the effect of the earthquake on the superstructure and the expected damage to structural and non-structural components.

4.2.4 Loss Assessment

Loss-assessment analyses are carried out by using the FEMA P-58 (ATC - Applied Technology Council 2012a) procedure implemented in the PACT software (ATC - Applied Technology Council 2012b). In order to obtain a loss-curve, a time-based performance assessment, that involves different steps as described in (Cardone and Perrone 2017), is performed for the five different configurations in exam: As-built, FRP strengthened, Base isolated, Base isolated + FRP, and Rebuilt.

4.2.4.1 Building Component Model

The building performance model assembled in PACT is a component-based model including the seismic performance, fragility and consequence function for each of the structural and non-structural components. The following input data are needed:

(i) *Basic building data*: including information on building size, geometry and the total replacement cost of the building;

(ii) *Vulnerable structural and non-structural components*: the fragility functions and the amount of components for each performance groups should be specified. Fragility specifications include the definition of a number of Performance Groups (PGs), relevant Fragility Functions (FFs) and Loss Functions (LSs). As showed in Figure 44, for this study the model was built by using the functions available in PACT (typical of the US construction standard) and the recent upgrades specifically developed for hollow clay brick infills and partitions (Cardone and Perrone 2015) and beam column joints (Cardone 2016). The consequence functions recently developed for the hollow clay brick infills and partitions (Del Vecchio et al. 2020) are used. This to properly account for the characteristics of buildings typical of the Mediterranean area.

(iii) *Structural analysis data*: the results in terms of maximum interstorey drift and peak floor acceleration obtained from NLTHs carried out by using the selected ground motions scaled at the nine different seismic intensities are used as input;

(iv) *Residual drift*: neglected in this study in order to remove this variable from the decisional process of demolition and reconstruction. Indeed, for RC building with very stiff infills characterized by a collapse mainly related to brittle failures due to the infill-to-structure interaction it does not significantly affect the results;

(v) *Collapse fragility functions*: available literature fragility functions specifically developed for existing RC buildings typical of the Mediterranean area (Cardone et al. 2018) have been implemented by authors in the PACT tool. They are defined by mean of a lognormal distribution with median value S_a (T*) = 0.4 g and dispersion β = 0.6 to account for record -to-record variability and modelling uncertainty in accordance with FEMA-58 recommendations (ATC - Applied Technology Council 2012a)(ATC - Applied Technology Council 2012b). With reference to the building in the retrofitted configurations, the collapse spectral acceleration at the fundamental period is assessed by using the numerical models. Since brittle failures govern the collapse of the building in the as built configuration, it is assumed that the collapse is achieved when a shear failure is detected in more than 50% of the main structural members (Galanis and Moehle 2015). Furthermore, the failure of the base isolation considering all the possible failure mode, including the extra-stroke displacement and the stress limitation in the pad, should be accounted (Cardone et al. 2019c)(Ragni et al. 2018). However, in this case study the shear failure due to the infill-to-structure interaction governs the collapse both in the base isolated and base isolated+FRP configurations. It is worth mentioning that this is due to the high stiffness of the infills as typically found in L'Aquila where thick infills are commonly used to have a good thermal insulation. This results in a spectral acceleration at the collapse, $S_a(T^*)$, of about 0.577g, 0.072g and 0.08, 0.721g, for the FRP strengthened, base isolated and base isolated + FRP, and rebuilt configurations, respectively (T^* is the average of the fundamental period of the structure)

(vi) *Hazard analysis*: the hazard curve implemented in PACT is defined in terms of Mean Annual Frequency of Exceedance (MAFEi) vs spectral acceleration $S_{a,i}$ (T^*) corresponding to the average of the fundamental period of the structure T^*. They are estimated through a modal analysis in SAP200 resulting in 0.22 s, for the as built, FRP strengthened and Rebuilt configurations, and 3.38 s, for the base isolated and base isolated +FRP configuration.

For each intensity measure (IM), a time-based performance assessment is carried out and expected losses have been calculated. Time-based performance assessment is accomplished in PACT with the evaluation of the building loss, which plots the total expected losses as a function of the annual probability of exceedance of repair cost of different amounts. The number of realizations used in this study is 500. Each realization consists in a unique set of simulated

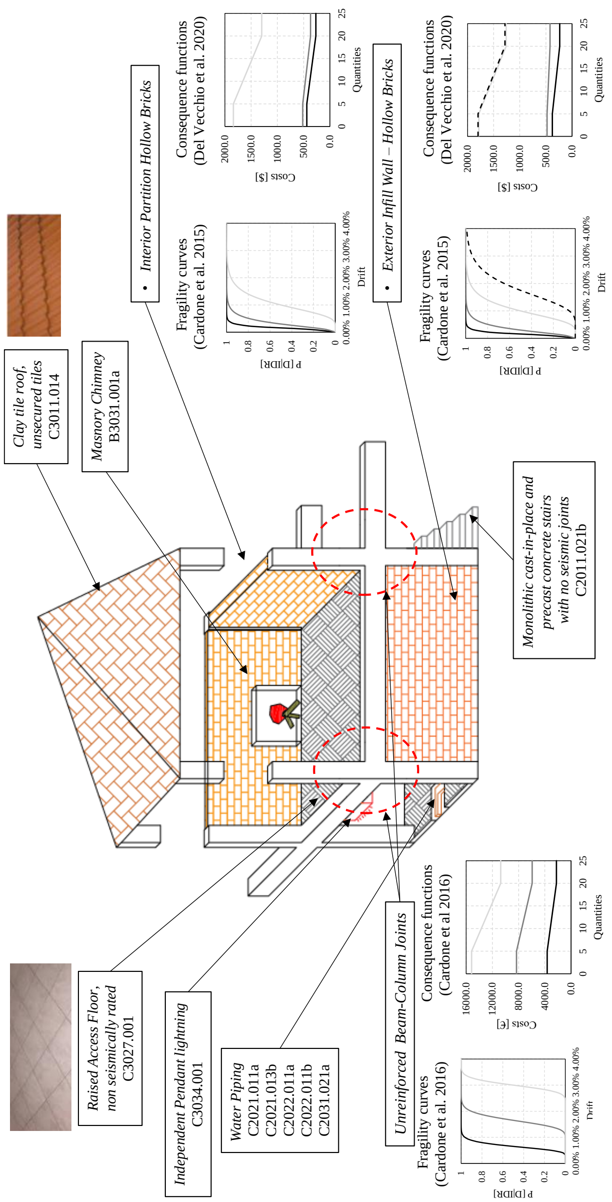

Figure 44. Component-based model for loss-assessment with focus on the adopted fragility and consequence functions.

structural response quantities (i.e., IDRs, PFAs) generated in PACT following a Monte Carlo simulation process, based on the uploaded NLTH results and assigned modelling dispersion β_m. The latter has been evaluated as the square root of the sum of the squares of two dispersion sources, i.e., the dispersion related to the level of the building definition and quality assurance β_c, and the dispersion related to the quality and completeness of the non-linear analysis model, β_q. In this study β_c and β_q have been set equal to 0.1 and 0.4 respectively, in accordance with FEMA-58 recommendations.

4.2.4.2 Assessment of the EALs

Time-based performance assessment, performed in the PACT tool, allows calculating the loss curve for all the configurations under investigation. The expected losses related to direct repair costs are expressed as percentage of the total building Reconstruction Cost, %RC, obtained by dividing the total losses by 1˙848˙000 € calculated as the product of the actual unitary reconstruction cost 1200€/m^2 of residential buildings in L'Aquila (Di Ludovico et al. 2017) times the surface area of the building of about 1˙540 m^2. The expected losses, related to the direct repair costs, are depicted in Fig 9 as function of the annual probability of exceedance repair costs, annual P, more detailed information can be found in available literature studies (ATC - Applied Technology Council 2012b; Cardone and Perrone 2017). A time-based performance assessment is carried out for each IM considering the hazard curve of the building site. More precisely, the probability of exceedance of the building loss resulting from each intensity-based analysis, is weighted by the annual frequency of occurrence of ground motions having an intensity that falls within a given interval centered around $S_{a,i}$ (T*). The time-based building loss curve is then evaluated by summing the previously mentioned contributions over the entire range of considered ground motions. Although the fitting of the data is suggested in loss assessment analyses when low number of performance points are available (O'Reilly and Calvi 2019), in this case the approximations related to the fitting are very large and this could affect the reliability of the results. In turn the binned value obtained from realizations are used, instead of a fitting with lognormal curves (Figure 45b). In this case, the lognormal seems not appropriate for approximating the EALs. As shown in Figure 45a reporting result of a loss curve for an intensity-based analysis for the case study building in the "as built" configuration, the curve fitted with the lognormal provides a large approximation to the binned value (i.e., the spheres), resulting in an underestimation of the effective $EAL_{s,direct}$ due to the smaller area under the curve. As a result, the related $EAL_{s,direct}$ curves have a rather flat trend with a fast increase of the repair cost corresponding to smaller increase of the probability of exceedance in the vicinity of the collapse.

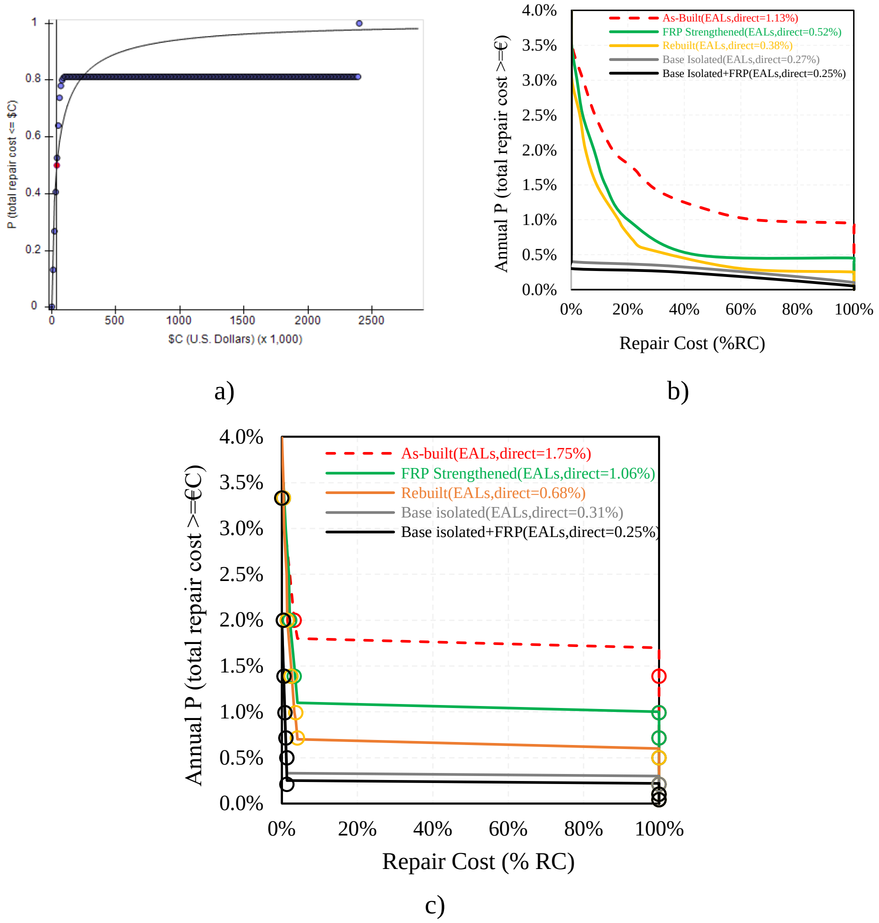

Figure 45. a) Loss distribution for as-built configuration for T_R 475 years, Loss curves related to direct repair costs for the case study building in the as-built and retrofitted configurations: b) lognormal fitting, c) binned value

The $EAL_{s,direct}$, calculated as the area below the loss curve, are reported in the legend of Figure 45, while the disaggregation of the repair costs for each IM and considering the contribution of four different component groups as-well-as of the collapse is reported in Figure 46. The components are grouped into: structural components (including beam-column joint subassemblies and stairs classified as Drift-sensitive), Infill and Partitions (Drift sensitive) and Plumbing and Electrical system (Acceleration sensitive) and Other non-structural components (including Lighting systems, Clay-tile roof, Masonry chimney and Floors classified as Acceleration sensitive).

The building in the as-built configuration has $EAL_{s,direct}$ about 1.75%, it complies with the outcomes of literature studies on infilled RC buildings typical of the Mediterranean area estimated considering refined numerical models (O'Reilly and Sullivan 2018) or simplified approaches for vulnerability assessment at regional scale (Polese et al. 2020). The FRP wrapping on beam-column joints allows to avoid the shear failure and to considerably increase the performance at the LSLS (PGA_C/PGA_D from 8% to 80%) and at collapse limit state. This results in a significantly reduction of the $EAL_{s,direct}$ to 1.06% by shifting the collapse to higher seismic actions with lower frequency (i.e. higher return period). It is worth mentioning due to lack of fragility functions specifically calibrated for FRP strengthened joints, the fragility functions of the as-built joints were used. This assumption does not significantly affect the estimation of the $EAL_{s,direct}$ since the contribution of structural members is almost negligible.

The building in the Rebuilt configuration have $EAL_{s,direct}$ of 0.68%, which is significantly lower than that of as-built one. This is because, without changing the geometry and, in turn, the lateral stiffness of the structural system, the use of reinforcement details compliant with the current code avoids the premature shear failure of primary structural members improving the performance at the LSLS (PGA_C/PGA_D from 8% to 100%) and at collapse limit state.

The use of the high efficiency retrofit solutions such as base isolation reduces the seismic demand on the superstructure, decreasing the accelerations and drift. Because seismic shear force demand on structural members significantly decrease, local failures are shifted to high return periods resulting in a significant reduction of the $EAL_{s,direct}$ to 0.31%. When base isolation is combined with local FRP strengthening interventions to achieve a PGA_C/PGA_D ratio equal to 100%, a further reduction of the $EAL_{s,direct}$ to 0.25% can be observed. No collapses were detected in the FPS devices since they were designed to sustain a displacement demand at LSLS. For higher intensities, the collapse of the superstructure is detected and thus, there is no need for a specific check on the FPS system.

The comparison in terms of the percentage reduction of the EALs respect to as-built configuration is reported in Table 7. It shows that the FRP strengthening allows to reduce the losses of about the 40%, the Rebuilt configuration of about the 61%, the base isolation of about the 82% and the base isolation combined with FRP of about the 86% respect to the as-built configuration. Furthermore, a significant increase in terms of the seismic safety respect to the as-built configuration can be achieved (i.e. +72%, +92%, +82% and + 92% for the FRP strengthened, Rebuilt, Base isolated and Base isolated+FRP configurations, respectively).

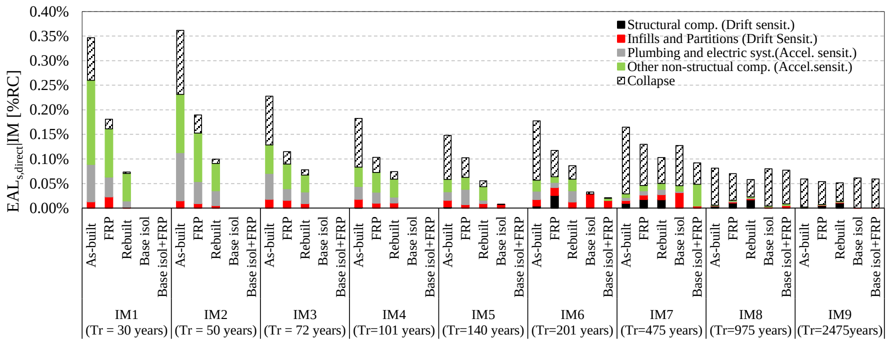

Figure 46. Disaggregation of direct repair costs at increasing IMs for each building configuration.

The disaggregation of the $EAL_{s,direct}$ depicted in Figure 46 in the expected repair cost of each of the structural and non-structural components for a given IM (namely return period T_R) provides important insights on the strength and weaknesses of each strengthening solution. It is worth noting that for each of the building configuration the sum of the $EAL_{s,direct}$ associated to each IM corresponds to the total $EAL_{s,direct}$ reported in Figure 45.

In particular, with reference to the as-built configuration low intensity earthquakes (i.e. IM1, IM2 and IM3) contributes to more than 50% of the total losses. This is related to the high frequency of occurrence of low intensity earthquakes in high seismicity regions such as Italy and to the high vulnerability of existing RC buildings that can be severely damaged at the non-structural components under low intensity earthquakes (Del Vecchio et al. 2020). The damage to non-structural components (i.e. the sum of infill and partitions, Plumbing and electrical systems and other non-structural components) is the majority of the repair cost until the IM4 and it is equally distributed between accelerations and drift sensitive non-structural components. Beyond IM4 the collapse of the buildings becomes dominant in the distribution of the repair costs. The $EAL_{s,direct}$ attributed to the collapse are function of the number of realizations resulted in collapse and the total cost of the building demolition and reconstruction and it cannot be further disaggregated. At large IMs the contribution of drift sensitive structural components becomes significant and higher than non-structural components.

The use of FRP wrapping in the seismic strengthening intervention improves the seismic performance of the case study building at the LSLS moving the collapse to high IMs. This results in a significant reduction of $EAL_{s,direct}$. In particular, the contribution of the collapse to $EAL_{s,direct}$ becomes higher than 50% between the IM6 (T_R=201 years) and IM7 (T_R=475 years). Indeed, the FRP system was designed to sustain the 80% of the seismic demand at LSLS. The distribution of the repair costs between the different components does not change significantly with respect to the as-built configuration since that FRP do not modify the lateral response of the building in terms of EDPs. The same considerations can be drawn for the Rebuilt configuration where the collapse becomes dominant in the $EAL_{s,direct}$ at the IM7 since the building is designed to sustain the 100% of the seismic demand suggested by the Italian building code (MIT 2018). At the same IM, the repair costs associated to the collapse characterize the $EAL_{s,direct}$ of the two base isolated configurations designed to sustain 90% and 100% of the seismic demand at LSLS. By contrast, the use of base isolation significantly reduces the $EAL_{s,direct}$ at low IMs, which are almost null until IM 5. This is due to the significant reduction of acceleration and drift demand on the superstructure, showing the benefits of a seismic protection strategy that is very effective in reducing $EAL_{s,direct}$ due to the frequent low intensity earthquakes.

Similar considerations can be drawn considering the $EAL_{s,indirect}$. The indirect losses related to the relocation of the occupants are evaluated considering the previously described approach considering the building downtime assessed by using the PACT software. With reference to the case study building, considering that it was occupied by 21 people and an annual repair time of a 44.2 days a total indirect loss of about 7391 € is computed. This cost is then normalized by reconstruction cost of the building resulting in $EAL_{s,indirect}$.= 0.40%. It is the 23% of the $EAL_{s,direct}$ remarking the importance of assessment of indirect costs to have reliable estimation of the losses. The same approach is used to assess the $EAL_{s,indirect}$ for all the retrofitted configurations. The direct comparison with the as-built configuration allows to assess the savings due to indirect losses ($\Delta EAL_{s,indirect,}$ see Table 7) about -40%,.-63%, .-82%, . -85%, the FRP, Rebuilt, Base isolated and Base isolated+FRP configuration, respectively. The reduction of the $EAL_{s,indirect}$ is due to the reduction in the downtime for the different retrofit solution considered due to the effectiveness of the strengthening intervention.

4.2.4.3 Cost of the strengthening interventions

In order to estimate the PBT, an estimation of the costs needed to implement the proposed retrofit solutions is required.

Table 7. Cost of the proposed retrofit solutions

	FRP	Rebuilt	Base isolated	Base isolated+ FRP
$\Delta_{PGAc/PGAd}^{*}$	+72%	+92%	+82%	+92%
$\Delta_{EALs,direct}^{*}$	-40%	-61%	-82%	-86%
$\Delta_{EALs.indirect}^{*}$	-40%	-63%	-82%	-85%
1) Direct cost (€)	195˙700	1˙848˙000	488˙543	(Base isol.) 488˙543 (FRP) 76˙000 (Base isol.) 214˙492

2) Repair cost related to strengthening	125˙140	-	214˙492	(FRP) 17˙680
3) Other costs (€)	133˙010	-	130˙131	130˙131
Total cost (€)	**453˙850**	**1˙848˙000**	**833˙166**	**926˙847**
Total cost (%RC)**	**24.5%**	**100%**	**45.1%**	**50.1%**

* Calculated respect to the As-built configuration (i.e. PGA_C/PGA_D = 8%, $EAL_{s,direct}$ = 1.75%, $EAL_{s,indirect}$ = 0.40%);
**Normalized by the total reconstruction cost of 1˙848˙000 €

All the direct and indirect costs related to the complimentary actions should be considered. In this paper, the actual strengthening costs monitored during the L'Aquila reconstruction process is considered to have reliable estimations. They were estimated by the practitioners engaged by the owners based on the Abruzzo region price list (STR.LL.PP. 2017) and then checked and approved by a government technical committee (Di Ludovico et al. 2017). The costs of the implementation of the retrofit technique are reported in Table 7 along with the benefits in terms of increased seismic safety ($\Delta_{PGAc/PGAd}$), reduced losses related to direct repair costs ($\Delta_{EALs,direct}$) and reduced losses related to indirect repair costs ($\Delta_{EALs,indirect}$) with respect to the as-built configuration. The costs are divided in three parts: direct costs (including the cost of the materials/devices, installation and finishing), repair costs related to strengthening interventions (including all the costs of the complimentary actions) and other costs (including the cost of safety measures, field installation, professional fees).

The cost of demolition and reconstruction (Rebuilt) is assumed equal to 1˙848˙000 € as discussed in the previous section. The cost analysis shows that the cost of FRP strengthening solution is about the 24.5% of the total reconstruction cost. This complies with the mean value of strengthening cost of the E-rated building of the L'Aquila database retrofitted with techniques different form base isolation, equal to 24% (Di Ludovico et al. 2017). Thus, by investing about 1/4 of the total reconstruction cost, a significant increase in the seismic safety (PGA_C/PGA_D) of about 72% and a reduction of the EALs of about the 40% can be achieved. The use of base isolation allows to achieve very high seismic performance (especially when combined with FRP system) with a cost of intervention of about the 50% of the %RC.

4.2.4.4 Pay-Back Time (PBT)

In order to compare the cost and the benefits of the proposed retrofit solutions by means of a unique parameter, the PBT of the economic investment is calculated. First, the curve representing the recovery of the initial investment should be evaluated. At the time of the initial investment (year zero), there is a debit equal to the cost of intervention (see last raw of Table 7). Every year the annual savings due to the reduction of direct and indirect EALs are deduct to the initial cost. The annual savings are evaluated through the difference between the $EAL_{AS\text{-}BUILT}$ and the $EAL_{RETROFIT}$ (Δ_{EALs}). The PBT can be easily calculated as the ratio between the initial cost and the annual savings.

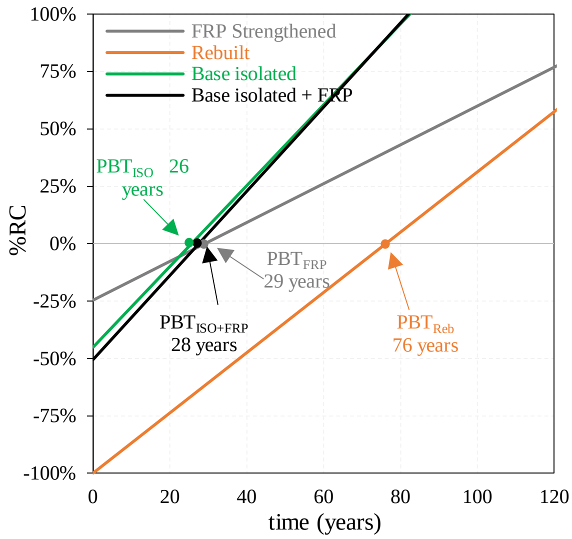

Figure 47. Pay-Back Time for the different retrofit solutions

From a graphic standpoint, the intersection between the curve representative of the initial investment in terms of %RC and its reduction due to annual savings (i.e. recovery of the investment curve) and the horizontal axis identifies the PBT. With reference to the case study building, the curves of the recovery of the investment and the PBT of the four proposed retrofit solutions are reported in Figure 47.

It is worth observing that the slope of the curves directly depends by the Δ_{EALs}. This is due to the assumption of neglecting the time value of money at this stage. Further details on the reliability of this assumption are provided at the end of this section. The strengthening solutions with high savings (high Δ_{EALs}) such as the ones employing base isolation have a steeper curve than FRP strengthened or Rebuilt configuration. This reflects the effectiveness of the strengthening solution in reducing the expected losses and thus, protecting the structural and non-structural components from expected damage and increasing the safety of the entire building against the collapse

The three retrofit solutions have a similar PBT in the range 26-29 years that is significantly smaller than the one associated to the Rebuilt solution (76 years). This remarks the convenience in the retrofitting of existing RC building respect to the demolition and reconstruction. Even though the retrofit solutions using base isolation have an high initial cost (45.1% and 50.1% for Base isolated and Base isolated+FRP, respectively), they have a PBT (26 years and 28 years, respectively) smaller than the FRP-based retrofit solution (29 years). This is because of the higher savings allowing for a faster recovery of the initial investment.

It is worth observing that the Rebuilt configuration, despite the benefits to the curve of losses, has a PBT higher than all the other retrofit solutions, due to the very high initial cost.

Note that base isolation and base isolation+FRP lead to a safety index at LSLS greater than the FRP-based solution.

The application to this case study building shows the reliability of the PBT as a meaningful parameter to drive the stakeholder in selecting the most convenient retrofit solution. In Figure 47 the PBT doesn’t take time value of money into account, thus leading to PBT lower than a discounted PBT. To account the present value of future cash inflows an assumption on the discount of the value of future cash flows to reflect what they're worth in the present day is needed. For this case study, a simulation of the discounted PBT was performed considering the discount rates provided by the Italian Ministry of

Economic Development. The discounted PBT was calculated using the discount rate and applied to the savings. The application of this procedure was implemented by the following formulation:

$$Savings_{disocunted} = \frac{Savings}{(1+c)^t} \tag{12}$$

where *"savings"* are calculated as above, *"c"* is the discount rate given by the Italian Ministry for each year to date, *"t"* is the time represented by the years. The discount rate comes from the database of the Italian Ministry of Economic Development. The value changes from year to year and is available up to the current year. In order to obtain the value for future years needed to calculate the PBT, a fittiing was made to the available data, as shown in Figure 48.

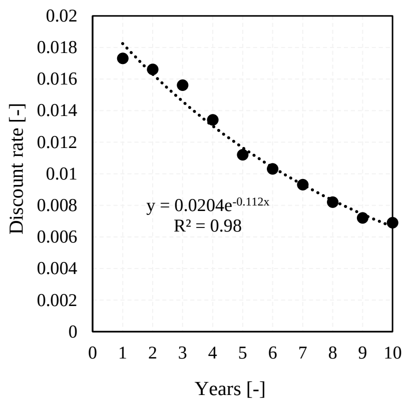

Figure 48. Fitting for the evaluation of discount rate

The time *'t'* represents the number of years from the application of retrofit interventions. Once all the parameters are available, the PBT was recalculated considering these variables and the results are shown in Figure 49.

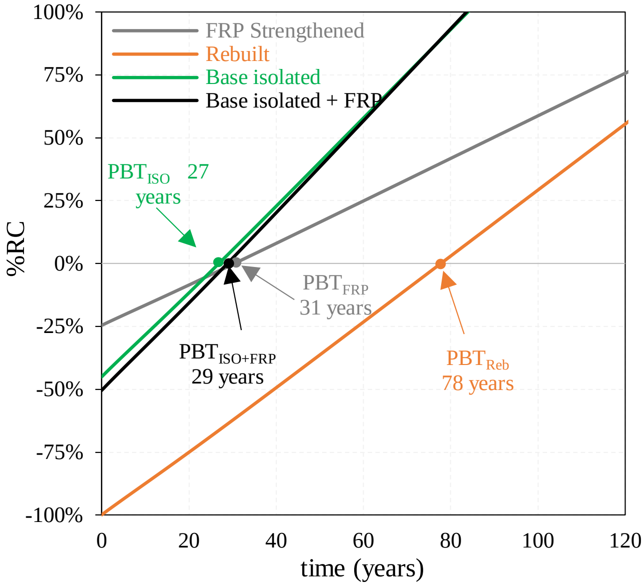

Figure 49. PBT accounting for the influence of the discount rate

The trend of the return on the economic investment does not change when the valuation is considered without the discount rate. There is a small change in the value of the PBT from 26-29 years to 31-34 years for the proposed retrofit solutions. Moreover, this is justified by the reduction in annual savings gains due to the discount rate, as shown in (Eq.12).

4.3 Pay-Back Time as design parameter

In order to validate the proposed methodology on a portfolio of RC buildings typical of the L'Aquila area, the study has been extended to the full database of existing RC buildings retrofitted by means of base isolation in L'Aquila (see Table 1). The results will be used to calibrate a simple relationship that can be used in the common design practice to estimate the PBT of base isolated buildings once that the cost of the intervention and the safety index (PGA_C/PGA_D) at the LSLS are known.

The calculation follows the framework described in Figure 40 and some assumptions, as described below, are made to define the loss curve of each of the buildings in the as-built and base isolated configuration from available data. In order to extent this approach to the entire database, the results of the seismic performance assessment carried out by the practitioners engaged by the owners are herein used to assess the $EAL_{s,direct}$. The actual retrofit costs and the safety index before and after the retrofit intervention are reported in Table 1. Furthermore, the $EAL_{s,direct}$ of the buildings in the as-built configuration was assumed equal to 1.50% according to available literature studies addressing the detailed or large-scale assessment of the EALs for infilled RC buildings typical of the existing buildings in the Mediterranean area (Cardone and Perrone 2017; Polese et al. 2020). This assumption does not allow to account for the building-to-building variability in the assessment of the $EAL_{s,direct}$ in the as-built configuration. However, it is strictly needed to extent the whole methodology to the entire dataset of buildings due to lack of data on the construction details for all the buildings. However, it is worth mentioning that the building characteristics are then included in the assessment of the performance of the retrofitted configurations by means of the analysis conducted by the practitioners in the assessment of the $\zeta_{e(RETROFIT)\ index}$. The $EAL_{s,direct}$ of the building in the retrofitted configuration by using base isolation alone or combined with other techniques is computed by using the approach suggested by the Italian guidelines for seismic risk assessment of constructions (Cosenza et al. 2018) that it provides accurate results, through a comparison with the results described above for the case study building in the base isolated configuration.

Similarly, the $EAL_{s,indirect}$ for the both the as-built and base-isolated configurations are assumed constant and equal to 0.40% and 0.07%. The sum of the $EAL_{s,direct}$ and $EAL_{s,indirect}$ provides the total EALs used to estimate the pay-back time for each building in the dataset.

The curves of the return of the economic investment for each of 59 buildings are depicted in Fig 12a (grey lines). The black curve is the best fitting of the full dataset defined by the equation %RC = -41.8% +1.46%*year. Where 41.8% is the mean cost of intervention of the full dataset of base-isolated buildings and 1.46% is the mean annual savings. The mean PBT of the full dataset is about 28.9 years (standard deviation of about 6.8 years) that is in agreement with the

PBT calculated based on refined analysis on the case study building. This confirms the applicability of the proposed procedure and the accuracy of the proposed simplified equation to have a first rough estimation of the PBT. In order to provide to the designer a useful and simple tool to assess the PBT and making proper cost-benefits considerations, the results of the calculation of the PBT for the full dataset of 59 buildings are used to derive a simple equation that correlates the PBT to the seismic performances, in terms of safety index (PGA_C/PGA_D) at LSLS. The latter is commonly used to quantify the effectiveness of a retrofit solution in the common design practice

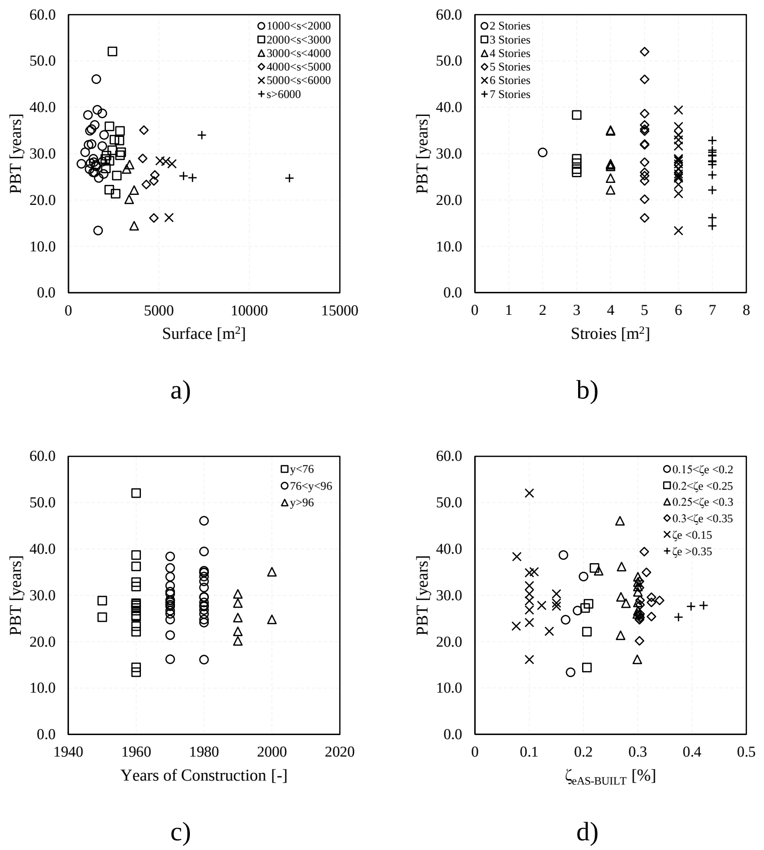

Figure 50. Correlation between the PBT and main characteristic of the building: a) Surface, b) Stories, c) Years of construction, d) Safety index in the as-built configuration

The objective of proposing a useful formulation to quantify PBT has led the author to correlate PBT with the main characteristics of the building such as surfaces, year of construction, number of floors and safety index for the as-built configuration, as shown in Figure 50.

The different variables are divided into subgroups to determine the global or local correlation with PBT.

As can be seen in Figure 50, no trends or correlations can be identified between the PBT and the different variables analyzed. In order to quantify convenience and safety, a correlation was also established between the PBT and the safety index, as shown in Figure 51b.

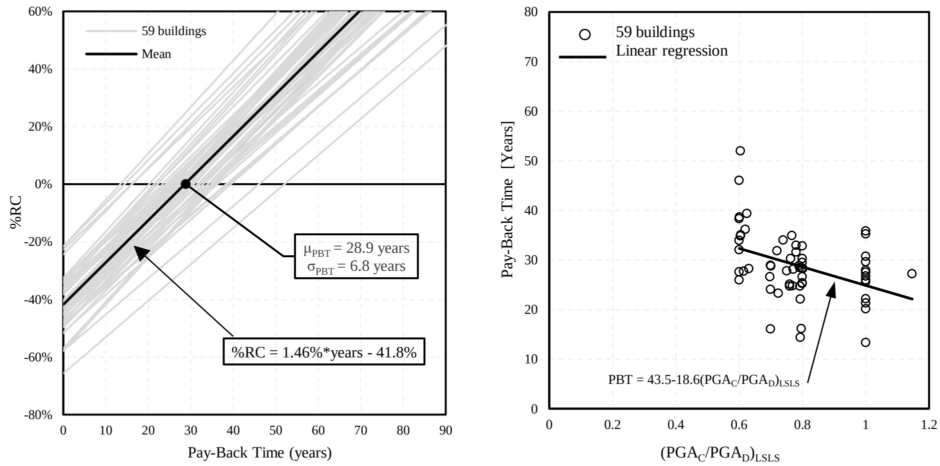

a) b)

Figure 51: Pay-Back Time for the database of 59 base isolated buildings in L'Aquila: (a) return of the investment curves; (b) interpolation of the PBT as function of the safety index $(PGA_C/PGA_D)_{LSLS}$

A linear regression is used to fit the data (see Figure 51b). A large scatter can be observed in terms of PBT. It is due to the different %RC and different safety index (PGA_C/PGA_D) associated to each building. The equation PBT = 43.5 – 18.6$(PGA_C/PGA_D)_{LSLS}$, outlines that higher is the seismic performances achieved and more convenient, namely lower PBT, is the proposed base isolation retrofit solution. If the mean ratio $(PGA_C/PGA_D)_{LSLS}$ = 0.80 of the full dataset of 59 buildings is used in the proposed equation, a PBT of about 28.6 year very close to the mean reported in Fig. 12a is obtained. It is worth noting that due to lack of data the proposed equation can be used only for safety index ranging between 0.60 and 1.15. This equation can be a useful tool to define the target safety index·$(PGA_C/PGA_D)_{LSLS}$ for the design of the base isolation system considering the desired PBT. It is worth mentioning that this is a preliminary tentative of deriving a simple formulation to assess the PBT and the results cannot be generalized to all type of buildings. Due to limitations of the dataset of buildings and the high dispersion in fitting the data due to the high variability of actual retrofit costs, no general conclusion can be drawn. Further research studies are needed to extent this results to a larger dataset of building considering different sites.

CHAPTER 5 – A TOOL FOR THE RAPID ASSESSEMENT OF THE PBT KNOWING THE MAIN BUILDING CHARACTERISTICS

The methodology proposed in the previous section has been implemented in a simplified tool that allows the estimation of PBT once the main building characteristics are known.

The main scope is to provide to designers a simple tool to evaluate the benefits of different retrofit solutions and calculate the related PBT without performing the sophisticated calculations showed in the previous section. The PBEE framework discussed in the previous section is fully implemented in this tool. However, some simplifications are needed to allow the software to perform a structural analysis knowing only the main building characteristics. The main assumptions, simplifications and the strategy for the implementation in a Matlab code are discussed in the following

5.1 Simplified methodology

The procedure implemented in this tool is based on the methodology described above. A simplified approach has been adopted to perform some analyses (Figure 52). It consists of:

- **Building definition:** The structural analysis needed to assess of the seismic performance of the building and the EDPs for the successive damage analyses, relies on non-linear analysis of the structural system reduced to 2D multi degree of freedom (MDOF) with number of degrees of freedom corresponding to the number of the building floors. The simplified model adopted is justified by the consistency of the EDPs with the refined model that allows this assumption.
- **Hazard Analysis:** the approach discussed in the previous section is fully implemented in the code, the hazard analysis defines the hazard curve, considering nine return periods ranging from 30 to 2475 years, expressed as MAFE (Mean Annual Frequency Expected) vs the $S_a(T_1)$ spectral acceleration at the fundamental period of the buildings. It is worth mentioning that the proposed tool does not perform the hazard analysis itself. Thus, the response spectra should be provided as input. Other software allowing an easy record selection can be used for this purpose (e.g. Rexel, (Iervolino et al. 2010)).

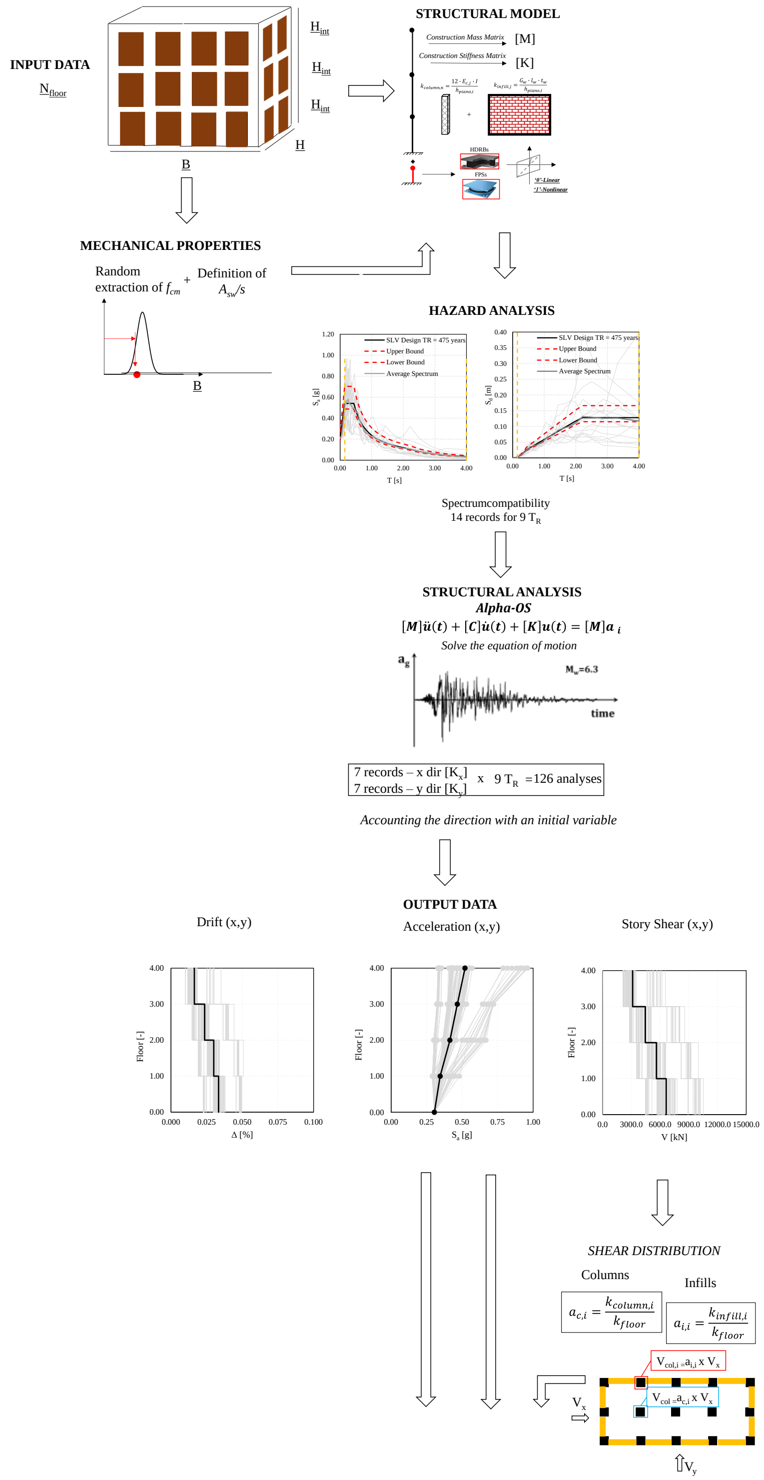

Figure 52. Flow chart of the main tool functionalities

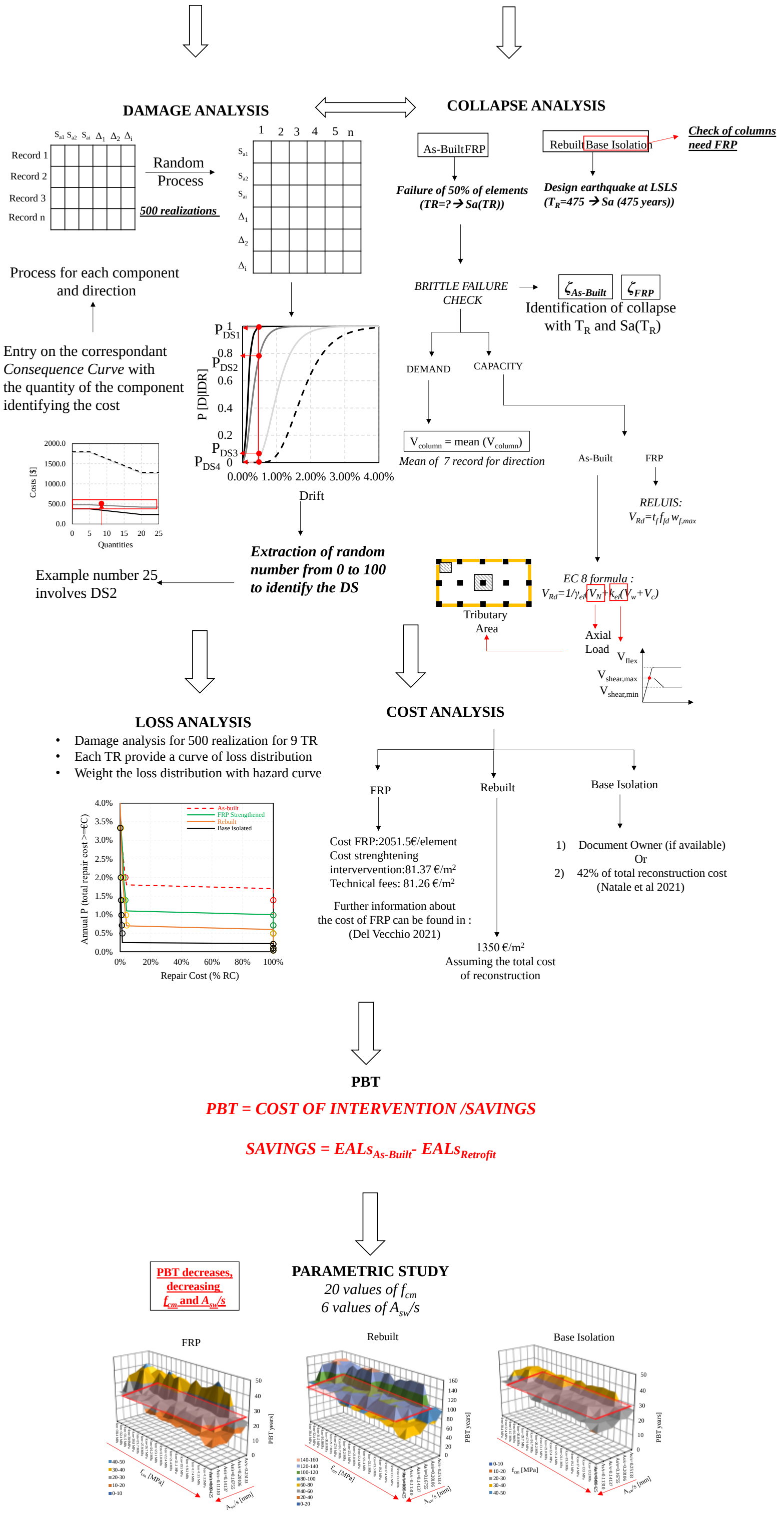

Figure 52. Flow chart of the main tool functionalities (Continue)

- **Structural analyses and seismic performance assessment:** the vulnerability of the structure and the EDPs should be assessed using NLTHs relying on the simplified 2D models previous described. In order to properly assess the drift and acceleration demand of RC buildings with stiff infill, their contribution to the lateral response should be properly considered. The seismic performance is evaluated by checking the brittle failure of the structure by comparing the capacity of the columns with the stress based on the series of NLTHs located under the building. The collapse of the structure is considered to occur when more than 50% of the structural elements collapse (Galanis and Moehle 2015). The return period of the collapse and, consequently, the associated spectral acceleration required for the successive loss analyses are defined
- **Estimation of Engineering Demand Parameters (EDPs):** the approach discussed in the previous section is fully implemented in the code, the EDPs are calculated for the as-built configuration and for the isolated configuration, because the FRP and the rebuilt configuration are assumed to have the same EDPs as those in the as-built configuration, since the FRP does not change the dynamic properties of the structure (Bakis et al. 2002) and the main change in the rebuilt configuration is the seismic details that are missing in the as-built configuration. The EDPs are estimated for the set of NLTHs for both directions, and the MDOF model is solved by using the numerical method, α- OS SPLITTING METHOD (Combescure and Pegon 1997)
- **Evaluation of damage and losses:** the damage analysis is based on the procedure implemented in PACT (ATC - Applied Technology Council 2012a) with some simplifications adopted. The fragility curves of the main drift and acceleration sensitive components are used: Infill, partition walls, beam-column connection, chimney, tiles, cold/hot water pipe, raised floor, lightning, low voltage, plumbing. They are available by the mean and CoV value in the PACT library and in the

literature for the last development related to infill (Cardone et al. 2018) and beam-column joints (Cardone 2016). In the context of fragility curves, there is the consequence curve defined by two values for the quantity and two for the cost: upper and lower values, then a linear function is implemented for the quantity between the two boundaries. The loss assessment analyses allow to evaluate the EALs for the four configurations studied and to define the decision variable in terms of the PBT.

- **Identification of potential weakness:** the assessment of the building in the as-built configuration allows to evaluate the vulnerability, the potential structural weakness as-well-as the main sources of economic losses. The explicit modelling of infills allows to identify the premature shear failure at the top of the columns as commonly found in the post-earth- quake damage surveys in the aftermath of recent seismic events in the Mediterranean area.
- **Design of the retrofit alternatives:** the retrofit solutions considered are mainly three techniques: the application of FRP to increase the capacity of the column, as the interaction with rigid infills leads to premature shear failure due to lack of seismic details. The capacity of the columns with the installation of the FRP system is calculated according of the approach suggested by the ReLUIS guidelines (2011), considering the maximum possible length, w_{max}, of the FRP for the capacity. The brittle failure test is performed again, and the collapse of this configuration is evaluated based on the same hypothesis as the one described above. Application of the base isolation system requires modification of the structural model, adding another degree of freedom to the floors. Two possible behaviors can be chosen for the base isolation system: linear, for a simplified analysis if the equipment allows this choice, or hysteretic elastic-plastic with hardening, which is more appropriate for the isolated system. The base isolation is designed to withstand the design earthquake in accordance with current

codes at LSLS (475 years), giving the structure a safety index of one. To guarantee this value, because, as described in (Natale et al. 2020) sometimes the base isolation cannot fix all the failures of the columns, a combined FRP intervention is considered, applying this system to the columns that fail after the installation of the base isolation. In the rebuilt configuration, the structure is demolished and rebuilt according to modern rules that guarantee the capacity of the building for 475 years design earthquake. Thus, a spectral collapse acceleration associated with a return period of 475 years is considered for the base isolation and the rebuilt configuration, which consequently results in a safety index of one.

- **Estimation of the cost of intervention, annual savings and PBT:** The PBT is evaluated as the ratio between the cost of each technique and the respective savings as the difference between the EALs in the as-built configuration and the EALs as a result of applying the retrofit solution. The cost is assessed for the FRP taking into account three contributions: a value of 2051.5 €/element , value of 81.37 €/m^2 for the strengthening connected with intervention and 81.26 €/m^2; for the base isolation is obtained from the owner of the document if possible, otherwise it is assumed a cost equal to 40% of the total reconstruction cost, for the reconstruction is assumed a value of 1350 €/m^2

5.2 Implementation in a MATLAB code

The whole procedure is implemented in MATLAB code, which consists of different scripts representing the steps of the described methodology.

5.2.1 Input

The first script, i.e. the first step, is the definition of the main characteristics of the building. The required input data are:

- Mass, it is proposed to calculate the mass as in finite element software concentrating in the master joint and thus taking into account the mass of the beam, column, infill, stairs and balcony
- Geometry of the columns, base and height necessary to evaluate their contribution to the stiffness (the stiffness of the beams is neglected since an infinitely rigid bending behavior is assumed) and to the capacity.
- Interstorey height, for the stiffness of columns and infills.
- Number of floors, two values must be given, the first for the as-built configuration (fixed base), the second for the configuration with base isolation, adding one unit to the previous value, representing the degree of freedom of the isolation system.
- Extension (length), shear modulus and thickness of the infills necessary to evaluate the stiffness and the maximum capacity expressed by the F_{peak} (Eq.5) of the elastic branch in the behavior of (Panagiotakos and Fardis 1996).
- Resistance of concrete and steel.
- Variable for the behavior of the base isolation system, "*0*" for linear behavior, "*1*" for elastic-plastic with hardening behavior.
- 14 data sets, according to the spectrum compatibility analyzes, the relative scale factor for the nine-return period and the duration of the data set (initial and final time) with the interval time, dt.
- Variable for selecting the time interval for recordings, "0" the original time interval, "1" the time interval selected by the user (specifying relative parameters).
- Parameters for defining the base isolation system: two types of devices can be modelled, the friction pendulum system and the elastomeric bearing; since the structure is an MDOF, the isolation system has grouped all the devices used on the columns.
- The value of the integration coefficient is between (-1/3.0), the numerical damping of the chosen method depends on this value.

Two clarifications are necessary to better identify the function of the tool in terms of concrete resistance, since the purpose of the work is to perform a parametric study on different types of buildings retrofitted using the base isolation, where the f_{cm} (compression concrete resistance) and the ratio A_{sw}/s (the mechanical percentage of transverse reinforcement) are varied. 20 values of the concrete resistance were extracted by a random process from a Gaussian distribution based on the data shown in (Masi and Vona 2009) on the concrete resistance in the existing buildings. In connection with this, 6 values for the ratio A_{sw}/s were chosen, namely two diameters for the transverse reinforcement (φ 6- φ 8) and three values for the distance between two consecutive reinforcements (20-25-30 cm).

Regarding the modeling of the base isolation system, as described above, two behaviors are available, the linear and the bilinear (which identifies the elastic-plastic with the hardening behavior). For the linear behavior, the equivalent stiffness, k_{eff} is the only necessary parameter, while for the bilinear behavior four parameters must be specified: the elastic stiffness, k_a, the post-elastic stiffness, k_b, the yielding force, F_y and the yielding displacement, d_y. For the frictional pendulum system (FPS), k_b and F_y can be identified by the equation, while $k_{a,}$ is assumed (in this work) equal to 400 kN/m (Ponzo et al. 2015) the yielding displacement is calculated as follows:

$$d_y = \frac{F_y}{k_b} \tag{13}$$

For the elastomeric bearing, instead, the parameters were determined based on (Pellecchia et al. 2021), which allow to identify a bilinear behavior of this device through an energy equivalence The formula used to calculate the required parameters is as follows:

$$\Delta = d_{max}^2\left(\pi^2\xi_{eff}^2 - 6\pi\xi_{eff} + 4\right) \tag{14}$$

$$F_y = \frac{1}{5}k_{eff}\left[d_{max}\left(\pi\xi_{eff} + 2\right) \mp \sqrt{\Delta}\right] \tag{15}$$

$$k_b = \pm\frac{k_{eff}\left[\sqrt{\Delta} + d_{max}\left(\pm 3 \mp \pi\xi_{eff}\right)\right]}{5d_{max}} \tag{16}$$

$$k_a = 5k_b \tag{17}$$

$$d_y = \frac{1}{4}\left[d_{max}\left(2 - \pi\xi_{eff}\right) \mp \sqrt{\Delta}\right] \tag{18}$$

where ξ_{eff} is the damping of the device usually provided by the owner

The input of all the given data allows to perform a structural analysis, a damage analysis and a loss analysis and to obtain the payback time for the different retrofit solutions studied, combined with the safety index, ζ_e, achieved for each of them to evaluate the best solution.

5.2.2 Dynamic properties of the structure

The properties of the columns and the infill defined in the input domain allow the stiffness matrix to be defined, and the mass matrix is also determined.

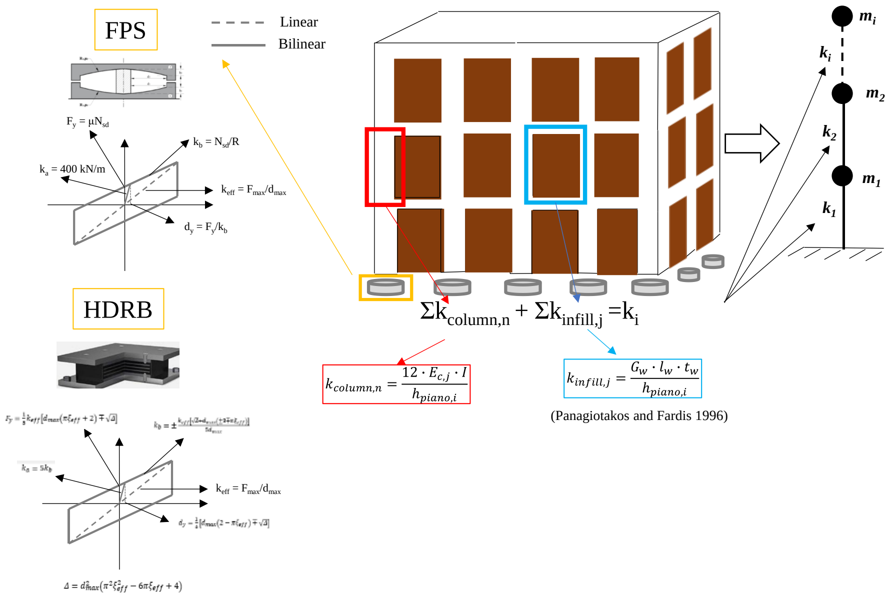

Figure 53. MDOF model and stiffness definition

In accordance with the adopted model, a MDOF (Multi-Degree of Freedom) (Figure 53), the mass matrix is a diagonal matrix that contains on the main diagonal the value of the mass of each floor, as shown in Figure 54

$$\begin{bmatrix} m_1 & 0 & 0 & 0 \\ 0 & m_2 & 0 & 0 \\ 0 & 0 & \dots & 0 \\ 0 & 0 & 0 & m_i \end{bmatrix}$$

Figure 54. Mass Matrix

The stiffness associated with each degree of freedom (mass) takes into account the stiffness of the columns and the infills of the floor, both in the x and y directions. The beams are neglected in the evaluation of the stiffness. The stiffness of the columns is calculated assuming a cantilever restrained at the top and bottom, which is why the following formula was used:

$$k_{column,i} = \frac{12 \cdot E_{c,j} \cdot I}{h^3_{piano,i}} \tag{19}$$

where the $E_{c,j}$ is the modulus of elasticity of the concrete, denoted by the subscript *'j'*, as it varies with the different values of the concrete obtained from the random process, and its evaluation is carried out according to the rule (Infrastrutture and Trasporti 2018), *I* is the inertia of the column (which varies with direction and is equal to $BH^3/12$ or $HB^3/12$, *B* and *H* are the base and the height of the column, respectively), and $h_{piano,i}$ is the interstorey height. The stiffness of the infill walls is calculated using Eq.2 The total stiffness is simply calculated as the sum of the stiffness of the columns and the infill walls, taking into account the direction of study. The script automatically takes into account the different directions through an initial variable defined in the input (which is defined as default and does not need to be chosen by the user). The stiffness matrix in accordance with the structural model has the following form:

$$\begin{bmatrix} k_1+k_2 & -k_2 & 0 & 0 \\ -k_2 & k_2+k_3 & -k_3 & 0 \\ 0 & -k_3 & \dots & -k_n \\ 0 & 0 & -k_n & k_n \end{bmatrix}$$

Figure 55. Stiffness Matrix

As for the direction, also for the different configurations as-built (FPR/Rebuilt) and the isolated base, a preliminary variable has been defined in the input that allows the code to perform the analysis for both structural models.

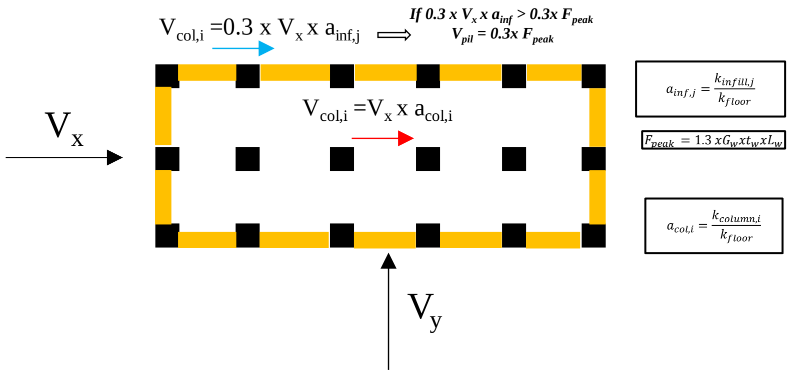

Figure 56. Distribution of the shear on the columns

The ratio between the value of the stiffness of each column and the infills compared to the value of the total stiffness of the floor makes it possible to determine a coefficient suitable to distribute the shear forces to each component. For the columns interacting with the infills, the shear of the infill was measured, and for the others, the shear due to their stiffness (Figure 56).

The identification of the mass and stiffness matrix allows the code to evaluate the damping matrix and the dynamic properties of the structure. The damping matrix is evaluated by proportionality with the mass and stiffness matrix and the Rayleigh coefficient:

$$C = \alpha_0 \cdot M + \alpha_1 \cdot K \tag{20}$$

where α_0 and α_1 are the Rayleigh coefficients assuming the following formulations:

$$\alpha_0 = \frac{2\omega_i\omega_j(\xi_i\omega_j - \xi_j\omega_i)}{(\omega_j^2 - \omega_i^2)} \tag{21}$$

$$\alpha_1 = \frac{2(\xi_i\omega_i - \xi_j\omega_j)}{(\omega_j^2 - \omega_i^2)} \tag{22}$$

where ω_i ,ω_j ,ξ_i and ξ_j are the frequency and damping ratio for the first two modes of vibration of the structure.

An eigenanalysis is performed, the eigenvalues and eigenvectors are obtained and from them the frequency and period of the structure are obtained.

5.2.3 Numerical integration

The 14 records (7 for each direction, x and y) provided in the input phase are imposed to the MDOF and the dynamic equation is solved using the α- OS SPLLITING METHOD (Combescure and Pegon 1997). In order to take into account the change of the stiffness matrix for each computational step, considering that each DOF has a linear behavior, except for the DOF related to the base isolation system, which allow the choice between two options, namely linear and elastic-plastic with hardening, a script is implemented in the method to recover the matrix at each step in order to obtain the correct seismic response of the model.

The output data provided by the solution of the 14 records are the profile of acceleration, drift, and shear. The script solved the equation of motion for 14 records for 9 return periods for a total of 126 analyses for a single configuration. Assuming that the analyses are performed for two configurations, as-built and base isolated, a total of 252 analyses are performed. Moreover, the variability of the f_{cm} is considered, which is equal to the value 20 in this work. For a single building, the script performs 5040 analyses, usually with an elapsed time of 2 hours, but several parameters affect this result.

In order to perform the successive verification necessary to identify the collapse of the structure and the efficiency of the retrofit solution, and to obtain further information for the damage analyses, the stresses acting on the columns are evaluated for each data set and, of course, for each return period.

The output data provides the shear for each floor. This shear is multiplied by the coefficient based on the previously determined stiffness of the columns and infills, which gives the value of the shear measured by each column and infill in the story. As described earlier, the free columns, i.e., the columns that do not interact with the infill walls, are loaded by their stiffness, while the columns that interact with the infill walls are loaded by the shear force of the infill walls. In this method, it is assumed that the shear force transmitted by the infills is 1/3 of the total shear force of the infills due to their stiffness. This assumption is consistent with various experimental tests where it has been observed that a mechanism of three bracing occurs at the infill walls subjected to seismic action.

In accordance with (Iervolino et al. 2007), the value of shear for performing the brittle check is provided by the average of the 14 records (7 for each direction), to obtain a single value for comparison with the capacity of the column, the procedure is applied for all return periods. This assumption can be used based on the compatibility analyses of the spectrum performed in the search for suitable records and on the number of records selected.

In this procedure, a further assumption is made regarding the shear force exerted by the infills on the columns. If the shear force derived from the analyses, which is assumed to be 1/3 of the total shear force, exceeds 1/3 of the capacity of the infill, F_{peak} (Equ), this last shear force is assumed to be the stress. The result of this procedure is a vector of stresses on each column, which makes it possible to obtain a unique value for the relationship between capacityand demand for the brittle check.

5.2.4 Verification and collapse definition

The brittle failure tests are performed for the different configurations in exam. The first test refers to the as-built configuration to determine the number of failed columns and consequently the collapse that occurs when more than 50% of the elements fail. The collapse is associated with a defined return period, which allows to determine the spectral acceleration of the collapse required for the analysis of the successive losses.

The verification of the brittle failure on the as-built configuration is performed by comparing the previously defined stress with the capacity of the column. The capacity of the column is evaluated using the EC8 formula (CEN 2004a), which is also known as the Bikinis formula.

$$V_R = \frac{1}{\gamma_{el}}[V_N + k_{el}(V_w + V_c)] \tag{23}$$

where:

γ_{el} is assumed to be 1.15 for the primary elements

$$V_N = \frac{(h-x)}{2L_v} min(N; 0.55\ f_c A_c) \tag{24}$$

where:

h is the total height of cross the section

x is the height of the compression part of the cross section (depth of the neutral axis)

N is the axial compressive force (is equal to zero if it is a tensile force)

L_v is the cutting gap

A_c is the area of the section

f_c is the compressive resistance of the concrete

The assumptions considered are: the depth of the neutral axis was assumed equal to the cover concrete and the axial force is evaluated by the area of influence on the column.

$$k_{el} = \left[1 - 0.05 min\left(5, \mu_{\Delta,pl}\right)\right] \tag{25}$$

where:

$\mu_{\Delta,pl} = \theta_m - \theta_y / \theta_y = \mu_\theta - 1$ is equal to the ratio between the plastic part of the chord rotation and the yielding rotation.

k_{el} is considered equal to one, so no deterioration in shear is assumed (Figure 57).

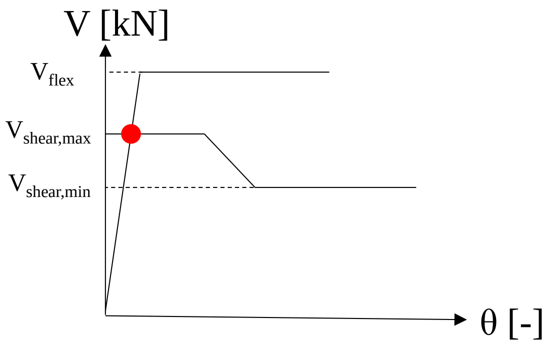

Figure 57. Shear behavior for cyclic loads

This assumption can be justified by the premature failure of the structural component due to lack of seismic details.

$$V_c = \left[0.16max(0.5; 100\rho_{tot})\left(1 - 0.16min\left(5; \frac{L_v}{h}\right)\right)\sqrt{f_c}A_c\right] \quad (26)$$

where:

ρ_{tot} is the geometrical percentage of longitudinal steel

$$V_w = \frac{A_{sw}}{s} f_y (h - c) \quad (27)$$

where:

A_{sw} is the area of the stirrups

s is the distance between two successive stirrups

The tests are performed for the x and y directions for the 9-return period under consideration. In each story, the failures in the x and y directions are combined to determine the total number of collapsed columns. The first return period in which more than 50% of the elements fail then determines the collapse return period for the floor. The minimum return period between all floors is the return period of the collapse of the structure.

The same procedure is followed for the configuration retrofitted with the FRP system, but the checks are performed only for the columns that failed in the as-built configuration. The capacity is evaluated as described below:

$$V_{R,FRP} = t_f \cdot f_{fd} \cdot w_{f,max} \tag{28}$$

Where the t_f is the thickness of the FRP, assumed in this work equal to 0.266 mm, the f_{fd} is the design resistance for the FRP equal to:

$$f_{fd} = \eta \frac{f_d}{\gamma_{FRP}} \tag{29}$$

where f_d is the resistance of the FRP, assumed equal to, 2580 MPa, η and γ_{FRP} are corrective coefficient, assumed equal to 1 and 1.1 respectively.

The w_{max} is the maximum usable length for the FRP defined as:

$$w_{f,max} = B \cdot cos\theta \tag{28}$$

Where B is the base (replace with H in the case of the other direction) of the columns, θ is the applied angle of the FRP, which is assumed to be equal to 45. The collapse is evaluated as for the as-built configuration, but for this retrofit solution, in conjunction with the return period that identifies the collapse, if more than 50% of the elements fail, another return period is calculated, always using the same procedure described previously, when the first failure occurs. The last procedure aims to define the safety index for the retrofit technique used.

The verification of the brittle failure of the columns is also performed when the configuration of the base isolation is analyzed. In this case, the column load capacity calculated with the Biskinis formula, and the stress evaluations described previously, obviously related to the isolated configuration, are compared. The aim is to determine the number of columns that fail after the application of the base isolation system, in order to quantify the further costs incurred by the local strengthening measures with e.g. FRP.

In the case of the FRP solution, the costs are evaluated on the basis of the number of retrofitted columns, assuming a value of 2051.5 €/column, combined with the cost of reinforcement measures of 81.37 €/m^2 and technical costs of 81.26 €/m^2. The sum of all these contributions makes it possible to estimate the cost of the FRP solution. The same cost values are used to evaluate the columns reinforced with FRP in the base isolated configuration.

5.2.5 Damage and Loss Analysis

The structural analysis is followed by the assessment of damage for each component of the buildings through an analysis of losses. The loss assessment procedure is based on FEMA-58 (ATC - Applied Technology Council 2012a)and used in the software PACT. A simplified model is adopted and described below. The steps involved are:

i) *Demand simulation*: A vector containing the EDPs (i.e., peak floor accelerations, peak floor velocity, peak floor drift ratio, and residual story drift ratio at each level in each direction), in this case peak floor acceleration and peak floor drift ratio, from each analysis is compiled. A matrix is created containing the results of one analysis in the rows (7 for each direction) and the values of a demanding parameter in the columns (depending on the number of floors). The entries in the matrix are assumed to be a joint lognormal distribution and are manipulated to compute a vector of median demands (the median vector derived from the set of analyses), variances (or dispersion), and a correlation matrix indicating how each demand parameter varies with respect to the other demand parameters in the set.

After this manipulation, the terms of the diagonal dispersion matrix are augmented using a square root sum approach to account for additional modeling uncertainties and ground motion uncertainties (in the case of scenario-based assessments). The resulting simulated demand rates are statistically consistent with the original demand rate, but better represent the range of possible responses that the building could experience for a given intensity of ground motion ((ATC - Applied Technology Council 2012a).

ii) *Collapse Determination*: For each realization, it is determined whether collapse has occurred or not. Collapse acceleration was defined, as previously described, for the four configurations studied: as-built, FRP, reconstruction, and base isolation. For the FRP system and the as-built system, the spectral acceleration is defined by an evaluation of the collapse, while for the rebuilt configuration and the base isolation, a spectral acceleration corresponding to a return period of 475 years is assumed, as described previously. The spectral acceleration is calculated by an additional script that implements the construction of the spectrum for the different return periods at the site. Thus, once the return period of the collapse and the period of the structure are defined, this script allows the evaluation of the corresponding acceleration. The Figure 58 shows a collapse fragility function for a hypothetical building.

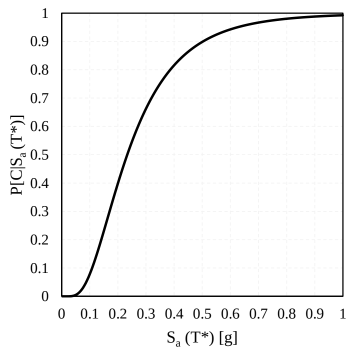

Figure 58. Collapse fragility function for hypothetical building

As an example, a ground motion intensity with a spectral acceleration of 0.5 g, there is a 15% probability of collapse for the fundamental vibration of the building. To determine if a collapse has occurred, a random number between 1 and 100 is generated at each realization. If the random number is less than or equal to the value of the conditional collapse probability multiplied by 100 (i.e., 0.15 × 100 = 15), the collapse is considered to have occurred in that realization. If the number is greater than 15, the collapse is assumed not to occur (ATC - Applied Technology Council 2012a)

iii) *Damage Calculation:* If no collapse has occurred, the damage suffered by each component is calculated. To determine the damage for each realization where collapse did not occur, a vector of simulated demands is determined and a damage state is determined using the fragility functions associated with each performance group, represented in this work by: Infill and partition wall and beam-columns joints, masonry chimney, raised floor, cold/hot water piping, independent lightning, low voltage, sanitary waste, tile roof. The fragility functions are extrapolated using the mean and CoV. Two types of fragility are used in the work, which are mainly related to the acceleration and drift sensitive components. The overall building damage state for realization is the aggregate of damage states in each performance group. Random number generation is used to determine the damage state for each component based on the assigned fragility function.

- *Sequential damage:* Sequential damage states must occur in sequential order, with one state occurring before another is possible. Each sequential damage state represents a progression to higher levels of damage as demand increases. Figure 59 illustrates hypothetical fragility functions for three sequential damage states and a hypothetical realization demand

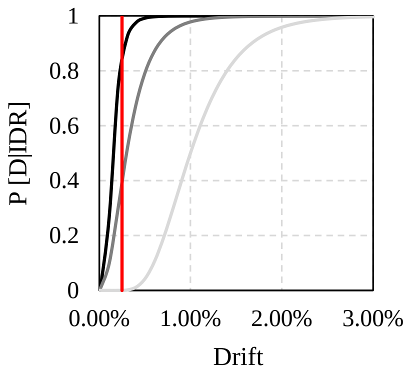

Figure 59. Hypothetical fragility function

Each sequential damage state is assigned a range of numbers. For example, DS1 ranging from (P1 × 100) to (P2× 100), and DS2 ranging from (P2× 100 + 1) to (P3 × 100), where Pi is the inverse probability of incurring damage state “i” at the demand level for the realization, as indicated by the fragility assigned to the performance group. A random number below (P1× 100) indicates that no damage has occurred; a random number between (P_i × 100) and (P_{i+1} × 100) indicates damage state P_i has occurred. For example, the probability of not incurring DS1 or higher is $P_1 = 1 – 0.75 = 0.25$; the probability of not incurring DS2 or higher is $1 – P_2 = 1 – 0.23 = 0.77$; and the inverse probability of not incurring DS3 is $P_3 = 1 – 0.06= 0.94$. Therefore, the range of numbers assigned to no damage would be 1 to 25; the range assigned to DS1 would be 26 to 77; the range assigned to DS2 would be 78 to 94; and the range assigned to DS3 would be 95 to 100. A random number of 97 would indicate that a component has incurred DS3 for the realization. (ATC - Applied Technology Council 2012a)

iv) *Loss Calculation:* The definition of DS allows one to evaluate the loss to realization using the consequence curve for each performance group uploaded in the script with the upper and lower bounds for quantity and cost (a hypothetical consequence curve is shown in Figure 60

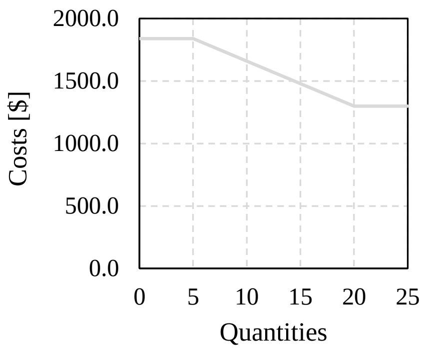

Figure 60. Hypothetical consequence curve

The valuation of losses, assuming a simplified approach, is done by identifying the quantity on the curve related to the group of outputs analyzed and determining the corresponding cost value. The quantities of each performance group are identified in different ways. For the infill and beam-column joint, they are calculated from the design documents, while for the other components used in the work, a tool provided by the ATC must be used (ATC - Applied Technology Council 2012c). For a single structure, the total damage is the sum of the damage sustained by each performance group evaluated as described above.

Loss distributions are developed by repeating the calculation of damage and loss for a large number of realizations and sorting the values in ascending (or descending) order to allow calculation of the probability that the total loss will be less than a given value for a given intensity of earthquake (intensity-based assessment). For example, if damage calculations are performed for 1,000 realizations and the realizations are compiled in ascending order, the repair costs with a 90% probability of exceedance are the repair costs calculated for the realization with the 100th largest cost, since 90% of the realizations had higher calculated costs. (ATC - Applied Technology Council 2012a)

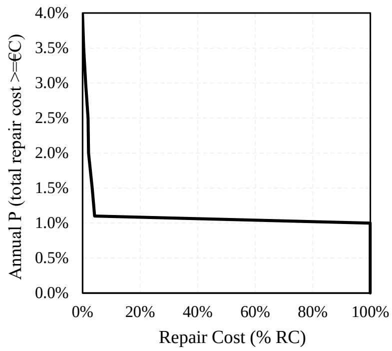

Figure 61. Hypothetical loss distribution

v) *Time Based Assessment:*

Time-based assessments produce a loss curve that represents the total value of a loss (e.g., the cost of repairs) as a function of the annual rate at which that loss is exceeded. The curve is constructed using the results of a series of intensity-based assessments in the specific case 9 (as the selected return period), weighted based on the frequency of occurrence as indicated in a seismic hazard curve for the site.

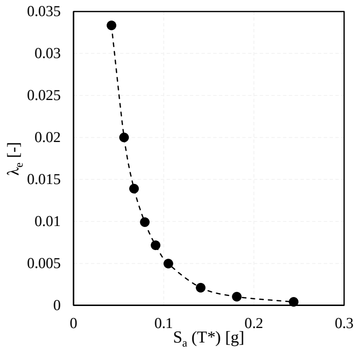

Figure 62. Hypothetical seismic hazard curve

The Figure 62 shows a representative seismic hazard curve in which the annual frequency of exceedance of earthquake intensity, λ(e), is plotted against earthquake intensity e. Earthquake intensity is typically measured as spectral acceleration at the first natural vibration period of the building.

The hazard curve for the site is used with the Eq. 30 to calculate the annual probability that the damage, L, will exceed a value, l:

$$P(L > l) = \int_0^{\lambda} P(L > l|E = e)d\lambda(e) \tag{30}$$

where the term P(L>l|E=e) is the loss curve obtained from an intensity-based assessment for intensity, e., while the dλ(e) is the interval between two succeive probability of occurrence, defined as their difference.

The loss curve (or EAL-Expected Annual Losses) is constructed by: (1) multiplying each loss curve by the annual frequency of occurrence in the interval corresponding to the earthquake intensity used to construct the curve; and (2) summing the annual frequencies for a given value of the loss.

The EALs or loss curves are calculated for the as-built configuration and for the three different retrofit solutions tested by the entire procedure described.

The difference between the $EAL_{As\text{-}built}$ and the $EAL_{RETORIFT}$ for the three solutions estimates the savings that each technique provides in one year. To estimate the corresponding PBT, the ratio of the cost of the technique to the savings is determined. The costs are evaluated for the different retrofit solutions: for the FRP, as described in the section above, for the base isolation, derived in this work from the original design document, for the rebuilt a cost of 1350 €/m^2 is assumed. In the context of the payback period, the safety index of the as-built and the FRP configuration is given in order to obtain a double information, one technical and one economic.

5.3 Application to the case study buildings

MATLAB code was used to conduct a parametric study of the convenience of base isolation in existing buildings. Six case studies retrofitted with base isolation, have been analyzed. The results in terms of accelerations, drift, EALs (for the existing and the retrofitted configurations), safety index and payback time have been obtained.

The parametric study is mainly related to two variables, the resistance of concrete, f_{cm}, (20 values were considered) and the ratio A_{sw}/s (6 values were considered), the mechanical percentage of the transverse reinforcement.

In order to validate the performance of the MATLAB code, the first analysis performed was the case study presented in the previous section, so that a comparison can be made with more refined analyses.

The second building (Figure 63) is located in Modena, it has a rectangular plan with dimensions 13.0 m x 27.0 m and a total height of 16.4 m. It is six floor buildings with an interstorey height of about 2.4 m, at the ground floor and 2.8 m at the upper levels. The building is regular in plan and in the elevation. The structural system consists of RC moment resisting frames. The material properties were identified by means of in-situ destructive and non-destructive testing. The resulting concrete compressive strength f_{cm}, is about 21.9 MPa while the yielding stress of steel, f_{ym} is about 430.0 MPa. The soil type was classified C according to NTC (2018).

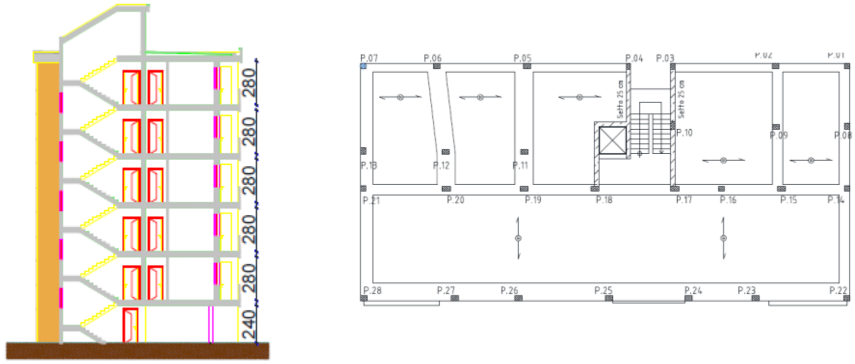

a) b)

Figure 63. Case study building 2: a) building front view and b) plan view and moment resisting frames

The geometry of beams and columns change floor-to-floor. The cross-sections of the columns are 400x300, 450x250 mm at the ground, 350x300, 400x250 mm at the first floor and 300x300, 300x250 mm at the others floor. The cross-sections of the beams are 500x200 and 1000 x 200 mm for the external beams and 600x200 and 700x200 mm for the internal beams at all floors. The columns are reinforced with 4ϕ16 deformed steel longitudinal bars at the ground, 4ϕ14 from the first to the fourth floor, while they have 4ϕ12 at the sixth floor. The stirrups are ϕ6/150 on columns and ϕ6/150 at beam ends.

The third building (Figure 64) is located in Avellino, it has a rectangular plan with dimensions 30.55 m x 14.55 m and a total height of 10.5 m. It is two floor buildings with an interstorey height of about 3.6 m, at the ground floor and 3.4 m at the upper level. The building is regular in plan and in the elevation. The structural system consists of RC moment resisting frames. The materials properties were identified by means of in-situ destructive and non-destructive testing. The resulting concrete compressive strength f_{cm}, is about 18.7 MPa while the yielding stress of steel, f_{ym} is about 401.5 MPa. The soil type was classified B according to NTC (2018).

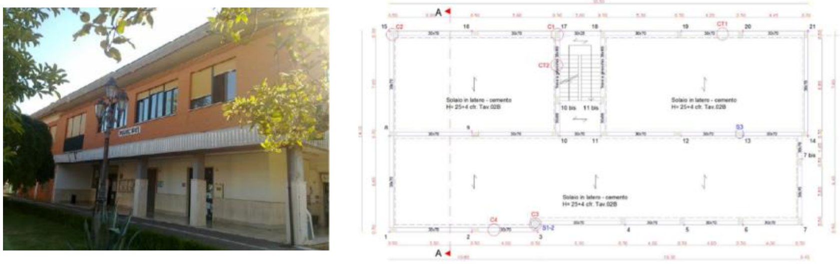

a) b)

Figure 64. Case study building 3: a) building front view and b) plan view and moment resisting frames

The geometry of beams and columns change floor-to-floor. The cross-sections of the columns are 500x300, 300x250 mm at the ground, 400x300, 300x400 mm at the first floor and 300x300 at the loft. The cross-sections of the beams are 300x700 for the external beams and 300x600 for the internal beams at all floors. The columns are reinforced with 4ϕ12 deformed steel longitudinal bars at all floors. The stirrups are ϕ6/150 on columns and ϕ8/200 at beam ends.

The fourth building (Figure 65) is located in Tolentino, it has a rectangular plan with dimensions 41.1 m x 12.2 m and a total height of 12 m. It is two floor buildings with an interstorey height of about 3 m. The building is regular in plan and in the elevation. The structural system consists of RC moment resisting frames. The materials properties were identified by means of in-situ destructive and non-destructive testing. The resulting concrete compressive strength f_{cm}, is about 12.0 MPa while the yielding stress of steel, f_{ym} is about 459.0 MPa. The soil type was classified C according to NTC (2018).

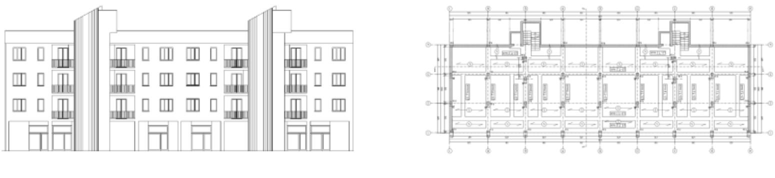

a) b)

Figure 65. Case study building 4: a) building front view and b) plan view and moment resisting frames

The geometry of beams and columns change floor-to-floor. The cross-sections of the columns are 400x300, 300x450 mm at the ground, 350x250, 300x400 mm at the other floors. The cross-sections of the beams are 200x700 for the external beams and 600x200 for the internal beams at the ground floor, 150x600 for the external beams and 600x200 for the internal beams at the other floors. The columns are reinforced with 6ϕ16 deformed steel longitudinal bars at the ground floor, 4ϕ16 at the first floor, 4ϕ14 at the second floor and 4ϕ12 at the third floor. The stirrups are ϕ8/150 and ϕ6/200 on columns and ϕ8/150 and ϕ6/200 at beam ends.

The fifth building (Figure 66) is located in Tolentino, it has a rectangular plan with dimensions 65.5 m x 10.0 m and a total height of 9.10 m. It is two floor buildings with an interstorey height of about 2.7 m. The building is regular in plan and in the elevation. The structural system consists of RC moment resisting frames. The materials properties were identified by means of in-situ destructive and non-destructive testing. The resulting concrete compressive strength f_{cm}, is about 10.3 MPa while the yielding stress of steel, f_{ym} is about 453.0 MPa. The soil type was classified C according to NTC (2018).

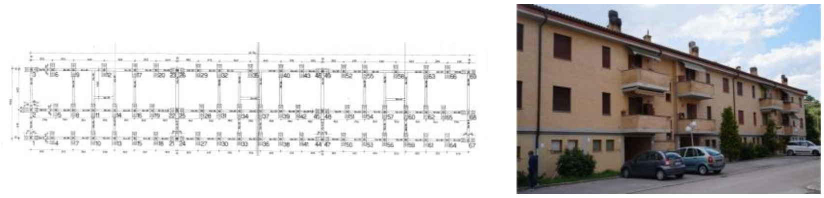

a) b)

Figure 66. Case study building 5: a) building front view and b) plan view and moment resisting frames

The geometry of beams and columns change floor-to-floor. The cross-sections of the columns are 300x300 at all floors. The cross-sections of the beams are 300x400 for the external beams and 500x200 for the internal beams at all floors. The columns are reinforced with 4ϕ14/6ϕ16 deformed steel longitudinal bars at the ground floor, 4ϕ14 at the first floor, 4ϕ14/4ϕ11 at the second floor. The stirrups are ϕ6/200 on columns and ϕ8/300 and ϕ6/150 at beam ends.

The sixth building (Figure 67) is located in Roma, it has a rectangular plan with dimensions 27.9 m x 37.9 m and a total height of 30 m. It is ten floor buildings with an interstorey height of about 3.0 m. The building is regular in plan and in the elevation. The structural system consists of RC moment resisting frames. The materials properties were identified by means of in-situ destructive and non-destructive testing. The resulting concrete compressive strength f_{cm}, is about 25.0 MPa while the yielding stress of steel, f_{ym} is about 430.0 MPa. The soil type was classified C according to NTC (2018).

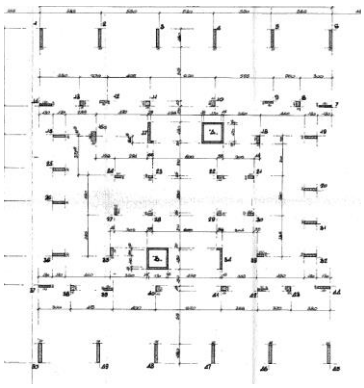

a) b)

Figure 67. Case study building 6: a) building front view and b) plan view and moment resisting frames

The geometry of beams and columns change floor-to-floor. Due to the high variability in cross section and reinforcement the list of characteristics is avoided in the work.

The implementation in the MATLAB code was done in the same way for all buildings. Once the data were entered, two configurations (as built and base isolated) were analysed for each building, for 20 values of f_{cm} and 6 values of A_{sw}/s, assuming that the A_{sw}/s had no effect on drift and acceleration, and the analyses were performed for nine return periods with 14 records. 5040 analyses were performed for each building to estimate drift and accelerations. Estimation of EALs and PBT was performed for each value of f_{cm} and A_{sw}/s for a total of 120 values.

First, the masses of each floor were determined, taking into account all contributions such as columns, beams, infill, balconies, etc. The masses for all buildings are listed in Table 8:

Table 8. Masses implemented in the tool for each building

Floor/Building	1	2	3	4	5	6
1	349	353	482	549	586	1202
2	346	360	432	534	585	1193
3	338	359		461	487	1190
4	236	359		261		1187
5		359				1185
6		285				1184
7						1183
8						1182
9						1167
10						1141

*the masses are expressed in ton

The data relating to geometry, such as the height between floors or the size of the column, are those described above.

The infills are characterized by a value of G_w equal to 1580 MPa with a thickness of 0.2 m.

For each building, a spectral compatibility was performed in accordance with the LSLS spectrum of the site. The results for building 1 were presented in the previous section, while those for the other buildings are given below.

For the case study building 2 the spectrum compatibility (Figure 68) was performed with the code compliant design spectrum on a soil type C, in Modena, at different return period.

Table 9. Record selected for the building 2

Record	Location	Year	Station	M_w	Soil Type	Distance JB	Direction	PGA	PGV	I_a	I_d
[-]	[-]	[-]	[-]	[-]	[-]	[-]	[-]	[g]	[m/s]	[m/s]	[-]
1	Campano Lucano (aftershock)	1981	ST97	5.2	B	15	EW	0.021	0.012		16.50
							NS	0.020	0.016		14.15
2	Izmit (aftershock)	1999	ST3266	5.8	C	27	EW	0.031	0.025		14.18
							NS	0.050	0.041		8.09
3	Kalamata	1986	ST163	5.9	B	11	EW	0.240	0.315		4.65
							NS	0.272	0.235		7.36
4	Umbria Marche (aftershock)	1997	ST225	5.6	A	23	EW	0.053	0.051		7.24
							NS	0.063	0.052		7.72
5	Lazio Abruzzo (aftershock)	1984	ST152	5.5	C	24	EW	0.037	0.026		17.22
							NS	0.034	0.025		15.45
6	Umbria Marche (aftershock)	1997	ST83	5.6	B	26	EW	0.045	0.032		14.48
							NS	0.037	0.038		14.52

7	Izmit (aftershock)	1999	ST3270	5.8	D	27	EW	0.071	0.062		10.33
							NS	0.067	0.062		11.77

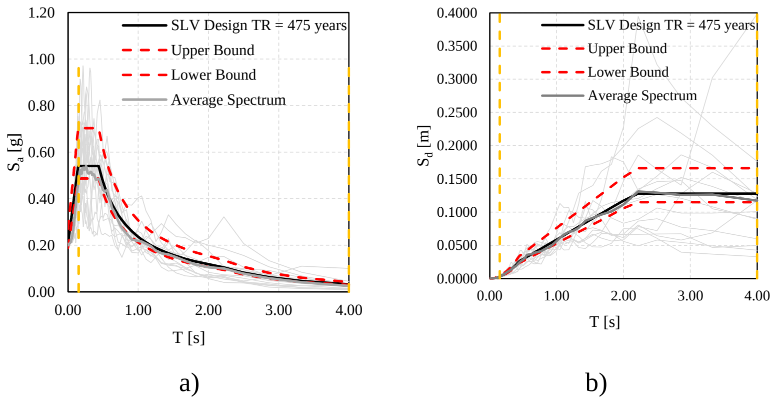

Figure 68: Spectrum compatibility for building 2: a) acceleration and b) displacement

For the case study building 3 the spectrum compatibility (Figure 69) was performed with the code compliant design spectrum on a soil type B, in Avellino, at different return period.

Table 10. Record selected for the building 3

Record	Location	Year	Station	M_w	Soil Type	Distance JB	Direction	PGA	PGV	I_a	I_d
[-]	[-]	[-]	[-]	[-]	[-]	[-]	[-]	[g]	[m/s]	[m/s]	[-]
1	Campano Lucano	1980	ST98	6.9	A	25	EW	0.06	0.044		16.35
							NS	0.06	0.059		13.79
2	Izmit (aftershock)	1999	ST772	5.6	C	41	EW	0.017	0.013		15.88
							NS	0.024	0.016		11.54
3	Izmit (aftershock)	1999	ST3270	5.1	D	39	EW	0.045	0.036		9.22
							NS	0.036	0.024		15.83
4	Izmit (aftershock)	1999	ST3266	5.8	C	27	EW	0.031	0.025		14.18
							NS	0.05	0.041		8.09
5	Umbria Marche	1997	ST223	6	C	22	EW	0.172	0.145		8.75
							NS	0.106	0.118		11.12
6	Umbria Marche	1997	ST83	5.7	B	25	EW	0.039	0.040		19.84
							NS	0.053	0.060		16.53
7	Aigion	1995	ST1331	6.5	B	43	EW	0.084	0.150		11.63
							NS	0.093	0.096		13.58

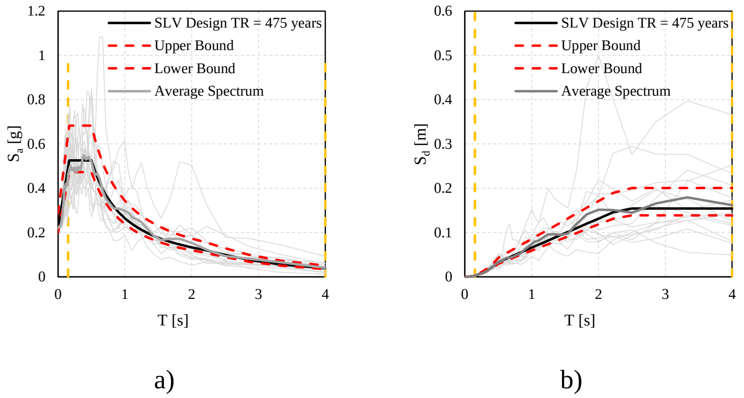

Figure 69. Spectrum compatibility for building 3: a) acceleration and b) displacement

For the case study building 4 and 5 the spectrum compatibility (Figure 70) was performed with the code compliant design spectrum on a soil type C, in Tolentino, at different return period.

Table 11. Record selected for the building 4-5

Record	Location	Year	Station	M_w	Soil Type	Distance JB	Direction	PGA	PGV	I_a	I_d
[-]	[-]	[-]	[-]	[-]	[-]	[-]	[-]	[g]	[m/s]	[m/s]	[-]
1	Izmit (aftershock)	1999	ST3266	5.8	A	27	EW	0.031	0.025		14.18
							NS	0.05	0.041		8.09
2	Umbria Marche	1997	ST223	6.00	C	22	EW	0.172	0.145		8.75
							NS	0.106	0.118		11.12
3	Manesion	1989	ST1330	5.2	D	24	EW	0.027	0.026		9.83
							NS	0.026	0.022		16.21
4	Kalamata	1986	ST164	5.9	C	10	EW	0.215	0.327		5.41
							NS	0.297	0.323		5.77
5	Umbria Marche	1997	ST83	5.7	C	25	EW	0.039	0.04		19.84
							NS	0.053	0.06		16.53
6	Izmit (aftershock)	1999	ST3273	5.8	B	25	EW	0.141	0.089		7.08
							NS	0.071	0.094		7.89
7	Izmir	1992	ST43	6.00	B	30	EW	0.029	0.036		14.87
							NS	0.039	0.068		8.47

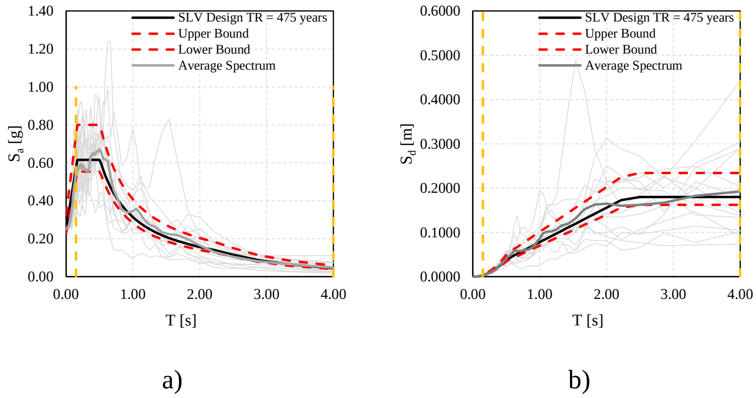

Figure 70. Spectrum compatibility for building 4-5: a) acceleration and b) displacement

For the case study building 6 the spectrum compatibility (Figure 71) was performed with the code compliant design spectrum on a soil type C, in Rome, at different return period

Table 12. Record selected for the building 6

Record	Location	Year	Station	M_w	Soil Type	Distance JB	Direction	PGA	PGV	I_a	I_d
[-]	[-]	[-]	[-]	[-]	[-]	[-]	[-]	[g]	[m/s]	[m/s]	[-]
1	Campano Lucano (aftershock)	1981	ST97	5.2	B	15	EW	0.021	0.012		16.5
							NS	0.020	0.016		14.1
2	Izmit (aftershock)	1999	ST3266	5.8	C	27	EW	0.031	0.025		14.2
							NS	0.050	0.041		8.1
3	Kalamata	1986	ST163	5.9	B	11	EW	0.240	0.315		4.7
							NS	0.272	0.235		7.4
4	Umbria Marche (aftershock)	1997	ST225	5.6	A	23	EW	0.053	0.051		7.2
							NS	0.063	0.052		7.7
5	Lazio Abruzzo (aftershock)	1984	ST152	5.5	C	24	EW	0.037	0.026		17.2
							NS	0.034	0.025		15.5
6	Umbria Marche	1997	ST83	5.7	B	25	EW	0.039	0.04		19.8
							NS	0.053	0.06		16.5
7	Izmit (aftershock)	1999	ST3270	5.8	D	27	EW	0.071	0.062		10.3
							NS	0.067	0.062		11.8

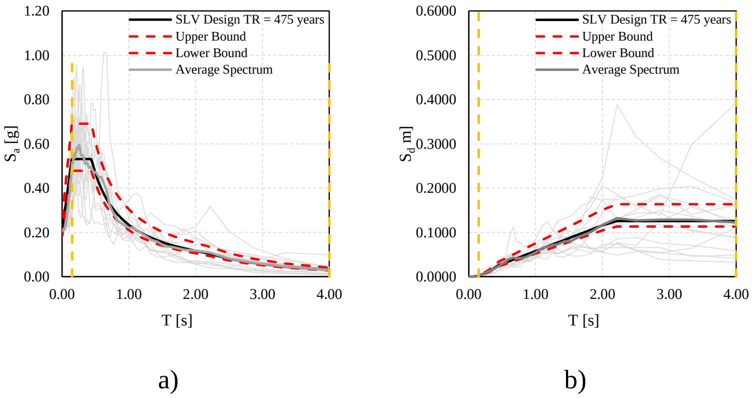

Figure 71. Spectrum compatibility for building 4-5: a) acceleration and b) displacement

The parameters for the isolation system were provided, different types of devices were used for the different buildings. For the building 1 a double concave friction pendulum FIP D-L 3700/800, for building 2 an elastomeric device, SI -550-126 was used, for building 3 a high damping rubber bearing, TDRI 600- NM -125 was used, in building 4 a high damping rubber bearing, TDRI 500- SM -126 was used, in building 5 a high damping rubber bearing, TDRI 450- SM -126 was used, at least in building 6 a high damping rubber bearing TDRI 650- HM -150 was used. The data available in the owner's list was used to define a linear or bilinear behavior for the base isolation system. The last data necessary to proceed with the analyzes and the results were the quantities needed for the damage analysis, such as the infills, the beam-column connections, the raised floor, etc.; some of them are calculated by design, others by using a tool provided by the (ATC) that allows defining these quantities based on the use of destination of each floor and the square meters of the floor, more details can be found in (ATC - Applied Technology Council 2012c)

5.3.1 Validation of the code

To validate the code and prior to conducting the parametric study for the existing building, a comparison of building 1 was conducted between the results of the refined analyses using SAP2000 and those of the code in terms

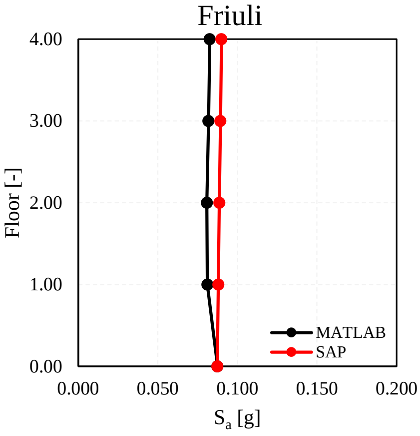
Friuli
4.00
3.00
2.00
1.00
0.00
Floor [-]
0.000
0.050
0.100
0.150
0.200
S_a [g]
MATLAB
SAP

a)

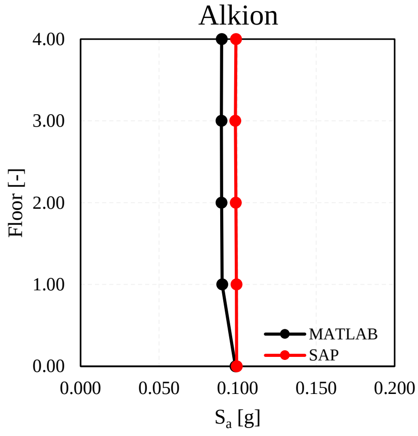
Alkion
4.00
3.00
2.00
1.00
0.00
Floor [-]
0.000
0.050
0.100
0.150
0.200
S_a [g]
MATLAB
SAP

b)

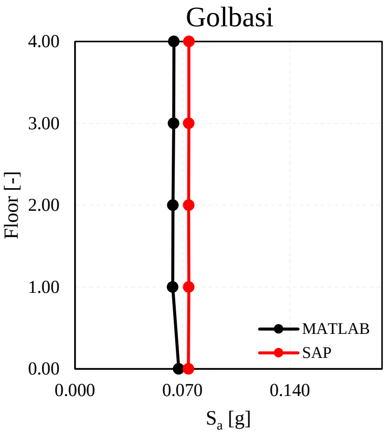
Golbasi
4.00
3.00
2.00
1.00
0.00
Floor [-]
0.000
0.070
0.140
S_a [g]
MATLAB
SAP

c)

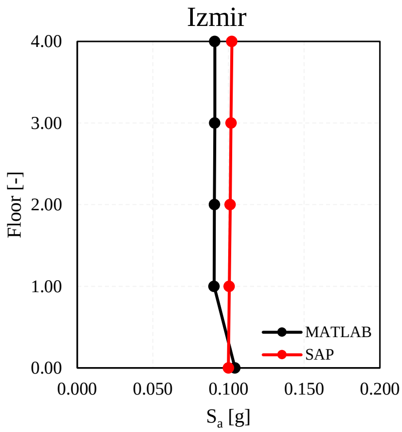
Izmir
4.00
3.00
2.00
1.00
0.00
Floor [-]
0.000
0.050
0.100
0.150
0.200
S_a [g]
MATLAB
SAP

d)

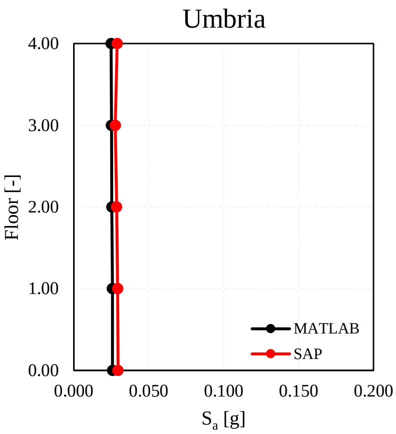
Umbria
4.00
3.00
2.00
1.00
0.00
Floor [-]
0.000
0.050
0.100
0.150
0.200
S_a [g]
MATLAB
SAP

e)

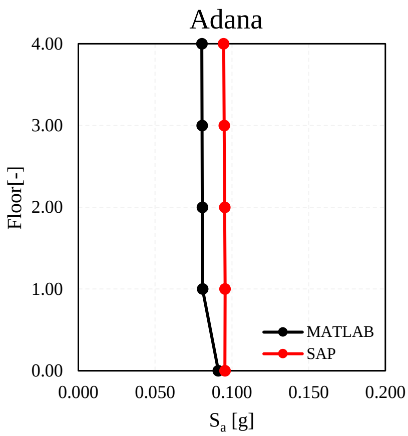
Adana
4.00
3.00
2.00
1.00
0.00
Floor[-]
0.000
0.050
0.100
0.150
0.200
S_a [g]
MATLAB
SAP

f)

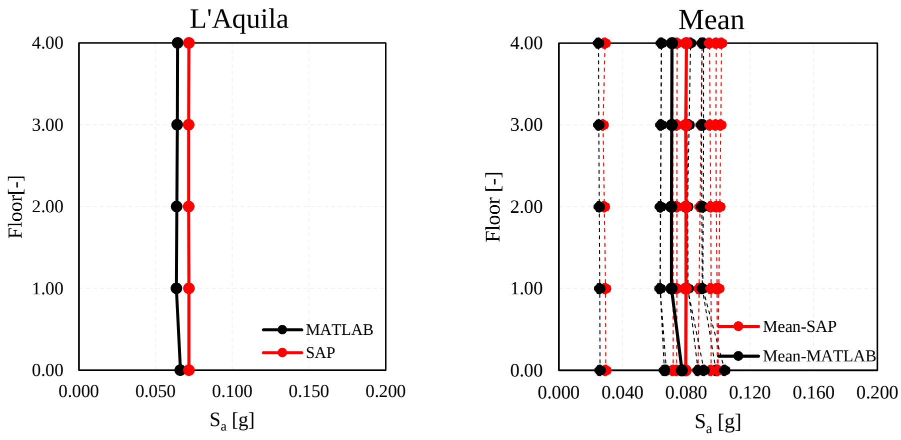

g) h)

Figure 72. Comparison between the acceleration estimate with MATLAB code and SAP2000 for base isolated configuration at LSLS: a) record 1, b) record 2, c) record 3, d) record 4, e) record 5, f) record 6, g) record 7, h) mean

of displacements and accelerations for the as-built and the base isolated configuration.

As with the building, the properties of the base isolation are concentrated in a single degree of freedom. In particular, the stiffness for the linear and bilinear behavior takes into account the stiffness of all the devices used on the building. In this case, the 24 friction pendulums used in the 3D model are modelled as a single isolation device with a radius of curvature of 3.7 m and a maximum displacement of 400 mm, but considering an axial load equal to the sum of the axial load acting on each device to estimate the k_b (Eq.10) and in the same way the k_a. The described procedure must be applied each time to model the base isolation. A comparison was made between the recordings at LSLS from the previous spectral compatibility in terms of drift and acceleration.

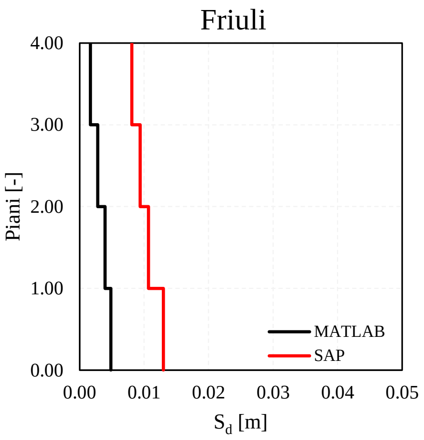
Friuli
Piani [-]
4.00
3.00
2.00
1.00
0.00
0.00 0.01 0.02 0.03 0.04 0.05
S_d [m]
MATLAB
SAP

a)

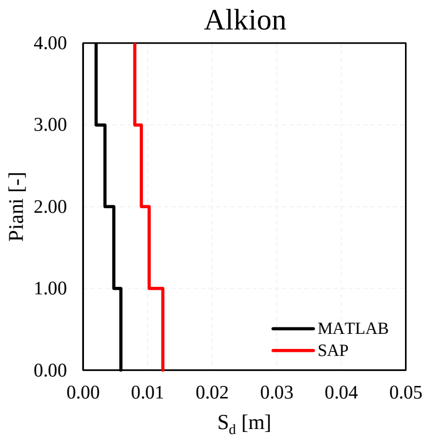
Alkion
Piani [-]
4.00
3.00
2.00
1.00
0.00
0.00 0.01 0.02 0.03 0.04 0.05
S_d [m]
MATLAB
SAP

b)

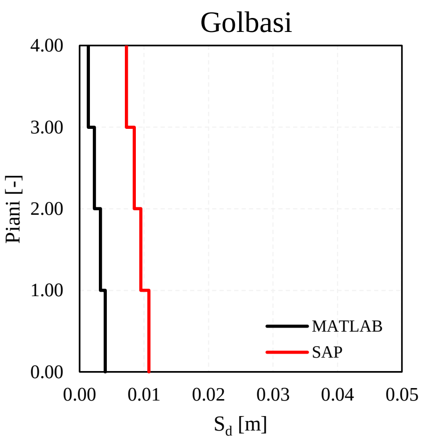
Golbasi
Piani [-]
4.00
3.00
2.00
1.00
0.00
0.00 0.01 0.02 0.03 0.04 0.05
S_d [m]
MATLAB
SAP

c)

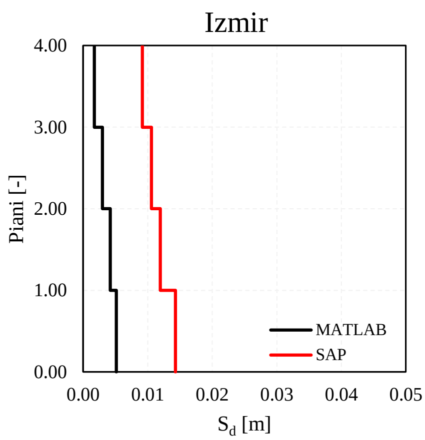
Izmir
Piani [-]
4.00
3.00
2.00
1.00
0.00
0.00 0.01 0.02 0.03 0.04 0.05
S_d [m]
MATLAB
SAP

d)

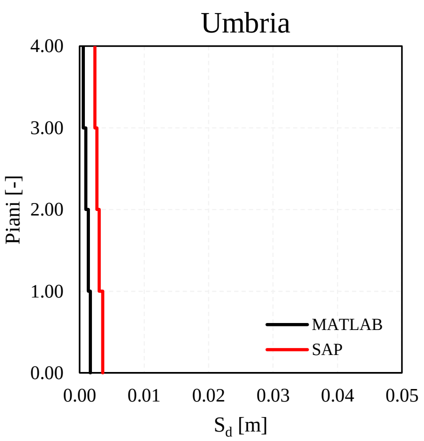
Umbria
Piani [-]
4.00
3.00
2.00
1.00
0.00
0.00 0.01 0.02 0.03 0.04 0.05
S_d [m]
MATLAB
SAP

e)

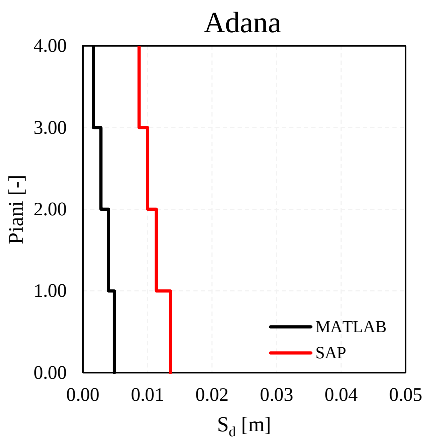
Adana
Piani [-]
4.00
3.00
2.00
1.00
0.00
0.00 0.01 0.02 0.03 0.04 0.05
S_d [m]
MATLAB
SAP

f)

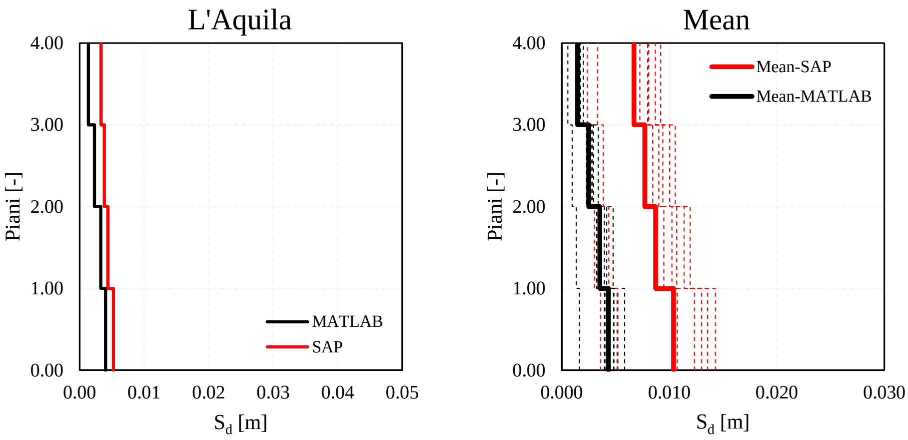

g) h)

Figure 73. Comparison between the drift estimate with MATLAB code and SAP2000 for base isolated configuration at LSLS: a) record 1, b) record 2, c) record 3, d) record 4, e) record 5, f) record 6, g) record 7, h) mean

As you can see in Figure 72-73, the results of the refined analyses and the simplified approach agree very closely with the MATLAB code, highlighting the usefulness of the code for the base isolation configuration. The same comparisons were made for the fixed-base configuration, as shown in Figure 74-75:

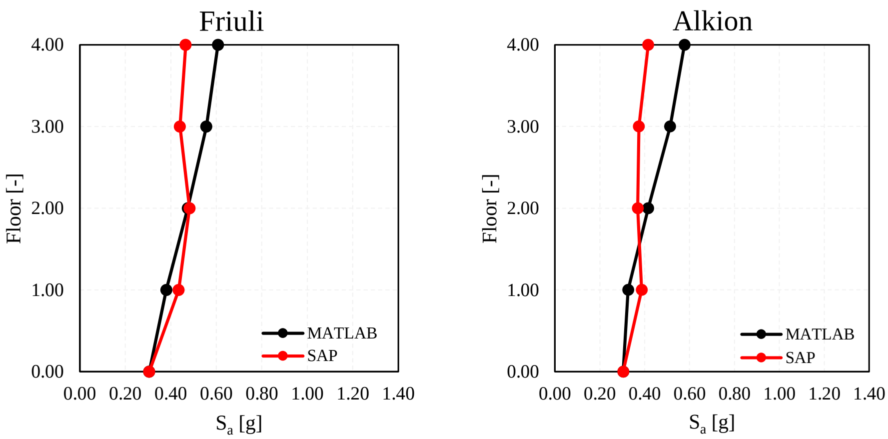

a) b)

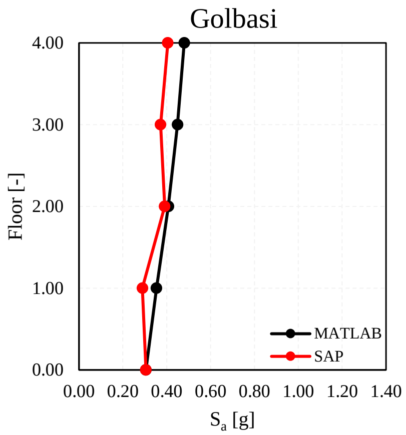
Golbasi
4.00
3.00
2.00
1.00
0.00
Floor [-]
0.00 0.20 0.40 0.60 0.80 1.00 1.20 1.40
S_a [g]
MATLAB
SAP

c)

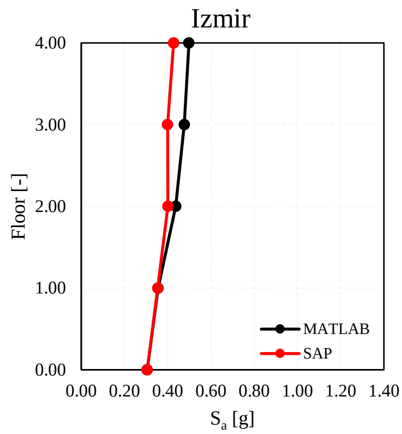
Izmir
4.00
3.00
2.00
1.00
0.00
Floor [-]
0.00 0.20 0.40 0.60 0.80 1.00 1.20 1.40
S_a [g]
MATLAB
SAP

d)

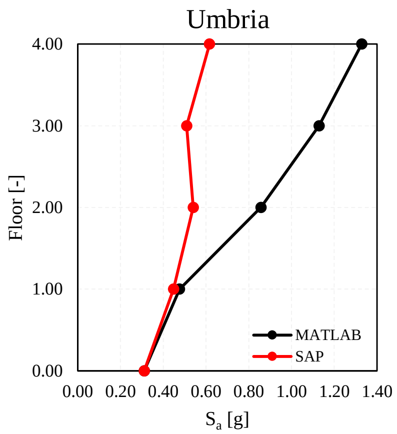
Umbria
4.00
3.00
2.00
1.00
0.00
Floor [-]
0.00 0.20 0.40 0.60 0.80 1.00 1.20 1.40
S_a [g]
MATLAB
SAP

e)

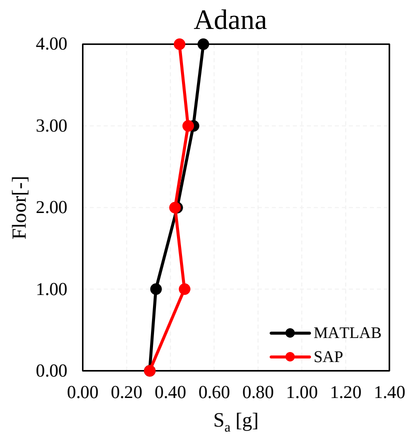
Adana
4.00
3.00
2.00
1.00
0.00
Floor[-]
0.00 0.20 0.40 0.60 0.80 1.00 1.20 1.40
S_a [g]
MATLAB
SAP

f)

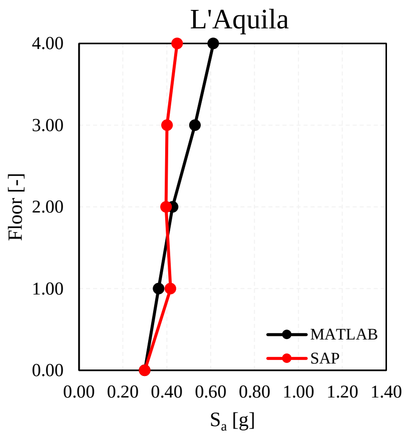
L'Aquila
4.00
3.00
2.00
1.00
0.00
Floor [-]
0.00 0.20 0.40 0.60 0.80 1.00 1.20 1.40
S_a [g]
MATLAB
SAP

g)

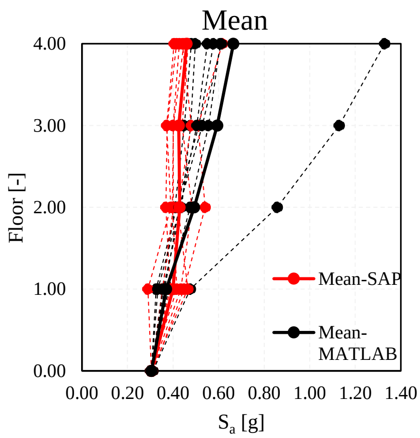
Mean
4.00
3.00
2.00
1.00
0.00
Floor [-]
0.00 0.20 0.40 0.60 0.80 1.00 1.20 1.40
S_a [g]
Mean-SAP
Mean-MATLAB

h)

Figure 74. Comparison between the acceleration estimate with MATLAB code and SAP2000 for fixed based configuration at LSLS: a) record 1, b) record 2, c) record 3, d) record 4, e) record 5, f) record 6, g) record 7, h) mean

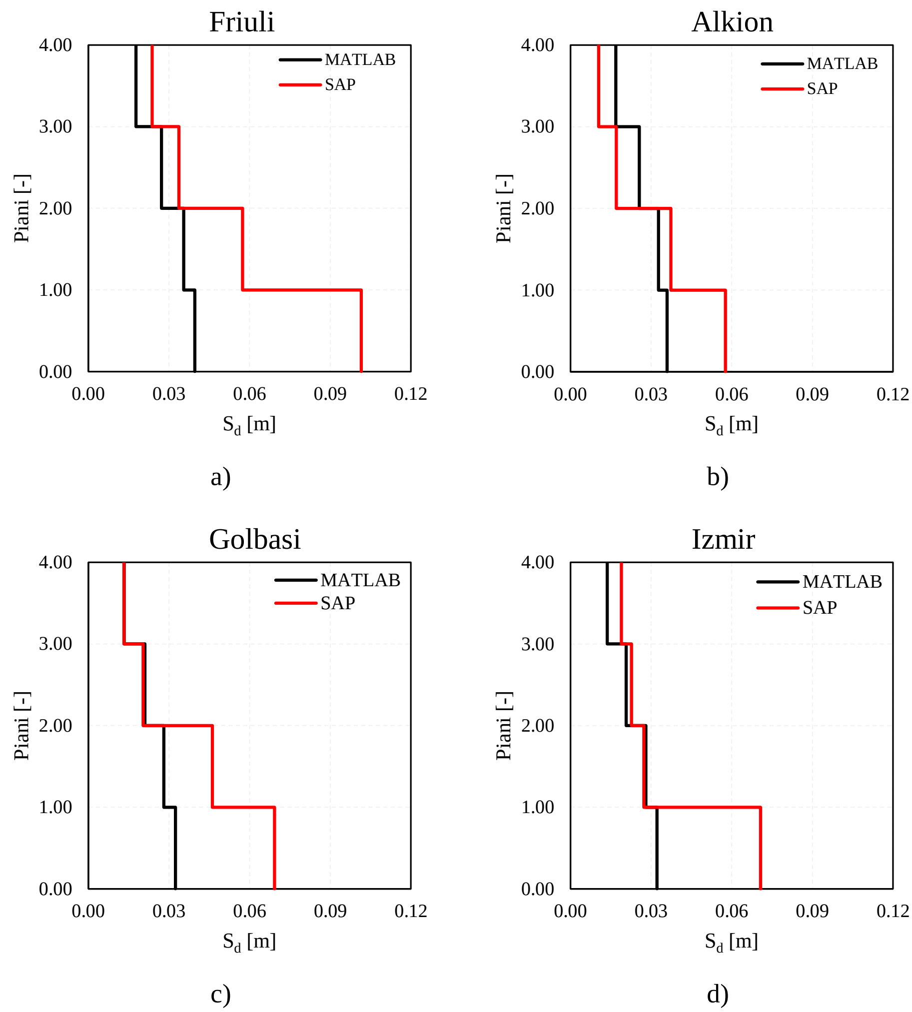

a) b)

c) d)

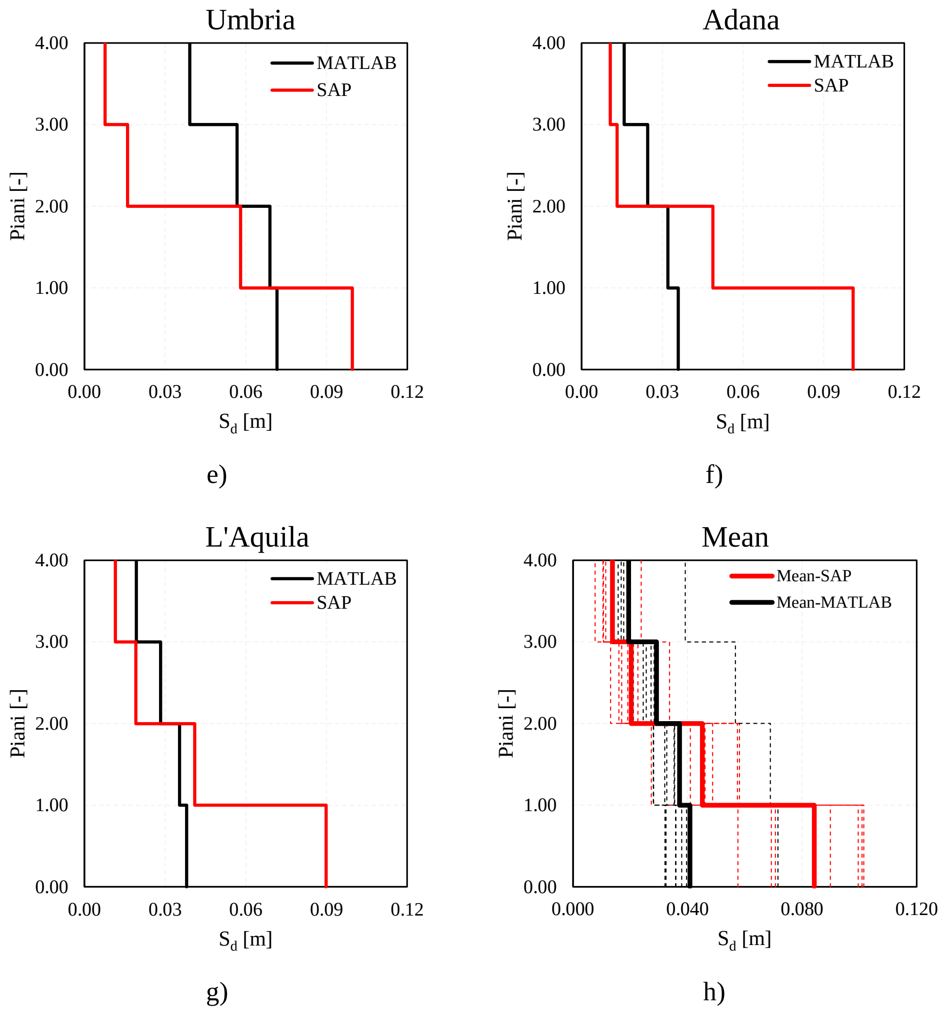

Figure 75. Comparison between the drift estimate with MATLAB code and SAP2000 for fixed based configuration at LSLS: a) record 1, b) record 2, c) record 3, d) record 4, e) record 5, f) record 6, g) record 7, h) mean

The agreement is not very strict in this case, but considering the contribution of drift and acceleration in the as-built configuration with a return period lower than the LSLS, the gap between the results is not significant in terms of the final result for the estimation of the PBT. In fact, the comparison at the lower bound, e.g., DS for a return period of 50 years, shows a large agreement, as shown in Figure 76-77:

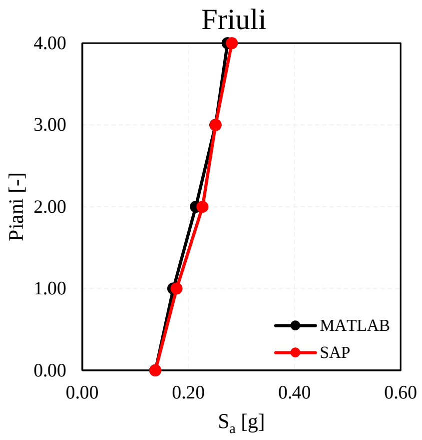
Friuli
Piani [-]
4.00
3.00
2.00
1.00
0.00
0.00
0.20
0.40
0.60
S_a [g]
MATLAB
SAP

a)

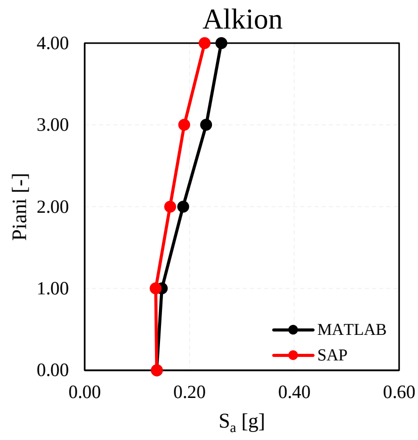
Alkion
Piani [-]
4.00
3.00
2.00
1.00
0.00
0.00
0.20
0.40
0.60
S_a [g]
MATLAB
SAP

b)

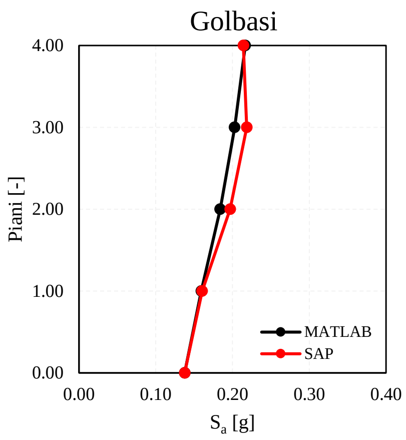
Golbasi
Piani [-]
4.00
3.00
2.00
1.00
0.00
0.00
0.10
0.20
0.30
0.40
S_a [g]
MATLAB
SAP

c)

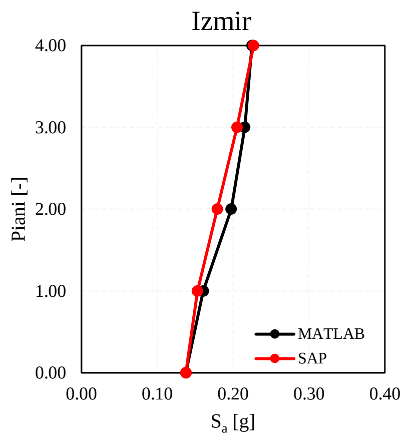
Izmir
Piani [-]
4.00
3.00
2.00
1.00
0.00
0.00
0.10
0.20
0.30
0.40
S_a [g]
MATLAB
SAP

d)

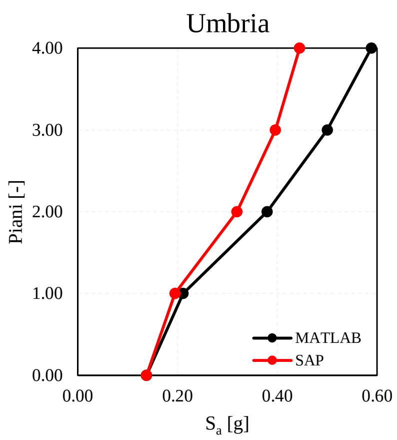
Umbria
Piani [-]
4.00
3.00
2.00
1.00
0.00
0.00
0.20
0.40
0.60
S_a [g]
MATLAB
SAP

e)

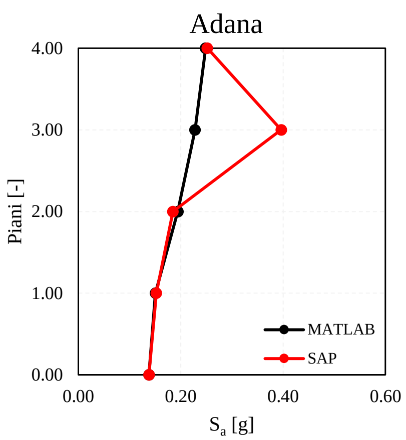
Adana
Piani [-]
4.00
3.00
2.00
1.00
0.00
0.00
0.20
0.40
0.60
S_a [g]
MATLAB
SAP

f)

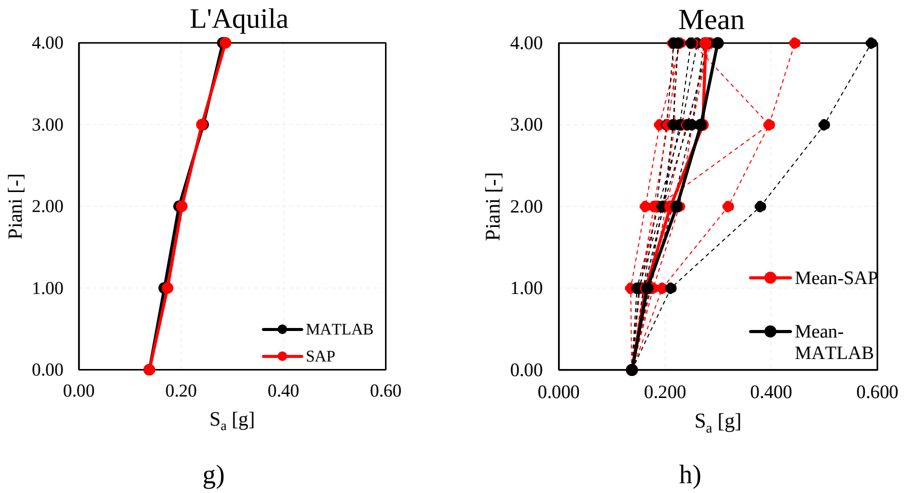

Figure 76. Comparison between the acceleration estimate with MATLAB code and SAP2000 for fixed based configuration at DS: a) record 1, b) record 2, c) record 3, d) record 4, e) record 5, f) record 6, g) record 7, h) mean

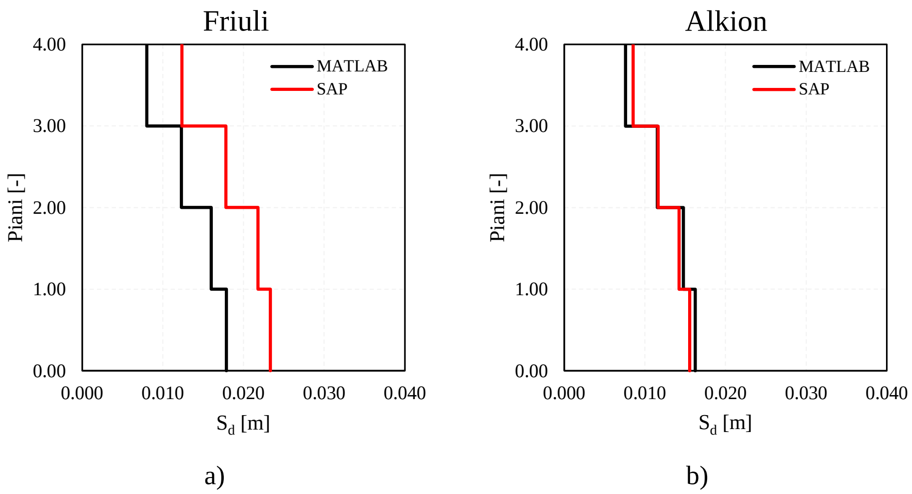

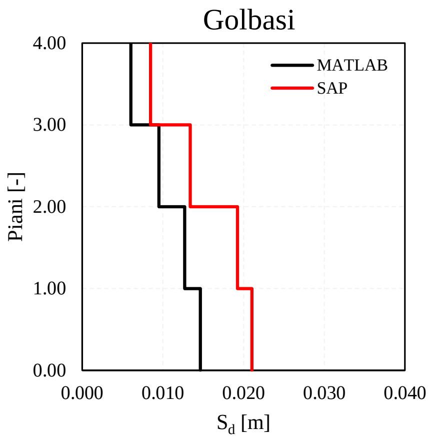
Golbasi
MATLAB
SAP
Piani [-]
S_d [m]
4.00
3.00
2.00
1.00
0.00
0.000
0.010
0.020
0.030
0.040

d)

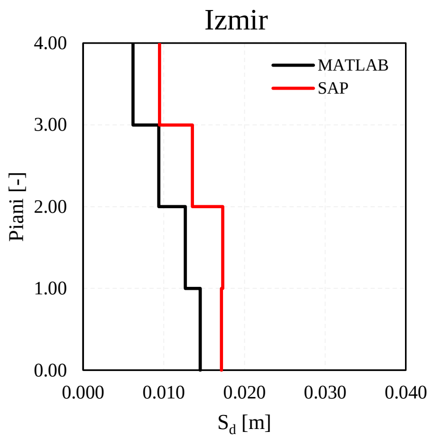
Izmir
MATLAB
SAP
Piani [-]
S_d [m]
4.00
3.00
2.00
1.00
0.00
0.000
0.010
0.020
0.030
0.040

e)

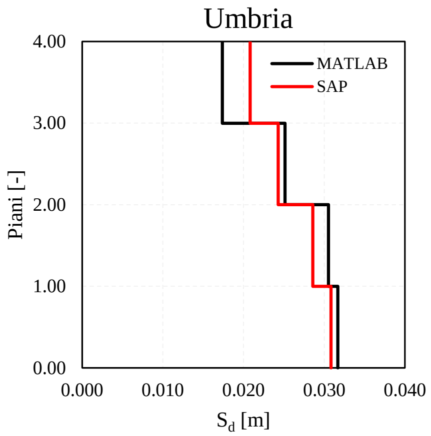
Umbria
MATLAB
SAP
Piani [-]
S_d [m]
4.00
3.00
2.00
1.00
0.00
0.000
0.010
0.020
0.030
0.040

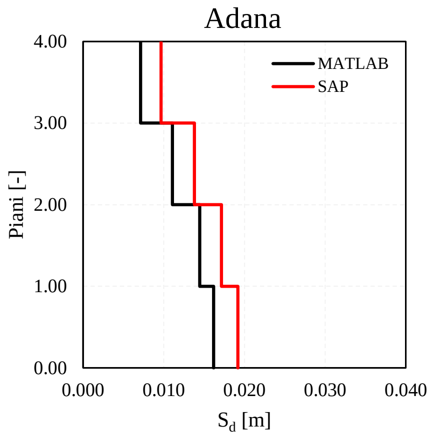
Adana
MATLAB
SAP
Piani [-]
S_d [m]
4.00
3.00
2.00
1.00
0.00
0.000
0.010
0.020
0.030
0.040

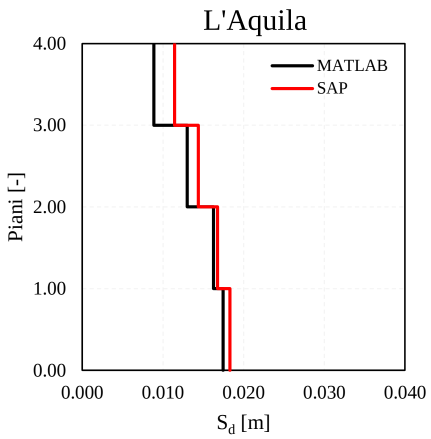
L'Aquila
MATLAB
SAP
Piani [-]
S_d [m]
4.00
3.00
2.00
1.00
0.00
0.000
0.010
0.020
0.030
0.040

g)

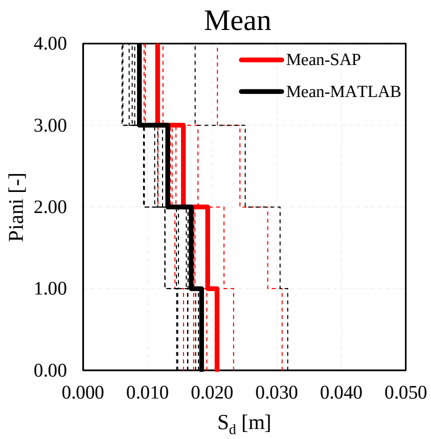
Mean
Mean-SAP
Mean-MATLAB
Piani [-]
S_d [m]
4.00
3.00
2.00
1.00
0.00
0.000
0.010
0.020
0.030
0.040
0.050

h)

Figure 77. Comparison between the drift estimate with MATLAB code and SAP2000 for fixed based configuration at DS: a) record 1, b) record 2, c) record 3, d) record 4, e) record 5, f) record 6, g) record 7, h) mean and all records, i) mean

The results show the usefulness of the code for solving the dynamic equation with a simplified approach and its suitability for the goal proposed by the work. In the following section, a correspondence with the final results in terms of PBT and EAL is described.

5.4 Results

The results in terms of drift and acceleration, EALs and PBT are shown.

Figure 78 shows the drift and acceleration for building 1 for as-built/FRP/rebuilt (Figure 78a,c,e,g) and base isolation (Figure 78b,d,f,h) configuration. A significant reduction in EDPs (acceleration and drift) is observed. The drift is reduced by about 1/8 in both directions on the ground floor and 1/11 in both directions on the upper floor, while the acceleration is reduced by about 1/5 in both directions on the ground floor and 1/7 in the x-direction and 1/9 in the y-direction on the upper floor.

The variation of f_{cm} and A_{sw}/s have a significant effect on the loss curve of the as-built configuration, as can observe in Figure 79. The value of EALs decreases with increasing f_{cm} and increasing A_{sw}/s. The increase in f_{cm} and A_{sw}/s is accompanied by an increase in the capacity of the columns, which plays a significant role in the evaluation of collapse in the loss analysis, as described.

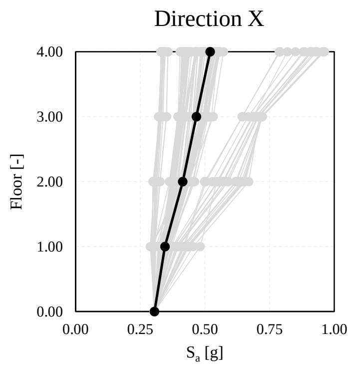

a)

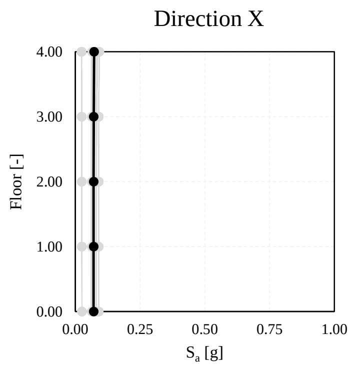

b)

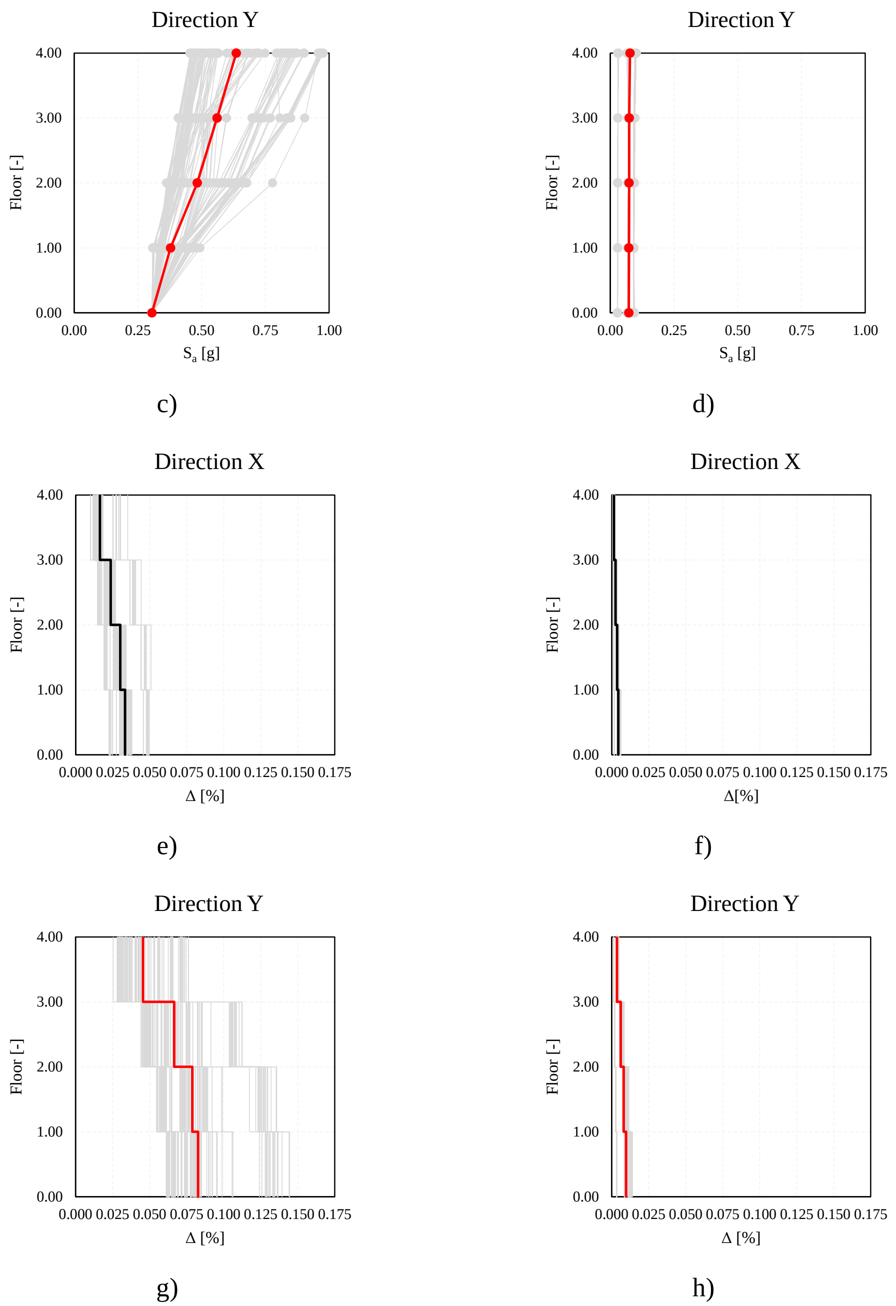

Figure 78. Acceleration in x direction for a) as-built , b) base-isolated configuration and in y direction for c) as-built , d) base-isolated, drift in x direction for e) as-built , f) base-isolated configuration and in y direction for g) as-built , h) base-isolated for building 1

The value of EALs ranges from 2.65% to 1.76%, with the highest value corresponding to the lowest value of f_{cm} of 7.9 MPa and A_{sw}/s of 0.09425 mm related to a transverse reinforcement with a diameter of 6 mm and a spacing of 300 mm, and the lowest value corresponding to the highest value of f_{cm} of 38.4 MPa and A_{sw}/s of 0.2533 related to a transverse reinforcement with a diameter of 8 mm and a spacing of 200 m.

Considering the average of the six values of the ratio A_{sw}/s for a given f_{cm}, obtaining 20 EALs values, one for each f_{cm}, the maximum value is 2.56%, the minimum value is 1.95% and the average value is 2.15%.

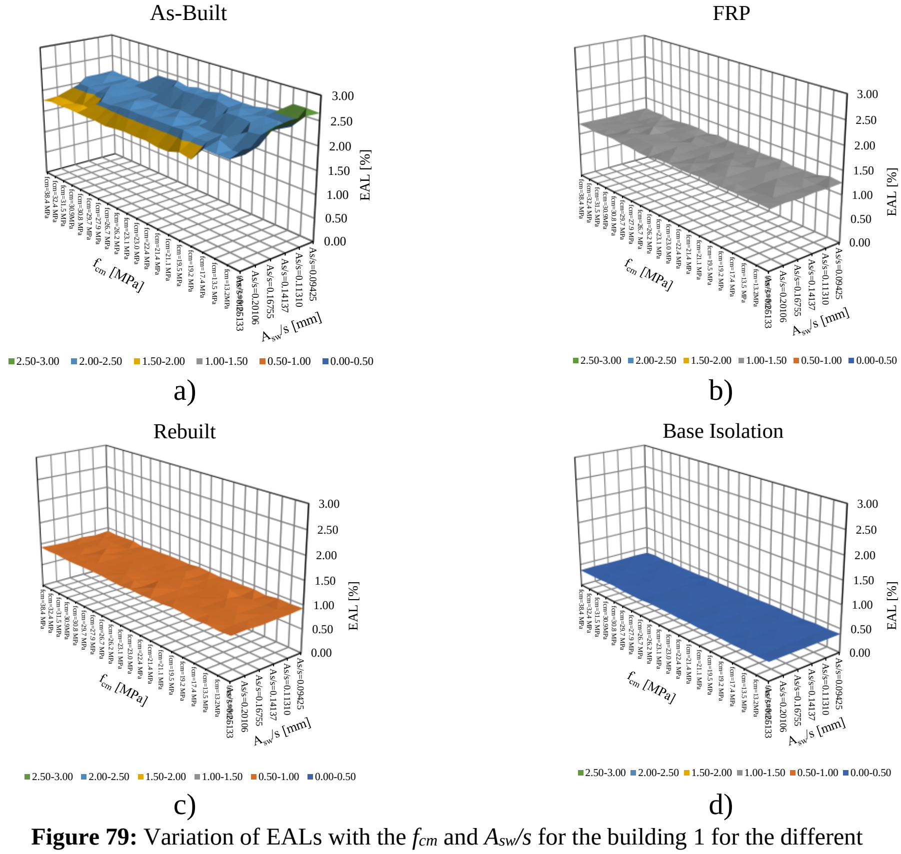

Figure 79: Variation of EALs with the f_{cm} and A_{sw}/s for the building 1 for the different configuration: a) As-Built, b) FRP, c) Rebuilt, d) Base Isolation

As for the EALs for the retrofit configurations, as can observe in Figure 79, the variability is quite low. The FRP configuration features an EALs of about 1.20%, the rebuilt configuration features an EALs of about 0.90%, and the base isolation configuration features an EALs of about 0.37%. Despite the variability of the f_{cm} and the A_{sw}/s, the retrofit solution achieves the same safety index for all values of the parameters. A comparison of the curves highlights the effectiveness of base isolation compared to the other two techniques. Although base isolation and rebuilt achieve the same safety index, the EALs of the isolated configuration is lower than that of the rebuilt because acceleration and displacement are further reduced, as shown in Figure 78.

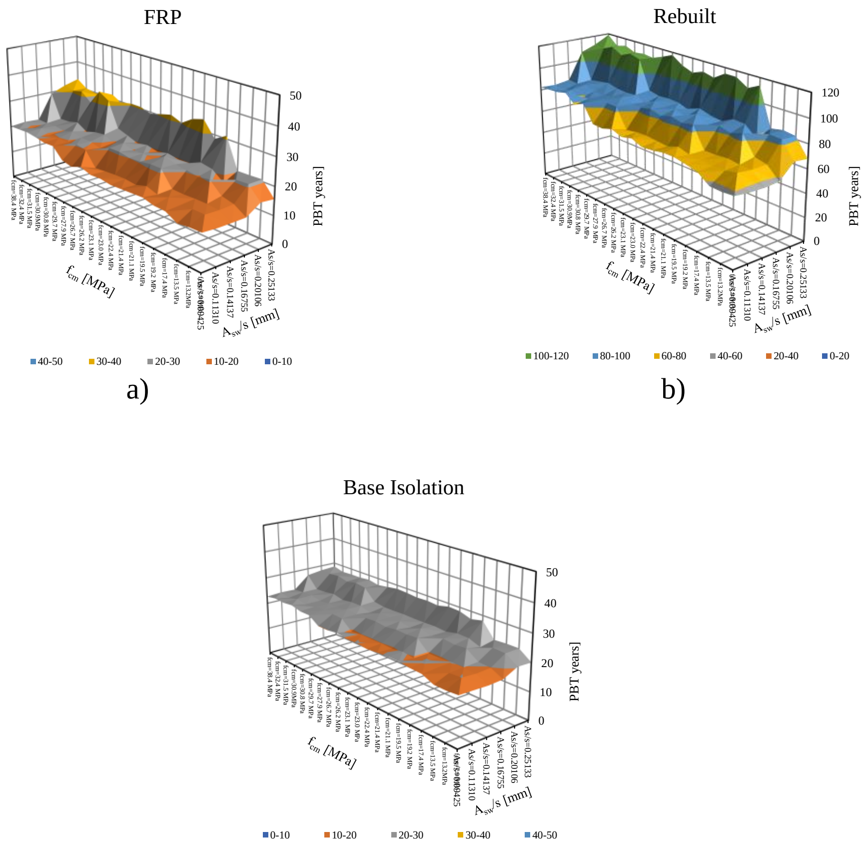

c)

Figure 80: Variation of PBT with the f_{cm} and A_{sw}/s for the building B1 for the different configuration: a) FRP, b) Rebuilt, c) Base Isolation

The trend of EALs has a direct impact on the variability of PBT. The PBT is the ratio between the cost of the retrofit technology and the savings. The savings is the difference between the EALs in the as-built configuration and the EALs for the retrofitted configurations. As can be observed in Figure 80, the PBT increases with increasing f_{cm} and A_{sw}/s, showing a trend opposite to that of the EALs. In fact, as shown in Figure 80, the EALs for the retrofitted solutions is not variable but assumes a constant value, while the EALs for the as-built increases with decreasing f_{cm} and A_{sw}/s, so that the savings increase for lower values of f_{cm} and A_{sw}/s. Since the proportionality between the PBT and savings is indirect, this justifies the trend shown. The PBT for the FRP configuration ranges from 13 to 33 years, with the lowest value for f_{cm} of 7.9 MPa and A_{sw}/s of 0.09425 and the highest value for f_{cm} of 38.4 MPa and A_{sw}/s of 0.25133. Estimating the mean of the six A_{sw}/s values for a given f_{cm} value yields 20 PBT values. The maximum value is 26 years, the minimum value is 14 years, and the average value is 21 years. For the rebuilt configuration, the PBT ranges from 58 to 119 years, with the lowest and highest values corresponding to the same f_{cm} and A_{sw}/s for the FRP. Taking the 20 values of PBT by the average of the six values of A_{sw}/s for each f_{cm}, the maximum value is 98 years, the minimum is 61 years, and the average is 83 years. At last, the base isolation configuration has a PBT between 18 and 29 years, with the same correspondence with f_{cm} and A_{sw}/s of FRP and Rebuilt. The mean of the six A_{sw}/s values for each f_{cm} gives a maximum value of 25 years, a minimum of 19years and a mean of 23 years. Considering the mean value obtained, the FRP has a PBT of 23 years, the rebuilt of 83 years, and the base isolation of 23 years. The FRP and base isolation have comparable PBT, despite the difference in installation costs, which are higher for the base isolation.. The highest value of the PTB in terms of rebuilt is due to the high costs corresponding to the total cost of reconstruction.

An important result highlighted in all retrofit solutions, and especially in base isolation, is the great convenience of use in an as-built configuration with very low seismic performance.

Figure 81 shows the drift and acceleration for building 2 for the as-built/FRP/Rebuilt (Figure 81a, c, e, g) and the base isolation (Figure 81b, d, f, h). A significant reduction in EDPs (acceleration and drift) is observed. Drift in the x-direction is reduced by 1/12 on the ground floor and 1/16 on the upper floor, while in the y-direction it is reduced by 1/7 on the ground floor and 1/10 on the upper floor. Acceleration is reduced by 1/4 in both directions on the ground floor, while it is reduced by 1/16 in the x-direction on the top floor and by 1/10 in the y-direction.

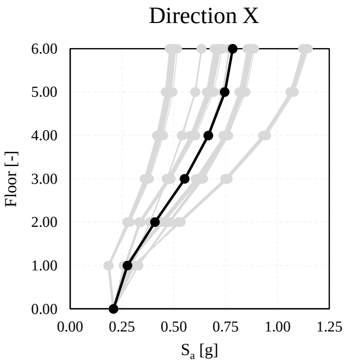
Direction X
Floor [-]
6.00
5.00
4.00
3.00
2.00
1.00
0.00
0.00 0.25 0.50 0.75 1.00 1.25
S_a [g]

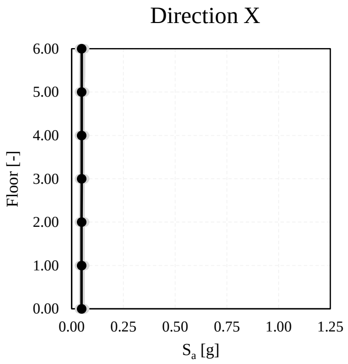
Direction X
Floor [-]
6.00
5.00
4.00
3.00
2.00
1.00
0.00
0.00 0.25 0.50 0.75 1.00 1.25
S_a [g]

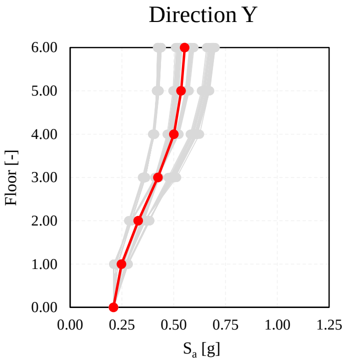
Direction Y
Floor [-]
6.00
5.00
4.00
3.00
2.00
1.00
0.00
0.00 0.25 0.50 0.75 1.00 1.25
S_a [g]

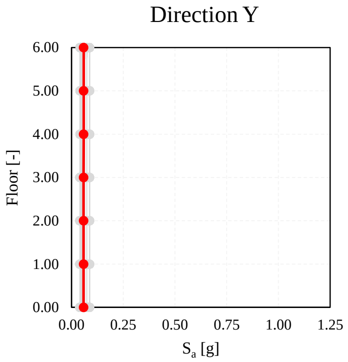
Direction Y
Floor [-]
6.00
5.00
4.00
3.00
2.00
1.00
0.00
0.00 0.25 0.50 0.75 1.00 1.25
S_a [g]

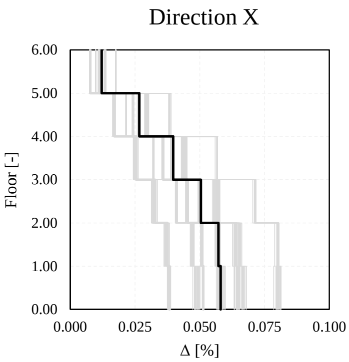
Direction X
Floor [-]
6.00
5.00
4.00
3.00
2.00
1.00
0.00
0.000 0.025 0.050 0.075 0.100
Δ [%]

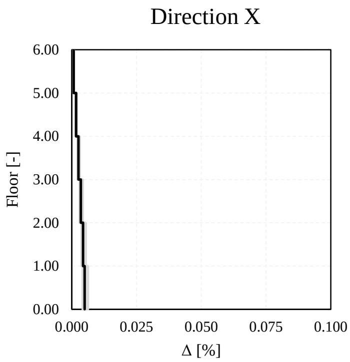
Direction X
Floor [-]
6.00
5.00
4.00
3.00
2.00
1.00
0.00
0.000 0.025 0.050 0.075 0.100
Δ [%]

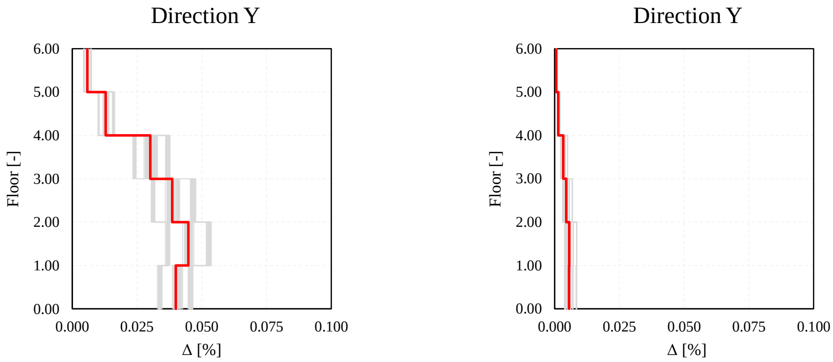

Figure 81. Acceleration in x direction for a) as-built, b) base-isolated configuration and in y direction for c) as-built, d) base-isolated, drift in x direction for e) as-built, f) base-isolated configuration and in y direction for g) as-built, h) base-isolated for building 2

In this case, the variability of f_{cm} and A_{sw}/s has a small effect on the EALs, for all configurations both as-built and retrofit (Figure 82). The complete absence of variability in the as-built configuration is due to the collapse achieved by the interaction between the column and the infill. The number of columns in contact with the infill is more than 50% of the elements of the floor, so the collapse is achieved at a very low return period, due to the low seismic performance of the structure, although the mechanical properties increase. The EALs for the as-built configuration ranges from 3.16% to 2.92%, showing the highest value for the lowest value of f_{cm} of 8.1 MPa and A_{sw}/s of 0.09425 and the lowest for an f_{cm} of 41.3 MPa and A_{sw}/s of 0.2533.

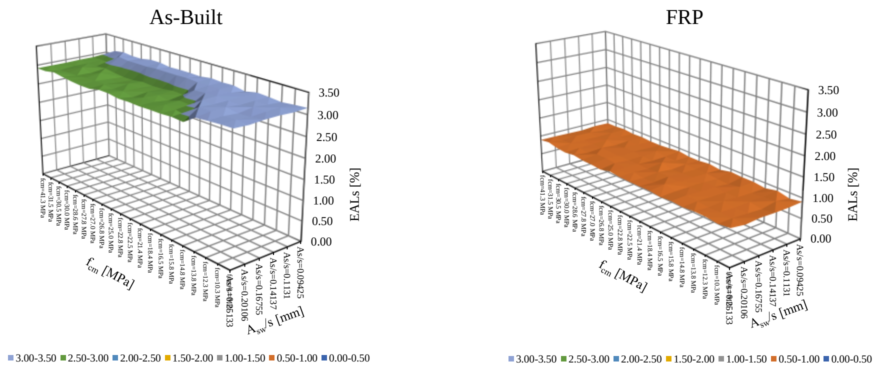

a) b)

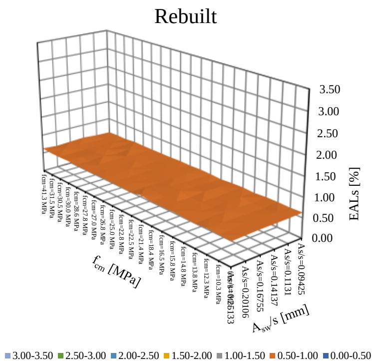

c)

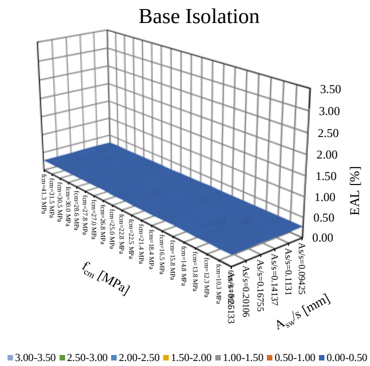

d)

Figure 82. Variation of EALs with the f_{cm} and A_{sw}/s for the building 2 for the different configuration: a) As-Built, b) FRP, c) Rebuilt, d) Base Isolation

Considering the average of the six values of the ratio A_{sw}/s for a given f_{cm} and obtaining 20 values of the EALs, one for each f_{cm}, the maximum value is 3.15%, the minimum value is 2.93% and the average value is 3.02%. As for the EALs for the retrofit configuration, the FRP is characterized by an EALs of about 0.89%, the rebuilt by an EALs of about 0.62% and the base isolation by an EALs of about 0.28%. Despite the variability of the f_{cm} and the A_{sw}/s, the retrofit solutions achieve the same safety index for all values of the parameters. Indeed, the FRP guarantees a safety index of 0.46, while the rebuilt and the base isolation guarantee a safety index of 1.00, so that the collapse loses its role in the evaluation of the loss curve. A comparison of the curves highlights the effectiveness of base isolation compared to the other two techniques. Although base isolation and rebuilt achieve the same safety index, the EALs of the isolated configuration is lower than that of the rebuilt because accelerations and drift are higher reduced, as shown in Figure 81.

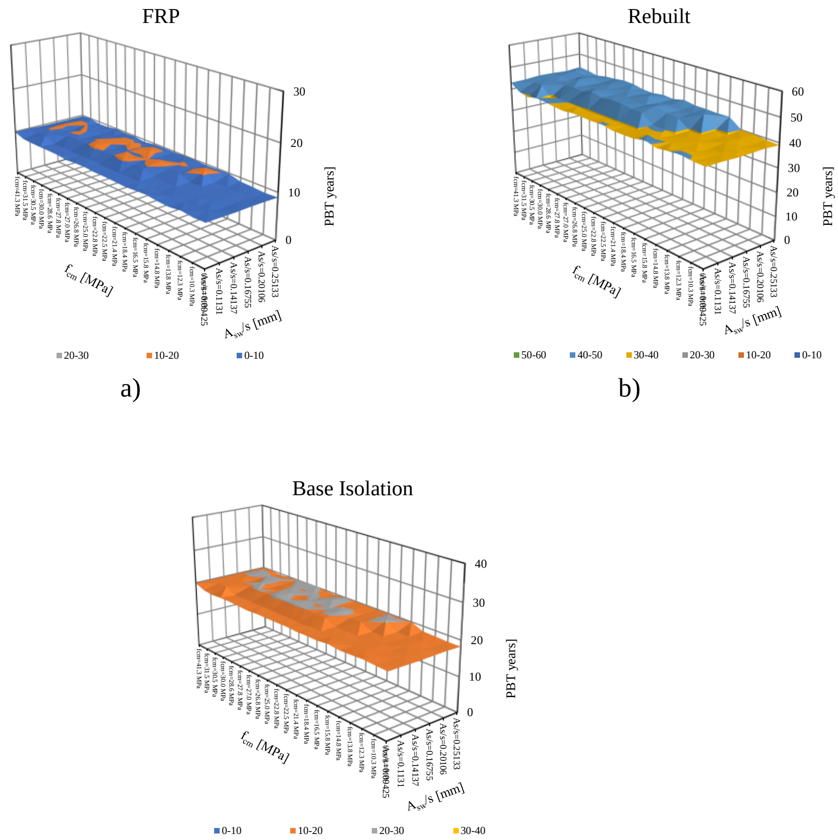

c)

Figure 83. Variation of PBT with the f_{cm} and A_{sw}/s for the building B2 for the different configuration: a) FRP, b) Rebuilt, c) Base Isolation

The low variability in EALs for the as-built configuration mirrors the low variability in PBT for the three-retrofit configurations in exam. Indeed, the PBT for the FRP configuration ranges from 9 to 10 years. 20 values of PBT are obtained by estimating the mean for the six values of A_{sw}/s for a given f_{cm}. The maximum value is 10 years, the minimum value is 9 years, and the mean value is 9 years, which confirms that the influence of the parameters is not present. For the rebuilt configuration, the PBT ranges from 40 to 44 years. When the 20 values of PBT are obtained by averaging the six values of A_{sw}/s for each f_{cm}, the maximum value is 43 years, the minimum value is 39 years, and the mean value is 42 years. At last, the base isolation configuration has a PBT between 18 and 20 years. The mean of the six values of A_{sw}/s for each f_{cm} gives a maximum value of 20 years, a minimum of 18 years and a mean of 19 years. Considering the mean value obtained, the FRP has a PBT of 9 years, the rebuilt one of 42 years and the base isolation of 19 years. In this case, the PBT for the FRP and the base isolation is not comparable due to the high different initial costs, but an important difference refers to the achieved safety index, which is equal to 1 for the base isolation, while 0.46 for the FRP.

PTB's highest value for rebuilt is due to its high cost, which is equal to the total cost of reconstruction.

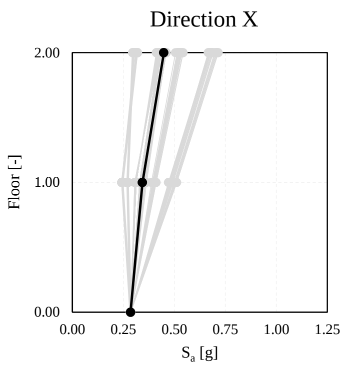

a)

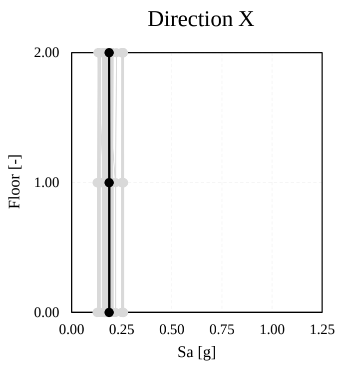

b)

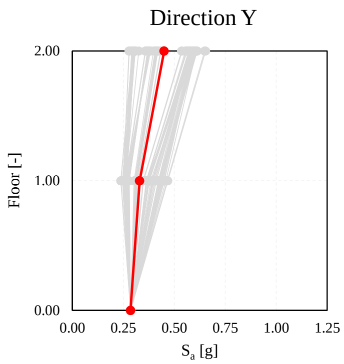

c)

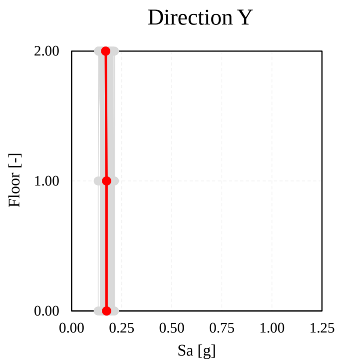

d)

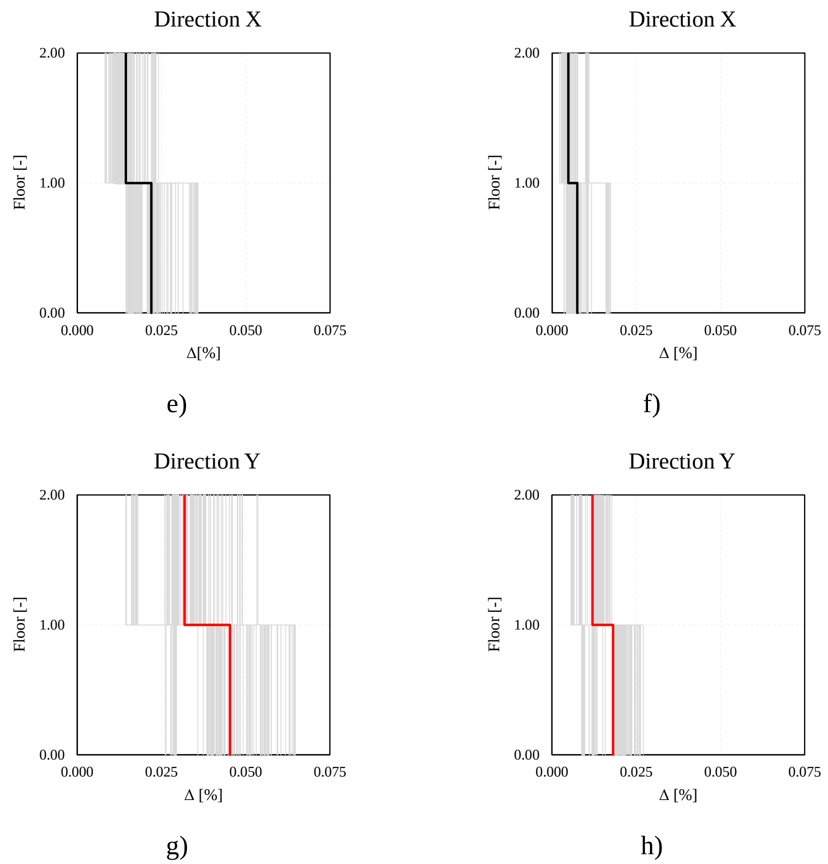

Figure 84. Acceleration in x direction for a) as-built, b) base-isolated configuration and in y direction for c) as-built, d) base-isolated, drift in x direction for e) as-built, f) base-isolated configuration and in y direction for g) as-built , h) base-isolated for building 3

Figure 84 shows the drift and acceleration for building 3 for the as-built/FRP/rebuilt (Figure 84a, c, e, g) and base isolation (Figure 84b, d, f, h). A reduction in EDPs (acceleration and drift) is observed. Drift in the x-direction is reduced by about 1/3 at both the base and the top, while in the y-direction it is reduced by about 1/2 at both the base and the top. For acceleration, the reduction is about ½ in both x and y directions on the ground and upper floor.

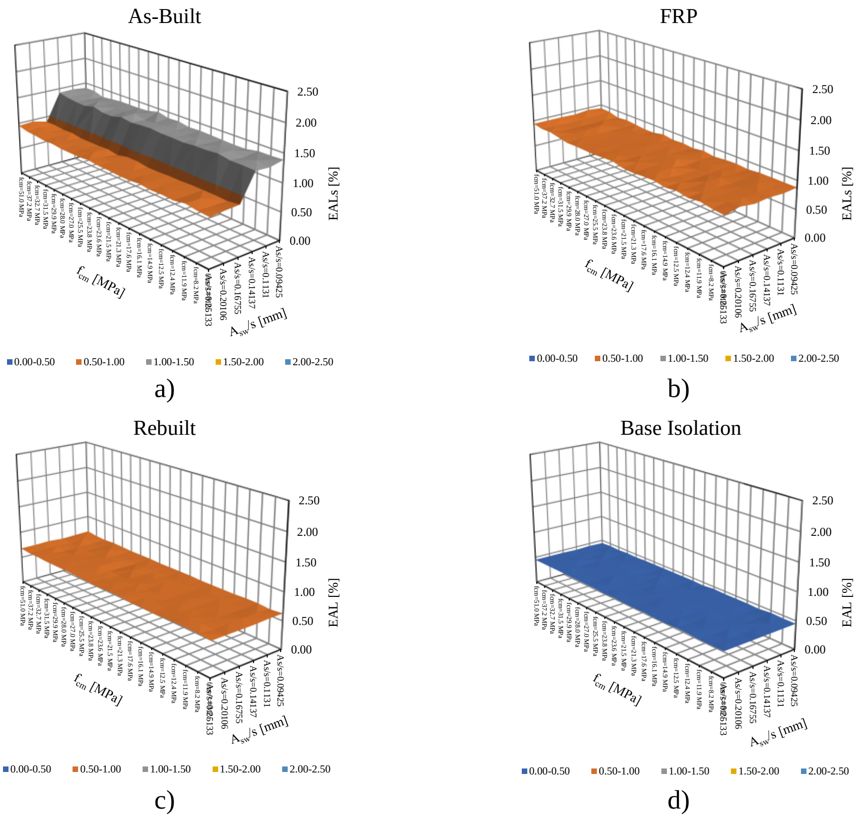

Figure 85: Variation of EALs with the f_{cm} and A_{sw}/s for the building B3 for the different configuration: a) As-Built, b) FRP, c) Rebuilt, d) Base Isolation

The EALs of the as-built configuration show the influence of A_{sw}/s, but not of f_{cm}. As can be seen in Figure 85, the EALs are constant for the first three values of A_{sw}/s, then decrease, and remain constant. The capacity of the column is affected by these three values. Transverse reinforcement increases the contribution to shear capacity more than f_{cm}, resulting in a collapse with a higher return period, which explains the trend shown in Figure 85a.

The EALs for the as-built configuration range from 1.38% to 0.88%, where the first value is assumed for all f_{cm} and the first three values of A_{sw}/s, while the second value is for the other values of A_{sw}/s. The maximum, minimum and average values obtained from the 20 values by averaging the reinforcement parameters are 1.18%, 1.11% and 1.13%, respectively. As can be seen in Figure 85b, c, d, the FRP, rebuilt and base isolation have a constant EALs for all values of f_{cm} and A_{sw}/s equal to 0.88%, 0.64% and 0.45%, respectively. The base isolation shows (Figure 85d) the largest reduction in EAL compared to the other two retrofit solutions. This highlights the effectiveness of the technique in reducing losses even in low-rise buildings.

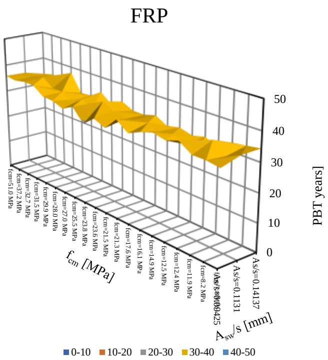

a)

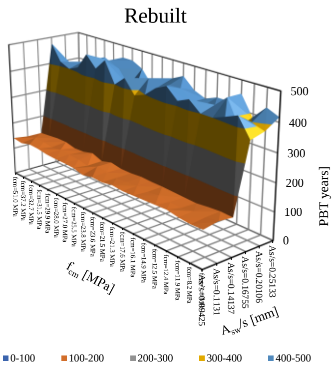

b)

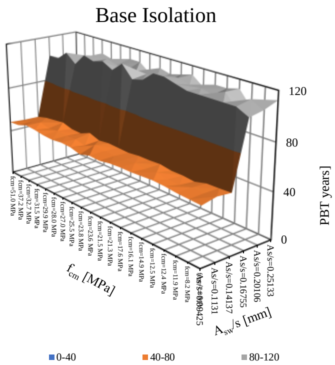

c)

Figure 86. Variation of PBT with the f_{cm} and A_{sw}/s for the building B3 for the different configuration: a) FRP, b) Rebuilt, c) Base Isolation

As can be seen in Figure 86, the PBT for the FRP configuration was estimated for only three values of A_{sw}/s, since for the other values the EALs in the as-built configuration and the FRP configuration are the same and no savings were provided. The good seismic performance of the as-built configuration resulted in this phenomenon, indicating the inability of the FRP for this case. The value of the PBT is almost 33 years. For both the base isolation and the rebuilt configuration, variability of the PBT with the A_{sw}/s is observed in agreement with the variability of the EALs in the as-built configuration. The value of PBT for the rebuilt configuration ranges from 476 to 123 years. With a maximum, minimum and mean of 20 f_{cm} values, obtained with the mean of 6 A_{sw}/s values, equal to 296, 263, 277 years; while for the base isolation the PBT ranges from 116 to 47. With a maximum, minimum and mean of 20 f_{cm} values, obtained with the mean of 6 A_{sw}/s values, equal to 82, 71, 79 years

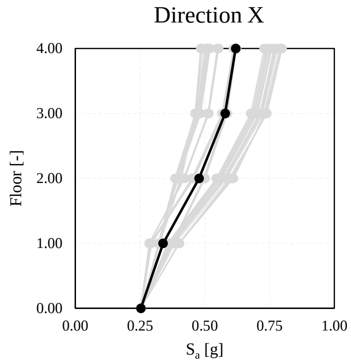

a)

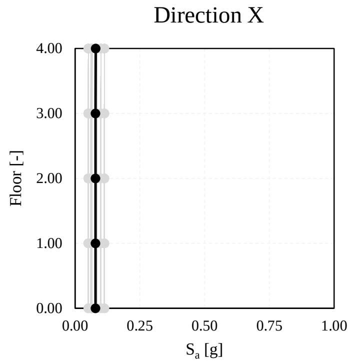

b)

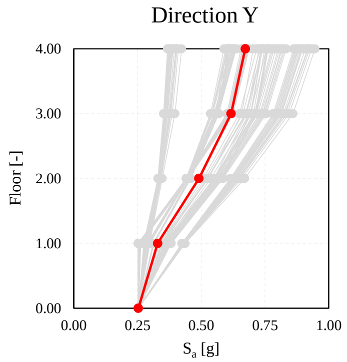

c)

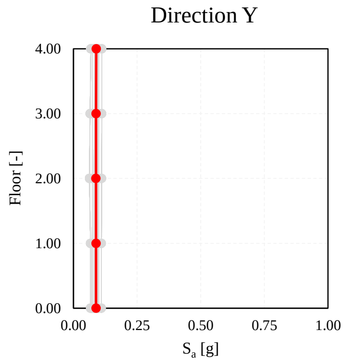

d)

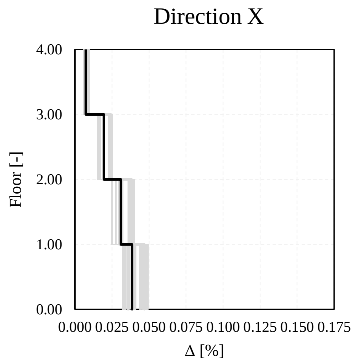

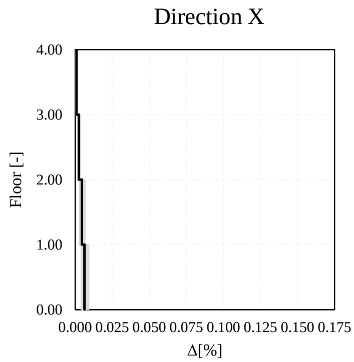

e) f)

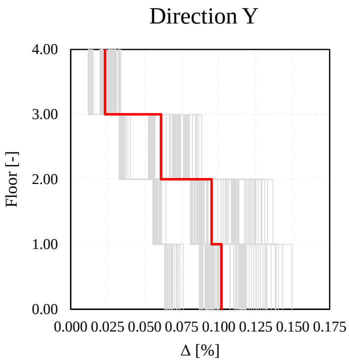

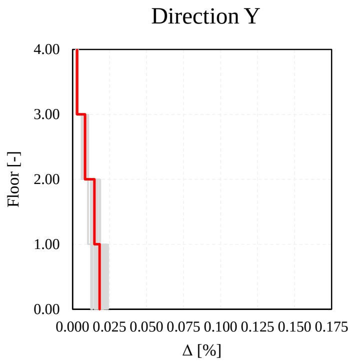

g) h)

Figure 87. Acceleration in x direction for a) as-built, b) base-isolated configuration and in y direction for c) as-built, d) base-isolated, drift in x direction for e) as-built, f) base-isolated configuration and in y direction for g) as-built, h) base-isolated for building 4

Figure 87 shows the drift and acceleration for building 4 for the as-built/FRP/rebuilt (Figure 87a, c, e, g) and base isolation (Figure 87b, d, f, h). A reduction in EDPs (acceleration and drift) is observed. Drift in x-direction is reduced by 1/6 on the ground floor and 1/8 on the top, while in y-direction it is reduced by 1/5 on the ground floor and 1/8 on the top. Acceleration is reduced by 1/ on the ground floor and 1/8 on the top, in both x and y directions.

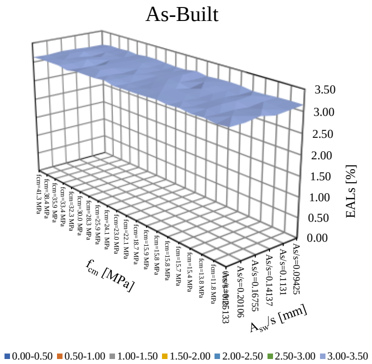

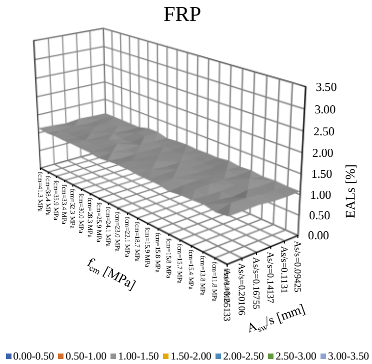

a) b)

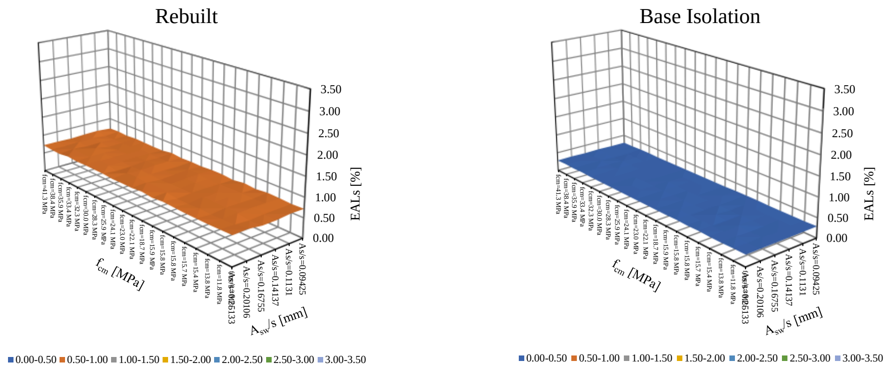

c) d)

Figure 88. Variation of EALs with the f_{cm} and A_{sw}/s for the building B4 for the different configuration: a) As-Built, b) FRP, c) Rebuilt, d) Base Isolation

The EALs for the as-built configuration were not affected by the variability of the resistance concrete f_{cm} and the transverse reinforcement A_{sw}/s, as in the previously described cases. The reason, similar to the previous cases, is the interaction between infills and columns, because more than 50% of the elements (columns) are connected to the infills, so they fail at a very low return period and the increase in f_{cm} or A_{sw}/s is not sufficient to cope with the increased demand due to the stiffness of the infills. The EALs is about 3.14%. For the FRP, rebuilt and base isolation, the EALs is constant, as in the previous cases, and is not affected by the parameters in exam. It is equal to 1.10%, 0.72% and 0.28%, respectively.

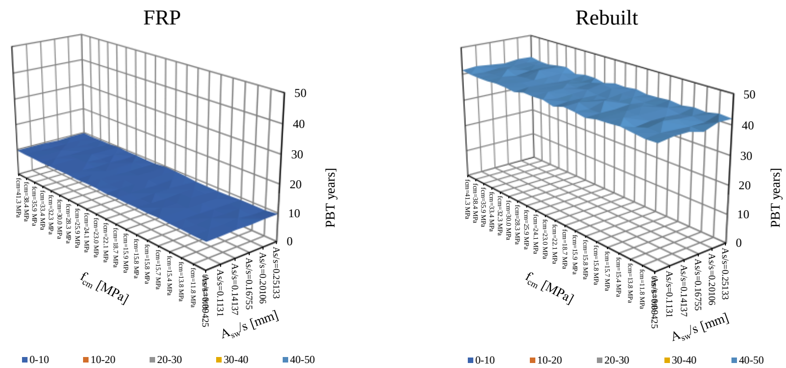

a) b)

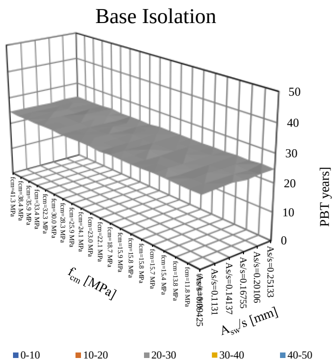

c)

Figure 89: Variation of PBT with the f_{cm} and A_{sw}/s for the building B4 for the different configuration: a) FRP, b) Rebuilt, c) Base Isolation

The lack of variability in the EALs is reflected in the PBT for the solution studied. The PBT for the FRP configuration is about 10 years, for the rebuilt configuration about 41 years, and for the base isolation about 24 years. Although the PBT of the base isolation is higher than that of FRP, the safety index achieved by the base isolation is equal to 1.00, while for FRP it is 0.72. Thus, the longer time of recovery of economic investment can be justified by the increase of safety, which guarantees that the losses in case of seismic event will be significantly reduced, unlike FRP, which is likely to cause more losses and costs in case of seismic event.

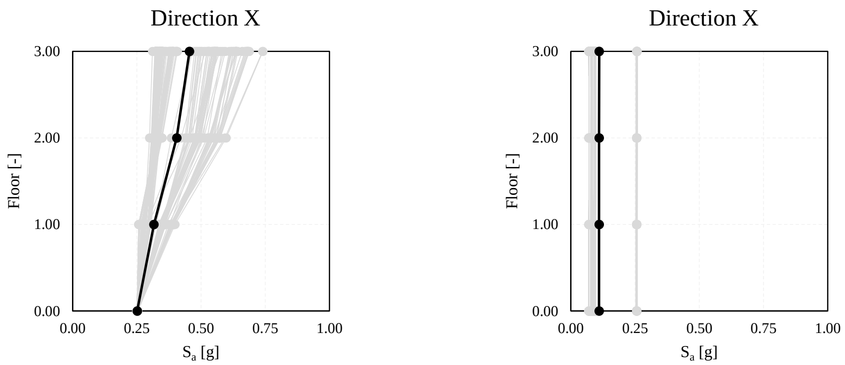

a)   b)

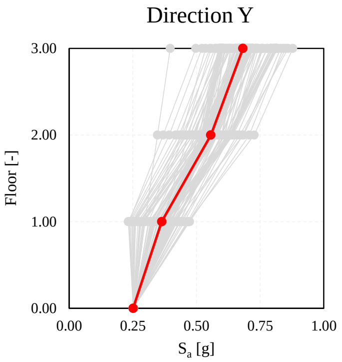

c)

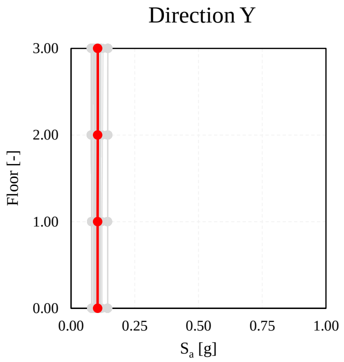

d)

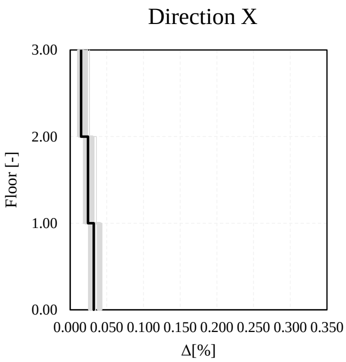

e)

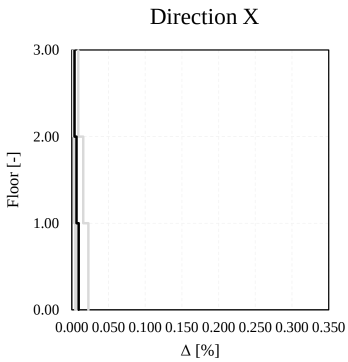

f)

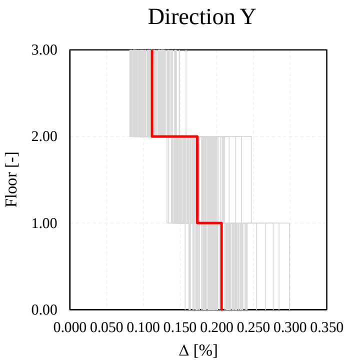

g)

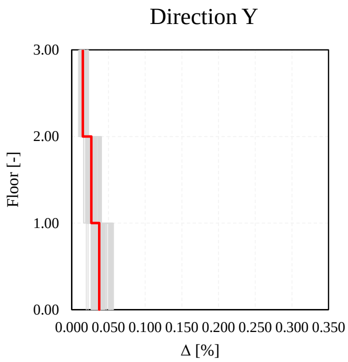

h)

Figure 90. Acceleration in x direction for a) as-built, b) base-isolated configuration and in y direction for c) as-built, d) base-isolated, drift in x direction for e) as-built, f) base-isolated configuration and in y direction for g) as-built, h) base-isolated for building 5

Figure 90 shows the drift and acceleration for building 5 for the as-built/FRP/rebuilt (Figure 90a, c, e, g) and base isolation (Figure 90b, d, f, h). A reduction in EDPs (acceleration and drift) can be observed. Drift in the x-direction has a reduction of about ¼ on ground floor and top, while in the y-direction it is about 1/5 on ground floor and 1/8 on the top. For acceleration, the reduction is about 1/2 and 1/4 on ground floor and top, in x-direction and about 1/5 and 1/7 on ground floor and top, in the y-direction.

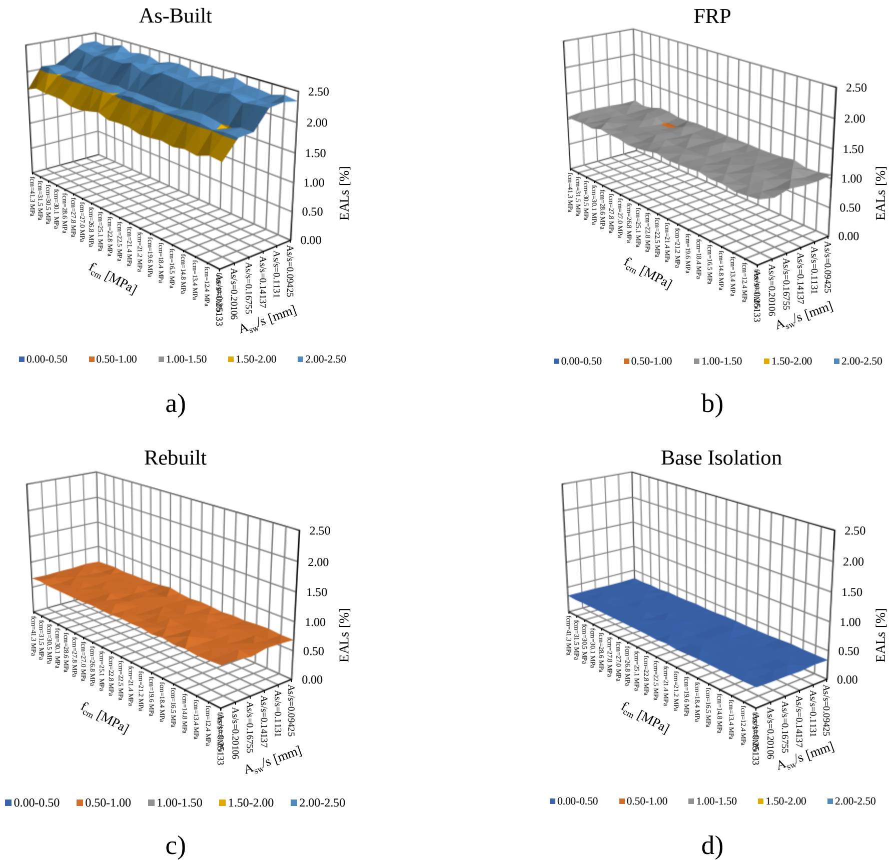

Figure 91. Variation of EALs with the f_{cm} and A_{sw}/s for the building B5 for the different configuration: a) As-Built, b) FRP, c) Rebuilt, d) Base Isolation

The variability of the A_{sw}/s affects the EALs for the as-built configuration, which decrease as the parameter increases, while the f_{cm} does not affect the loss curve. The EALs for the A_{sw}/s range from 2.43% to 1.65%, while the maximum, minimum and mean values for the 20 values of f_{cm} by averaging the six values of A_{sw}/s are 2.15%, 2.08% and 2.13%, respectively, highlighting the absence of variability with f_{cm}. As for FRP, rebuilt and base isolation, both A_{sw}/s and f_{cm} do not condition EALs. The values are 1.05%, 0.69%, and 0.33%, respectively.

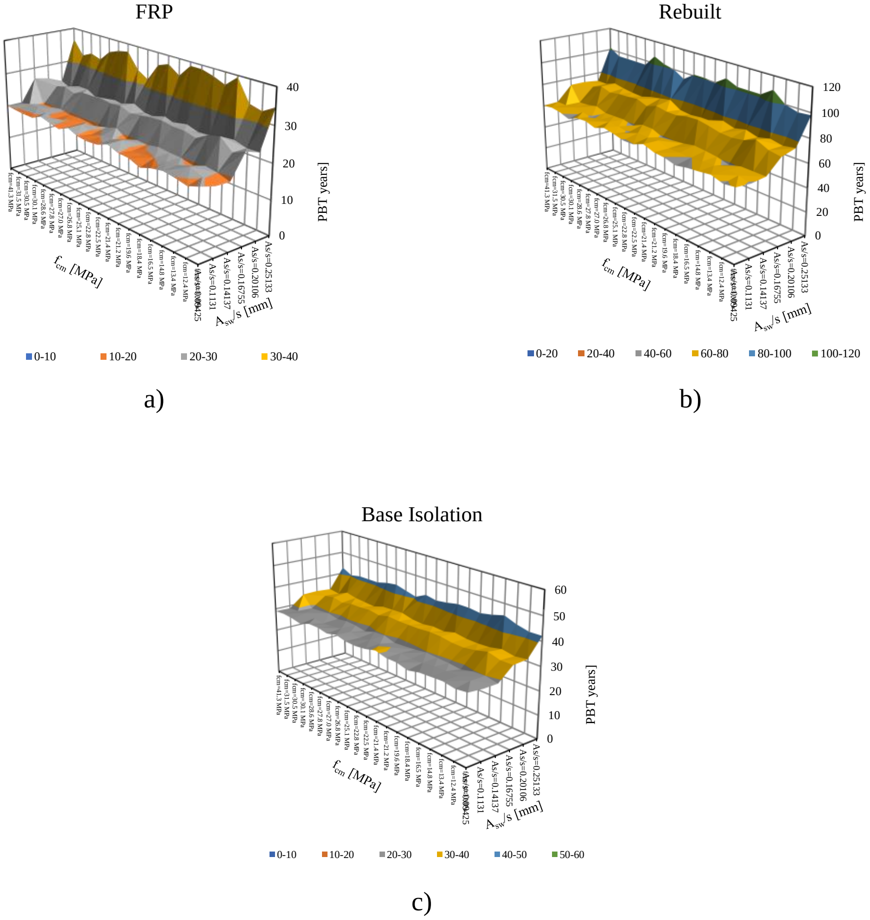

Figure 92. Variation of PBT with the f_{cm} and A_{sw}/s for the building B5 for the different configuration: a) FRP, b) Rebuilt, c) Base Isolation

The PBT for all retrofit solutions show the same trend, decreasing with decreasing A_{sw}/s, while remaining constant with f_{cm}. This mirrors the trend of EALs with indirect proportionality, as described above. The FRP configuration has a PBT between 19 and 40 years, while the variability with the f_{cm} shows the maximum, minimum, and mean values of the 20 f_{cm} values averaged over the six A_{sw}/s values for each f_{cm}, equal to 26, 24, and 23 years, respectively, highlighting the lack of variability with the f_{cm}. For the rebuilt, the range with A_{sw}/s is from 57 to 109 years, while the variability with the f_{cm}, shows the maximum, minimum and mean values of the 20 values of f_{cm} averaged over the six values of A_{sw}/s for each f_{cm} equal to 74, 71, 72 years. At last for the base isolation, the PBT with A_{sw}/s ranges from 28 to 45 years, while the variability with the f_{cm} shows the maximum, minimum, and mean values of the 20 values of f_{cm}, averaged over the six values of A_{sw}/s for each f_{cm} equal to 34, 32, 33 years.

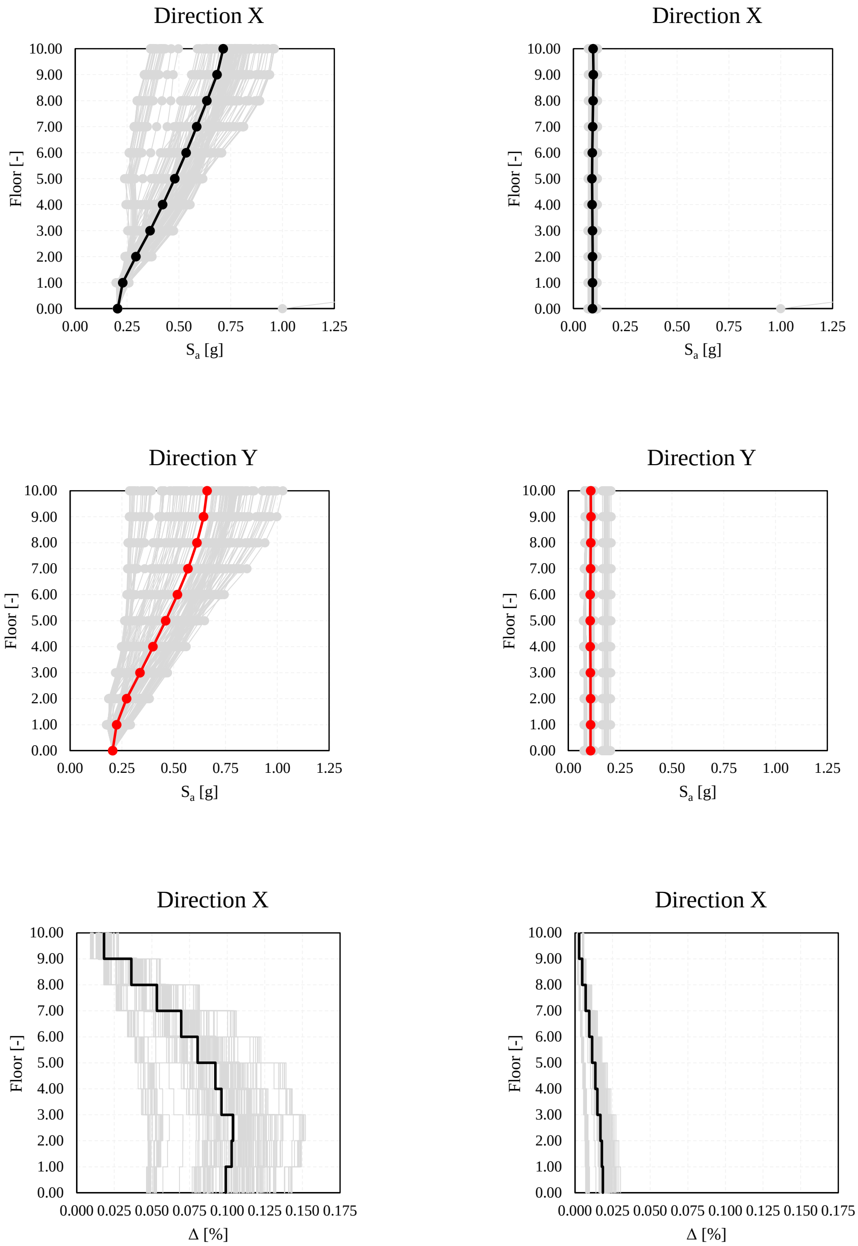

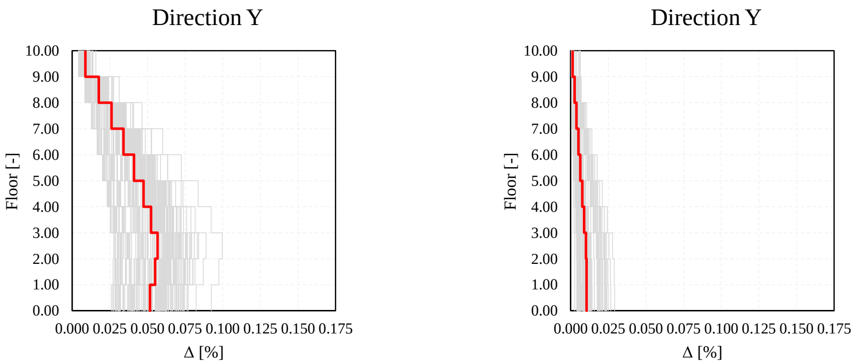

Figure 93. Acceleration in x direction for a) as-built, b) base-isolated configuration and in y direction for c) as-built, d) base-isolated, drift in x direction for e) as-built, f) base-isolated configuration and in y direction for g) as-built, h) base-isolated for building 6

Figure 93 shows the drift and acceleration for building 6 for the as-built/FRP/rebuilt (Figure 93a, c, e, g) and base isolation (Figure 93b, d, f, h). A reduction in EDPs (acceleration and drift) is observed. Drift decreases by about 1/5 and 1/7 in both x and y directions on the ground floor and top, respectively, the acceleration decreases by about 1/2 and 1/7 in x direction at on the ground floor and top, respectively, and by about 1/2 and 1/6 in y direction on the ground floor and top, respectively.

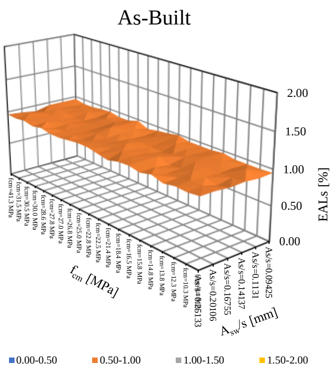

a)

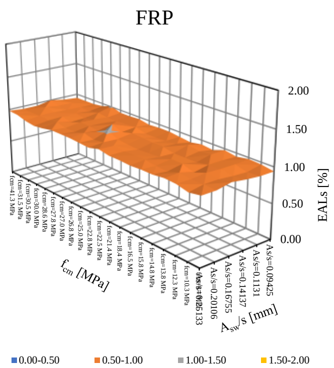

b)

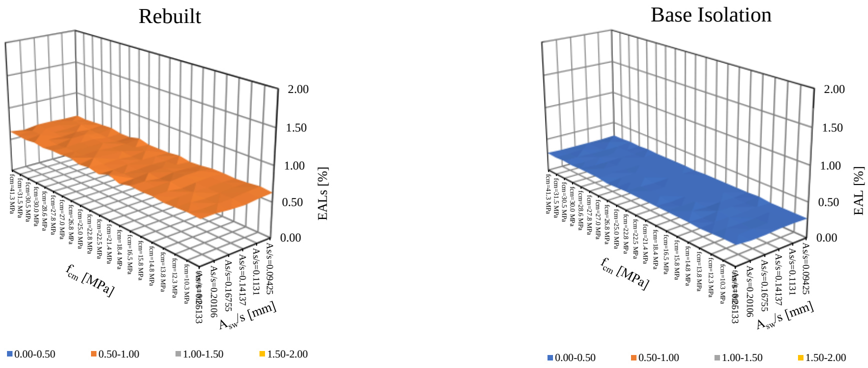

c) d)

Figure 94. Variation of EALs with the f_{cm} and A_{sw}/s for the building B6 for the different configuration: a) As-Built, b) FRP, c) Rebuilt, d) Base Isolation

As in the previous cases, the variability of A_{sw}/s and f_{cm} does not affect the evaluation of the EALs for the as-built configuration, which is constant and equal to 0.95%. The low value of the EALs for the as-built configuration is due to the recent years of construction. The seismic rules applied during the construction gets the building quite effective respect to the seismic actions. Indeed, it shows a safety index of as-built equal to 1.00. The application of the FRP isn't able to improve the seismic performance, indeed the EALs is equal to 0.95%, although the variation of f_{cm} and A_{sw}/s, it doesn't vary. Furthermore, the parameters in exam don't affect both the rebuilt and base isolation configuration, indeed they show an EALs constant, equal to 0.63% and 0.28%, respectively.

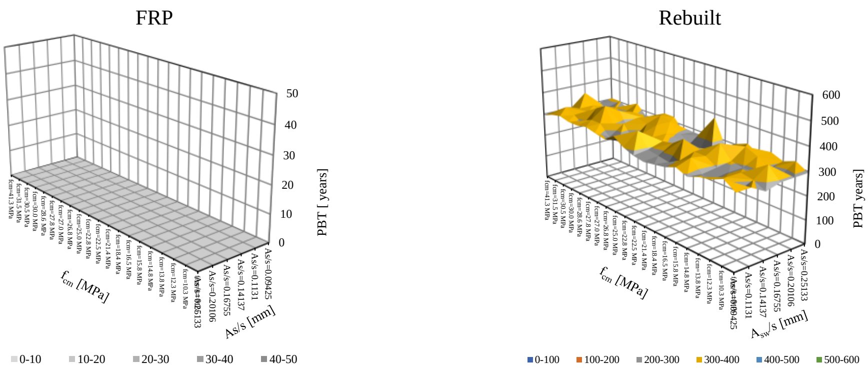

a) b)

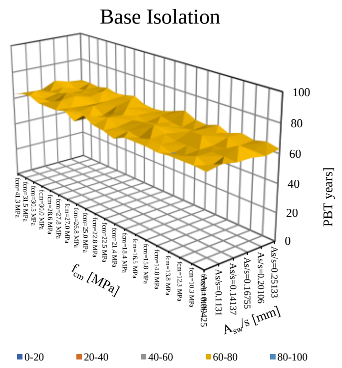

c)

Figure 95. Variation of PBT with the f_{cm} and A_{sw}/s for the building B6 for the different configuration: a) FRP, b) Rebuilt, c) Base Isolation

Due to the same value of EALs of the as built and FRP configuration, it isn't possible to define a PBT for this configuration, because no savings are gained during the time, indeed no improvement in seismic performances are taken by the FRP. While the rebuilt and the base isolation configuration show a constant PBT for all value of f_{cm} and A_{sw}/s equal, respectively, to 307 and 64 years

5.5 Discussion of results

The following Table 13 summarizes the main characteristics and the main results in terms of EALs and Pay-back time, for the six buildings analyzed. In addition, the safety index for the as-built and FRP configuration was given.

Table 13. Main characteristics and results for the 6 buildings in exam

	N Piani	PGA	Zona Sism	Sup Piano	Età	f_{cm}	f_{ym}	LC	Costo FRP	Costo Rebuilt	Costo Iso	Costo Iso
	[-]	[g]	[-]	[m^2]	[years]	[MPa]	[MPa]	[-]	[€]	[€]	[€]	[%]
1	4	0.305	1	434	60	16.8	309.0	2	369905.6	2079000.0	833166.0	40.0
2	6	0.209	2	351	-	21.9	430.0	3	568709.7	2843100.0	1492930.0	52.5
3	2	0.285	1	592	-	18.7	401.5	2	293369.1	1800900.0	861553.5	53.9
4	4	0.253	1	626	-	12.0	459.0	3	526166.4	3380400.0	1891255.4	55.9
5	3	0.251	1	874	80	10.3	453.0	2	870826.2	3539700.0	2058603.9	58.2
6	10	0.205	2	887	90	25.0	430.0	2	2502151.2	11974500.0	6456246.9	53.9

$\zeta_{AS\text{-}BUILT}$	ζ_{FRP}	$EAL_{As\text{-}Built}$	EAL_{FRP}	$\Delta EALs$	PBT_{FRP}	$EAL_{REBUILT}$	$\Delta EALs$	$PBT_{REBUILT}$	EAL_{ISO}	$\Delta EALs$	PBT_{ISO}

	[%]	[%]	[%]	[%]	[%]	[years]	[%]	[%]	[years]	[%]	[%]	[years]
1	60	100	2.15	1.23	0.92	21	0.91	1.24	83	0.37	1.78	23
2	29	46	3.02	0.89	2.13	9	0.62	2.40	42	0.28	2.74	19
3	83	100	1.13	0.88	0.25	44	0.64	0.49	277	0.45	0.68	79
4	33	72	3.14	1.10	2.04	10	0.72	2.42	41	0.28	2.85	24
5	59	100	2.13	1.05	1.07	24	0.69	1.43	72	0.33	1.79	33
6	100	100	0.95	0.95	0.00	28	0.63	0.33	307	0.28	0.68	64

The results related to EALs and PBT refer to the mean of the 20 values of f_{cm}, taking the average of the 6 values of A_{sw}/s for each of them.

As can be seen in the Table 13, the EALs for the as built configuration shows variability, although some structures have the same characteristics. The maximum value of EALs is related to the building with a higher number of floors (Buildings 2), where a higher shear value was measured due to the mass, leading to premature failures, while building 4, despite having a lower number of floors, has the same EALs value but is characterized by a higher PGA value. A difference is shown between building 1 and 4, although the same number of stories and a different PGA, higher for building 1. The difference is due to the interaction with the infills, since building 4 is characterized by infills with greater length, which cause a greater shear value on the columns, resulting in failures of all columns with interaction, causing 50% of the elements to fail at a very low return period. Moreover, the two buildings with the higher EALs values are characterized by the lower value of $\zeta_{AS-BUILT}$. As for the PGA, buildings 4 and 5 have the same value since they are located in the same site. The difference in EALs is due to the dimensions in the floor plan, as building 5 has a larger plane compared to building 4 with a very high number of columns. Although the PGA value is the same (and the masses are also the same), the shear has to be distributed over more columns, so each of them has a lower value. This leads to a shear failure in building 4 that precedes the one in building 5.

The EALs values for the three retrofit solutions for all analyzed buildings are similar due to the close correlation with the collapse calculation. The FRP collapse was determined when more than 50% of the reinforced elements fail, and this value is used to calculate the EALs. For all buildings, this occurs when the safety index is 80%, while the ζ_{FRP} value given in the table is calculated when the first column fails, and the values are similar for all buildings, with a return period of 475 years, except for building 2 and 4, where the dimensions of the column (30x30) and the interaction with infills, respectively, do not allow a higher safety index. The collapse of the rebuilt building and the base isolation was defined for a safety index of 1.00, moreover a difference between the EALs of the two retrofit solutions can be observed. The reduction of EDPs, such as acceleration and drift, allows a lower loss curve for the base isolation than for the rebuilt.

The most important parameter provided by the code is the PBT, both for the base isolation and for the other retrofit solutions considered. The PBT is directly related to the cost of the technology and the savings achieved. As Table 13 shows, the highest PBT are for the building with the lowest and highest height (2 floors -10 floors), with values far from the others. In fact, the savings (ΔEALs) obtained by applying the base isolation are the lowest, due to the good seismic performance of the as-built configuration. The number of floors is not the only variable related to PBT. Indeed, a building with a lower number of floors than another may have a higher PBT, for example, building 1 and 5 with 4 and 3 floors, respectively. Moreover, building 1 has a higher PGA than building 5 and has a lower PBT even though it has the same seismic performance expressed by the $EALs_{AS\text{-}BUILT}$. In fact, the cost of building 5 is higher than building 1, so the same savings will take more time to pay back the economic investment. The difference in installation costs is due to the different dimensions of the building. On the other hand, buildings with the same floor and different PGA can have the same PBT, as for building 1 and building 4, which are in two different locations with different PGA. In fact, despite the higher installation cost and lower PGA, building 4 has more savings than building 1 due to very low seismic performance causing high losses with premature collapse.

Buildings with the same PGA, such as 4 and 5, show different values for PBT. Building 4 has a lower PBT value than building 5, which is due to the higher savings from the installation of the base isolation. The low seismic performance of building 4 resulted in significant savings as expressed in the ΔEALs compared to building 5, which has a good seismic response. In addition, the costs for these buildings are comparable.

The base isolation considerations can be applied to the rebuilt and the FRP. A comparison between the three retrofit solutions shows that the FRP has the lowest PBT, followed by the base isolation and finally the rebuilt.

This could indicate that the FRP solution is cheaper than the others, but an important point is that the safety index guaranteed by the FRP might be lower compared to that of the base isolation and the rebuilt. This leads to additional costs in case of a seismic event after retrofit, which are avoided in the other two retrofit solutions. Therefore, the base isolation might be the more convenient and useful solution in terms of safety and economy.

On the other hand, the parametric study has shown that the convenience of the base isolation may vary with different parameters. It is clear that the number of floors is an important parameter for evaluating the usefulness of base isolation. The lower the number, the worse the convenience, and the seismic performance of the as-built is another parameter that plays a crucial role in the convenience.

CHAPTER 6 – BASE ISOLATED INFRASTRUCTURES

The effectiveness of seismic retrofitting by using base isolation is not limited to buildings, but it can be extended to all other existing constructions, especially to infrastructures, which protection is strategic for the resilience of modern communities in seismic prone areas. Indeed, the failure or downtime of a bridge during an earthquake could have severe consequences in terms of loss of lives and direct and indirect monetary losses. For example, part of acity could be excluded from rescue, increasing the number of fatalities. In recent years, seismic events demonstrated that the performance of existing RC bridges is poor. For this reason, different retrofit solutions have been developed to enhance seismic performances of existing bridges. The base isolation is widely used because the structural system (piers and deck) has an optimal configuration for their installation. The frequent use of base isolation on the infrastructure, especially on the bridge, has driven the continuous research and development of new devices targeting the increasing effectiveness of the devices with a moderate cost. In the previous chapters, the different isolation devices available on the market are illustrated. In this chapter attention is given to a novel isolation device: the Ball Rubber Bearing (BRB) that is studied from an experimental and analytical standpoint as part of the period spent abroad at the Middle Est Technical University (METU) within this PhD program.

6.1 Novel isolation devices: Ball Rubber Bearing

The Ball Rubber Bearing (BRB) devices combine the practical use and the low maintenance cost of elastomeric bearing with a friction-based dissipation provided by the steel balls in the inner core (Ozkaya et al. 2011). They belong to the category of elastomeric bearings using the insert in the core and to achieve high performances. The configuration is comparable to this of the Lead Rubber Bearing (LRB), with low carbon steel balls in the inner core rather than a lead core. The work aims at developing a design-oriented formulation to estimate the equivalent damping, the characteristic strength and the lateral stiffness of BRBs. In order to calibrate and validate the proposed formulation, experimental tests available in literature are collected. In addition, further 15 experimental tests are performed with different level of maximum displacement and axial pressure to clear identify the effect of such variables on the damping. Simple considerations on the influence of the different design parameters are discussed and used to calibrate a reliable design formulation to be used in the design practice. Furthermore, the work aims at assessing the influence of short-term lateral creep on the hysteretic response of different rubber bearings, namely EB and BRBs. To this end, experimental tests on different elastomeric bearings under imposed lateral displacement are performed. For each device, the lateral response is measured, and the advantages and disadvantages are discussed in terms of strength, stiffness, energy dissipation and equivalent damping. The loss of load under sustained lateral displacement is experimentally assessed and the effects of creep in the design procedure of a base isolated system are discussed. Despite of the analytical and experimental studies the recent development of the device involve further study to deeply analyze different aspect of the bearing, from the long terms effect to the variable influencing its behavior.

6.1.1 Experimental Characterization

Two experimental campaigns were carried out on BRB devices: one aiming at studying the role of displacement and axial load on the hysteretic response of the bearings, and the other one aimed at investigating the effects of horizontal creep.

6.1.1.1 Experimental program to assess the influence of displacement ad axial load

In this campaign the Ball Rubber Bearing (BRBs) with geometry depicted in Figure 96 were tested. They are composed by an alternance of rubber layers (15 mm thick) and steel shims (2 mm thick). A special mixture of neoprene and natural rubber is used (Ozkaya et al. 2011). Natural rubber with a nominal stiffness of 60 Shore A Durometer was used (Caner et al. 2015). 17.5 mm thick steel plates (st37-(1980)) are vulcanized to elastomers under pressure and with heat activated bonding agent at the top and the bottom of the device. The diameter of the bearings, *D*, is 500 mm and the total height about 66 mm (without steel plates) with a shape factor of about 7. Inner hole has a diameter of 165 mm, *d*, and it is filled with steel balls to increase energy dissipation. The steel balls used in these specimens have a diameter of 1.65 mm and they are made with low-carbon steels. This type of material is used to contain the cost of the device. Although the stainless steel has a higher resistance to corrosion, in such a type of bearings the steel balls are located in the inner hole surrounded by rubber glued to the steel plates. This protects the steel balls from exterior environment

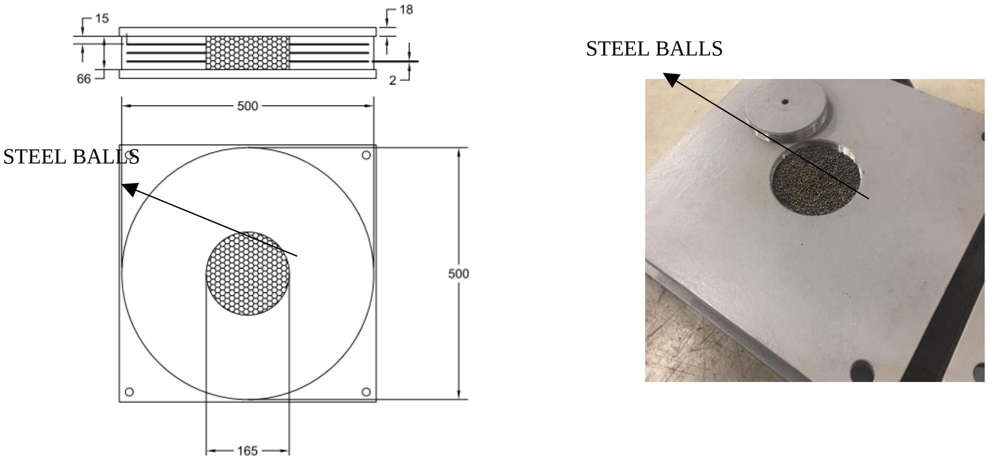

(a) (b)

Figure 96. Geometry (a) and front view (b) of the tested BRBs (dimensions in mm).

The test setup used to carry out the experimental tests is depicted in Figure 97. It consists in two oleo-dynamic actuators applying the constant axial load and the cyclic horizontal displacement. Load cells and linear variable displacement transducer (LVDT) are used to monitor the load and displacement.

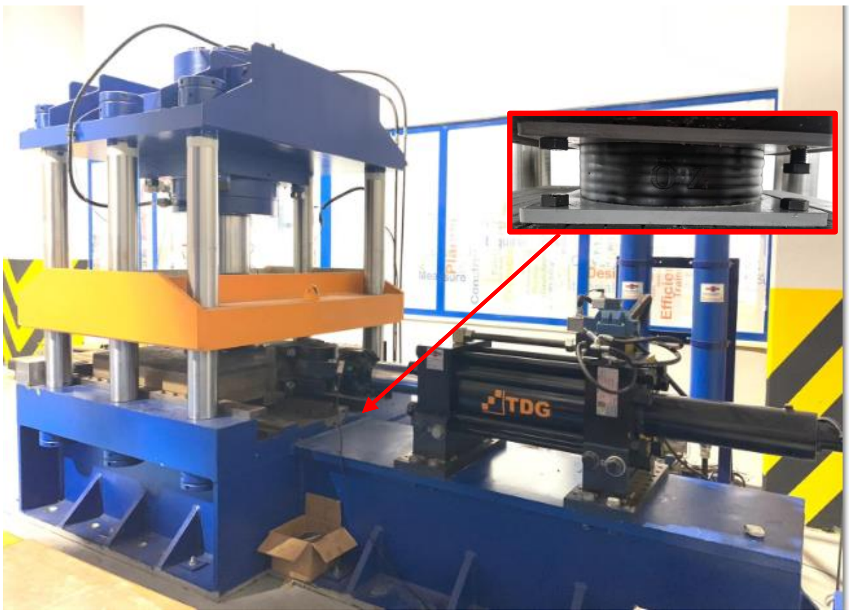

Figure 97. Test setup

The devices are tested in individually and connected to a steel plate connected to the horizontal actuator, as showed in Figure 97.

Table 14. Experimental program

Test n.	Axial Pressure [MPa]	Displacement [mm]	γ [%]
P3_d15	3	15	25
P3_d30	3	30	50
P3_d45	3	45	75
P3_d60	3	60	100
P3_d75	3	75	125
P6_d15	6	15	25
P6_d30	6	30	50
P6_d45	6	45	75
P6_d60	6	60	100
P6_d75	6	75	125
P9_d15	9	15	25
P9_d30	9	30	50
P9_d45	9	45	75
P9_d60	9	60	100
P9_d75	9	75	125

The experimental program consists of 15 tests on BRB device with the same geometric characteristic for all the tests. The tests can be grouped in three bins characterized by an increasing axial pressure. 3, 6 and 9 MPa (labelled as P3, P6 and P9, respectively). Devices are tested at five different maximum displacement: 15 mm, 30mm, 45mm, 60mm and 75mm (labelled as d15, d30, d45, d60, d75). Also, the shear deformation (γ) is reported in Table 14.

The three different level of axial pressure are selected to reproduce the service and seismic load condition of an isolation device belonging to bridge structures. Three cycles at the maximum displacement are performed for each test to assess the stability of the bearing. The loading rate is the maximum speed allowable for the setup. The tests were conducted on the same specimen for 15 times checking that no damage interested the bearings.

The experimental observations for the third cycle of the tests, is depicted in Figure 98, Figure 99 and Figure 100 at the tests with 3 MPa, 6 MPa and 9 MPa axial pressure, respectively. To clearly show to the reader the hysteretic response and remove the effects of the first loading branch, only the third cycle of the tests is reported. However, it is worth mentioning that no degradation effects (e.g. scragging/Mullins effects) were observed during the first cycles.The main experimental results are also summarized in Table 15 in terms of F_{max}, the maximum recorded force, calculated as the mean of the value in positive and negative direction, $Q_{d,BRB}$, the characteristic strength, equal to the intersection of the cycle with the vertical axis (i.e. at an imposed displacement equal to zero), and calculate as the average absolute between the two values (negative and positive), d_{max}, the maximum imposed displacement, P_{ver}, the axial load applied on the bearings, E_d, the energy dissipation provided by the real cycle, equal to the area under the curve, E_w, the energy dissipation provided by an equivalent cycle having characterized by F_{max} and d_{max} and β_{eq}, the equivalent damping (calculated according to Eq.31).

$$\beta_{eq} = \frac{E_d}{4\pi \cdot E_s} = \frac{E_d}{2\pi \cdot k_{eff} \cdot d_{max}^2} = \frac{E_d}{2\pi \cdot F_{max} \cdot d_{max}} \tag{31}$$

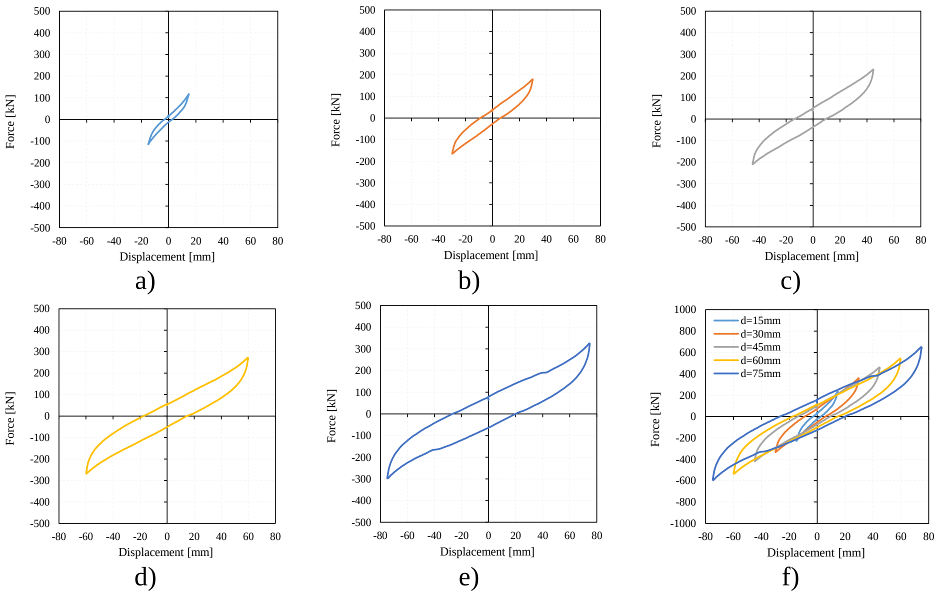

Figure 98. Cyclic response of tested BRBs at 3 MPa axial pressure: a) d_{max}=15mm; b) d_{max}=30mm; c) d_{max}=45mm; d) d_{max}=60mm; e) d_{max}=75mm; f) comparison of the cyclic response at different maximum displacement.

Figure 98a shows the hysteretic response of the ball rubber bearing tested at d_{max}= 15 mm under 3 MPa axial pressure. The maximum force in the positive direction is about of 117 kN while in the negative direction is -114 kN, with a damping ratio about of 7.6%. By increasing the displacement demand to d_{max} = 30mm, (see Figure 98b) the maximum force increases to 179 kN and -166 kN, in the positive and negative direction, respectively. Also the damping ratio increases to 11.3%. The same trend is found for the other tests at d_{max}= 45mm (see Figure 98c), d_{max}=60mm (see Figure 98d) and d_{max}=75mm (see Figure 98e). The maximum force increases to 229 kN, 272, kN and 325 kN in the positive direction, while in the negative direction to -208 kN, -268 kN and -297 kN, for d_{max} equal to 45 mm, 60 mm and 75 mm, respectively. The related damping ratio is equal to 11.5%, 11.5% and 12.5%.

The energy dissipation for a d_{max} = 75 mm is about 22.8 times higher than the one at d_{max} = 15mm, 5.0 times the one at d_{max} = 30mm, 2.6 times the one at d_{max} = 45 mm and 1.6 times that at d_{max} = 60mm. Despite of the significant increase in the energy dissipation by increasing the displacement demand, a significant increase in the damping can be observed only moving from d_{max} =15 mm to the d_{max} =30mm. Beyond d_{max} = 30 mm, the increasing displacement demand does not produce a significant increase in the damping. This is because of the contemporary increase of the product of the of maximum force, F_{max}, and maximum displacement, d_{max}, that reduce the damping as remarked in Eq. (1).

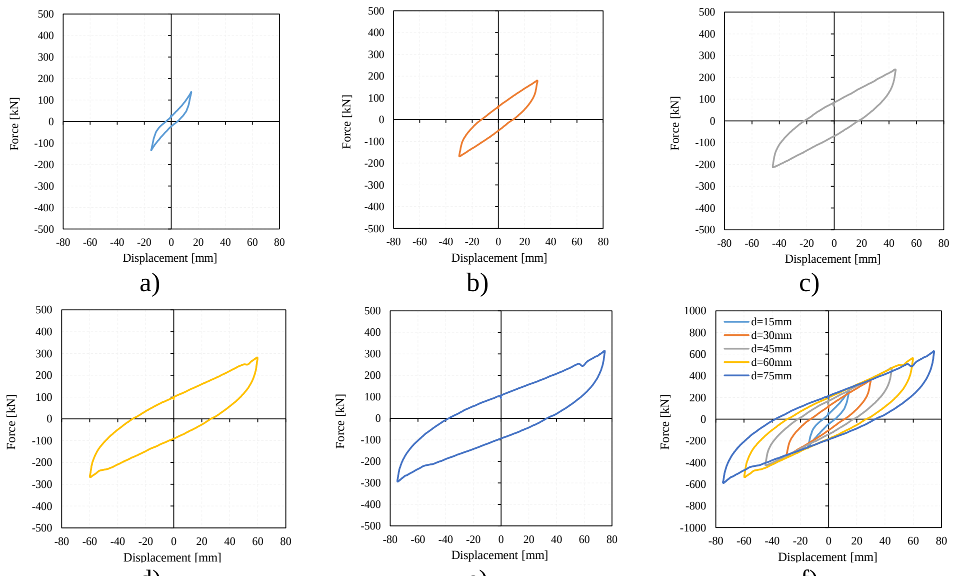

Figure 99. Cyclic response of tested BRBs at 6 Mpa axial pressure: a) d_{max}=15mm; b) d_{max}=30mm; c) d_{max}=45mm; d) d_{max}=60mm; e) d_{max}=75mm; f) comparison of the cyclic response at different maximum displacement

Figure 99a shows the hysteretic response of the ball rubber bearing tested at d_{max}= 15 mm under 6 MPa axial pressure. The maximum force in the positive direction is about of 138 kN while in the negative direction is -134 kN, with a damping ratio about of 10.9%. By increasing the displacement demand to d_{max}= 30mm, (see Figure 99b) the maximum force increases to 179 kN and -169 kN, in the positive and negative direction, respectively. Also the damping ratio increases to 17.4%. The same trend is found for the other tests to d_{max} = 45mm (see Figure 99c), d_{max} = 60mm (see Figure 99d) and d_{max} = 75mm (see Figure 99e). The maximum force increases to 237 kN, 282, kN and 313 kN in the positive direction, while in the negative direction to -213 kN, -267 kN and -294 kN, for d_{max} equal to 45 mm, 60 mm and 75 mm, respectively. The energy dissipation for a d_{max} = 75 mm is about 18.5 times higher than the one at d_{max} = 15mm, 4.5 times the one at d_{max} = 30 mm, 2.2 times the one at d_{max} = 45 mm and 1.3 times that at d_{max} = 60mm. In line with the results of the previous tests, despite of the increase in the energy dissipation with the increasing maximum displacement, a significant increase in the damping can be observed only moving from d_{max} = 15 mm to d_{max} = 30 mm.

Figure 100a shows the hysteretic response of the ball rubber bearing tested under 9 Mpa axial pressure and at d_{max}= 15 mm. The maximum force in the positive direction is observed to be 178 kN while in the negative direction is -165 kN, with an equivalent damping ratio about of 13.1%. By increasing the displacement demand to d_{max}= 30mm, (see Figure 100b) the maximum force increases to 216 kN and -202 kN, in the positive and negative direction, respectively. Also, the damping ratio increases to 23.0%. The same trend is found for the other tests to d_{max} = 45 mm (see Figure 100c), d_{max} = 60mm (see Figure 100d) and d_{max} = 75 mm (see Figure 100e). The maximum force increases to 275 kN, 337, kN and 383 kN in the positive direction while in the negative direction to -247 kN, -313 kN and -357 kN, for d_{max} equal to 45 mm, 60 mm and 75 mm, respectively. The related damping ratio is equal to 23.1%, 21.8% and 21.6%.

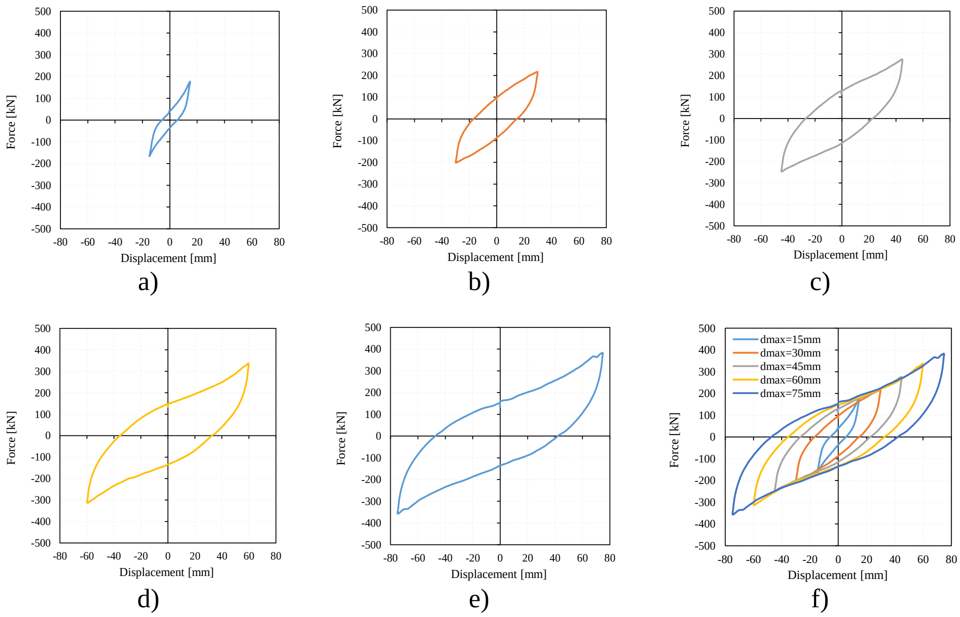

Figure 100. Cyclic response of tested BRBs at 9 Mpa axial pressure: a) d_{max}=15mm; b) d_{max}=30mm; c) d_{max}=45mm; d) d_{max}=60mm; e) d_{max}=75mm; f) comparison of the cyclic response at different maximum displacement

The energy dissipation for a d_{max} =75 mm is about 18.0 times higher than the one at d_{max}= 15mm, 4.2 times the one at d_{max}=30mm, 2.2 times the one at d_{max}=45 mm and 1.4 times that at d_{max}=60mm. A slight decrease in the damping can be observed for the last two tests at d_{max} = 60 mm and 80 mm.

As described in the section above, the maximum positive and negative force in the cycle don’t correspond, although some difference can be justified and expected the difference in some cases is around the 10%. The maximum force always has been recorded in the positive load direction (i.e. the direction of the first load). This can be related to the relocation of the inner steel balls that may cause a non-symmetric response.

As shown in the Figure 98,99,100, a ripple in the hysteretic response can be observed for the high displacement demand (i.e., between 50 and 70mm). This can be attributed to the relocation of the ball in the inner core.

Table 15. Experimental data and results

Test n.	F_{max}^{+} [kN]	F_{max}^{-} [kN]	F_{max} [kN]	Q_d^{+} [kN]	Q_d^{-} [kN]	Q_d [kN]	d_{max} [mm]	P_{ver} [kN]	E_d [kNmm]	β_{eq} [%]
1	117.3	-114.4	115.9	10.5	-10.5	10.5	15	600	1644.6	7.61
2	179.0	-165.7	172.4	29.3	-29.3	29.3	30	600	7312.5	11.32
3	229.4	-208.4	218.9	37.8	-37.8	37.8	45	600	14240.3	11.58
4	271.8	-267.5	269.7	50.8	-50.8	50.8	60	600	23376.2	11.53
5	325.3	-297.4	311.4	64.1	-64.1	64.1	75	600	36594.4	12.5
6	138	-134.3	136.2	22.9	-22.9	22.9	15	1200	2756.3	10.86
7	179.4	-168.9	174.2	52.5	-52.5	52.5	30	1200	11344.1	17.37
8	236.6	-212.8	224.7	70.2	-70.2	70.2	45	1200	23226.2	18.34
9	281.6	-267	274.3	90.9	-90.9	90.9	60	1200	38514.1	18.67
15	313.4	-293.9	303.7	93.9	-93.9	93.9	75	1200	50722.7	17.76
10	177.5	-165.3	171.4	39.8	-39.8	39.8	15	1800	4187.0	13.11
11	216	-201.6	208.8	87.6	-87.6	87.6	30	1800	18008.9	23.00
12	275.4	-246.5	261.0	115.3	-115.3	115.3	45	1800	34006.7	23.12
13	336.7	-313.1	324.9	135.1	-135.1	135.1	60	1800	53354.1	21.84
14	383.4	-356.9	370.2	136.3	-136.3	136.3	75	1800	75215.5	21.61

The results reported in Table 15 clearly show the influence of some design parameters, such as the axial load pressure and the imposed maximum displacement on the maximum strength, F_{max}, the characteristic strength, $Q_{d,BRB}$ and on the equivalent damping, β_{eq}. A close comparison of the test results can be useful to draw important considerations as reported in the following.

6.1.1.2 Experimental program on creep

In this campaign, two different types of rubber bearings are tested: Elastomeric Bearing (EBs) and Tube Ball Rubber Bearing (TBRBs) as depicted in Figure 101. They both have the same geometry, and they are composed of multiple layers of rubber (15 mm thick) and steel shims (2 mm thick). The outer rubber layers typically have a thickness equal to half of that of the inner layers. A special mixture of neoprene and natural rubber is generally used to form the rubber layer (Ozkaya et al. 2011). Natural rubber with a nominal stiffness of 60 Shore A Durometer was selected in the mix design (Caner et al. 2015). 15 mm thick steel plates (st37-(1980)) are vulcanized to the elastomers under pressure and with heat activated bonding agents at the top and the bottom of the device. The diameter of the bearings, *D*, is 300 mm, and the total height about 85 mm with a shape factor of about 3. The inner hole has a diameter of 100 mm, *d*, and it is empty for the classic EBs (see Figure 101a) or filled with steel balls for TBRBs (see Figure 101b) to increase energy dissipation by means of friction. The steel balls used in the TBRBs have a diameter of 1.65 mm and they are produced from low-carbon steels.

The Tube Ball Rubber Bearing (Figure 101b) is similar to the Ball Rubber Bearing with the addition of a flexible rubber tube that protects the central hole from deterioration. Explicitly, the tube is used to prevent the adjacent rubber of the central core from any probable damage due to the rolling of steel balls under cyclic loads. The circular rubber tube has an outer diameter of 100 mm, and it is 85 mm in height. It has a thickness of 5 mm, and it is manufactured from the same rubber used for the isolation device.

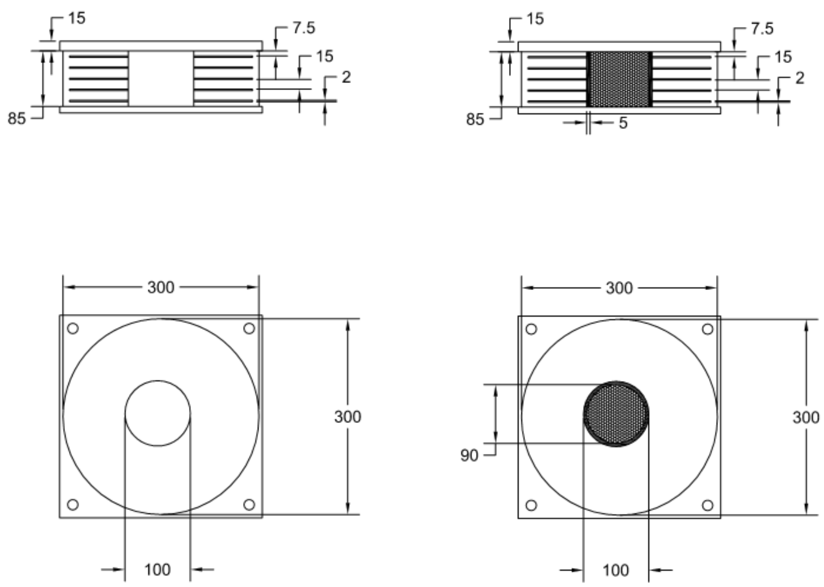

a) b)

Figure 101. Geometric dimensions (in mm) and overview of the tested specimens: a) Elastomeric Bearing (EB), b) Tube Ball Rubber Bearing (TBRB)

The test setup used to carry out the experimental tests on the two different devices is depicted in Figure 102. It consists of two oleo-dynamic actuators applying the constant axial load and the cyclic horizontal displacement. The load cells and the linear variable displacement transducer (LVDT) are used to monitor the load and displacement.

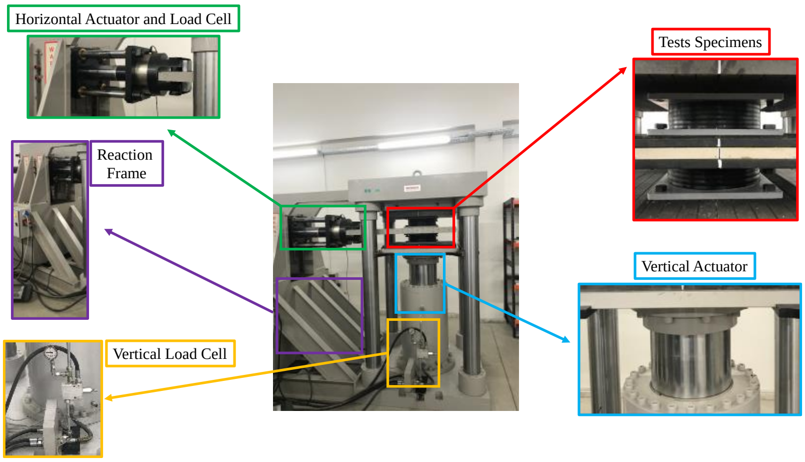

Figure 102. Test setup

The devices are tested in couples and connected to an intermediate steel plate connected to the horizontal actuator, as showed in Figure 102. Each device is connected to the test setup by means of 8 M20 steel bolts (4 for each face of the isolator). The testing program consists of 6 tests for each device, as described in Table 16, the tests were executed under constant laboratory temperature of about 10 degrees. In addition, a pre-test is carried out before Test 1 to stabilize the hysteretic response of the bearing. A target displacement of 40 mm is achieved performing three cyclic loads, under a pressure of 3 MPa.

Table 16. Test matrix for each bearing (EBs, TBRBs)

Test n.	Axial pressure [MPa]	N. cycles	Rate [mm/s]	Displacement [mm]	Holding time [s]	Objective	Notes
1	3	3	2.5	40	-	Reference	Assess the hysteretic response
2	3	Monotonic	2.5	5	1800	Creating Creep	Benchmark for test 3 (rate effects)
3	3	Monotonic	$1.6 \cdot 10^{-3}$	5	1800	Creating Creep	Benchmark for test 2 (rate effects)
4	3	Monotonic	2.5	40	1800	Creating Creep	-
5	3	3	2.5	40	-	Verification	Comparison with test 1 (influence of creep)
6	6	3	2.5	40	-	Influence of axial load	Comparison with test 5 (axial load effect)

The first test (Test 1) aims at assessing the hysteretic response of the bearing under cyclic loads to be used as a reference test for the following comparisons. Three repetitions are performed at the target displacement of 40 mm, corresponding to the half-height of the bearing and reproducing a typical displacement demand in bearings under a small magnitude earthquake at the serviceability limit state. The second and third tests aim at assessing the effects of the loading rate on the lateral creep of the bearing. A first monotonic ramp is performed to achieve the target displacement of 5 mm. Then, this displacement is held constant for a time of 1800 s (30 min). The holding displacement, d_{hold}, is calculated as the thermal displacement achieved by a 50 m span RC bridge subjected to a thermal gradient of 10 °C. This thermal gradient value is chosen because it is the average daily variation of temperature in cities such as Ankara, Naples and New York. The displacement is calculated assuming a linear variation of the thermal distortion (Eq.32):

$$d_{hold} = \alpha \cdot \Delta T \cdot L = 1 \times 10^{-5}(°C^{-1}) \times 10°C \times 50000\, mm = 5\, mm \quad (32)$$

where: α is the linear temperature expansion coefficient of concrete (1×10^{-5}(°C^{-1})), ΔT is the daily temperature variation and L is the bridge span.

The loading rate used in Test 2, 2.5 mm/s (equivalent to 150 mm/min), is the maximum loading rate of the testing machine. In Test 3 the minimum loading rate of the testing machine, 0.0016 mm/s (equivalent to 0.096 mm/min), is used to achieve the target displacement. This is very close to the loading rate of 0.083 mm/min recommended by AASHTO code for the thermal test. Test 4 aims at inducing lateral creep under the same target displacement (40 mm) and the same loading rate (2.5 mm/s) of the reference test, Test 1. Test 5 aims at assessing the influence of creep on the hysteretic response of the bearing, while Test 6 aims at assessing the influence of a high axial pressure (6 MPa instead of 3 MPa as in all the other tests) on the cyclic response. These axial pressures are common for bridge bearings and lower than those commonly found in buildings (Ozkaya et al. 2011). This is in accordance with Mellon and McKee (1994) suggesting that, for steel reinforced bearings, the average axial load pressure should not exceed 6.9 MPa. Furthermore, the AASTHO LRFD (2015) suggests that the compressive stress on the steel reinforced elastomeric bearing should be limited to 1.25 ksi (8 MPa). The test results and a discussion on the effects of the loading rate test, creep and axial pressure are reported in the following sections.

The hysteresis performances of the two tested bearings are reported in Figure 103 (see Figure 103a and Figure 103b for EBs and TBRBs, respectively). In order to have a clear hysteretic response unaffected by the initial loading branch, only the response of the third cycle is reported. A direct comparison of the two devices is reported in Figure 104c It is worth noting that, as described above, the devices are tested in couples. Thus, the measured force reported in the following graphs refers to two isolators. The damping is calculated through Eq.33:

$$\beta_{eq} = \frac{E_d}{4\pi \cdot E_s} = \frac{E_d}{2\pi \cdot k_{eff} \cdot d_{max}^2} \qquad (33)$$

where the dissipated energy, E_d, is the area of the cycle shown in Figure 103, k_{eff} is the secant stiffness to the maximum strength that can be calculated as the ratio of the maximum force, F_{max}, and the maximum imposed displacement, d_{max}. Q_d is the force where the displacement is equal to zero. Please note that E_d is a function of Q_d. The main results of the cyclic tests are also summarized in Table 18.

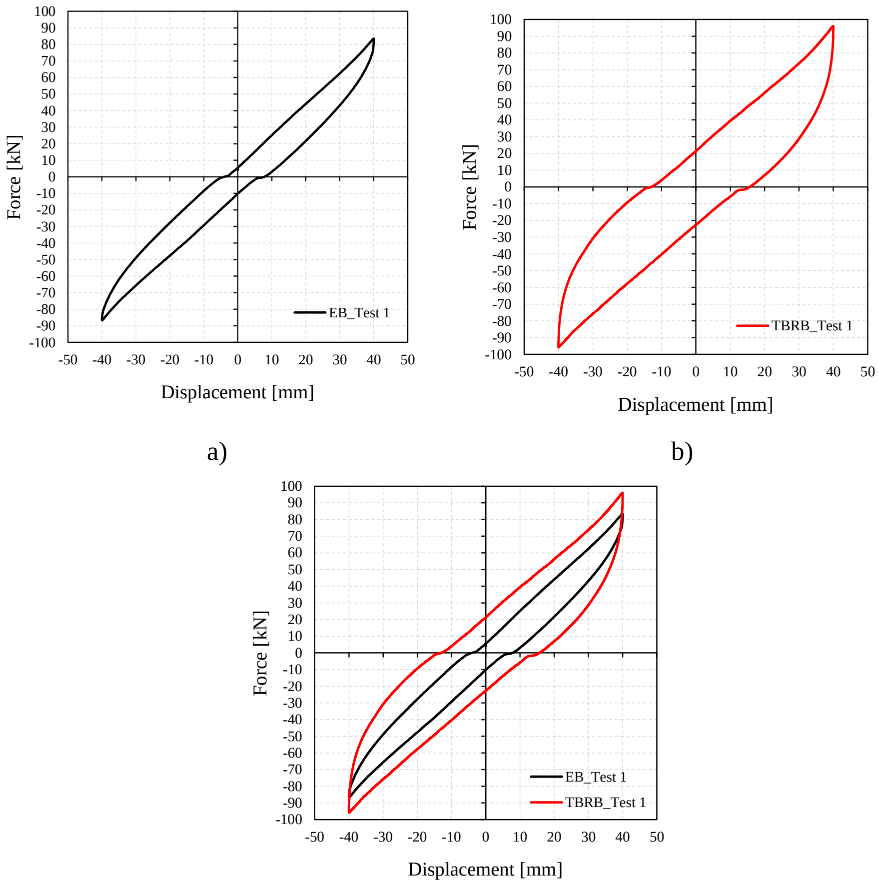

a) b)

c)

Figure 103. Results of Test 1: a) Elastomeric Bearings (EBs), b) Tube Ball Rubber Bearings (TBRBs), c) comparison of EBs and TBRBs

Figure 103a shows the hysteretic response of the elastomeric bearings. The maximum force in the positive load direction is about 85 kN with a similar response in the negative load direction. The damping ratio is about 7% similar to test results available in literature (Roeder and Stanton 1984). Figure 103b shows the hysteretic response of the tube ball rubber bearings (TBRBs, red dashed line); the maximum force in the positive load direction is about 97 kN. The specimen exhibited a similar response in the negative load direction. The damping ratio is about 15%, similar to the result from previous tests performed on ball rubber bearings (Ozkaya et al. 2011).The comparison between the hysteretic response of the EBs and TBRBs is depicted in Figure 103c. It reveals the benefits of the steel balls in increasing the energy dissipation capacity by means of friction. The presence of the steel balls results in an increased energy dissipation and damping to 110% corresponding values in the EBs. This makes the TBRBs an effective and economically feasible solution for the design of base isolated constructions. Further details on the influence of creep and axial load on the cyclic response are reported in the following part of this paper.

As discussed in (Ozkaya et al. 2011) many variables affect the damping of BRBs. The main parameters are the dimension of the steel balls, the shape factor (which also takes into account the dimension of the central hole), the magnitude of the displacement, and the vertical pressure. All parameters have mutual effects on the damping, and this makes the prediction of the damping a challenging task. The TBRBs tested in this study show a damping ratio lower than the damping commonly observed in BRB devices (Ozkaya et al. 2011). This can be attributed to the larger shape factor (*D/d*) caused by the reduction of the diameter of the central hole, *d*, due to the presence of the rubber tube.

The results of tests 2, 3 and 4 in which a target displacement (5 mm or 40 mm) is imposed and held constant for 1800 s for the two different bearings, EBs and TBRBs, are reported in Figure 104 and Figure 105, respectively. For each test, the displacement history (Figure 104-105a, d, g), the recorded force (Figure 104-105b, e, h), and the losses in terms of force expressed as the loss ratio F/F_{max}, (Figure 104-105c, f, i) are shown. Six-time steps are chosen to calculate the loss ratio: 0 s, 1s, 100s, 600s, 1200s and 1800s, where 0 s corresponds to the time at which the target displacement is achieved.

Table 17. Results of the creep test on EBs and TBRBs

			EBs			TBRBs		
Test n.	Rate [mm/s]	Displacement [mm]	F_{max} [kN]	F_{min} [kN]	$(F/F_{max})_{min}$ [-]	F_{max} [kN]	F_{min} [kN]	$(F/F_{max})_{min}$ [-]
2	2.5	5	12.1	6.6	0.54	14.5	8.2	0.57
3	$1.6 \cdot 10^{-3}$	5	12.0	10.2	0.85	27.4	23.6	0.86
4	2.5	40	86.4	70.2	0.82	99.7	82.9	0.83

A maximum force of about 12.0 kN is achieved in Test 2 and Test 3 for the EBs; this suggests that the change of loading rate from 2.5 to 1.6 x 10^{-3} does not play a significant role on the maximum achieved lateral force for the elastomeric bearing. Instead, the influence of the loading rate can be observed in the reduction of the maximum force during the holding time. In fact, as depicted in Figure 104c and 104f, Test 2 and Test 3 show different ratios of F/F_{max}.

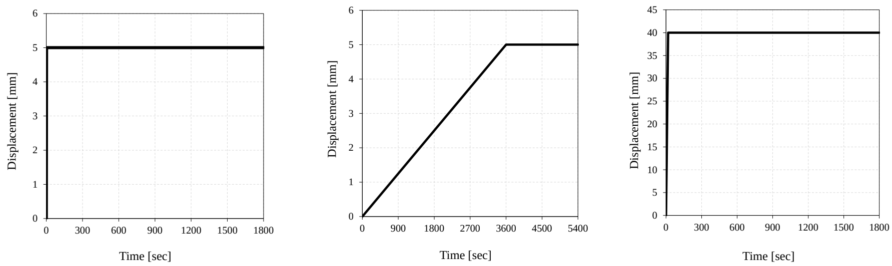

a) b) c)

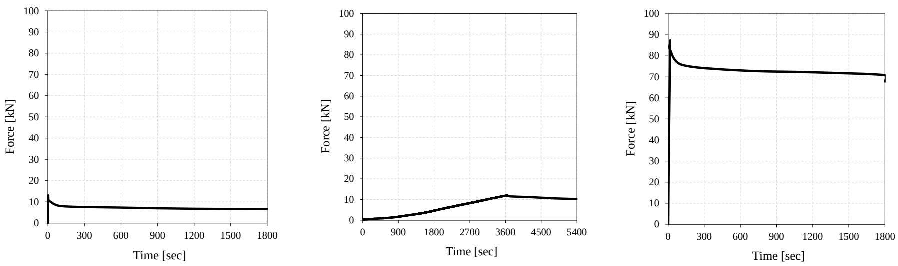

d) e) f)

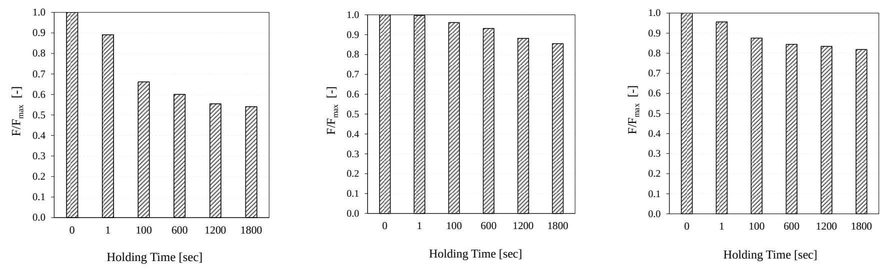

g) h) i)

Figure 104. Creep tests for the Elastomeric Bearing (EBs), a-b-c) EBs_Test 2, d-e-f-) EBs_Test 3, g-h-i) EBs_Test 4

Test 2 shows a minimum ratio of F/F_{max} equal to 0.54 while for Test 3 the same ratio is equal to 0.85. This observation suggests that a higher loading rate results in higher losses under the condition of sustained displacement. As expected, increase in the displacement demand results in a higher level of maximum force equal to 86.4 kN (Figure 104h). As depicted in Figure 104i, and reported in Table 2, the ratios F/F_{max} are similar to those of Test 3 (Figure 104f), with a minimum equal to 0.82. The comparison of the loss of maximum force for Test 2 and Test 4, depicted in Figure 104c and Figure 104i respectively, suggests that increasing the maximum displacement demand while maintaining the same loading rate decreases the loss in lateral force.

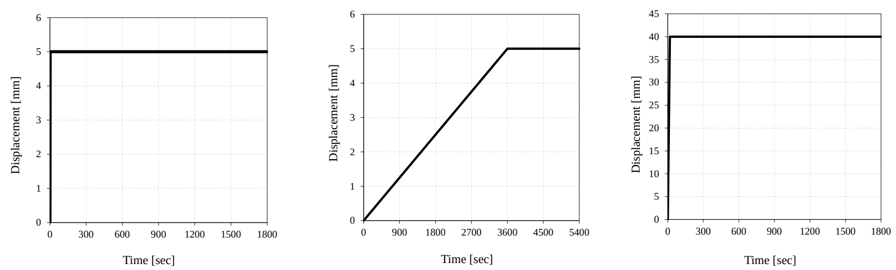

a) b) c)

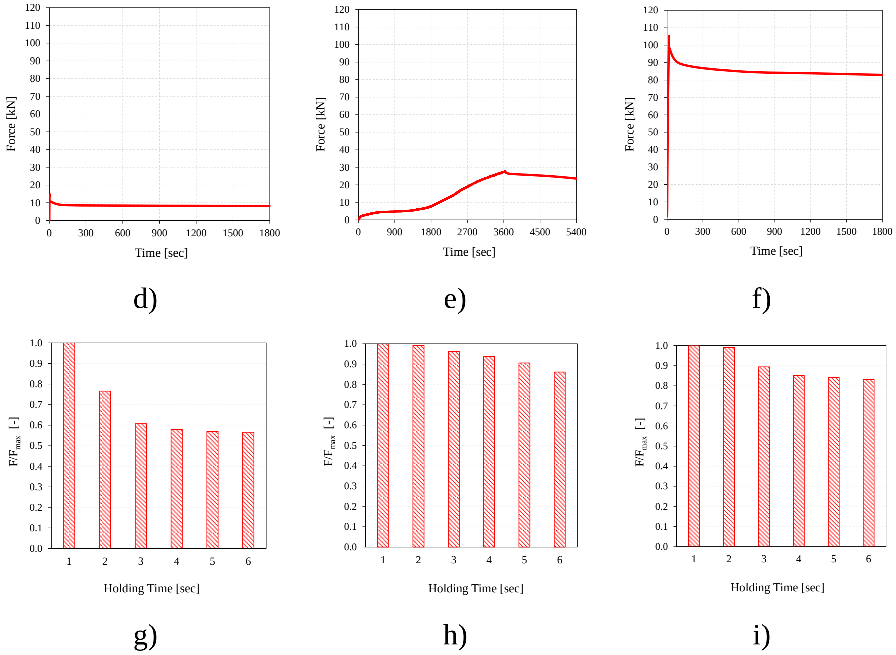

Figure 105. Creep tests for the Tube Ball Rubber Bearing (TBRBs), a-b-c) TBRBs_Test 2, d-e-f) TBRBs_Test 3, g-h-i) TBRBs_Test 4

For TBRB, higher maximum lateral forces, F_{max}, of about 14.5 kN and 27.4 kN are achieved in Test 2 and Test 3 as compared to the same EB tests; see Figure 105b and 105e respectively. This observation suggests that the loading rate plays a significant role on the maximum achieved force when steel balls are introduced in an elastomeric bearing (TBRB). The maximum force in a TBRBs is function of the characteristic strength Q_d, of the post elastic stiffness, K_2, of the maximum displacement, d_{max}, and of the yield displacement, d_y.

$$F_{max} = Q_d + K_2(d_{max} - d_y) \tag{34}$$

The characteristic strength is strongly influenced by the friction, μ, that is function of the peak friction angle, φ_p (Ozkaya et al. 2011). The different loading rate may significantly affect the friction between steel balls, probably increasing the peak friction angle by decreasing the loading rate leading to an increase of the maximum force. Further studies on this topic are suggested.

Different losses can be observed in terms of the ratio F/F_{max}, as depicted in Figure 105c-105f. Thus, the loading rate also plays a role in the reduction of

F_{max} at a constant displacement. Test 2 shows higher losses than Test 3, with minimum F/F_{max} ratios equal to 0.57, and 0.86 respectively. By increasing the displacement demand, the maximum force increases to 99.7 kN (Figure 105h). As depicted in Figure 105i, and reported in Table 2, the ratios F/F_{max} are similar to those of Test 3 (Figure 105f), with a minimum equal to 0.83. The comparison of the loss of maximum force for Test 2 and Test 4, depicted in Figure 105c and Figure 105i respectively, suggests that increasing the maximum displacement demand while maintaining the same loading rate decreases the loss of force.

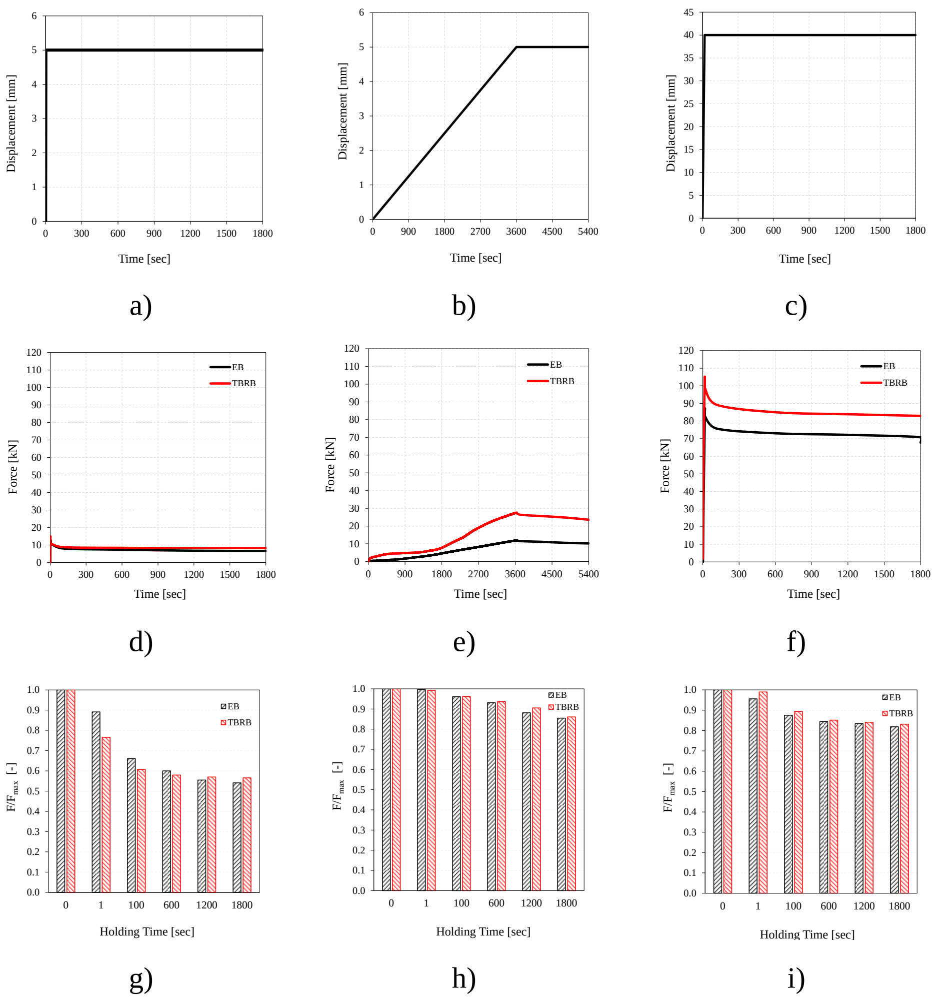

Figure 106. Comparison creep's tests between EBs and TBRBs: a-b-c) EBs-TBRBs_Test 2, d-e-f) EBs-TBRBs_Test 3, g-h-i) EBs-TBRBs_Test 4

The comparison of the responses of EBs (black line) and TBRBs (red dashed line) under imposed lateral displacement is reported in Figure 106. The elastomeric bearing and the tube ball rubber bearing achieved different maximum force at the same imposed displacement (Figure 106b, e, h) due to the resistance of the steel balls. The tube ball rubber bearing shows a higher strength than the elastomeric bearing, resulting in high dissipation capacity. Furthermore, by comparing Figure 106b and Figure 106e it can be understood that the strength capacity of the tube ball rubber bearing is influenced by the loading rate. This is due to the internal friction between the steel balls under cyclic loading. The elastomeric bearing and the tube ball rubber bearing show similar losses for Test 2, Test 3, and Test 4 (Figure 106c-f-i). In fact, as reported in Table 3, the minimum F/F_{max} ratio is similar: 0.54 and 0.57 in Test 2, 0.85 and 0.86 in Test 3, 0.82 and 0.83 in Test 4 for EBs and TBRBs respectively. The comparison of Test 2 and Test 4 results for EB and TBRBs suggests that the creep at 5 mm of sustained displacement does not significantly affect the response of either bearing. Indeed, the strength capacity of the bearing increases and the losses decrease. In order to assess the cyclic response of the bearings after larger sustained displacement (40 mm at Test 4) a cyclic test is repeated and the results are compared with that of the reference test, Test 1.

A cyclic test with three repetitions is performed at the target displacement of 40 mm and an average vertical pressure of about 3.0 MPa (Test 5) for both the EBs and TBRBs after they have been subjected to Tests 2, 3 and 4 to develop creep. The same test is then repeated by increasing the axial pressure to 6.0 MPa (Test 6). This is to assess the influence of degradation due to creep and of the axial load on the hysteretic response of the elastomeric bearing. In order to quantify the influence of these variables on the cyclic response, the results of Test 5 and Test 6 are compared with those of the reference Test 1. The results are depicted in Figure 107 and Figure 108 respectively for EBs and TBRBs and summarized in Table 3 in terms of the characteristic strength, Q_d, maximum absolute force, F_{max}, post-elastic stiffness, k_2, energy dissipated per cycle, E_d, and equivalent damping, β_{eq}.

Table 18. Results of cyclic tests

			EBs					TBRBs				
Test n.	Axial pressure [MPa]	Config.	Q_d [kN]	F_{max} [kN]	k_2 [kN/m]	E_d [kNmm]	β_{eq} [%]	Q_d [kN]	F_{max} [kN]	k_2 [kN/m]	E_d [kNmm]	β_{eq} [%]
1	3.0	reference	4.1	85.0	2022.5	1470.0	6.9	18.1	96.0	1947.5	3501.8	14.5
5	3.0	post-creep	7.7	85.0	1932.5	1450.0	6.8	23.8	94.9	1777.5	3473.2	14.6
6	6.0	post-creep	7.6	85.0	1835.0	1632.5	7.6	41.3	130.0	2217.5	7113.6	21.8

Figure 107a and Figure 107b show the hysteretic response of the EBs at 3.0 MPa and 6.0 MPa of axial pressure after being subjected to creep. The comparison of Test 5 with the reference Test 1 is depicted in Figure 107c, which shows a perfect overlapping of the hysteretic responses. This suggests that the creep tests have not resulted in any modification of the rubber properties. This is confirmed by experimental results reported in Table 3. Test 5 is characterized by a maximum force of about 85.0 kN which matches the maximum force recorded during the reference Test 1. In turn, similar energy dissipation and damping can be observed. The dissipated energy is about 1470 kNmm and 1450 kNmm, while the damping is about 6.9% and 6.8% respectively for Test 1 and Test 5.

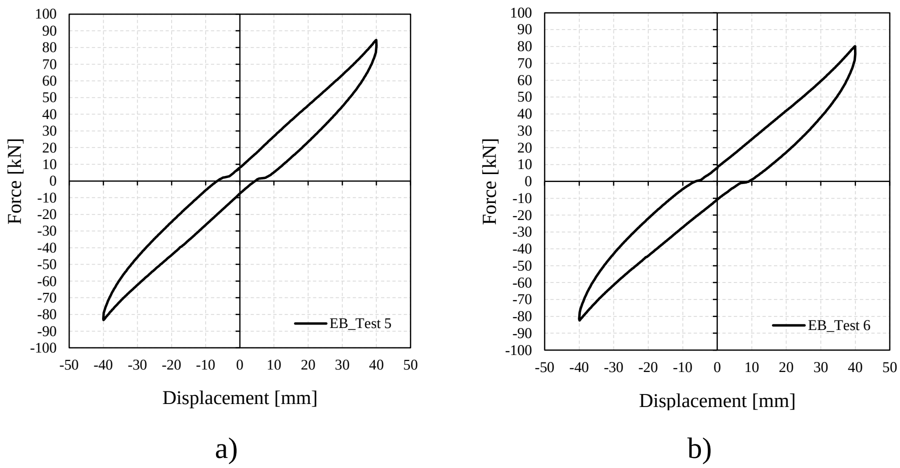

a) b)

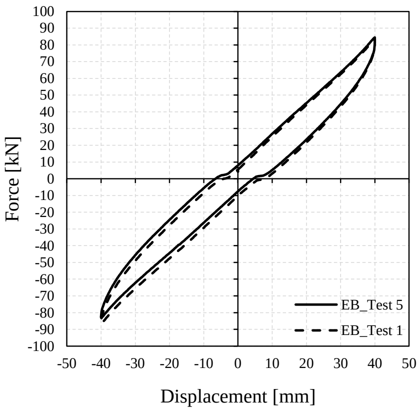

c)

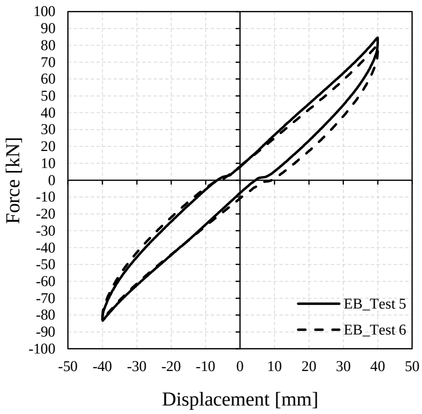

d)

Figure 107. a) EBs_Test 5, b) EBs_Test 6, c) Comparison between EBs_Test 1 and EBs_Test 5, d) Comparison between EBs_Test 5 and EBs_Test 6

The cyclic response of the EBs subjected to 6.0 MPa vertical pressure and the direct comparison with Test 5 at 3.0 MPa axial pressure is reported in Figure 107d. In this case, the vertical pressure does not have significant influence on the cyclic response of the EBs. Indeed, a maximum absolute lateral force of about 84 kN similar to reference Test 1 is recorded. Similarly, the dissipated energy of about 1632 kNmm and damping of about 7.6% does not significantly differ from the previous tests.

Figure 108a and Figure 108b show the hysteretic response of the TBRBs at 3.0 MPa and 6.0 MPa of vertical pressure after being subjected to creep. The comparison of Test 5 with the reference Test 1 is depicted in Figure 108c, which shows a perfect overlapping of the hysteretic responses. This suggests that the creep tests have not modified the rubber properties. This is confirmed by experimental results reported in Table 18. Test 5 is characterized by a maximum force of about 94.9 kN which matches the maximum force recorded during reference Test 1. In turn, similar energy dissipation and damping can be observed. The dissipated energy is about 3502 kNmm and 3473 kNmm, while the damping is about 14.5% and 14.6% respectively for Test 1 and Test 5.

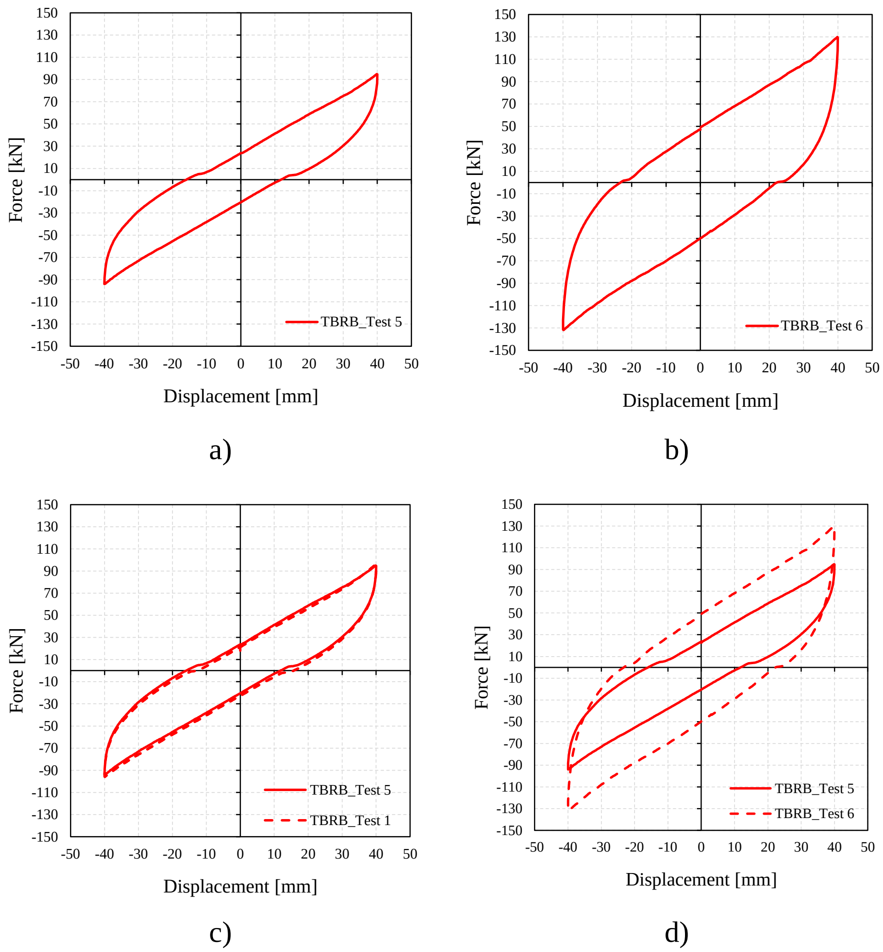

Figure 108. a) TBRBs_Test 5, b) TBRBs_Test 6, c) Comparison between TBRBs_Test 1 and TBRBs_Test 5, d) Comparison between TBRBs_Test 5 and TBRBs_Test 6

The cyclic response of the TBRBs subjected to 6.0 MPa vertical pressure and the direct comparison with Test 5 at 3.0 MPa vertical pressure is reported in Figure 108d. In this case the axial pressure has significant influence on the cyclic response of the TBRBs. Indeed, a maximum lateral force of about 130 kN is achieved. This is significantly higher than the maximum recorded during the reference Test 1, resulting in a higher dissipated energy of about 7114 kNmm and damping of about 21.8%.

6.1.2 Analytical model of the main BRB's characteristics

The experimental tests carried out, in the second experimental campaign, to investigate the influence of the axial pressure and maximum imposed displacement on the damping are used to draw preliminary considerations on the variability of the damping and other response parameters (F_{max} and $Q_{d,BRB}$) of the BRBs.

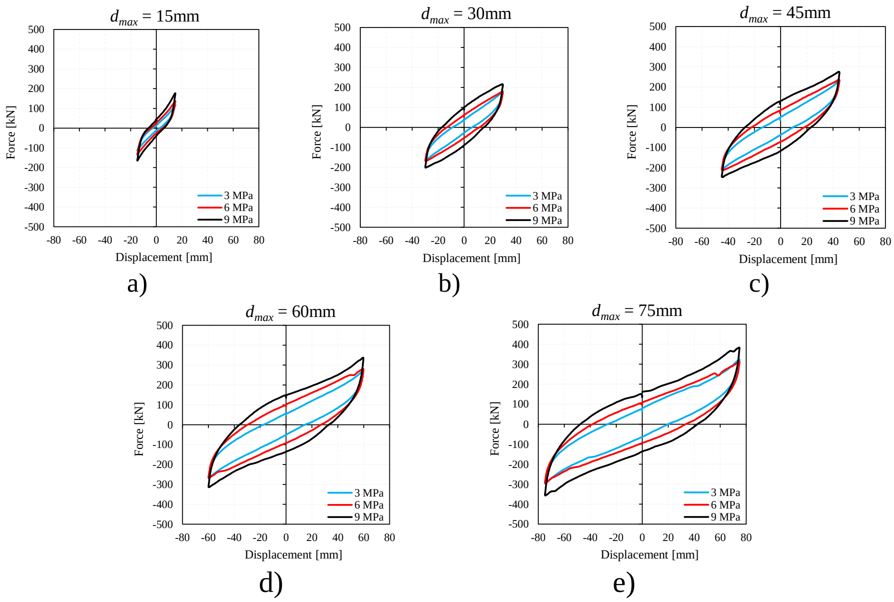

Figure 109. Variability of the hysteretic response with the axial pressure at different maximum imposed displacement: a) d_{max}=15mm, b) d_{max}=30mm%, c) d_{max}=45mm, d) d_{max}=60mm%, e) d_{max}=75mm

In order to assess the influence of axial pressure on the hysteretic response of the tested BRBs, the previous tests are grouped in Figure 109 considering tests at the same imposed maximum displacement, d_{max}.

Figure 109 remarks that for each level of the maximum imposed displacement the increase in axial pressure corresponds to a direct increase of the energy dissipation (the area within the hysteretic cycle). According to the results reported in Table 3, such an increase respect to the test under 3 MPa axial pressure can be quantified in 67.6% and 154.6% for a d_{max}=15mm, 55.1% and 146.3 % for a d_{max}=30mm, 63.1% and 138.8 % for a d_{max}=45mm, 64.8%and 128.2 % for a d_{max}=60mm, 38,6% and 105.5 % for a d_{max}=75mm, respectively for tests under 6 MPa and 9 MPa axial pressure.

Both the F_{max} and $Q_{d,BRB}$ increase by increasing the axial pressure and the imposed displacement. However, it should be noted that the percentage increase in the $Q_{d,BRB}$ is higher than the percentage increase of the F_{max} (see Figure 110a, b, d, e). According to Naim & Kelly (1999), the damping is directly proportional to $Q_{d,BRB}$ and indirectly proportional to F_{max}, thus, to quantify their effect on the damping, the ratio $Q_{d,BRB}/F_{max}$ should be computed.

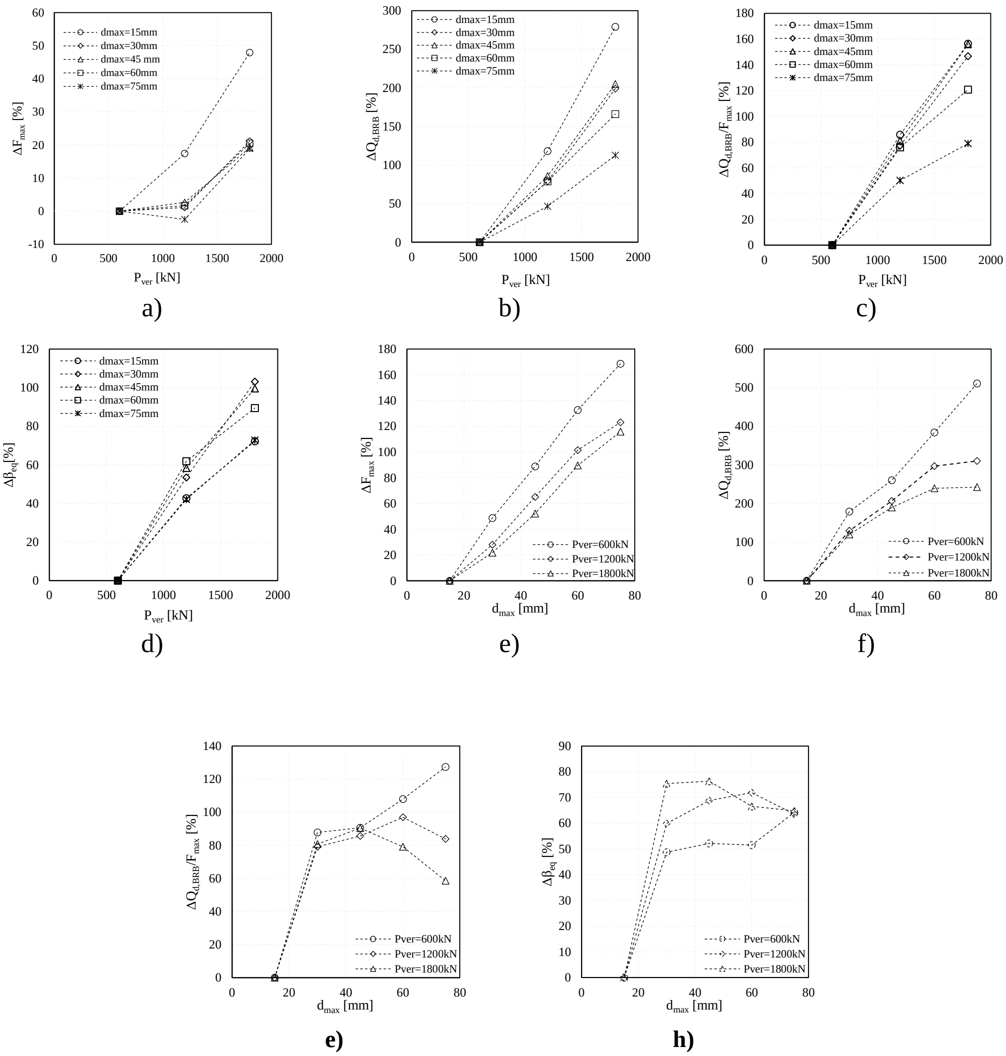

Figure 110. Percentage increase of F_{max}, $Q_{d,BRB}$ and $Q_{d,BRB}/F_{max}$ as function of P_{ver} and d_{max}: ΔF_{max} vs. P_{ver} a); $\Delta Q_{d,BRB}$ vs. P_{ver} b); $\Delta Q_{d,BRB}/F_{max}$ vs. P_{ver} c); $\Delta \beta_{eq}$ vs. P_{ver} d); ΔF_{max} vs. d_{max} e); $\Delta Q_{d,BRB}$ vs. d_{max} f); $\Delta Q_{d,BRB}/F_{max}$ vs. d_{max} g); $\Delta \beta_{eq}$ vs. d_{max} h)

Table 19. Comparison of experimental results for tests at same maximum displacement.

	Test n.	P_{ver} [kN]	E_d [kNmm]	ΔE_d [%]	F_{max} [kN]	ΔF_{max} [%]	$Q_{d,BRB}$ [kN]	$\Delta Q_{d,BRB}$ [%]	$Q_{d,BRB}/F_{max}$ [-]	$\Delta Q_{d,BRB}/F_{max}$ [%]	*β_{eq} [%]	$\Delta\beta_{eq}$ [%]
d_{max}=15mm	1	600	822.3	-	115.9	-	10.5	-	0.09	-	7.61	-
	6	1200	1378.2	67.6	136.1	17.4	22.9	118.1	0.17	85.7	10.86	42.7
	10	1800	2093.5	154.6	171.4	47.9	39.8	279.0	0.23	156.3	13.11	72.3
d_{max}=30mm	2	600	3656.3	-	172.3	-	29.3	-	0.17	-	11.32	-
	7	1200	5672.1	55.1	174.2	1.1	52.5	79.2	0.30	77.2	17.37	53.4
	11	1800	9004.5	146.3	208.8	21.2	87.6	199.0	0.42	146.7	23.00	103.2
d_{max}=45mm	3	600	7120.2	-	218.9	-	37.8	-	0.17	-	11.58	-
	8	1200	11613.1	63.1	224.7	2.6	70.2	85.7	0.31	80.9	18.34	58.4
	12	1800	17003.4	138.8	260.9	19.2	115.3	205.0	0.44	155.9	23.12	99.7
d_{max}=60mm	4	600	11688.1	-	269.7	-	50.8	-	0.19	-	11.53	-
	9	1200	19257.1	64.8	274.3	1.7	90.9	78.9	0.33	75.9	18.67	61.9
	13	1800	26677.1	128.2	324.9	20.5	135.1	165.9	0.42	120.8	21.84	89.4
d_{max}=75mm	5	600	18297.2	-	311.3	-	64.1	-	0.21	-	12.5	-
	15	1200	25361.4	38.6	303.6	-2.5	93.9	46.5	0.31	50.2	17.76	42.1
	14	1800	37607.8	105.5	370.1	18.9	136.3	112.6	0.37	78.9	21.61	72.9

**The percentage in this case represents the unit for damping.*

As showed in Figure 110c,f the variability of the ratio $Q_{d,BRB}/F_{max}$ better catches the variability of the equivalent damping than the single variables $Q_{d,BRB}$ and F_{max}. This is quite evident comparing the trend of $Q_{d,BRB}/F_{max}$ with that of the percentage variation of the damping (Figure 110d,h). The trends are very similar and this remarks the strong correlation of the damping and the ratio $Q_{d,BRB}/F_{max}$. This is accounted into Eq. (2), where the theoretical equivalent damping is directly proportional to the $Q_{d,BRB}/F_{max}$.

Previous studies identified the main variables characterizing the hysteretic response of BRB devices. In addition to the axial pressure, σ, and maximum displacement, d_{max}, whose effects are quantified in this work, the diameter of the central hole, d, and the dimension of the steel balls, d_{sb}, may significantly affect the damping (Ozkaya et al. 2011). In order to study the influence of each variable on the lateral response of BRBs and the effects on the damping, experimental data available in literature (Ozkaya et al. 2011; Caner et al. 2015) are collected in an unique database including all tests available on BRBs.

All the bearing characteristics as well as the experimentally measured parameters are reported in Table 4 along with the ratio of the experimentally over the predicted damping, $\beta_{eq}^{pred}/\beta_{eq}^{exp}$.To reproduce the hysteretic response of the BRBs and to simplify the analytical calculation of the damping, the hysteretic response of BRBs is linearized as depicted in Figure 111.

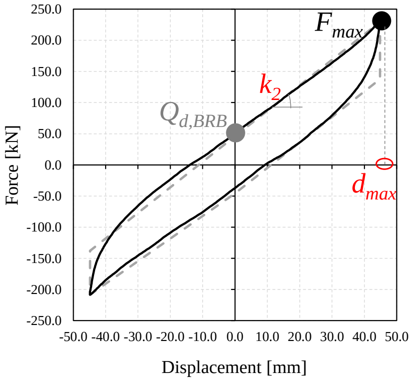

Figure 111. Bilinear behaviour of BRB

The damping can be assessed by using the following formulation (Naeim and Kelly 1999) derived from Eq.31 assuming that the dissipated energy can be approximated by the area of a rectangle of height $2Q_{d,BRB}$ and base $2d_{max}$:

$$\beta_{eq} == \frac{4 \cdot Q_{d,BRB}}{2 \cdot \pi \cdot F_{max}} \tag{35}$$

The main design parameters are the characteristic strength, $Q_{d,BRB}$, the target displacement, d_{max} and the post-elastic stiffness, k_2. Considering that the product of k_{eff} times d_{max} is the maximum strength F_{max}, the damping ratio can be expressed as function of the ratio $Q_{d,BRB}/F_{max}$. The latter was found as the parameter with the strongest correlation with the damping based on the previously discussed experimental results (see Table 19). Based on Eq 2 once that the characteristic strength and the maximum force (or in alternative the post-elastic stiffness, k_2) is defined, the damping can be easily calculated. In order to obtain a predictive formulation of these parameters, the correlation with the main design variables is shown in Figure 112 and Figure 113.

Table 20. Experimental data using for the prediction model

	Label	D	d	h	σ	P_{ver}	d_{max}	$*Q_{d,BRB,exp}$	$k_{2,exp}$	$*F_{max,exp}$	$\beta_{eq,exp}$	$\beta_{eq,pred}$	$\beta_{eq,pred}/\beta_{eq,exp}$
	[-]	[mm]	[mm]	[mm]	[MPa]	[kN]	[mm]	[kN]	[kN/mm]	[kN]	[%]	[%]	[-]
(Ozkaya,2011)	1	300	100	85	1.7	120	44.0	20.0	0.97	62.5	20.37	17.16	0.84
	2	300	60	85	2.8	198	84.0	13.0	0.62	65.0	12.73	20.05	1.57
	3	300	80	85	2.8	198	54.0	26.3	0.84	71.5	23.37	18.00	0.77
	4	300	100	85	2.8	198	54.0	21.5	0.92	71.0	19.28	19.03	0.99
	5	300	120	85	2.8	198	54.0	28.6	1.03	84.0	21.69	20.06	0.92
	6	300	150	85	2.8	198	54.0	32.0	0.80	75.0	27.16	21.61	0.80
	7	300	150	85	1.7	120	28.1	12.0	0.68	31.0	18.00	18.10	1.01
	8	300	150	85	1.7	120	28.1	12.0	1.18	45.0	18.00	18.10	1.01
	9	300	150	85	1.7	120	71.4	36.0	0.67	84.0	26.00	22.56	0.87
	10	300	80	85	1.7	120	34.0	30.0	0.71	54.0	20.00	15.10	0.75

	11	300	80	85	1.7	120	50.2	24.0	0.77	62.5	22.00	16.76	0.76
	12	300	80	85	1.7	120	61.2	26.5	0.75	72.5	24.00	17.90	0.75
	13	300	120	85	0	0	45.0	5.7	0.82	42.5	8.46	17.00	2.01
	14	300	120	85	1.7	120	54.0	19.5	0.98	72.5	17.12	19.22	1.12
	15	300	120	85	2.8	198	54.0	28.6	1.03	84.0	21.69	20.06	0.92
	16	300	120	85	4.3	304	44.3	20.5	1.22	74.5	17.52	20.21	1.15
	17	300	120	85	5.7	403	44.0	20.8	1.24	75.5	17.50	21.24	1.21
	18	300	120	85	7.1	502	43.5	22.5	1.31	79.5	18.02	22.26	1.24
	19	300	100	85	2.8	198	17.9	7.8	1.59	36.0	13.69	15.31	1.12
	20	300	100	85	2.8	198	73.1	24.3	0.75	78.8	19.64	20.99	1.07
	21	300	100	85	4.2	297	17.9	9.8	1.89	43.4	14.30	16.38	1.14
	22	300	100	85	4.2	297	49.3	32.3	1.25	93.6	21.93	19.61	0.89
	23	300	100	85	5.6	396	17.0	14.3	2.20	51.7	17.56	17.36	0.99
	24	300	100	85	5.6	396	33.2	25.0	1.45	73.1	21.78	19.02	0.87
(Caner	25	300	100	85	0	0	42.5	3.0	0.51	24.5	9.30	15.71	1.69
	26	300	100	85	1.5	106	42.5	4.2	0.66	32.4	11.70	16.85	1.44
	27	300	100	85	3	212	42.5	4.8	0.84	40.5	14.70	18.00	1.22
(Natale	TBRBs_Test1	300	90	85	3	212	40.0	9.1	0.97	48.0	14.51	17.22	1.19
	TBRBs_Test5	300	90	85	3	212	40.0	11.9	0.89	47.5	14.56	17.22	1.18
	TBRBs_Test6	300	90	85	6	424	40.0	20.7	1.11	65.0	21.77	19.51	0.90
This work	P3_d15	500	165	66	3	600	15	10.5	7.12	115.1	7.61	7.97	1.05
	P3_d30	500	165	66	3	600	30	29.3	4.80	172.3	11.32	9.51	0.84
	P3_d45	500	165	66	3	600	45	37,8	4.04	218.9	11.58	11.05	0.95
	P3_d60	500	165	66	3	600	60	50.8	3.66	269.7	11.53	12.60	1.09
	P3_d75	500	165	66	3	600	75	64.1	3.30	311.3	12.50	14.14	1.13
	P6_d15	500	165	66	6	1200	15	22.9	7.65	136.1	10.86	14.44	1.33
	P6_d30	500	165	66	6	1200	30	52.5	4.08	174.2	17.37	15.98	0.92
	P6_d45	500	165	66	6	1200	45	70.2	3.45	224.7	18.34	17.53	0.96
	P6_d60	500	165	66	6	1200	60	90.9	3.06	274.3	18.67	19.07	1.02
	P6_d75	500	165	66	6	1200	75	93.9	8.89	303.6	17.76	20.61	1.16
	P9_d15	500	165	66	9	1800	15	39.8	4.07	171.4	13.11	20.91	1.60
	P9_d30	500	165	66	9	1800	30	87.6	3.25	208.8	23.00	22.46	0.98
	P9_d45	500	165	66	9	1800	45	115.3	3.17	260.9	23.12	24.00	1.04
	P9_d60	500	165	66	9	1800	60	135.1	3.13	324.9	21.84	25.54	1.17
	P9_d75	500	165	66	9	1800	75	136.3	2.80	370.1	21.61	27.09	1.25
												Media	1.09
												Cov	0.24

*The maximum force, Fmax, and characteristic strength of the tests reported in Ozakaya et al. 2011, Caner et al. 2015 and Natale et al. 2021 refers to two bearings. In this study the experimental forces of these testing programs are divided by two to report to a single bearing.

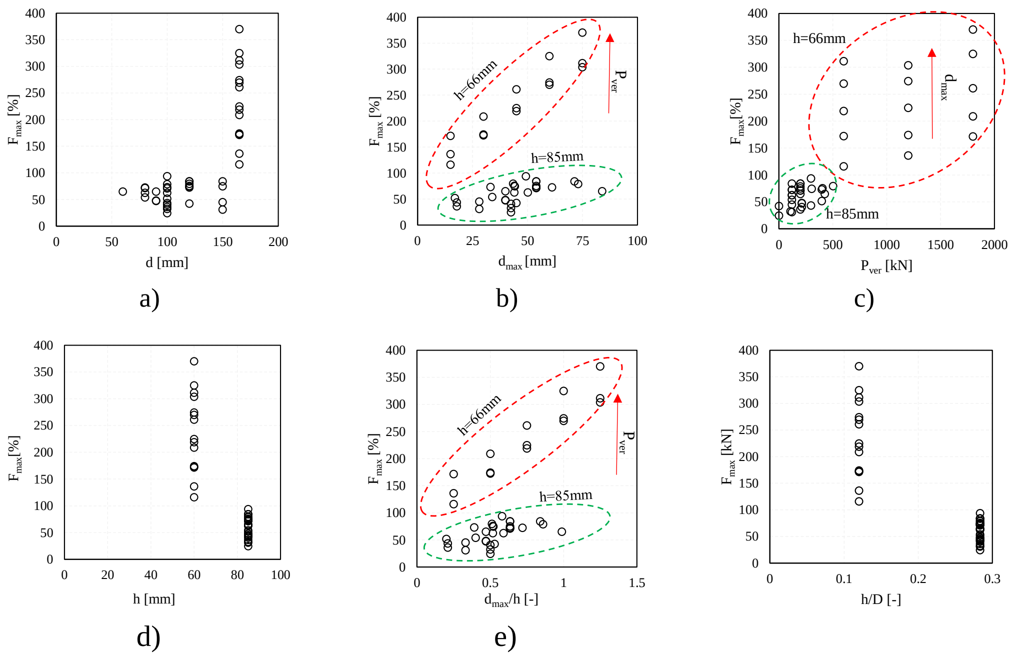

Figure 112. Correlation of the maximum force with different parameters of BRBs: a) dimension of the central hole, *d*; b) maximum displacement, d_{max}; c) Axial Load, P_{ver}; d) height, *h*; e), maximum displacement to height ratio, d_{max}/h; f) height to diameter ratio,*h/D*

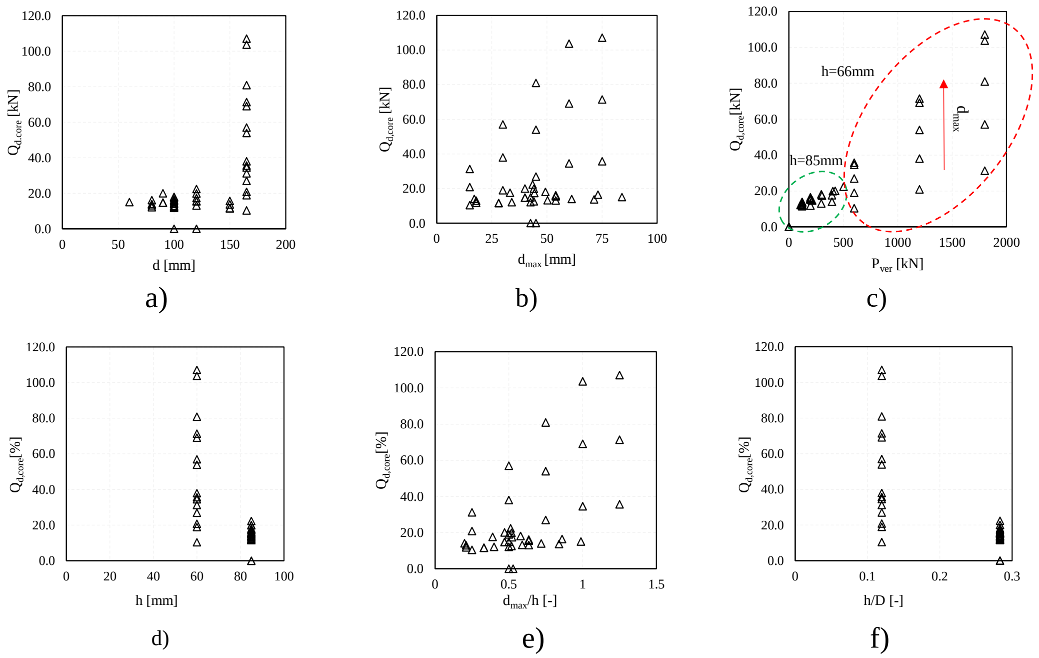

Figure 113: Correlation of the characteristic strength due to the core with different parameters of BRBs: a) dimension of the central hole, *d*; b) maximum displacement, d_{max}; c) Axial Load, P_{ver}; d) height, *h*; e), maximum displacement to height ratio, d_{max}/h; f) height to diameter ratio,*h/D*

The number of variables characterizing the collected dataset and their mutual variability do not allow to show a clear trend of the design parameters. However, despite of the test-to-test variability some basic considerations can be done. A direct proportionality between the characteristic strength and the maximum with the imposed displacement, d_{max}, the dimension of the central hole, *d*, and the axial load pressure, P_{ver}, can be observed in Figure 112 a,b,c and Figure 113a,b and c, respectively. By contrast, $Q_{d,core}$ and F_{max} decrease by increasing the bearing height, *h*, as showed in Figure 112d and Figure 113d, respectively. The same correlation can be found comparing these variables against the shape factor *h/D*. It is worth noting that in such a kind of bearings, the strength mainly depends by the contribution of stell balls that is a function of the volume of the inner core. For this reason, the results are equally sensitive to the bearing height (Figure 112d and Figure 113d) and to the shape factor

(Figure 112f and Figure 113f). For the same reason, the strength is not sensitive to the lateral stiffness of the rubber (GA/tr). Thus, this variable that commonly affect the response of rubber bearing is not considered in the derivation of the analytical relationships.

Grouping the test data reported in Figure 112b, c, d and Figure 113c in subgroups of tests with the same height (i.e. h equal to 66 mm and 85 mm) a significant variability can be observed. In particular by reducing the specimen height an increase of the F_{max} and $Q_{d,core}$ can be observed . Furthermore, as remarked by the red arrows in Figure 112b, e, the maximum force (F_{max}) for a fixed d_{max} or d_{max}/h increases by increasing the axial load P_{ver}. Both F_{max} and $Q_{d,core}$ increase by increasing the d_{max} for a fixed P_{ver}, as remarked in Figure 112c and Figure 113c.

According to these observations, four design variables, namely the axial load (P_{ver}), the dimension of the central hole (d), the maximum displacement (d_{max}) and the height (h), of BRB devices are selected for fitting the proposed design equations for $Q_{d,BRB}$ and F_{max}. In addition, the ratio $Q_{d,BRB}/F_{max}$ is selected to fit the proposed design equation of damping to have more accurate predictions.

6.1.2.1 Prediction of BRBs characteristics and maximum strength

The experimental response of the BRB is composed of two different contributions: the contribution of elastomeric part (rubber and steel shims) and the contribution of the central core characterized by the friction between steel balls. As discussed in Ozkaya et al (2011), the characteristic strength of the BRB, $Q_{d,BRB}$, can be evaluated as the sum of two terms, the characteristic strength due to the elastomeric part of the bearing, $Q_{d,EB}$, and the characteristic strength due to the steel ball, $Q_{d,CORE}$.

$$Q_{d,BRB} = Q_{d,EB} + Q_{d,CORE} \tag{36}$$

The $Q_{d,CORE}$, as reported in Ozkaya et al (2011), is function of the friction coefficient and the axial load. When no axial load is applied, $Q_{d,CORE}$ can be neglected and the $Q_{d,BRB}$ is equal to the characteristic strength of the elastomeric part of the bearing. The lack of experimental data does not allow a proper calibration of the $Q_{d,EB}$, thus, in this study the $Q_{d,EB}$ is assumed equal to :

$$Q_{d,EB} = \frac{\pi}{2} \times \beta_{eff,mean} \times G \times A \times \frac{d_{max}}{h} \quad (37)$$

where G, is the shear modulus of the rubber, assumed equal to 1 MPa (Ozkaya et al. 2011), A, is the area of the elastomer, d_{max}/h, is the shear deformation, h, is the height of the rubber and β_{eff} is the damping of the elastomeric bearing assumed equal to the mean of the tests in Table 21.

Table 21. Experimental damping for the prediction of $Q_{d,EB}$

	Label [-]	β_{eff} [%]	$\beta_{eff,meean}$ [%]
(Ozkaya et al 2011)	13	8.46	7.81
(Caner et al 2015)	25	9.30	
(Natale et al. 2021)	EB_Test1	6.90	
	EB_Test5	6.80	
	EB_Test6	7.60	

The axial pressure acting on the central core, P_{core} is a portion of the total applied axial pressure that can be calculated by using a distribution coefficient, ψ, as the product of the total axial load and the distribution coefficient. This coefficient can be assumed constant and equal to 0.5 as suggested in Ozkaya et al. (2011). However, in this study in order to better capture the experimental response of the tests available in the database a further equation is proposed to reproduce the variability of the distribution coefficient with the aspect ratio D/d. This allows to account for the increasing axial pressure acting on the central core by decreasing the core diameter d. The following equation is proposed:

$$\psi = 0.2064 \times e^{0.3949 \times D/d} \quad (38)$$

The equation is a best fitting of the experimental results. However, the variables and their functional relationship are selected according to basic theoretical principles of confinement. Indeed, according to the most diffused confinement models (Mander et al. 1988), the effectiveness of confinement increases by decreasing the diameter of confined core, d, (the dimensions of the inner hole in the case of BRB devices). This happens because the volume of the confined core increase by increasing the diameter, and thus the effectiveness of the confinement decreases under a fixed lateral pressure.

$Q_{d,core}^{exp}$ is computed from the experimental data on $Q_{d,BRB}^{exp}$ subtracting the $Q_{d,EB}$. $Q_{d,core}^{exp}$ is plotted in Figure 114a against the P_{core} for all the tests available in Table 4. The tests are grouped in different bins of uniform ranges of the maximum displacement demand, d_{max}. They are plotted in Figure 114a in different colours together with the dashed line representing the best fitting of each bin. The slope of the dashed line (representing the friction coefficient, μ) increases by increasing the maximum imposed displacement until d_{max} of about 60 mm. Then it is assumed minor or equal to 0.09 that is a value comparable with the friction of the FPS system and with the value of lubricated steel-steel surface. This observation is made due to the friction between steel balls that increases by increasing the maximum achieved displacement due to geometric relocation of the balls. Once that the friction coefficient of each bin is defined, it is related to the mean maximum displacement of the bin and plotted in Figure 114b. The best fitting between friction coefficient, and maximum lateral displacement, is expressed by a power function (Eq.6).

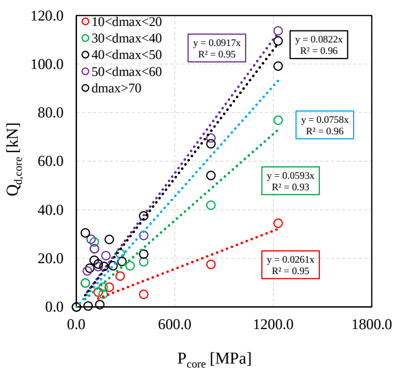

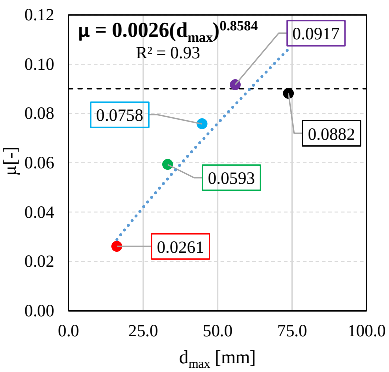

Figure 114. Investigating the friction coefficient of the steel balls: characteristic strength vs. core axial pressure a); mean friction coefficient vs. maximum displacement b)

$$\mu = 0.0026 \times d_{max}^{0.8584} \leq 0.09 \qquad (39)$$

Although the power function well interpolates the mean experimental data, a large dispersion can be observed with each bin respect to the dashed line (see Figure 114a). This is due to the other variables influencing the characteristic strength, $Q_{d,CORE}$, such as the diameter of the central hole, d, reflecting the amount of steel balls and the axial pressure insisting on the steel core.Once that the design variables are known a multi-linear regression (Su et al. 2012) based on the Ordinary Least Squares method is used to correlate these variables with the characteristic strength of the core, $Q_{d,core}$. This results in Eq. 7 having a R^2 = 0.90, R_{adj} = 0.90 and R_{multi} = 0.95.

$$Q_{d,core}^{pred} = -32.8 + 0.0059 \times d \times \mu \times P_{CORE} + 0.50 \times h \qquad (40)$$

As reported in the section above when no axial pressure is applied the contribution of the steel balls to the characteristic strength should be neglected. This is due to lack of experimental data on tests with zero or low axial pressure. Thus, when P_{ver}, and contextually P_{CORE}, is equal to 0, the $Q_{d,CORE}$ have to be assumed equal to zero in calculating the $Q_{d,BRB}^{pred}$.

The prediction of the $Q_{d,BRB}$. are plotted in Figure 115a against the experimental results. The comparison outlines a satisfactory matching with mean equal to 1.15 and coefficient of variation (CoV) equal to 0.57. The large dispersion is related to two tests for which the proposed model significantly overestimates the experimental response. These tests are characterized by design variables similar to other tests but a significant difference in the measured characteristic strength. The latter is mainly related to the relocation of steel balls in the inner core that is actually not easy to predict.

According to the simplified schematization of the BRB response depicted in Figure 111, the maximum strength at a fixed displacement can be computed using the following equation:

$$F_{max} = Q_{d,BRB} + k_2 \times d_{max} \qquad (41)$$

The post-elastic stiffness k_2 is strongly influenced by the maximum imposed lateral displacement. Experimental results (see Test_21 and Test_22 in Table

4) show that by increasing the maximum displacement demand d_{max} a reduction of the k_2 can be observed. Also, the dimension of the central hole, *d*, plays a crucial role in the definition of the k_2 (see Test_2 and Test_5 in Table 4). The results reported in Table 4 outline that the axial pressure does not have a significant influence on the post-elastic stiffness, in fact considering test 16 and 17, where all the variables are the same except for the axial pressure, fixed at 4.3 and 5.7 MPa, respectively, k_2 is very similar and equal to 2.44 kN/m and 2.49 kN/m. For this reason, the post-elastic stiffness is estimated through a multilinear regression assuming as design variables d_{max}, *d* and *h*. The relation is expressed by the Eq. 10:

$$k_2 = 16.5 - 0.2 \times h + 6360.4 \left({}^{1}\!/_{(d \cdot d_{max})} \right) \qquad (42)$$

The multilinear regression is characterized by a R^2 equal to 0.84, while a R^2_{adj} equal to 0.83.

The comparison between analytical predictions and experimental results is reported in Figure 115b. It shows a satisfactory matching with a mean ratio k_2^{pred}/k_2^{exp} equal to 1.02 and CoV equal to 0.45.

Once that $Q_{d,BRB}$ and k_2 are estimated the maximum strength, F_{max}, can be computed by using the Eq.34. The proposed equation well matches the experimental results with a mean of the ratio $F_{max}^{pred}/F_{max}^{exp}$ equal to 1.02 and CoV equal to 0.35 (see Figure 115c).

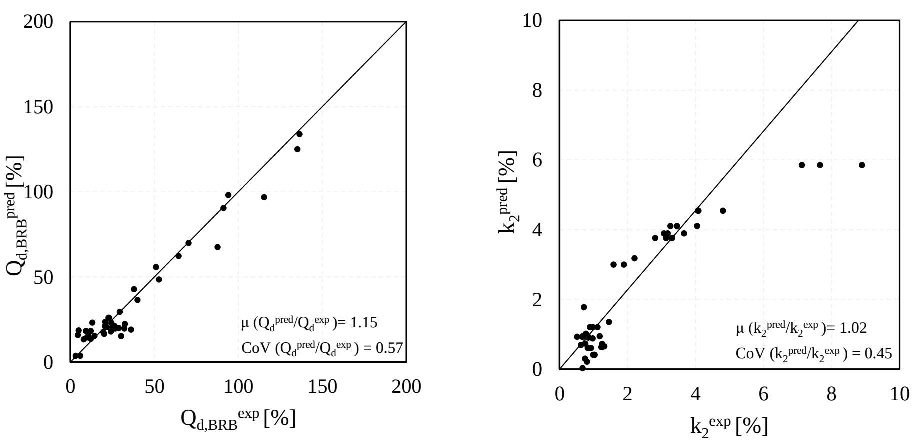

a) b)

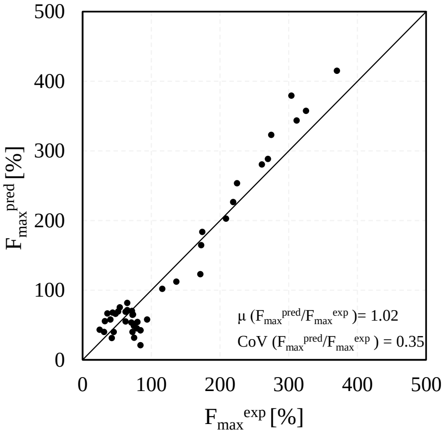

c)

Figure 115. Comparison of experimental results and analytical predictions in terms of: a) Characteristic strength, b) Post-Elastic stiffness, c) Maximum force

6.1.2.2 Prediction of damping for BRBs

Once that the maximum force (Eq. 41) and the characteristic strength (Eq. 40) are computed, the damping ratio can be estimated by using Eq. 2. The comparison of the predicted damping $\beta_{eq}^{pred}$and the experimental one, β_{eq}^{exp}, is reported in Figure 116a. The comparison outlines that the proposed procedure to calculate the equivalent damping provides a reasonable matching with experimental results, resulting in a mean ratio $\beta_{eq}^{pred}/\beta_{eq}^{exp}$ equal to 1.16 and CoV equal to 0.28.

In order to have more accurate estimations of the damping, a multi-linear regression (Su et al. 2012) based on the Ordinary Least Squares method of the ratio $Q_{d,BRB}/F_{max}$ as function of the maximum displacement, d_{max}, the dimension of the central hole, d, the vertical load, P_{ver}, and the BRB height, h, is proposed in Eq.(10):

$$Q_{d,BRB}\big/F_{max} = -0.94 + 0.00017 \times P_{ver} + 0.00081 \times d + 0.00162 \times d_{max} + 0.012 \times h \qquad (43)$$

As reported in the section above, $Q_{d,BRB}$ and F_{max} decrease with the increasing height of the bearing. By contrast, the ratio $Q_{d,BRB}/F_{max}$ increase with the increasing height of the damping. This is due to the volume of the steel balls located in the core that increase with the height of the device, enhancing the damping ratio.

The comparison of the experimental and predicted damping ratios by using Eq. () with the direct estimation of the $Q_{d,BRB}/F_{max}$ ratio by using Eq. (43) is depicted in Figure 116b. The comparison shows a good match with a mean ration $\beta_{eq}^{pred}/\beta_{eq}^{exp}$ equal to 1.09 and CoV equal to 0.24. It has an higher accuracy respect to the estimation of the damping by calculating separately $Q_{d,BRB}$ and F_{max} by using Eq. (40) and Eq. (41).

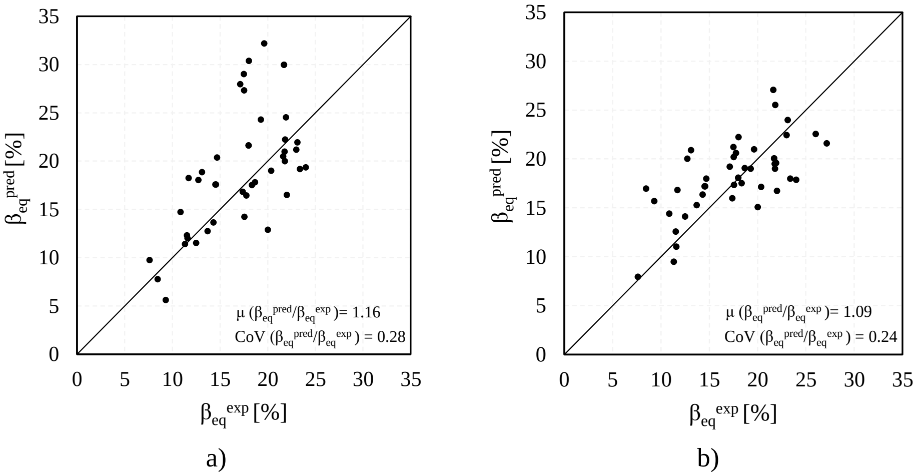

Figure 116. Comparison of experimental results and analytical predictions in terms of damping a) $Q_{d,BRB}/F_{max}$ calculated through regression, b) $Q_{d,BRB}$ and F_{max} calculate as single parameter

Even though the proposed equations well match experimental results, caution is recommended in their extension to BRBs with characteristic falling out of the range used for their calibration. In particular, the equations have been validated for BRBs devices with D = 300 mm, 66 mm ≤ h ≤ 85mm, 0 MPa ≤ σ ≤ 7.1 MPa, 17 mm ≤ d_{max} ≤ 84 mm, 80 mm ≤ d ≤ 165 mm, G=1 MPa, d_{sb}=1.65mm, 10mm≤t_w≤15mm.

6.1.2.3 Influence of Design Variables

In order to assess the reliability of the proposed predictive equations considering a variation of some of the design variables, further comparisons between the experimental damping and the predicted one are proposed. Figure 117a,b show the variability of the damping with the maximum displacement for fixed pressure and dimension of central core (d =100 mm and d =165 mm, in Figure 117a and Figure 117b, respectively). In this case the predicted trends satisfactorily match the experimental ones demonstrating the reliability of the proposed equations in selecting the optimal design parameters in terms of d_{max}. Figure 117c and 117d, show variability of the damping with the dimension of central hole fixing both the d_{max} and the axial pressure. In this case the matching is not good. However, the proposed model is still capable of catching the increasing trend of the damping by increasing the centre hole diameter and axial pressure.

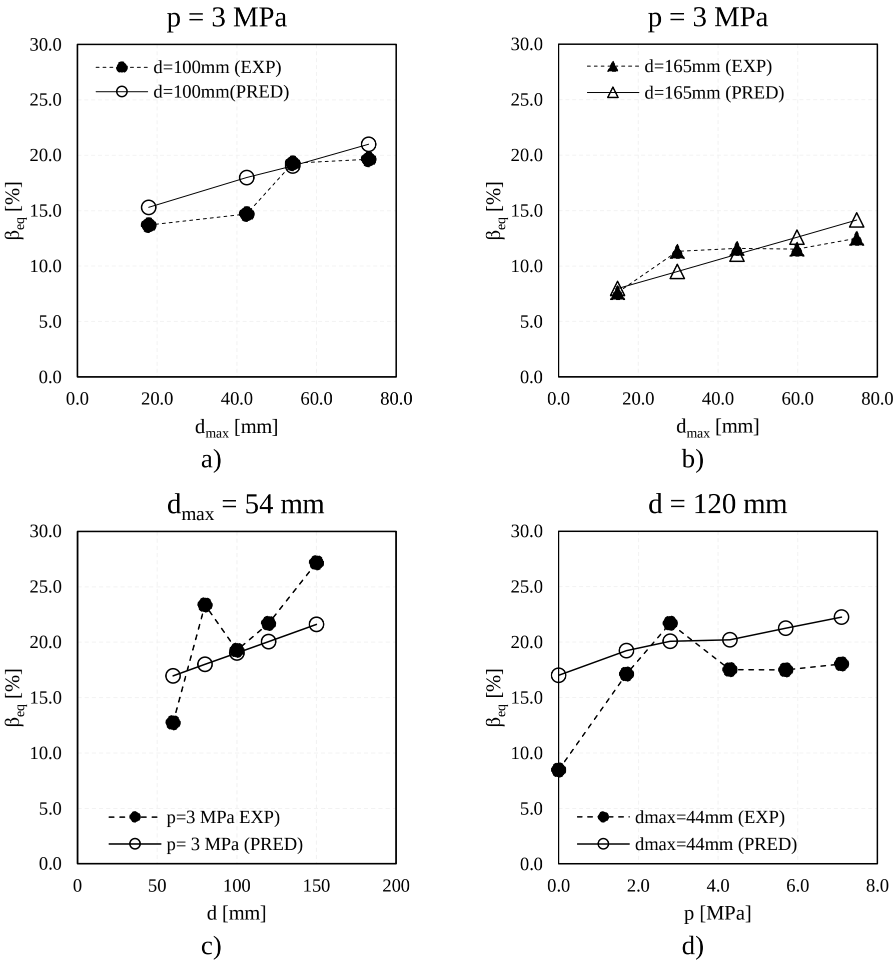

Figure 117. Comparison experimental vs prediction trend, variability of damping: a) with maximum displacement for h =85mm, b) with maximum displacement for h =60mm, c) with dimension of central hole, d) with axial pressure

A parametric study is carried out in order to show the sensitivity to design variables of the proposed equations. In particular, the variability of the equivalent damping, β_{eq}, with the maximum displacement demand, d_{max}, the diameter of the central core, d and the axial pressure, P_{ver} is analysed. The proposed analytical model is applied by fixing one or more variables within the range of calibration of the proposed model. Eq. (10) is used to assess the ratio $Q_{d,BRB}/F_{max}$, then used to calculate the damping ratio by means of Eq. (2).

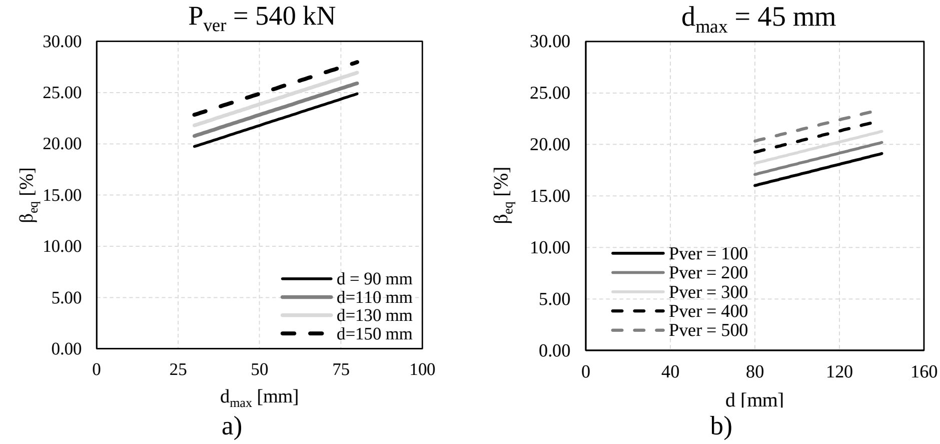

Figure 118. Parametric study on the damping a) Dependence from d and d_{max}, b) Dependence from d and P_{ver}

Figure 118a shows the variability of the equivalent damping with the maximum displacement demand and the diameter of the central hole. In this case, the axial load is fixed at 540 kN taken as the mean of the full dataset of experimental tests. It is worth noting that the damping increases by increasing the displacement demand, d_{max}. In particular, an increase of about the 37% can be observed by increasing the displacement of about four times. This is due the increase of the characteristic strength, $Q_{d,BRB}$,. Indeed, as reported in Eq. (6) there is a direct increase of the increasing friction with the increasing d_{max}. This is confirmed, bythe experimental results of test 19 (at d_{max} equal to 17.9 mm) and test 20 (at d_{max} equal to 73.1 mm) showing that an increase of the the displacement demand of about four times result in an increase of the damping of about 43%. Figure 118b shows the variability of the equivalent damping with the dimension of the central hole, d, and the axial pressure. The trends are obtained by fixing the maximum target displacement, d_{max}, to 45 mm (mean of the dataset reported in Table 4). The trends show that the equivalent damping increases by increasing the diameter of the central core. This is due to the increase of the ratio $Q_{d,BRB}/F_{max}$ that directly depends on d. Indeed, comparing the results of Test_4 and Test_5, where only the variable is d, an increase of the damping ratio of about 12% can be observed moving from a d equal to 100 mm to d equal to 120 mm.

Similarly, the increase of the axial pressure produces and increasing of the characteristic strength resulting in and increase the damping. Considering test 14 and test 15 in Table 4 tested at the axial load of about 120 kN and 200 kN, respectively, an increase of the axial load, P_{ver}, results in an increase of the damping of about the 25%. The comparison between the results of the parametric study and the experimental data highlights the reliability of the proposed analytical model in the selection of the optimal design variables.

6.1.3 Long terms effects on BRB

Typically, seismically isolated structures are not restrained against lateral loads or displacements for a number of reasons. These reasons include but are not limited to the service lateral load restraints detrimentally affecting the seismic performance of the structure, the initial cost of the restraints, replacement of the restraints after a seismic event, and a lack of certainty as to the performance of the restraints. Furthermore, the designer should consider that service load characteristic design response may significantly influence the design of isolated structures, with particular emphasis on bridges. Lateral loads (such as wind or braking loads) and thermal loads are two of the main design parameters for bridges and bridge expansion joints. The target performance under wind and braking induced lateral loads aims to have bearings with high initial stiffness (k_1) and characteristic strength (Q_d) in order to minimize lateral displacements Conversely, under thermal expansion/contraction, the bearings should have low initial stiffness (k_1) and yield force (Q_d) in order to reduce the actions transmitted to piers or abutments. The different desired behaviors may coexist in the same bearing if the different rates of occurrence of the two service conditions are considered. Indeed, the rate of service loading is currently considered to be slower than earthquake-induced displacement but faster than imposed service-level displacements such as creep, shrinkage, and seasonal and daily thermal expansion and contraction.

For instance, in the case of LRB (Lead Rubber Bearing), because of the lead core, under slow displacement demand such as those related to shrinkage/creep/thermal loads, the yield force is low (commonly assumed equal to 0.33*$Q_{d,seismic}$), while under fast displacement demand, such as wind or braking loads, the yield force is assumed equal to 0.5*$Q_{d,seismic}$. BRBs can provide a similar response to LRBs because the inner friction developed by the steel balls behaves similarly to the lead core.

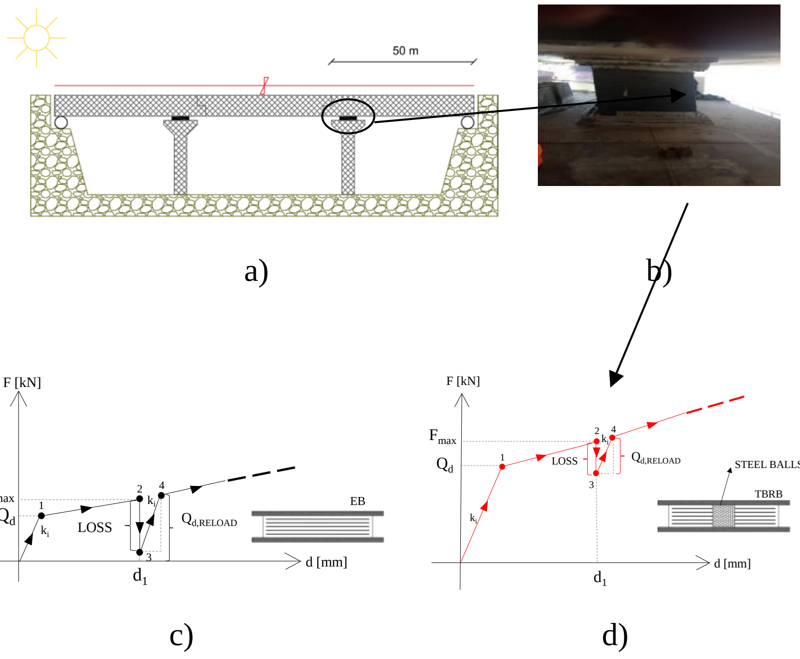

Figure 119. Long span bridge subjected to thermal distortion a), Displacement of bearing subjected to service condition on long span bridge b), Creep effect in terms of losses related to the Q_d: c) EBs, d) TBRBs

For many bridges, the forces induced by thermal expansion/contraction are less of a concern for the design of the structure than service lateral load resistance. This is especially true for short-span structures in low seismic zones where a high Q_d for service loads can make the isolation bearings too stiff to achieve optimum performance of the isolation system for seismic loading. For this reason, the small amount of creep in the ball-filled elastomeric bearings could be a positive attribute. In some very long, continuous bridges (see Figure 119a, b) the forces induced in the bearings due to imposed thermal expansion/contraction are more of a concern than lateral load resistance.

Once the isolation system is subjected to a service condition, lateral force and displacement are achieved in the bearings and held (point 2 in Figure 119c,d). During this holding time, it is possible to observe a loss in the force (moving from point 2 to point 3 in Figure 119c, d). This loss, as shown in the section above, depends on the type of the bearings and the imposed lateral displacement. In order to quantify such a loss as a function of the characteristic strength Q_d, the ratio $(F_{max}-F_{min,1800})/Q_d$ is presented in Figure 120.

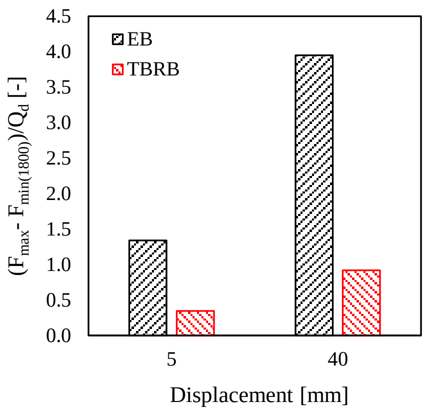

Figure 120. Ratio between the losses and the characteristic strength of the EB and TBRB

The EBs and TBRBs, the bearings analyzed in this study, are characterized by different values of loss of loads, see Figure 120. In particular, the EBs have shown a very high loss of load, about 1.3 times and 4.0 times Q_d at 5 mm and 40 mm imposed displacement respectively. By contrast, the TBRBs showed a limited loss of load of about 0.3 Q_d and 0.9 Q_d at 5 mm and 40 mm imposed displacement respectively.

This loss of load becomes critical in the design of the EBs because under exceptional load conditions (i.e. an earthquake event), they have to overcome a characteristic strength, Q_d, higher than they were designed for.

Indeed, with reference to the load path in Figure 119, assuming that an earthquake occurs when the bearing is at point 3 (it is not a rare condition since it happens on a daily-basis due to, for example, thermal distortions), the EBs will not perform as designed and the force transmitted to the piers, $Q_{d,reload}$ will be 1.3-to-4 times higher than the initial one, Q_d. This is because to activate the bearing the $Q_{d,reload}$ (point 4 in Figure 119d) should be achieved. By contrast, this phenomenon is not significant for TBRB devices. Indeed, at a displacement of 5 mm, the $Q_{d,reload}$ is about 0.3 the initial $Q_{d.}$ suggesting that the devices need a force lower than the design one to be re-activated. Also, at large sustained displacement of about 40 mm the loss of $Q_{d,reload}$ is about equal to the initial Q_d, making the phenomenon insignificant for the reloading stages.

In conclusion, the TBRBs, when subjected to service load conditions that may generate relaxation and creep phenomena, are capable of guaranteeing the seismic performances they were designed for. It is worth mentioning that the results of this pioneering study cannot be generalized since only one type of bearing with a single geometric configuration has been tested. Further research is needed to better investigate this phenomenon.

6.2 Certification and acceptance of isolation device (curved surface sliders) for bridge

This section describes the certification and acceptance process for the curved surface devices. The design and controls are directly related to the recommendations in which the design is realized. The Italian code (NTC 2018) is inserted in the context of the European codes and in particular UNI EN 15129 (CEN 2009) and UNI EN 1337 (CEN 2004b). The NTC 2018 is perfectly in line with what the UNI EN proposes. Indeed, it separates the tests for certification from the tests for acceptance. Furthermore, according to NTC 2018, specific tests should be added for the different types of isolators.

Compliance with the harmonized European standard UNI EN 15129 (CEN 2009) and the CE marking are required by NTC 2018 for the certification process. The above-mentioned UNI EN 1519 provides for a system of evaluation and verification of constancy of performance to be applied. The objective of the certification process is to maintain functionality under the various conditions that will be tested during the life of the project.

Mandatory on-site verification for all types of devices is required by the 2018 NTC for the acceptance process; in addition, the required certification document must be reviewed by the construction manager and all non-compliant devices must be rejected. Geometric verification and dimensional tolerance could also be performed by the construction manager.

Laboratories that have adequate competence, equipment and organization can perform and certify the acceptance tests. Refer to the "Factory Production Control" section of UNI EN 15129 for the methodology for establishing the acceptance test plan and evaluation criteria. If certain conditions are met: i) sampling of the equipment has been carried out on the lots intended for the particular site by the site manager; ii) testing is carried out and certified by a laboratory with adequate competence, equipment and organization; iii) the above certificates explicitly state the site(s) where the supply will be used; factory production control carried out as part of the certification process can be used for the purpose of acceptance testing.

Finally, the devices subjected to certification or acceptance testing may be used in construction only if: i) the elements stressed in the non-linear range are replaced or if their resistance to fatigue at low load cycles is at least an order of magnitude greater than the number of test cycles; ii) and in any case, only after their perfect integrity and full functionality have been verified.

The number of devices to be tested is specified in NTC 2018 11.9.8.1. acceptance tests shall include at least 20% of the devices, in any case not less than 4 and not more than the number of devices to be implemented.

6.2.1 UNI EN 15129

The European standard for describing the certification and acceptance process of sliders with curved surfaces is UNI EN 15129. Additional tests required by national recommendations had to be integrated in UNI EN 15129. The entire process of certification and acceptance is described here in a brief summary. The Assessment and Verification of the Constancy of the Performance (AVCP) is described in Chapter 10 of UNI EN 15129. Verification of seismic protection devices in accordance with the requirements of UNI EN 15129 and the manufacturer's declared performance includes: i) identification of the product type; ii) verification of production at the manufacturer's plant, including evaluation of the product. The acquisition of the CE marking together with the type tests that constitute the certification process, constitutes the type product. According to UNI EN 15129 (10.2), type tests must be performed on full-scale sliders, including cyclic tests, to determine all mechanical properties of the sliders required for the design to ensure durability. Representative values of the mechanical properties of the sliders shall be confirmed by the test results.

The acceptance process is formed by the factory production control (FPC), which is the control of the production site. In order to ensure that the sliders conform in their essential characteristics to the declared performance, the manufacturer should maintain an FPC system according to UNI EN 15129 (10.3). The FPC includes control of raw materials and also some special tests for the devices.

These general rules apply to all types of sliders, while the curved surface sliders are specifically analyzed in section 8.3.4 of UNI EN 15129, defining the type tests (8.3.4.1) and the FPC tests (8.3.4.2).

The FPC tests that complete the acceptance of the devices are described here. For the slides with curved surfaces, the tests are listed in section 8.3.4.2 of UNI EN 15129 (Figure 121).

To complete the FPC tests, the following tests are required:

a) Vertical load bearing capacity (see Sect. 8.3.1.2.2.2 and 8.3.4.1.2 of UNI EN 15129);

b) Frictional resistance force under service conditions (see Sect. 8.3.1.2.2.5 and 8.3.4.1.3 of UNI EN 15129);

c) Test run P1, also called benchmark test (see Sect. 8.3.1.2.2.6 and 8.3.4.1.5 of UNI EN 15129).

According to Tab. 16 of UNI EN 1337- 2:2004 for raw materials and components, or in the case of other slippery materials, according to the provisions of the respective European Technical Approval (ETA), the tests shall be carried out
Based on the recommendations described, the acceptance protocol for curved surface sliders has been summarized in a European framework in Figure 121. Note that the national code and other authorities involved in the project may recommend adding further tests to the protocol. Foe example for the case study shown in the next section, the acceptance protocol presents a challenge: to ensure compliance with all European and Italian regulations, while guaranteeing compliance with the technical specifications of the Italian Railway System (RFI) and the Italian Road Federation (ANAS).

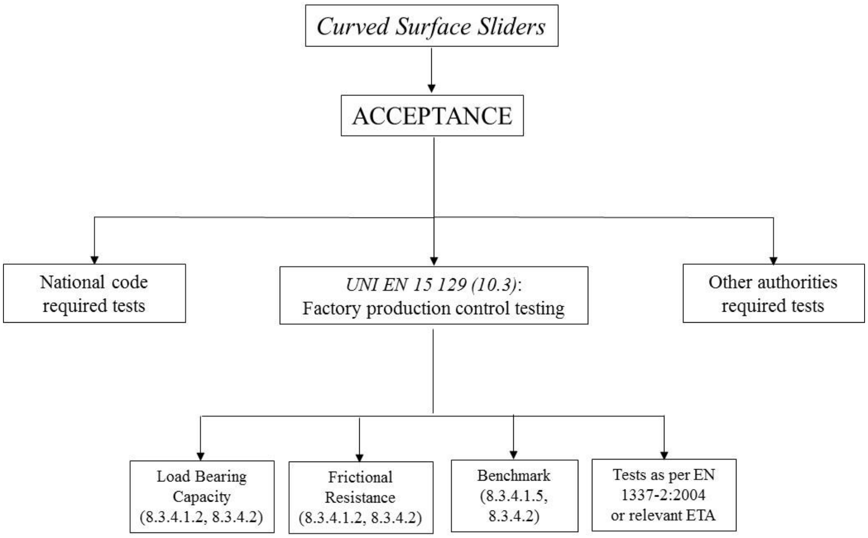

Figure 121. The acceptance for the curved surface sliders summarized in a flow-chart (Cademartori et al)

The Italian National Code (NTC 2018, 11.9.8) proposes to add an additional test to the protocol, called the Quasi Static Test. For the case study shown, the Italian Railway System (RFI) and the Italian National Road Association (ANAS) propose additional technical specifications to be considered in the acceptance process. Among all the tests proposed by the different authorities involved in the project, the one of RFI is added because it is similar to the tests of UNI EN 15129 but uses different loading conditions/set-up conditions/acceptance parameters. This test is not dealt with in the present work.

6.2.2 Application to a case study

Following the August 14, 2018 tragedy that killed 43 people when the viaduct collapsed on the A10, a strategic link in northern Italy, the Polcevera viaduct has been rebuilt with a seismic isolation devices.

Figure 122. View of the bridge (Cademartori et al. 2021)

The San Giorgio Bridge has a length of 1067 m and the road level is at an elevation of 40 m. The bridge has a steel-concrete composite deck with a total width of 29.8 m and a distance between supports of 7 m. Structurally, the bridge is a continuous girder with a length of 50 m for all spans except the three spans in the middle (with a length of 100 m and for the spans near the abutments, which are shorter).

The deck is seismically isolated from the piers. The structure was designed to resist seismic action, wind action, and thermal action, which is particularly important for a bridge 1067 m long with no intervening movement joints. The Figure 122 shows a top view of the bridge.

Figure 123. Plan view of the bridge with the piers' identification (Cademartori et al. 2021)

The bridge is equipped with the following devices (between brackets the nomenclature is given according to UNI EN15129), as shown in the plan view of Figure 123: i) two curved surface sliders (*"friction pendulums"*) on each pier from P2 to P17 with shear fuses for the device on the north side (*"combined devices: curved sliders + fuses"*) and without fuses for the device on the south side; ii) two multidirectional bearings on piers P1 and P18; iii) two multidirectional bearings on abutments A, west side, and abutment B, east side; (iv) a guided bearing at the center of the abutments; (v) two curved surface sliders on piers RP1-RP2-RP3 of the ramp; (vi) an elastomeric device at the center of abutment A of the ramp; (vii) two multidirectional bearings on abutment A of the ramp.

The base isolation was chosen to provide high deformability in case of a seismic event, to extend the period of vibration and to reduce the acceleration of the deck. In this context, transverse anchors provided by the fuses during the service condition, are installed to limit the movement due to wind or breaking. The fuses were calculated to break off in case of a seismic event.

To prevent direct contact between the steel deck and concrete piers during extreme seismic events, the deck is also equipped with transverse seismic anchors at each pier and transverse and longitudinal seismic anchors at the abutments. Movement joints are only provided at the three abutments.

6.2.2.1 Acceptance protocol test

The main objectives of the testing program carried out for the San Giorgio Bridge were: i) to ensure compliance with the technical standards in force; ii) to guarantee compliance with the planned performances; iii) to study the behavior of the devices in relation to the comments and regulations issued by the various authorities during the project approval procedure (e.g. the technical authority of the Italian Minister of Transport and the comments of the Commissioning Authority); iv) to study the durability and long-term behavior of the devices using all the available state-of-the-art tests in the field.

The acceptance protocol (UNI EN 15129 FPC tests plus tests required by national law) for the case study under investigation is presented here. In accordance with Tab 16 of UNI EN 1337- 2:2004, the characteristic material conformance tests were performed. In addition, other tests were performed under the supervision of RFI specialists based on their protocol. Table 1 lists the tests studied, the type of tests performed, and the standard to which each test refers (tests performed in accordance with RFI specifications are not included here).

Table 22. Summary of devices under investigation and relevant tests (see Figure 123 for labels) (Cademartori et al 2021).

CURVED SURFACE SLIDERS TYPE	**PIER**	**TEST**			
TYPE A: 3 SLIDERS ON THE 100 METERS BAYS	P9/3, P10/3 and P11/2	Load Bearing Capacity UNI EN 15129	Frictional Resistance UNI EN 15129	Benchmark UNI EN 15129	Quasi-Static NTC 2018
TYPE B: 4 SLIDERS ON THE 50 METERS BAYS	P2/3, P13/3, P2/2 and P12/2				
TYPE C: 4 SLIDERS ON THE BRIDGE RAMP	RP3/R2, RP3/R3, RP2/R2 and RP1/R2				

The following nomenclature is used: the number after “P” refers to the pier number as reported in Figure 123, while the number after the “/” refers to the location of the devices on the pier (“3” for the northern support and “2” for the southern supports). The supports located on the southern side are combined devices (curved surface sliders + shear fuses).

A critical discussion of the main problems encountered during the test program is described:

- the acceptance and certification processes were carried out contemporary, as the device was realized ad hoc, not commercially produced and specifically suited to the design requirements. Significant problems arise when there are matches between the acceptance and certification processes, as in this case, since the UNI EN15129 does not require full tests for the combined devices in the acceptance protocol, while it suggests only one test in the certification process. In fact, the combined devices must be tested with high priority to ensure that there are no unexpected interferences between the components that affect the behavior of the device. To this end, specific tests for the combined device were required by the building inspectorate for the case study under investigation (including tests in the transverse direction, break away tests on two sacrificial devices), but these have not been addressed in this work. Testing of the individual components should be carried out after the combined tests, as some modifications/retrofits may be required, as in the case study
- the loading bearing capacity test required an axial load from the gravity combination ULS of 1.3 NULS; the value of the vertical load is significantly high, especially for the modern bridge. This means that the facilities may not be able to have adequate capacity. In order to easily perform the tests, this constraint could be taken into account in the design of structures/infrastructure by consulting the available instruments of the laboratories in the region. Otherwise, a significant increase in time and cost for testing with non- conventional instruments should be considered. The regulations should provide for a simplified approach that ensures the same level of safety. The same issues may arise with displacement requirements.

- the design of small friction values may mean that the calibration forces of the laboratory equipment may be comparable to the forces to be measured; this may strongly influence the test results.

As discussed in the following sections, the interpretation of some tests of UNI EN 15129 is in some cases ambiguous or not always quantitative (see, for example, the definition of $F_{average}$ in the next section).

From here, a special focus is given to the benchmark test, which is the most important dynamic test within the requirements of UNI EN 15129 in the acceptance phase.

6.2.2.1.1 Benchmark Test

The benchmark test for curved surface sliders has two objectives related to the acceptance test required by UNI EN 15129:

1) Verification of cycle stability in terms of variation of test force with respect to average force.

2) Verification of the dynamic friction coefficient.

The table. indicates the method of load application (UNI EN 15129 8.3.4.1.5), where d_{bd} is defined as the maximum design displacement of the device. The device is subjected to a permanent vertical load N_{sd} (seismic combination)

Table 23. Load application method for the benchmark test (UNI EN 15129 8.3.4.1.5).

Type of test	Test run	Compression load N_s [kN]	Displacement d_0 [mm]	Peak velocity v_0 [mm/s]	Number of complete cycles
Benchmark	P1	N_{sd}	1 x d_{bd}	50	3

Any kind of oscillations are accepted, such as those caused by the stick-slip phenomenon. The motion shall be regular and uniform, in accordance with the acceptance criteria of UNI EN 15129 8.3.1.6. The force variation shall be within +/- 5% of the average restoring force, up to 85% of the maximum displacement required by the test protocol for each bearing displacement. The average restoring force is determined from the best fitting straight line determined by interpolating the least squares response between +/- 85% of the maximum displacement.

The requirement to satisfy the test can be summarized as:

for (-0.85) d_{bd} <d <(+ 0.85) d_{bd} : $F_{regression}$- (0.05$F_{average}$) <F_{test} <$F_{regression}$ + (0.05$F_{average}$) (44)

Other criteria concern the dynamic coefficient of friction. The value must be within the limits set by the structural engineer under the test conditions specified in UNI EN 15129 8.3.4.1.5. During the design phase, two limits are set for the dynamic coefficient of friction: a lower limit and an upper limit. It shall be verified that the value of the coefficient resulting from the tests is within these limits. The verification can be done by calculating the average dynamic coefficient of friction using the following formulae:

$$\mu = \frac{H}{2 \cdot (d^{+} + |d^{-}|) \cdot V_{load}} \quad (45)$$

where: H = area subtended by the curve, d + = maximum displacement, d- = minimum displacement, V_{load} = vertical load. This value should vary inside the lower/upper bound range.

Then, the final requirement is that:

$$\mu_{lower\ bound} < \mu < \mu_{upper} \quad (46)$$

As described in the above section, the benchmark test on P12/3 slider (label producer MAU112E19-10) is shown here. In the Figure 124, the hysteretic response of the slider is shown. Also shown in the Figure 125 are the displacement-time and force-time diagrams for the 3 cycles.

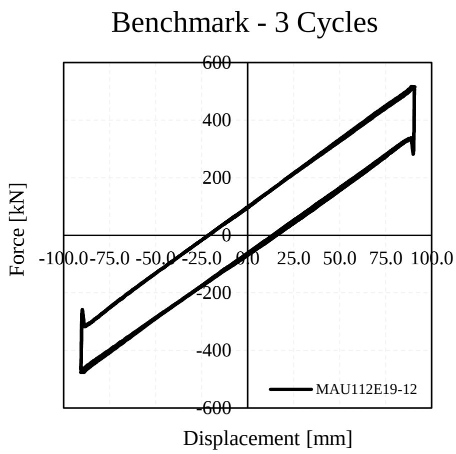

Figure 124. Displacement-force plot for the 3 cycles of the benchmark test

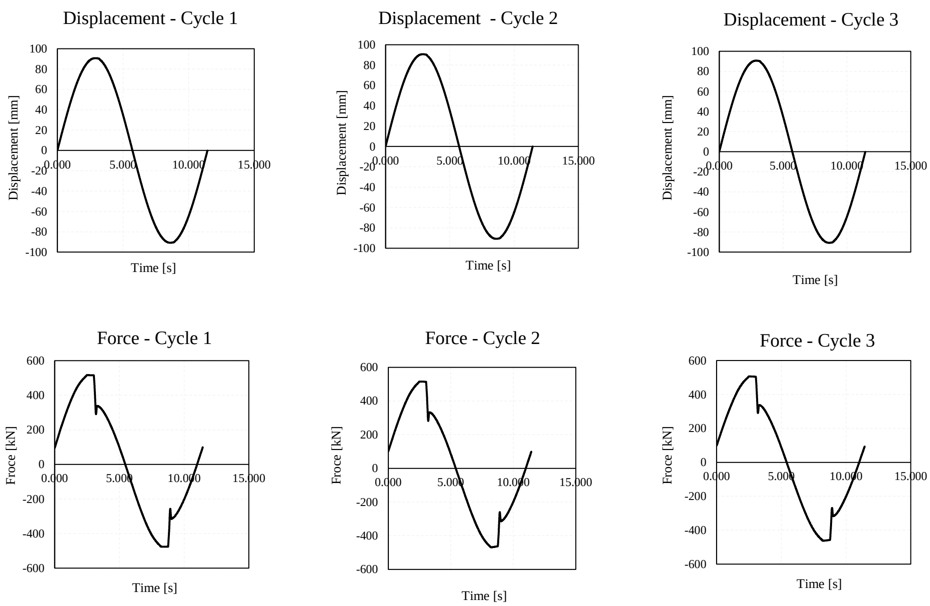

Figure 125. Displacements-time and forces-time plots for the 3 cycles.

The Figure 126 shows the verification of the cycle stability in terms of the variation of the test force at each step with respect to the average force for the three cycles. The check shows a continuous stability of the hysteretic response over the 3 cycles

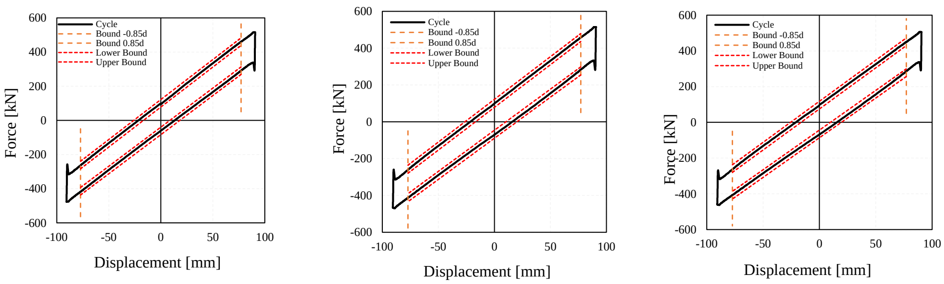

Figure 126. Stability check of the 3 cycles for the curved surface sliders

In accordance with Equation 3, the value of the dynamic friction coefficient in the three cycles was calculated and reported in Table 3.

Here is a summary of the dynamic coefficient of friction in the three cycles (Table).

Table 24. Summary of the dynamic frictional coefficient in the three cycles.

Cycle 1	Cycle 2	Cycle 3
0.5%	0.5%	0.5%

The UNI EN 15129 states that the average restoring force is to be determined from the best-fit straight line, which is determined by interpolating the least squares response ± 85% of the peak of the test displacement. The variation in horizontal force shall be less than ± 5% of the average restoring force, up to 85% of the peak test displacement at any level of displacement of the sliding isolator. Therefore, the procedure for determining the value of this average restoring force for which the 5% interval should be calculated may lead to different interpretations (i.e., in terms of the interval in which the test result should be contained to satisfy the test). It is clear that this mentioned value should depend on an average of the maximum forces reached during the test in accordance with the ± 85% of the test displacement peak, but a simpler explanation could help users.

Conclusions

The thesis presents the results of a research work on the effectiveness of base isolation as seismic protection strategy for existing RC buildings and bridges. In particular, it focused on the following aspects and goals: i) determine the effectiveness of base isolation compared to other techniques; ii) provide a comprehensive PBEE-based methodology to assess the PBT of different retrofit solutions; iii) develop a simplified tool to calculate the PBT based on the building main characteristics, iv) develop and validate through experimental test a new type of rubber bearing; v) assess the influence of creep and relaxation on the lateral response of this novel devices; vi) provide reliable design equations to predict the main bearing characteristics to be used in the design process; vii) clarifying the acceptance and qualification process of new bearings to be used on bridges. With reference to this objective, the main findings can be summarized as follows.

Base isolation is a seismic retrofit technique with high effectiveness. It allows not only to increase the structural safety of the building but also to protect the acceleration and drift sensitive non-structural components. This may result in a significant reduction of the expected annual losses (EALs) providing that the building and its content are properly modelled. The seismic analyses on base-isolated RC existing buildings performed in this study outlined that:

- When the building is modelled in the bare configuration, significant ductility demand can be observed on the superstructure. Thus, a nonlinear model seems more appropriate to reproduce the seismic response and properly assess and define the strengthening interventions on the structural members;
- When the infills are included in the structural model, the response of the structural system is mostly elastic. This is due to the high lateral stiffness of allow clay brick infills;

- The infills significantly changes the structural response of the super-structure. Although the drift demand is significantly reduced, they attract higher shear forces resulting in higher number of structural members (i.e. columns and beam-column joints) that need for further strengthening interventions combined with the base-isolation;

The main criticism to the widespread of base isolation as retrofit technique of existing buildings is the high initial cost. However, the direct cost should not be considered as meaningful decision variable since it does not account for the performance of the retrofitted building during its design life. To help practitioners to quantify and communicate the advantages of base isolation as seismic retrofit solution a refined framework to estimate the Pay-Back Time, namely the time needed for the return the economic investment of the retrofit solution, has been herein analyzed and discussed. To validate its application, it is applied to a case study building, evaluating the PBT related to four different retrofit solution (FRP, Rebuilt, Base Isolation and Base Isolation +FRP). Then it is extended to the entire database of RC buildings retrofitted by means of base isolation during the L'Aquila reconstruction process. This allowed to develop a simple formulation for the definition of PBT. The study allowed to draw the following conclusions:

- The results of (Non Linear Time Histories) NLTHs and the disaggregation of the (Expected Annual Losses) $EALs_{,direct}$ outline the main advantages and the disadvantages of all proposed solutions. Indeed, although FRP or the rebuilt are effective in increasing the seismic safety and reducing the probability of collapse they do not significantly act in reducing the $EALs_{,direct}$ under low intensity and more frequent earthquakes. By contrast, the high efficiency of the base isolation allows to significantly reduce the drift and acceleration demand on the superstructure resulting in a significant reduction of the $EALs_{,direct.}$

- The comparison in terms of PBT sheds new lights on how to identify the most convenient retrofit solution. The three retrofit solutions have a PBT in the range of 26–29 years that is significantly smaller than the one associated to the rebuilt solution (76 years). This remarks the potential convenience in the retrofitting of existing RC building with respect to the demolition and reconstruction
- Even though the retrofit solutions using base isolation have a high initial cost (45.1% and 50.1% for Base isolated and Base isolated + FRP, respectively, (1200 €/m^2, replacement cost)), they have a PBT (26 years and 28 years, respectively) smaller than the FRP-based retrofit solution (29 years). This is because of the higher savings allowing for a faster recovery of the initial investment
- The methodology has been extended to the full database of 59 base-isolated buildings in L'Aquila resulting in a mean PBT of about 28.9 years and a standard deviation of 6.8 years. These data have been used to calibrate a simple relationship that can be used in the common design practice to estimate the PBT of base isolated buildings once that safety index at LSLS is known (i.e. $PBT = 43.5 – 18.6 \cdot (PGA_C/PGA_D)_{LSLS.}$

Although a reliable framework to calculate the PBT is proposed it needs many detailed information on the building to be used, the lacking of these data not allow its application at the early stages of the design. To help practitioners in the calculation of the PBT and to compare different retrofit techniques based on the building main characteristics, a simplified software tool, based on the refined loss-assessment framework discussed before, has been developed in the MATLAB environment. This tool requires a few input data (geometry, number of floors, mechanical properties, base isolation system parameters) and it is able to perform a complete structural, damage and loss analyses, providing drift, acceleration, shear storey, EALs, (Expected Annual Losses) and PBT (Pay-Back Time) as output. At this stage three different retrofit solution are considered: FRP, Rebuilt and Base Isolation. In addition to investigate the influence of concrete compressive strength and transverse reinforcement, a parametric study has been performed. The application to six real case studies RC building retrofitted by means of base isolation to assess the reliability of this tool has been carried out. The main findings can be summarized as follows:

- This tool is very useful instrument to have a first insight on the retrofit solution leading to the lowest PBT. It requires very basic data and a short time of analysis if compared with a refined loss-assessment analysis. Furthermore, it provides results that are having a good agreement with the most refined framework previous described;
- The PBT decreases by decreasing the concrete compressive strength, f_{cm}, and the ratio A_{sw}/s. This remarks that the convenience in the use of base isolation increases as most as the seismic performance of the existing building are low.
- This framework allows to identify the boundaries of the convenience in the use of the base isolation. For instance, the PBT for the base isolation ranges from 19 to 79 years with the highest value for the lower buildings. The PBT, for the retrofit with FRP and the Rebuilt, ranges from 9 to 44 years and from 41 to 307 years, respectively. The base isolation always achieves $\zeta_{BaseIsolation}$ equal to 1.00 while FRP could have a ζ_{FRP} lower than to 1.00.

Further developments of this research work may be oriented to extend the proposed simplified tool to include a simplified approach to account for torsional effects on irregular buildings. This tool can be further developed to include other retrofit techniques such as steel braces or new infill walls and a comparison of the retrofit alternatives with a comprehensive cost/benefit methodology

Recent earthquakes demonstrated that the seismic performance of road infrastructures is critical to guarantee a rapid recover and to reduce direct and indirect economic losses. Bridges are commonly characterized by supporting devices with a high horizontal deformability for service loads, which may also serve as base isolation when properly designed. The research of cost-effective devices has a strong improvement in the last years. To this aim the study of new type of elastomeric device, namely Ball Rubber Bearing (BRB) is carried out. An experimental program consisting of 15 tests was carried out (in Ankara, during the visiting period at M.E.T.U-Middle East Technical University). The tests investigated the influence of axial load and horizontal displacement. To this purpose three values of axial load and five values of horizontal displacement are investigated. The main finding can be summarized as follows:

- The increase in vertical load, P_{ver}, in the displacement demand, d_{max}, and in the dimension of the central hole, d, (namely increase in the amount of steel balls) corresponds to a direct increase of the energy dissipation;

Bridges are subjected to a different type of loads that are not predominant in buildings, such as service loads, which have both short-term and long-term effects. Lateral movements must be allowed in order to avoid significant stress on the piers under thermal deformations. To this aim an experimental program investigating the lateral creep of the TBRB (Tube Ball Rubber Bearing) and EB (Elastomeric Bearing) has been carried out. In literature data on vertical creep are available but there aren't information on the lateral one is still lacking. The campaign consists in 6 tests for each device. One to assess the cyclic behavior of the bearing, three tests to evaluate the lateral creep, investigating two values of imposed displacement and two values of speed rate, one test to estimate the cyclic behavior after creep and the last one to investigate the influence of axial load. The assessment of the influence of creep and relaxation on the lateral response of this novel device outlined that:

- The comparison of hysteretic response showed the increasing performance of TBRBs respect to EBs, this is due to the use of steel balls providing an increase in the energy dissipation and equivalent damping ratio. The deterioration of the rubber related to the contact with the steel balls that can be observed in classic BRBs is reduced using inner flexible rubber tube;

- The creep tests at different sustained displacement (i.e 5 mm and 40 mm) do not provide significant modification on the hysteretic response of EBs and TBRBs.
- The loss of load is ranged between 1.3 and 4.0 Q_d and between 0.3 and 0.9 Q_d for the EBs and TBRBs, respectively, showing a different response on the re-load brunch after creep;
- With reference to EBs, the increase in the characteristic strength led to a $Q_{d,reload}$ higher than the one considered in the design. This may result in a significant increase of the shear forces is transmitted to the piers.
- This issue is not relevant for TBRBs. A $Q_{d,reload}$ lower or equal to the initial one makes these bearings effective even when an earthquake occurs while it is not in its initial position.

The results of this early work cannot be generalized since they refer to bearings with specified geometric and mechanical characteristics. Further studies are needed to investigate the variability of this phenomenon with respect to the bearing characteristics and to deeply investigate the TBRBs.

Recent development of a new type of bearing as the BRB show the lack of several instrument to an adequate design of a base isolation system with this type of device. To this aim different predictive equations for the main design parameter of the BRBs are proposed. All the data available in literature on BRBs are collected and best-fitting equations are proposed. Design equations for the equivalent damping, characteristics strength, stiffness and maximum force, have been herein proposed.

The main findings on this task can be summarized as follows:

- The characteristic strength percentage, $Q_{d,BRB}$, is higher than the increase in the maximum strength, F_{max}. This results in an increase of the equivalent damping by increasing the ratio $Q_{d,BRB}/F_{max}$;
- By contrast $Q_{d,BRB}$ and F_{max} decrease by increasing the bearing height, *h;*
- Four variables, namely P_{ver}, d_{max}, *d and h* are considered in fitting proper design equations to predict the characteristic strength, the maximum strength and the equivalent damping;
- The proposed equations satisfactorily match the experimental data in terms of $Q_{d,BRB}$ (Eq. 3) and F_{max} (Eq. 8). However, when the results of the predictions are used to assess the equivalent damping by means of Eq. (2) they may lead to overestimate the experimental damping of about the 16% on average;

  To have more reliable estimations of the equivalent damping the ratio $Q_{d,BRB}/F_{max}$ can be estimated by using Eq. (10), resulting in a mean of 1.09 and CoV of about 0.24.

The development and installation in-field of isolation devices are subjected to a qualification and acceptance process. In the European context the reference documents are the UNI EN 15129 and UNI EN 1137 in combination with national rules. This creates some difficulties in the definition of acceptance tests and in their interpretation of test results. To this aim a clarification of the main acceptance tests has been made with an application to a case study (Polcevera Bridge).

References

AASHTO AA of SH and T (2015) AASHTO LRFD Highway Bridge Superstructures

Aiello MA, Ciampoli PL, Fiore A, et al (2017) Influence of infilled frames on seismic vulnerability assessment of recurrent building typologies. Ing Sismica 34:58–80

Al-Hussaini T., Zayas VA, Constantinou MC (1994) Seismic Isolation of Multi-Story Frame Structure Using Spherical Sliding Isolation Systems. Buffalo, NY

ATC - Applied Technology Council FP-58 (2012a) Next-generation Seismic Performance Assessment for Buildings, Volume 1 – Methodology. Fed Emerg Manag Agency, Washington, DC

ATC - Applied Technology Council FP-58 (2012b) Next-generation Seismic Performance Assessment for Buildings, Volume 2 – Implementation Guide. Fed Emerg Manag Agency, Washington, DC

ATC - Applied Technology Council FP-58 (2012c) Next-generetion Seismic Performance Assessment for Buildings, Volume 3 - Supporting Electronic Material. Fed Emerg Manag Agency, Washington, DC

Baggio C, Bernardini A, Colozza R, et al (2007) Field Manual for post-earthquake damage and safety assessment and short term countermeasures (AeDES). ISPRA, Italy

Bakis CE, Bank LC, Brown VL, et al (2002) Fiber-Reinforced Polymer Composites for Construction — State-of-the-Art Review. ASCE J Compos Constr Constr 6:73–87. https://doi.org/1090-0268/2002/2- 73–87

Balsamo A, Di Ludovico M, Prota A, Manfredi G (2011) Masonry Walls Strengthened With Innovative Composites. In: Proc 10th International Symposium on Fiber-Reinforced Polymer Reinforcement for Concrete Structures. pp 1–18

Bondonet G, Filiatrault A (1997) Frictional Response of Ptfe Sliding Bearings at high frequencies. J Bridg Eng 2:139–148

Buckle IG, Mayes RL (1990) Seismic isolation: History, Application and Performance - A World View. Earthq Spectra 6:

REFERENCES

Cademartori M, Miano A, Fiorillo A, et al (2021) Functionale Acceptance Tests for the seismic isolation devices of the New San Giorgio Bridge in Genoa. In: COMPDYN - 2021

Calvi GM, Spaziante V (2009) La ricostruzione tra provvisorio e definitivo: il progetto C.A.S.E. Progett Sismica

Calvi PM, Calvi GM (2018) Historical development of friction-based seismic isolation systems. Soil Dyn Earthq Eng 106:14–30. https://doi.org/10.1016/j.soildyn.2017.12.003

Calvi PM, Ruggiero DM (2016) Numerical modelling of variable friction sliding base isolators. Bull Earthq Eng 14:549–568. https://doi.org/10.1007/s10518-015-9834-y

Caner A, Naghshineh AK, Erdal S (2015) Performance of ball rubber bearings in low-temperature regions. J Perform Constr Facil 29:1–6. https://doi.org/10.1061/(ASCE)CF.1943-5509.0000546

Cardone D (2016) Fragility curves and loss functions for RC structural components with smooth rebars. Earthq Struct 10:1181–1212. https://doi.org/10.12989/eas.2016.10.5.1181

Cardone D, Flora A, De Luca Picione M, Martoccia A (2019a) Estimating direct and indirect losses due to earthquake damage in residential RC buildings. Soil Dyn Earthq Eng 126:105801. https://doi.org/10.1016/j.soildyn.2019.105801

Cardone D, Flora A, Gesualdi G (2013) Inelastic response of RC frame buildings with seismic isolation. Earthq Eng Struct Dyn 42:871–889. https://doi.org/10.1002/eqe.2250

Cardone D, Perrone G (2015) Developing fragility curves and loss functions for masonry infill walls. Earthq Struct 9:257–279. https://doi.org/10.12989/eas.2015.9.1.257

Cardone D, Perrone G (2017) Damage and Loss Assessment of Pre-70 RC Frame Buildings with FEMA P-58. J Earthq Eng 21:23–61. https://doi.org/10.1080/13632469.2016.1149893

REFERENCES

Cardone D, Perrone G, Piesco V (2019b) Developing collapse fragility curves for base-isolated buildings. Earthq Eng Struct Dyn 48:78–102. https://doi.org/10.1002/eqe.3126

Cardone D, Rossino M, Gesualdi G (2018) Estimating fragility curves of pre-70 RC frame buildings considering different performance limit states. Soil Dyn Earthq Eng 115:868–881. https://doi.org/10.1016/j.soildyn.2017.11.015

Cardone D, Sullivan TJ, Gesualdi G, Perrone G (2017) Simplified estimation of the expected annual loss of reinforcedconcrete buildings. Earthq Eng Struct Dyn 46:

CEN (2004a) Eurocode 8 Design of structures for earthquake resistance

CEN (2009) UNI EN 15129 Anti-seismic devices - Comité Europeen de Normalisation

CEN (2004b) UNI EN 1337-Structural bearings - Part 2: Sliding elements

Clemente P, Martelli A (2018) Seismically isolated buildings in Italy: State-of-the-art review and applications. Soil Dyn Earthq Eng 1–17. https://doi.org/10.1016/j.soildyn.2017.12.029

Colangelo F (1999) Qualificazione risposta sismica pseudodinamica e modelli fenomenologici di portali di c.a tamponati con laterizio

Combescure D, Pegon P (1997) α-Operator splitting time integration technique for pseudodynamic testing error propagation analysis. Soil Dyn Earthq Eng 16:427–443

Computer, Structures (2007) SAP 2000. Linear and Nonlinear Static and Dynamic Analysis and Design of Three Dimensional Structures. CSi, Berkeley, CA

Constantinou MC, Caccese J, Harris H. (1987) Frictional characteristics of Teflons-steel interfaces under dynamic conditions. Earthq Eng Struct Dyn 15:751–759

Constantinou MC, Reinhorn AM, Watson R (1988) Teflon bearings in aseismic base isolation: experimental studies

Constantinou MC, Soong T., Dargush G. (1998) Passive Energy Dissipation Systems for Structural Design and Retrofit

REFERENCES

Cosenza E, Del Vecchio C, Di Ludovico M, et al (2018) The Italian guidelines for seismic risk classification of constructions: technical principles and validation. Springer Netherlands

Cosenza E, Di Sarno L, Chioccarelli E, et al (2009) L ' Ospedale del Mare in Napoli : il record europeo dell ' isolamento sismico

Cosenza E, Manfredi G (2000) Damage indices and damage measures. Prog Struct Eng Mater 2:50–59. https://doi.org/10.1002/(sici)1528-2716(200001/03)2:1<50::aid-pse7>3.3.co;2-j

CS.LL.PP. (2019) Istruzioni per l'applicazione dell'«Aggiornamento delle "Norme tecniche per le costruzioni"». Gazz Uff della Repubb Ital 35:1–337

Del Vecchio C, Di Ludovico M, Pampanin S, Prota A (2018) Repair costs of existing rc buildings damaged by the l'aquila earthquake and comparison with FEMA P-58 predictions. Earthq Spectra 34:237–263. https://doi.org/10.1193/122916EQS257M

Del Vecchio C, Di Ludovico M, Prota A (2020) Repair costs of reinforced concrete building components: from actual data analysis to calibrated consequence functions. Earthq Spectra 1–25. https://doi.org/10.1177/8755293019878194

Del Vecchio C, Di Ludovico M, Prota A (2021) Cost and effectiveness of fiber-reinforced polymer solutions for the large-scale mitigation of seismic risk in reinforced concrete buildings. Polymers (Basel) 13:. https://doi.org/10.3390/polym13172962

Derham CJ, Kelly JM, Thomas A. (1985) Nonlinear Natural Rubber Bearings for Seismic Isolation. Nucl Eng Des 84:417–428

Di Ludovico M, Prota A, Manfredi G (2019) Leggi di correlazione dannno costo per la definizione di scenari di perdite da sisma

Di Ludovico M, Prota A, Moroni C, et al (2017) Reconstruction process of damaged residential buildings outside historical centres after the L'Aquila earthquake: part II—"heavy damage" reconstruction. Springer Netherlands

Dolce M, Calvi GM (2010) La filosofia del progetto C.A.S.E. G dell'Ingegnere

REFERENCES

Dolce M, Cardone D, Marnetto R, et al (2003a) A New Added Damping Rubber Isolator (ADRI): Experimental Tests and Numerical Simulations. In: 8th World Seminar on Seismic Isolation, Energy Dissipation and Active Vibration Control of Structures. Yerevan, Armenia

Dolce M, Cardone D, Nigro D, Croatto F (2003b) The Effects of Friction Variability on the Response of Isolated Bridges. In: 8th World Seminar on Seismic Isolation, Energy Dissipation and Active Vibration Control of Structures

Dolce M, Cardone D, Ponzo FC, Di Cesare A (2004) Progetto di edifici con Isolamento Sismico

Dolce M, Serino G (2009) Technologies for the Seismic Isolation and Control of Structures and Infrastructures. state Art Earthq Eng Res Italy ReLUIS-DPC 2005-2008 Proj

DPC-ReLUIS (2011) Linee Guida Per Riparazione E Rafforzamento Di Elementi Strutturali, Tamponature E Partizioni (in Italian), Doppiavoce

Duerig TW, Melton KN, Stoeckel D, Wayman C. (1990) Engineering aspects of shape memory alloys. Butterworth-Heinemann Ltd, London

Fadi F, Constantinou MC (2009) Evalaution of simplified methods of analysis for structures with triple friction pendulum. Earthq Eng Struct Dyn 39:5–22. https://doi.org/10.1002/eqe

Fajfar P (2000) A non-linear analysis method for performance-based seismic design. Earthq Spectra 16:573–592

Fenz D., Constantinou MC (2008) Modeling triple friction pendulum bearings for response-history analysis. Earthq Spectra 24:1011–1028. https://doi.org/10.1193/1.2982531

Fib bulletin 90 (2019) Externally applied FRP reinforcement for concrete structures. Fédération internationale du béton (fib), 2019

Fico R, Sabino A, Pipponzi G, et al (2019) The emergency management and reconstruction process in small towns: the case of Barisciano (AQ). In: DYNAMIC INTERACTION OF SOIL AND STRUCTURE (DISS_19). L'Aquila

Frascadore R, Di Ludovico M, Prota A, et al (2015) Local strengthening of reinforced concrete structures as a strategy for seismic risk mitigation at regional scale. Earthq Spectra 31:1083–1102. https://doi.org/10.1193/122912EQS361M

Furinghetti M, Yang T, Calvi PM, Pavese A (2021) Experimental evaluation of extra-stroke displacement capacity for Curved Surface Slider devices. Soil Dyn Earthq Eng 146:106752. https://doi.org/10.1016/j.soildyn.2021.106752

Galanis PH, Moehle JP (2015) Development of collapse indicators for risk assessment of older-type reinforced concrete buildings. Earthq Spectra 31:1991–2006. https://doi.org/10.1193/080613EQS225M

Goulet CA, Haselton CB, Mitrani-Reiser J, et al (2007) Evaluation of the seismic performance of a code-conformingreinforced-concrete frame building—from seismic hazard tocollapse safety and economic losses. Earthq Eng Struct Dyn 36:1973–1997. https://doi.org/10.1002/eqe.694

Hanson RD (1993) State of the art and state of the practice in seismic energy dissipation. In: Proc. Of the ATC-17-1 Seminar. San Francisco, California

Housner GW, Bergman LA, Caughey TK, et al (1997) Structural Control: Past, Present, and Future. J Eng Mech 123:897–971. https://doi.org/10.1061/(asce)0733-9399(1997)123:9(897)

Hwang JS, Chang KC, Lee GC (1990) Quasi-static and dynamic sliding characteristics of Teflon- stainless steel interfaces. 116:2747–2762

Iervolino I, Galasso C, Cosenza E (2010) REXEL: Computer aided record selection for code-based seismic structural analysis. Bull Earthq Eng 8:339–362. https://doi.org/10.1007/s10518-009-9146-1

Iervolino I, Maddaloni G, Cosenza E (2007) Accelerogrammi naturali compatibili con le specifiche dell ' OPCM 3431 per l ' analisi sismica delle strutture

REFERENCES

Infrastrutture MD, Trasporti EDEI (2018) Aggiornamento delle «Norme tecniche per le costruzioni». Gazz Uff della Repubb Ital 1–198

Kawashima K (2001) Remarkable design example of recent application of seismic isolation to new and reconstructed viaducts in Japan. In: Proc. 7th World Seminar on Seismic Isolation, Energy Dissipation and Active Control Structures. Assisi, Italy

Kelly JM (1991) Dynamic and Failure Characteristics of Bridgestone Isolation Bearings

Kelly JM, Quiroz E (1992) Mechanical Characteristics of Neoprene Isolation Bearing

Kelly TE (2001) Base Isolation of Structures: design guidelines. Holmes Consult Gr Ltd

Kelly TE (1992) Skellerup Industries Lead Rubber Isolation Bearings: Experimental Properties

Mander JB, Priestley MJN, Park R (1988) THEORETICAL STRESS-STRAIN MODEL FOR CONFINED CONCRETE

Mannella A, Di Ludovico M, Sabino A, et al (2017) Analysis of the population assistance and returning home in the reconstruction process of the 2009 L'aquila earthquake. Sustain 9:. https://doi.org/10.3390/su9081395

Martelli A, Forni M (2009) State of art on application, R&D and design rules for seismic isolation, energy dissipation and vibration control for civil structures, industrial plants and cultural heritage in Italy and other countries. In: Proc 11th World Conference on Seismic Isolation, Energy Dissipation and Active Vibration Control of Structures. Guangzhou, China

Masi A, Vona M (2009) Estimation of the in-situ concrete strength: provisions of the european and italian seismic codes and possible improvements. RELUIS - Eurocode 8 Perspect from Ital Standpoint Work 67–77

Mellon FL, McKee JA (1994) Bridge Bearings. Natl Coop Highw Res Progr Synth Highw Pr. https://doi.org/10.1201/9781482266993-10

MIT (2018) Aggiornamento delle «Norme tecniche per le costruzioni» (in Italian). Supplemento ordinario n. 8 alla GAZZETTA UFFICIALE del 20-2-2018. Italy

REFERENCES

Morgan T., Whittaker AS (2001) Cyclic behavior of High Damping Rubber Bearing. In: 5th World Congress on Joints, Bearings and Seismic Systems for Concrete Structures

Naeim F, Kelly JM (1999) Design of Seismic Isolated Structures. Wiley: New york

Natale A, Del Vecchio C, Di Ludovico M (2020) Seismic retrofit solutions using base isolation for existing RC buildings: economic feasibilty and pay-back time. Bull Earthq Eng 19:483–512. https://doi.org/10.1007/s10518-020-00988-9

Natale A, Del Vecchio C, Di Ludovico M, et al (2021) Creep effects on elastomeric and ball rubber bearings unders sustained lateral loads. Struct Infrastruct Eng

O’Reilly GJ, Calvi GM (2019) Conceptual seismic design in performance-based earthquake engineering. Submitt to Earthq Eng Struct Dyn (on-line p: https://doi.org/10.1002/eqe.3141

O’Reilly GJ, Sullivan TJ (2018) Probabilistic seismic assessment and retrofit considerations for Italian RC frame buildings. Springer Netherlands

Ozkaya C, Akyuz U, Caner A, et al (2011) Development of a new rubber seismic isolator: ‘Ball Rubber Bearing (BRB).’ Earthq Eng Struct Dyn 1337–1352. https://doi.org/10.1002/eqe.1091

Panagiotakos TB, Fardis MN (1996) Seismic response of infilled RC frames structures. Prooceedings of the Eleventh World Conference on Earthquake Engineering, Mexico, Paper No. 225

Pellecchia D, Lo Feudo S, Vaiana N, et al (2021) A procedure to model and design elastomeric-based isolation systems for the seismic protection of rocking art objects. Comput Civ Infrastruct Eng 1–18. https://doi.org/10.1111/mice.12775

Polese M, Di Ludovico M, Gaetani d’Aragona M, et al (2020) Regional vulnerability and risk assessment accounting for local building typologies. Int J Disaster Risk Reduct 43:. https://doi.org/10.1016/j.ijdrr.2019.101400

Ponzo FC, Cesare AD, Leccese G, Nigro D (2015) Shaking table tests of a base isolated structure with double concave friction pendulum bearings. Bull New Zeal Soc Earthq

Eng 48:136–144

Porter K. (2003) An Overview of PEER's Performance-Based Earthquake Engineering Methodology. In: Ninth International Conference on Applications of Statistics and Probability in Civil Engineering

Ragni L, Cardone D, Conte N, et al (2018) Modelling and Seismic Response Analysis of Italian Code-Conforming Base-Isolated Buildings. J Earthq Eng 22:198–230. https://doi.org/10.1080/13632469.2018.1527263

Ricci P, De Luca F, Verderame GM (2011a) 6th April 2009 L'Aquila earthquake, Italy: Reinforced concrete building performance. Bull Earthq Eng 9:285–305. https://doi.org/10.1007/s10518-010-9204-8

Ricci P, Verderame GM, Manfredi G (2011b) Analytical investigation of elastic period of infilled RC MRF buildings. Eng Struct 33:308–319. https://doi.org/10.1016/j.engstruct.2010.10.009

Robinson W. (1982) Lead-rubber hysteretic bearings suitable for protecting structures during earthquakes. Earthq Eng Struct Dyn Struct Dyn 10:593–604. https://doi.org/10.2140/siaps.2011.2.5

Roeder C., Stanton J. (1984) Elastomeric bearings: state-of-the-art. 109:2853–2871

Ruggieri S, Porco F, Uva G (2020) A practical approach for estimating the floor deformability in existing RC buildings: evaluation of the effects in the structural response and seismic fragility. Springer Netherlands

Skinner RI, McVerry GH (1975) Base Isolation for increased earthquake resistance of buildings. Bull New Zeal Soc earthqauke Eng 8:93–101

Soong TT, Dargush G. (1997) Passive energy dissipation systems in structural engineering. John Wiley & Sons Ltd

STR.LL.PP. (2017) Abruzzo region price list 2017 Edition, Abruzzo, Italy

Su Y, Gao X, Li X, Tao D (2012) Multivariate multilinear regression. IEEE Trans Syst Man, Cybern Part B Cybern 42:1560–1573.

https://doi.org/10.1109/TSMCB.2012.2195171

Taylor AW, Lin A., Martin J. (1992) Performance of Elastomers in Isolation Bearings: a Literature Review. Earthq Spectra 8:279–304

Timsina S, Calvi PM (2021) Variable Friction Base Isolation Systems: Seismic Performance and Preliminary Design. J Earthq Eng 25:93–116. https://doi.org/10.1080/13632469.2018.1504837

Tyler RG (1977) Dynamic Tests on PTFE Sliding Layers under Erthquake Conditions. Bull New Zeal Natl Soc Earthq Eng 10:129–138

Verderame GM, De Luca F, Ricci P, Manfredi G (2010) Preliminary analysis of a soft-storey mechanism after the 2009 L'Aquila earthquake. Earthq Eng Struct Dyn 40:925–944. https://doi.org/10.1002/eqe.1069

Zayas VA, Low S, Mahin S. (1987) The Friction Pendulum System (FPS) Earthquake Resistign System: Experimental Report. Berkeley, California

(1980) DIN 17 100 - Steel for general structural purpose